06

III

# SELECTED HYDROLOGIC APPLICATIONS OF LANDSAT-2 DATA: AN EVALUATION

RECEIVED
JUL .. 1979
SIS/902.6

E 7.9-10.264
CR-162098

By

DAVID F. McGINNIS, JR., MICHAEL MATSON, AND DONALD R. WIESNET

23170

"Made available under NASA sponsorship
in the interest of early and wide dissemination of Earth Resources Survey
program information and without liability
for any use made thereof."

(E79-10264) SELECTED HYDROLOGIC APPLICATIONS OF LANDSAT-2 DATA: AN EVALUATION Final Report (National Environmental Satellite Service) 205 p HC A10/MF A01 CSCL 08H G3/43

N79-32603

Unclas
00264

# SELECTED HYDROLOGIC APPLICATIONS OF LANDSAT-2 DATA: AN EVALUATION

by

David F. McGinnis, Jr., Michael Matson, and Donald R. Wiesnet

Donald R. Wiesnet — Principal Investigator
David F. McGinnis, Jr. — Co-investigator
Michael Matson — Associate

National Oceanic and Atmospheric Administration
National Environmental Satellite Service
Environmental Sciences Group
Washington, D.C. 20233

Original photography may be purchased from
EROS Data Center

Sioux Falls, SD 57198

Final Report

Prepared for:
GODDARD SPACE FLIGHT CENTER
Greenbelt, Maryland 20771

# An Evaluation of Landsat-2

# for

# Soil Moisture Detection

# and for

# Snow Studies

by

David F. McGinnis, Jr., Michael Matson, and Donald R. Wiesnet

Final Report Contract # NAS-5399/A

1978

SELECTED HYDROLOGIC APPLICATIONS OF LANDSAT-2 DATA:

AN EVALUATION

TABLE OF CONTENTS


Executive Summary and Conclusions 1

Introduction 6

Part A - Snow Studies

Section 1. Introduction A-1

Section 2. Snow Extent Mapping A-4

American River Basin A-4

Description A-4

The 1975 Water Year A-7

The 1976 Water Year A-7

The 1977 Water Year A-13

Landsat MSS and NOAA VHRR Coverage A-17

GOES VISSR Coverage A-19

References A-22

Section 3. Snowmelt in the American River Basin A-24

Introduction A-24

Description of the GE Image 100 System A-24

Analysis of Landsat MSS Data A-25

Surface Data A-39

Precipitation A-39

Temperature A-40

Comparison of Areal Snow Extent: Conventional vs. GE Image 100 A-43

Discussion of Results A-48

GE Image 100 vs Conventional Procedure as a Snow Mapping Tool A-48

Snow Classification using the GE Image 100 A-49

Summary A-53

References A-55

Section 4. Snow in Forest Areas A-56
Introduction A-56
Objectives A-56

Data A-56

Data Analysis A-56

Summary A-62

References A-64

Section 5. Snowcover : Runoff Relation in American River Subbasins A-65

Introduction A-65

Description of Subbasins A-65

Data and Data Analysis A-66

Discussion of Results A-76

Summary A-78

References A-79

Part B - Soil Moisture Studies

Section 1. Introduction B-1

Section 2. Phoenix Test site B-2

Description of Site and Overview of Experiment B-2

Soil Sampling and Soil Moisture Data B-8

Microwave Study B-9

Gamma-Ray Study B-9

Equipment B-10

| | | |
|---|---|---|
| | Technique | B-11 |
| | Results | B-13 |
| | Soil Moisture Ground Measurements | B-22 |
| | Landsat Investigation - Visible and Near-IR | B-24 |
| | Introduction | B-24 |
| | Procedure | B-24 |
| | Results and Discussion | B-28 |
| | NOAA Investigation - Thermal IR | B-38 |
| | Conclusions | B-41 |
| | Summary of Soil Moisture | B-42 |
| | Future | B-43 |
| | References | B-45 |
| Section 3. | Luverne, Minnesota Soil Moisture Survey | B-48 |
| | Description of Test Site | B-48 |
| | Soil Moisture Experiments | B-48 |
| | The May 11-12, 1975, Experiment | B-48 |
| | Equipment | B-52 |
| | Technique | B-52 |
| | Results | B-53 |
| | Conclusions | B-65 |
| | The October 17, 1975, Experiment | B-67 |
| | Zeiss and AMPS Data | B-71 |
| | Multispectral Scanner Data | B-91 |
| | $M^2S$ Thermal IR Data and PRT-5 Data | B-100 |
| | Landsat Data | B-101 |
| | Conclusions | B-104 |

LIST OF ILLUSTRATIONS


| | | |
|---|---|---|
| Fig. 1. | Index map showing location of American River Basin, California. | A-5 |
| Fig. 2. | Drainage map of the American River Basin, California. | A-6 |
| Fig. 3. | Average snowfall of three stations in or near the American River Basin for 1975. The three stations are Squaw Valley, Twin Lakes, and Blue Canyon. | A-8 |
| Fig. 4. | 1975 snow buildup and melt in the American River Basin from NOAA-4 VHRR data. | A-9 |
| Fig. 5. | Areal snow extent in the American River Basin as determined by Environmental Products Branch/NESS from Landsat-1 and Landsat-2 MSS band-5 imagery. | A-10 |
| Fig. 6. | Three-day running mean of snow buildup and melt in the American River Basin from NOAA-4 VHRR data. | A-11 |
| Fig. 7. | Areal snow extent in the American River Basin as determined from GOES-2 imagery. | A-12 |
| Fig. 8. | Water content of snow at Alpha (near Wrights Lake), elev. 7,600 ft. (2316 m), comparing 1975-76 and 1976-77 with average. | A-15 |
| Fig. 9. | Monthly mean discharge of North Fork American River at North Fork Dam, Calif., for 1976 and 1977 water years. | A-16 |
| Fig. 10. | Comparison of SMS VISSR, NOAA VHRR, and Landsat MSS 5 sensors in mapping areal snow extent in the American River Basin for 1975. | A-21 |
| Fig. 11a. | Computer-generated snow classification for 8 May 1975. | A-29 |
| Fig. 11b. | Computer-generated snow classification for 17 May 1975. | A-30 |
| Fig. 11c. | Computer-generated snow classification for 13 June 1975. | A-31 |
| Fig. 11d. | Computer-generated snow classification for 22 June 1975. | A-32 |

| | | |
|---|---|---|
| Fig. 11e. | Computer-generated snow classification for 1 July 1975. | A-33 |
| Fig. 11f. | Computer-generated snow classification for 14 April 1976. | A-34 |
| Fig. 11g | Computer-generated snow classification for 23 April 1976. | A-35 |
| Fig. 11h. | Computer-generated snow classification for 20 May 1976. | A-36 |
| Fig. 11i. | Computer-generated snow classification for 29 May 1976. | A-37 |
| Fig. 12a. | Comparison of SCA as derived from Fig. 11b (solid line) with conventionally-derived SCA shown in Fig. 13a (dashed line) for 17 May 1975. | A-44 |
| Fig. 12b. | Comparison of SCA as determined from Fig. 11d (solid line) with conventionally-derived SCA shown in Fig. 13b for 22 June 1975. | A-45 |
| Fig. 13a. | Conventional SCA map for 17 May 1975. | A-46 |
| Fig. 13b. | Conventional SCA map for 22 June 1975. | A-47 |
| Fig. 14. | Graph showing Landsat brightness levels and radiation estimates of snowcover in deciduous and coniferous areas of the Adirondack Mountains. (After Eschner, et al., 1977). | A-61 |
| Fig. 15. | Sketch map showing the location of the Duncan Creek, Pilot Creek, and North Fork of Middle Fork American River subbasins. | A-67 |
| Fig. 16a. | Map of the Duncan Creek subbasin. | A-68 |
| Fig. 16b. | Map of the Pilot Creek subbasin. | A-69 |
| Fig. 16c. | Map of the North Fork of Middle Fork American River subbasin. | A-70 |
| Fig. 17a. | Daily discharge hydrographs of Pilot Creek and Duncan C Creek for March-June 1973, 1975, and 1976. | A-71 |
| Fig. 17b. | Daily discharge hydrographs of North Fork of Middle Fork American River for March-June 1973, 1975, and 1976. | A-72 |

LANDSAT-2 REPORT

SOIL MOISTURE SECTION

FIGURE CAPTIONS


Fig. 1. Index map showing the two survey lines near Phoenix, Ariz. B-3

Fig. 2a. Map showing northern third of test site near Phoenix, Arizona with details as to land use, row direction, and field sampling locations (from Blanchard, 1975, Appendix B). B-4

Fig. 2b. Map showing middle third of test site near Phoenix, Arizona, with details to land use, row direction, and field sampling locations. Legend found on Figure 2. (from Blanchard, 1975, Appendix B) B-5

Fig. 2c. Map showing southern third of test site near Phoenix, Arizona with details as to land use, row direction, and field sampling locations. Legend found on Figure 2. (from Blanchard, 1975, Appendix B) B-6

Fig. 3. View of the interior of the gamma ray survey aircraft showing the detector package and the electronic data collection system. (from Feimster, et al, 1975) B-12

Fig. 4. Definition of the gamma energy spectral pulse height windows used in the photopeak area equations. The letter labels refer to the following: T (counts in the $^{208}Tl$ window); U (counts in the window occupied by the higher energy $^{214}Bi$ gammas from the uranium decay chain); B (counts in the 1.6 MeV $^{214}Bi$ photopeak window); K (counts in the $^{40}K$ photopeak window); and L (lower energy background gamma counts around the 1.12 MeV $^{214}Bi$ photopeak. (from Feimster et al, 1975) B-14

Fig. 5. Portion of Landsat-1 image (3/17/75, 1967-17154, orbit 13,484) covering Phoenix and the area to the west of the city including the test site at Tolleson, Arizona. MSS band 5 (0.6-0.7μm) on left, MSS band 7 (0.8-1.1μm) on right. Computer-generated and enhanced. B-17

Fig. 6a. Enlarged segment of MSS band 5 shown in Figure 5, covering test site and the immediate vicinity around Tolleson, Arizona. B-25

Fig. 6b. Enlarged segment of MSS band 7 shown in Figure 5, covering test site and the immediate vicinity around Tolleson, Arizona. B-26

Fig. 7 Example of full-resolution contoured microfilm printout of MSS band 7 raw data counts, covering fields 94, 95, 97A, 97B, and portions of fields 91, 92, 93A, 98A, 99A, 99B, and 100A. B-27

Fig. 8. Volumetric water content in the 0.0 to 0.5-cm increment versus time for 3 days during March 1971. The solid line represents smoothed data and the symbols represent the measured values. (from Jackson, 1973) B-29

Fig. 9a. Regression analysis of percent soil moisture vs. MSS reflectance raw counts, MSS band 4, bare fields only (power fit). B-30

Fig. 9b. Regression analysis of percent soil moisture vs. MSS reflectance raw counts, MSS band 4, vegetated fields only (parabolic fit). B-31

Fig. 9c. Regression analysis of percent soil moisture vs. MSS reflectance raw counts, MSS band 6, bare field only (power fit). B-32

Fig. 9d. Regression analysis of percent soil moisture vs. MSS reflectance raw counts, MSS band 6, vegetated fields only, alfalfa (parabolic fit) and wheat (power fit) separated. B-33

Fig. 10. Combined plots of MSS bands 5 and 7 raw counts vs. soil moisture: a) MSS band 5, bare fields only (power fit); b) MSS band 5, vegetated fields only (straight-line fit); c) MSS band 7, bare fields only (power fit); d) MSS band 7, alfalfa only (parabolic fit); and e) MSS band 7, wheat only (logarthmic fit). B-34

Fig. 11 False-color aerial photograph of fields 94, 95, 97A, 97B as well as portions of fields 91, 92, 93A, 98A, 99A, 99B, and 100A, overprinted with MSS band 7 raw data from Landsat-1 image (3/17/75, 1967-17154). See Fig. 7. B-36

Fig. 12. SMS-2 8 km resolution thermal-IR (10.5-12.5μm) imagery of southwestern North America and eastern Pacific Ocean. Image on left was observed at 2015 GMT on 3/17/75. Image on right was observed at 1015 GMT on 3/18/75. Image in center was obtained by subracting temperatures measured on 3/18/75 from those measured on 3/17/75. B-39

Fig. 13. Enlarged portion of 8-km thermal-IR (10.5-12.5μm) image acquired by SMS-2 at 1015 GMT on 3/18/75. Area viewed covers southwestern U.S. (including Phoenix test site) and portions of Baja, California, and the Gulf of Baja. B-40

Fig. 14. Index map of Minnesota showing the location of Luverne. B-49

Fig. 15. Map of Luverne, Minnesota, test site showing flight line. B-50

Fig. 16. Soil map of Luverne, Minnesota, test site. U.S. Highway #75 is shown by dark bold line. Test site line is shown by dashes. Map taken from USDA soil map of Rock County, Minnesota. B-51

Fig. 17. Luverne, Minnesota, survey flight pattern-north half. The dashed lines labeled A through C and E indicate the positions of survey lines (from Feimster and Fritzsche, 1975). B-54

Fig. 18. Luverne, Minnesota, survey flight pattern-south half. The dashed lines labeled A through D indicate the positions of survey lines (from Feimster and Fritzsche, 1975). B-55

Fig. 19. Average adjusted gross count rate per mile for each of the four passes of line A (from Feimster and Fritzsche, 1975). B-64

Fig. 20. Average soil moisture per mile from airborne adjusted gross count rate and from soil samples (from Feimster and Fritzsche, 1975). B-66

Fig. 21. Location of the four fields selected in the October 17, 1975 soil moisture experiment. B-72

Fig. 22. Zeiss color IR photograph of field A. B-73

Fig. 23. Zeiss color IR photograph of fields B and C. B-74

Fig. 24. Zeiss color IR photograph of field D. B-75

Fig. 25. AMPS aerial color photograph of field A. B-76

Fig. 26. AMPS aerial color photograph of field B. B-77

Fig. 27. AMPS aerial color photograph of field C. B-78

Fig. 28. AMPS aerial color photograph of northern section of field D. B-79

Fig. 29. AMPS aerial color photograph of southern section of field D. B-80

Fig. 30. AMPS color IR photograph of field A. B-81

Fig. 31. AMPS color IR photograph of field B. B-82

Fig. 32. AMPS color IR photograph of field C. B-83

Fig. 33. AMPS color IR photograph of northern section of field D. B-84

Fig. 34. AMPS color IR photograph of southern section of field D. B-85

Fig. 35. AMPS black and white IR photograph of field A. B-86

Fig. 36. AMPS black and white IR photograph of field B. B-87

Fig. 37. AMPS black and white IR photograph of field C. B-88

Fig. 38. AMPS black and white IR photograph of the northern section of field D. B-89

Fig. 39. AMPS black and white IR photograph of the southern section of field D. B-9

Fig. 40. Typical laboratory curve of chernozem-type soil (from Condit, 1970), percent reflectance vs. wavelength. B-92

Fig. 41. Contoured radiance values for the channel 9 (0.760-0.860μm) of the multispectral scanner. Field B is shown. B-94

Fig. 42. Plot of average field radiance vs. wavelength for field A. B-95

Fig. 43. Plot of average field radiance vs. wavelength for field B. B-96

Fig. 44. Plot of average field radiance vs. wavelength for field C. B-97

Fig. 45. Plot of average field radiance vs. wavelength for field D. B-98

Fig. 46. A comparison of the channel 4 band (0.54-0.58μm) of the $M^2S$ and band 5 (0.5-0.6μm) of Landsat-2. Identical features on both bands are numbered. B-102

Fig. 47. A comparison of the channel 10 band (0.97-1.06μm) of the $M^2S$ and band 7 (0.8-1.1μm) of Landsat-2. Identical features on both bands are numbered. B-103

LIST OF TABLES

Snow Section


Table 1. Observed and forecast for the American River inflow to the Folsom Reservoir (in acre - feet x 1000) (based on data from California Department of Water Resources). A-14

Table 2. Landsat-derived snow extent measurements for the American River Basin, 1975. A-18

Table 3. Dates of available Landsat CCT's covering American River Basin, 1975 and 1976. A-26

Table 4. Range of reflectance in arbitrary units for various classes of snow. A-27

Table 5. Comparison of Conventional Analysis vs. Computer-Generated Analysis and breakdown of snowcover by class as percent of total basin area. A-

Table 6. Estimated surface and upper air temperatures at or near time of Landsat overpass, in degrees C. A-42

Table 7. Number of pixels by snow type and comparison of yellow and cyan snow to purple snow in percent. A-52

Table 8. Correlation analysis over snow survey sites (after Eschner, et al., 1977). A-57

Table 9. Satellite imagery data ranges, 1976 dimensionless values, absolute scale of 0 to 255 (after Eschner, et al., 1977). A-59

Table 10. Landsat image brightness and radiance estimates (after Eschner, et al., 1977). A-60

Table 11. Snow-cover area of American River subbasins in percent for 1973, 1974, 1976 using Landsat MSS band 5 imagery. A-73

Soil Moisture Section

Table 1. Summary of remote sensors used to collect data of Phoenix test site. B-7

Table 2. Net $^{40}K$ and $^{208}Tl$ gamma photopeak count rate from the March 18, 1975 survey. B-7

Table 3. Nonterrestrial backtround determined from the estimated radon activity using U/K method. (Nonterrestrial bkg = radon + aircraft + cosmic). B-19

Table 4. Nonterrestrial background computed from the adjusted gross count rate, fitted to photopeak area data. B-19

Table 5. Soil moisture values from soil samples weighted for the sampled 9-cm soil depth. B-23

Table 6. Comparison of soil moisture values determined from ground sampling and from aerial measurements. B-23

Table 7. Net $^{40}K$ and $^{208}Tl$ gamma photopeak count rates from the May 12, 1975 survey of line A at Luverne, Minnesota. B-57

Table 8. Air filter data. B-59

Table 9. Gamma spectral data used in U/K ratio comparisons. B-60

Table 10. Adjusted and averaged gross count rate per mile for line A. B-62

Table 11. Soil moisture for May 12, 1975 computed from averaged adjusted gross count rates in Table 10 and March 6, 1973 soil moisture data. B-62

Table 12. Comparison of the airborne gross count rate method and the ground-based soil moisture measurements per mile. B-63

Table 12a. Comparison of airborne gross count rate method and the ground-based soil moisture measurements per 2 miles. B-63

Table 13. $M^2S$ characteristics. B-68

Table 14. AMPS characteristics. B-69

Table 15. Zeiss characteristics. B-69

Table 16. Soil types found in Fields A, B, C, and D. B-69

Table 17. $M^2S$ spectral band vs. field radiance. B-99

# Executive Summary
# and
# Conclusions

## PART A: SNOW STUDIES

Snow events in the American River basin and subsequent runoff conditions are described for two years: a "typical" year, 1975; and a record drought year, 1977. For the 1975 data, a graph of snowcover plotted as a function of Julian day gave a correlation of 0.99+ for the seven measurements, while 11 NOAA VHRR measurements gave a correlation of 0.97. Thus, the use of Landsat or VHRR data to forecast the date of snowfree conditions in the river basin is a distinct possibility.

The use of satellite images in conjunction with ground based measurements can increase the effectiveness of getting the drought "message" across to the public.

The differing response of various sensors to snowcover measurements, previously demonstrated by several workers, should be taken into account by snow mappers. For example, 10 VISSR measurements of snowcover in the American River basin are, on the average, 3.5% lower than corresponding values from VHRR.

A comparison of conventional and computer-generated analyses of snowcover disclosed that the snow-cover area (SCA) ratio to computer-generated to conventional analysis ranged from 0.60 to 0.08. The ratio consistently dropped as a function of Julian day and was always least just before complete snowmelt. These findings were not unexpected, as pixel counts invariably are more precise than techniques that merely outline areas of snow. Further, the smaller the area of snowcover, the greater the error potential;

i.e., as the area of snowcover approaches zero, the percent error increases if the absolute area of measurement in error remains the same.

An analysis of snowcover extent by the GE Image 100 on a pixel by pixel classification, using MSS bands 5 and 7, resulted in much lower snowcover area figures. It was not possible using this technique to distinguish metamorphosed or "melting" snow areas, unambiguously. The current MSS bands are not optimum for measuring areas of metamorphosed or melting snowcover.

The low values of SCA as measured by computer-generated thematic mapping indicate the difficulty in properly defining the various themes representing SCA as viewed by Landsat. Previous studies have shown that conventionally derived NOAA/NESS SCA estimates agree well with ground observations. Nevertheless, even if the computer-generated thematic system produced snow maps equivalent to conventionally prepared maps, the computer-generated technique would be more time consuming and costlier at this stage.

Rather than classifying melting and non-melting snow, the thematic approach had instead apparently divided the melting or metamorphosed snow into various degrees of metamorphism: actively melting, early melting, and incipient melting. If this be true, the need for more detailed studies of the radiative properties of melting snow becomes more and more clear.

In a study of snow in forests, Landsat MSS when compared with NOAA VHRR visible imagery had a better signal-to-noise ratio and better sensitivity. Careful digital analysis in the Adirondack Mountains of New York indicate that forest type has a significant impact on reflectance. Deciduous and conifer areas show increases in radiance as a function of increasing wavelength. The converse is true for open areas. As forest areas are critical

for snowcover studies, careful controlled ground measurements of radiation are needed.

Snowcovered area was shown to be an important variable in runoff prediction by a stepwise multivariate analysis for several American River subbasins. Sateilite-derived SCA and day of year provided estimates of daily average runoff with a correlation of about 0.90, during seasons in which the recession curve of the hydrograph is fairly smooth.

## PART B: SOIL MOISTURE STUDIES

There is a real need for areally averaged soil-moisture values that reflect the condition of the watershed and its response to rainfall more accurately. We attempted to relate field studies of soil moisture near Phoenix, Arizona, and Luverne, Minnesota, to Landsat spectral reflectance measurements not only with ground truth but also with concurrent gamma-ray aircraft data and cooperatively with NASA PMIS (microwave) overflights.

At Phoenix, soil moisture values computed from the gamma-ray gross-count rate of the 18 March 1975 data are slightly higher than the ground-based measurements. The mean of the ground-sampled moisture values was nearly the same as that computed from the photopeak gamma-ray technique.

At Luverne, the gamma-ray adjusted gross-count-rate method gave an average soil moisture value of 28%, with mile-by-mile values ranging from 21-36%. Ground-based soil moisture measurements gave an average of 28%, with individual values ranging from 23%-36%. Thus the gamma-ray adjusted-gross-count technique provided a reliable source of corroboration for the areal soil-moisture values.

Gamma-ray aircraft surveys provided only <u>one</u> value for the entire Phoenix test site as a result of averaging many data points whose "footprint" was 150 m. The technique is limited by atmospheric contaminants, the need to fly at low (150 m) altitudes, and the need for prior ground calibration of a given test site.

Multispectral data can be used to establish a spectral signature for specific soil types. It is possible to detect significant changes in reflectance and relate these changes to changes in roughness

(i.e., tillage), soil moisture, or vegetative status. Identification of the causal factor is equivocal.

A comparison of MSS band 7 raw data (full resolution) over the Phoenix site superimposed on a false color near-IR aerial photo taken 27 hours later revealed that for alfalfa field 97A 0-2 cm soil-moisture values were lowest (13.70%), and band 7 reflectances were lowest (64). For alfalfa field 97B 0-2 cm soil-moisture values were highest (27.65%) and the band 7 reflectances were highest (84). This direct relationship of soil moisture to band 7 values held for all alfalfa fields sampled in the study.

The amount of useful information from visible and near-IR data is miniscule when compared to that provided by passive microwave radiometers and, potentially, from the thermal-IR. Further efforts to estimate soil moisture from remote platforms should place the emphasis on the microwave and the thermal IR portion of the spectrum where the most encouraging results have been achieved.

The use of the Geostationary Operational Environmental Satellite (GOES) thermal IR system to monitor soil moisture will not be feasible until the spatial resolution is improved from the current 8 km, and unless computer compatible tapes are made available.

## INTRODUCTION

This report was prepared as a result of a grant to the National Oceanic and Atmospheric Administration/National Environmental Satellite Service (Investigation No. 23170, Contract No. NAS-53991A). It is prepared in two sections: Part A, which deals with snow studies, and Part B, which deals with soil moisture studies. The purpose of this report is to evaluate our ability to extract useful information from Landsat-2 data, and to apply it to current needs of the National Oceanic and Atmospheric Administration's hydrologists. As can be seen throughout this report, the authors have continually tried to examine Landsat data and compare it with the current operational NOAA series of polar-orbiting satellites and the geostationary series (GOES).

The authorship of the report is a team effort, but nevertheless, certain sections are primarily authored by individuals. In Part A, section one and two were written by Wiesnet, sections three, four, and five were written by McGinnis. Sections one and two of Part B were written by McGinnis and section three by Matson. Each has reviewed the others' contributions and the ranking of each author represents the amount of time (work) spent on the entire project. Please note that the references are found at the end of each section for the readers' convenience.

Landsat-2 was in no way different from Landsat-1 with respect to sensors. We have stressed the Multispectral Scanner or MSS data. Our results differ from the Landsat-1 report (Wiesnet, et al., 1975) in the fact that we have narrower objectives, i.e., snow and soil moisture, and in the increased use of computer compatible tape data (CCT's), rather than

the use of photointerpretive techniques.

We lament our inability to obtain aircraft/satellite coordination on our experiments, but all concerned must realize that the acquisition of NASA aircraft data precisely in step with the satellite is indeed very rare. The limitations of project priorities, weather, and equipment failure make coordination of aircraft overflights a nearly impossible task. We were able to get aircraft data from gamma-ray overflights performed by EG&G, Inc. under contract, and these data have been included in Part B.

The access to NOAA imagery and image processing systems has been of great help to us, and we have freely used and relied on NOAA data, computer facilities, and equipment. Whether this report answers more questions than it raises is for the reader to determine. It certainly offers some interesting conclusions, but it is also clear that many unanswered questions remain.

Acknowledgements. John A. Pritchard of NESS has been our reliable source of expertise on computer processing throughout this project. His original and innovative computer programs have been a great help, without which many of the figures in this report would not have been possible. David G. Forsyth has been involved in computer processing as well as a myriad of other details. Lt. Craig P. Berg of the NOAA Corps and Darrell Macklin worked on sections of both the snow and soil moisture portions of the report. We acknowledge with thanks, EG&G for furnishing the gamma-ray material; National Weather Service for coordinating the gamma-ray overflights; Prof. A.R. Eschner, J.M. Lillesand, and D.E. Meisner on whose work most of Part B, section 4 is based. Lastly, we acknowledge the painstaking work of Mrs. Olivia Smith, who as a typist is rated simply "expert".

## INTRODUCTION

Snow, being the supplier of water for human, agricultural, and industrial consumption, is a vital water resource in arid areas of the world. A complex reservoir system, such as that in California, effectively transports snow runoff to meet the demands of cities and farms. However efficient these systems, better snow/runoff forecasts are always needed. The snow studies presented in this report attempt to evaluate the role satellites, principally Landsat, can provide in improving these snow/runoff forecasts.

Four chapters discuss various snow parameters and problems encountered with snowpacks in mountains. Section 2 evaluates several years of snow extent mapping in the American River basin--a review and update of our Landsat-1 study (Wiesnet, et al., 1975). Snow-extent mapping from satellite imagery has successfully evolved into an operational mode with 30 basins in the western United States currently evaluated by NESS throughout the melt season. Snowmelt in the American River basin is reevaluated in Section 3 and updates work begun in our first Landsat study. The major emphasis in this study incorporates analyses performed on the G.E. Image 100 Interactive Multispectral Image Analysis System. A summary of the work done by Eschner, et al. (1977) regarding snow in forest areas performed as an adjunct to this study constitutes Section 4. Multiple regression analyses for three subbasins in the American River basin relating snowmelt runoff to various meteorological and satellite measurements are investigated in Section 5.

This portion of the report represents another step toward application of Earth-orbiting satellite data to the real day-to-day problems of water

resource studies, research, and management. As a research paper it does not attempt to be comprehensive, rather it attempts to demonstrate by simple examples, that new ways of assessing or monitoring the snowpack will come only after we fully understand the type, quantity, and quality of information inferable from satellite orbit.

References

Eschner, A.R., Lillesand, J.M., and Meisner, D.E., 1977: Satellite Remote Sensing of Snowcover in the Adirondack Mountains, Final Report, 88 pp., NOAA/NESS Grant No. 04-5-158-43.

Wiesnet, D.R., McGinnis, D.F., and McMillan, M.C., 1975: Evaluation of ERTS Data for Certain Hydrological Uses, Final Report to NASA/GSFC, Contract No. 432-641-14-04-03, 92 pp.

## Snow Extent Mapping

The capability of Landsat MSS and NOAA VHRR to measure the areal extent of snow in river basins on a repetitive basis has been amply demonstrated. (Barnes and Bowley, 1968; Wiesnet, 1974; Wiesnet et al., 1974; Rango, 1975; Meier, 1975; Schneider, et al., 1976). This section will report in some detail on the snow extent in the American River basin which lies on the western slopes of the Sierra Nevada in California just west of Lake Tahoe (Fig. 1). In our original proposal, we had planned to include the Feather River basin as well, but this latter area was also included in a snow study by A.J. Brown, California Department of Water Resources, under the Advanced Systems Verification Test (ASVT) program of NASA (Rango, 1975, p. 6). Therefore, it was deleted from our plans as duplicative.

The fertile Sacramento and San Joaquin valleys of California depend heavily on the Sierra Nevada snowpack to provide water for agricultural use as well as for municipal and industrial use. Nearly 50% of the average annual runoff takes place during the April-July snowmelt. The California State Cooperative Snow Survey Program began in 1929 to measure snow and to forecast hydrologic runoff. Water management in California is as sophisticated as anywhere in the world. The State has been quick to recognize the potential of satellite data collection and satellite snow observations (Brown, 1975).

### A. The American River basin

1. Description. This rugged mountain basin lies between the city of Sacramento and Lake Tahoe. It covers 5,601 $km^2$. The Central Sierra Snow Laboratory lies just outside the basin boundary (Figure 2). Much of the basin receives more than 152 cm (60 inches) of precipitation

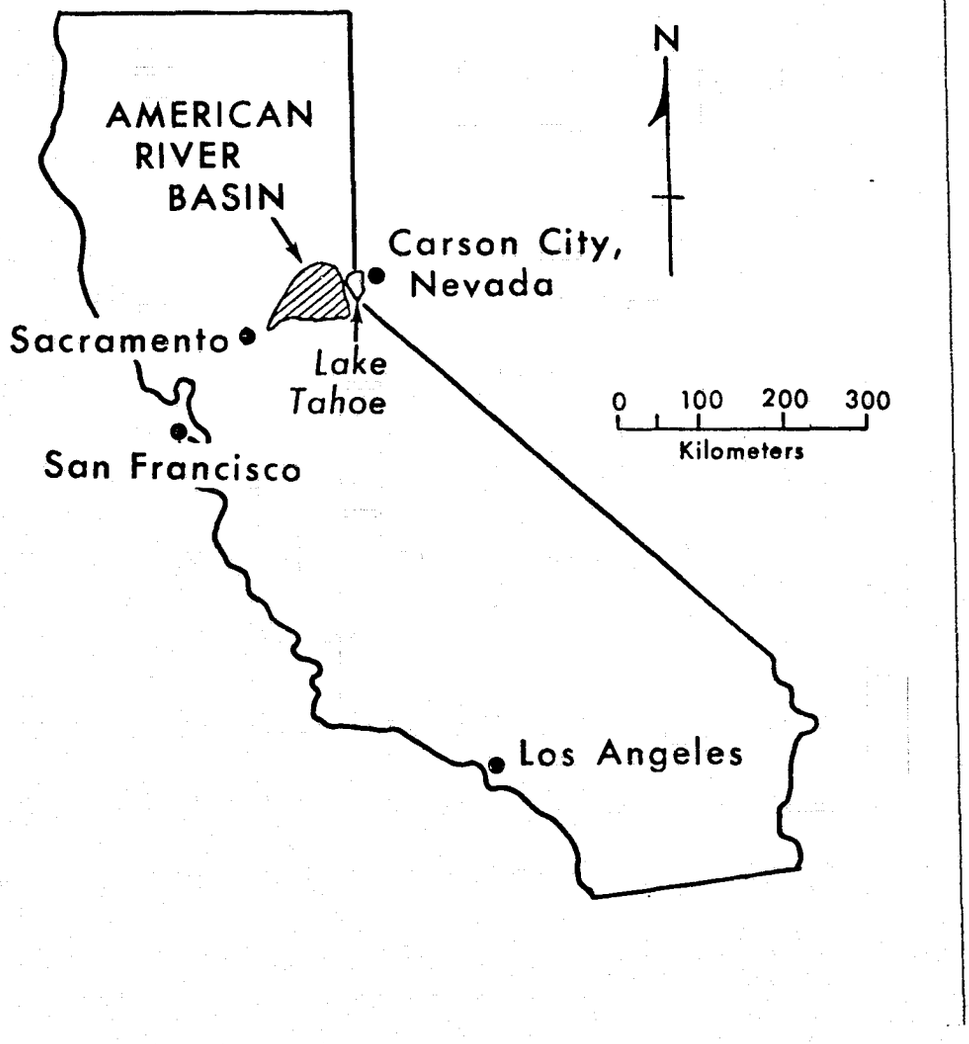



Figure 1. Index map showing location of American River Basin, California.

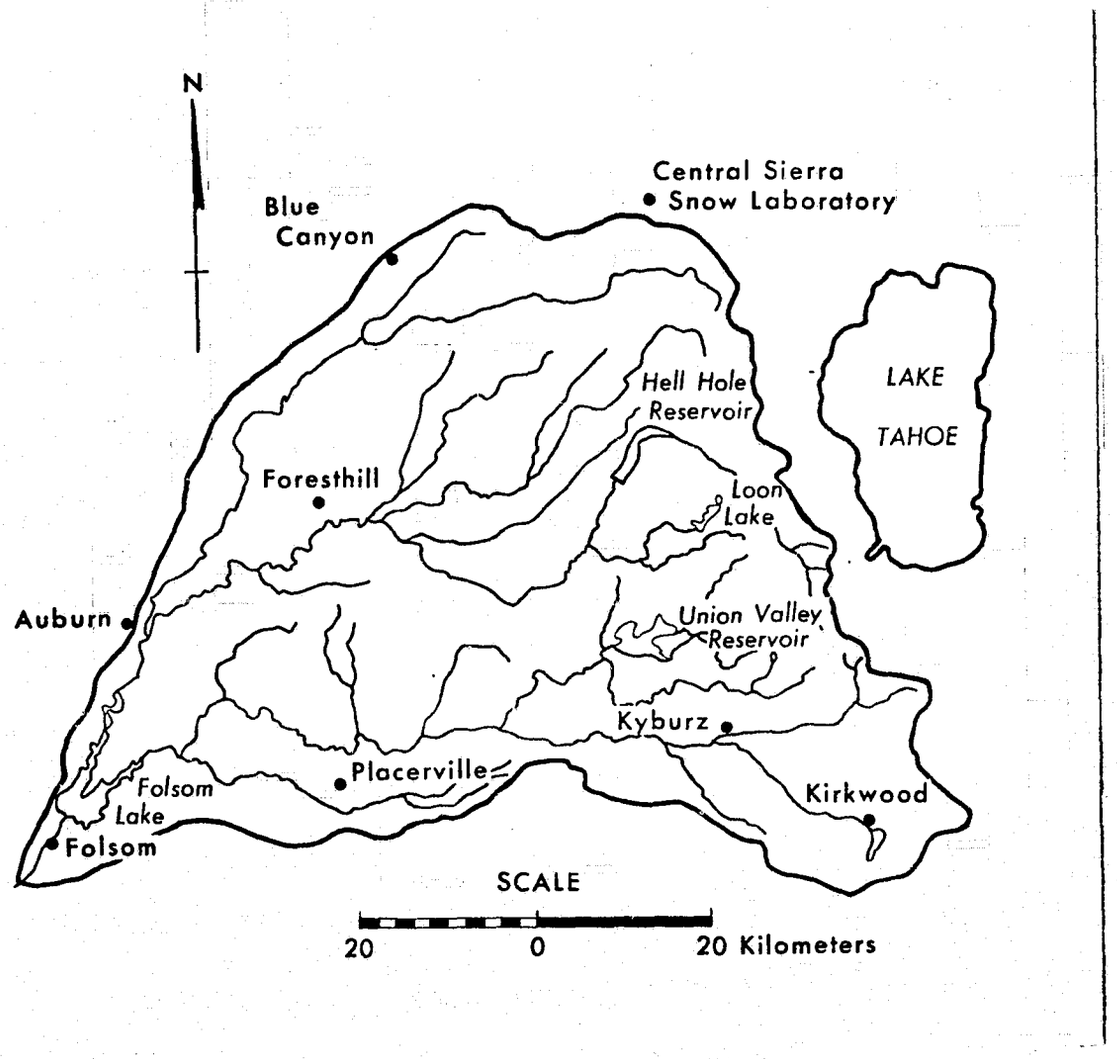



Figure 2. Drainage map of the American River Basin, California.

REPRODUCIBILITY OF THE
ORIGINAL PAGE IS POOR

largely in the form of snow. In the spring and summer, clear skies predominate and facilitate satellite observations. Runoff is about 102 cm (40 inches) per year, and reaches a peak during the April-June period.

2. The 1975 water year. In the American River basin the snowpack built up slowly in November through January, but heavy snows fell in early February, changing the outlook for water supply from near drought conditions to a higher-than-average year. Figure 3 shows the seasonal distribution of snowfall. The snow-extent build-up recorded by NOAA VHRR images (figure 4) shows a dramatic rise during the first week of February from 22% to 62% in the snow-covered area (SCA). The rapid decline thereafter was due chiefly to lower level melting. Once into Spril, the melting of the snowpack assumes a fairly stable rate. Snowfall and snowstorms decrease in amount and number.

The Landsat MSS record of melt (figure 5) appears much smoother than the NOAA VHRR, because of fewer observations, but is at about the same rate.

Comparison with the 3-day running mean of the NOAA VHRR-derived SCA data shows even closer similarities (figure 6). Comparison with the GOES values (figure 7) shows that GOES consistently detects less snow than Landsat; this phenomenon is attributed to the different spectral response of the two sensors; GOES peaking farther in the near-IR receives less visible radiation (Schneider and McGinnis, 1977).

3. The 1976 water year. This was the ghird driest year of the century in California. Only about 76 cm (30 inches) of precipitation fell over the American River basin as an offshore high-pressure system

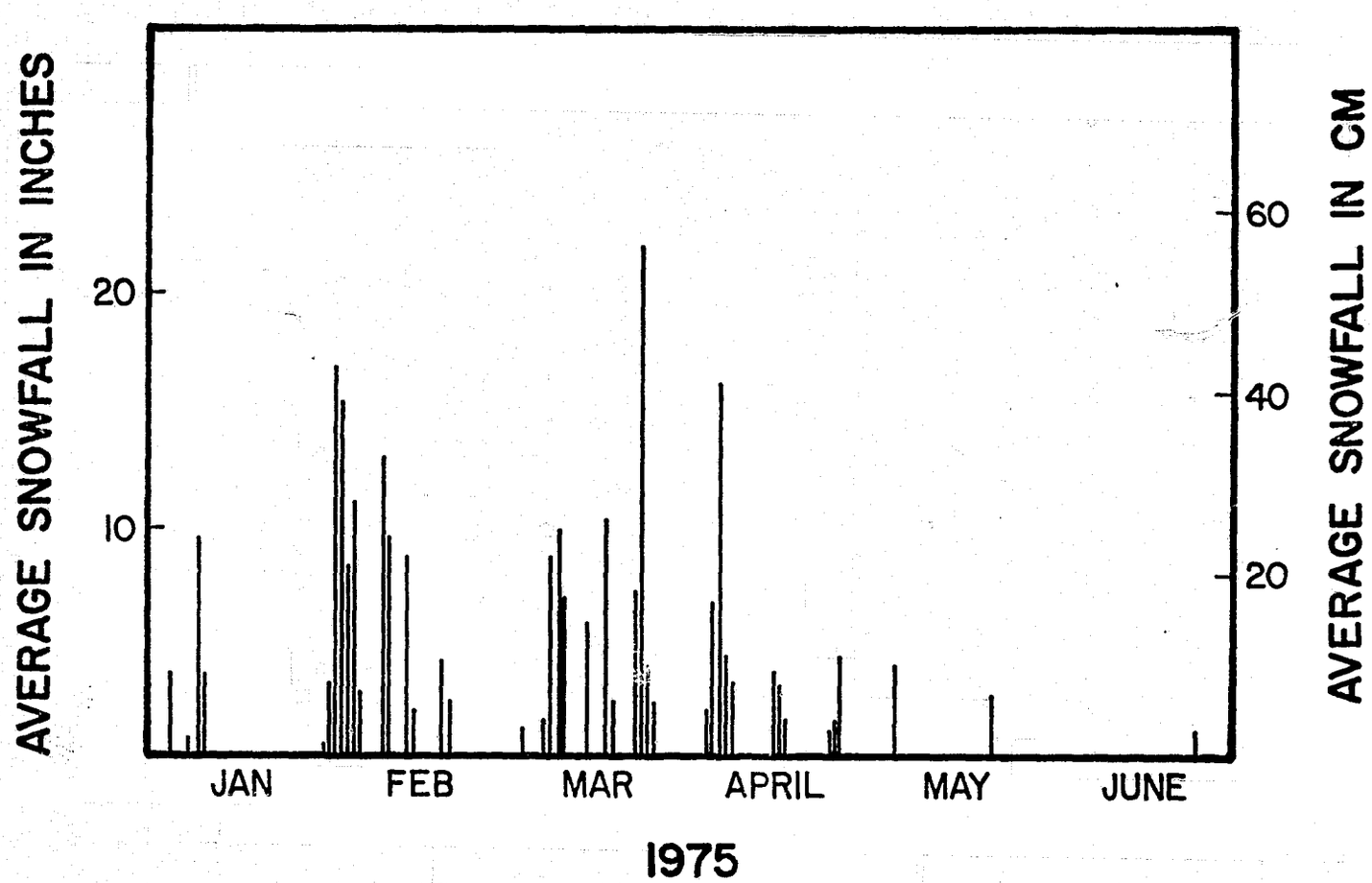



Figure 3. Average snowfall of three stations in or near the American River Basin for 1975. The three stations are Squaw Valley, Twin Lakes, and Blue Canyon.

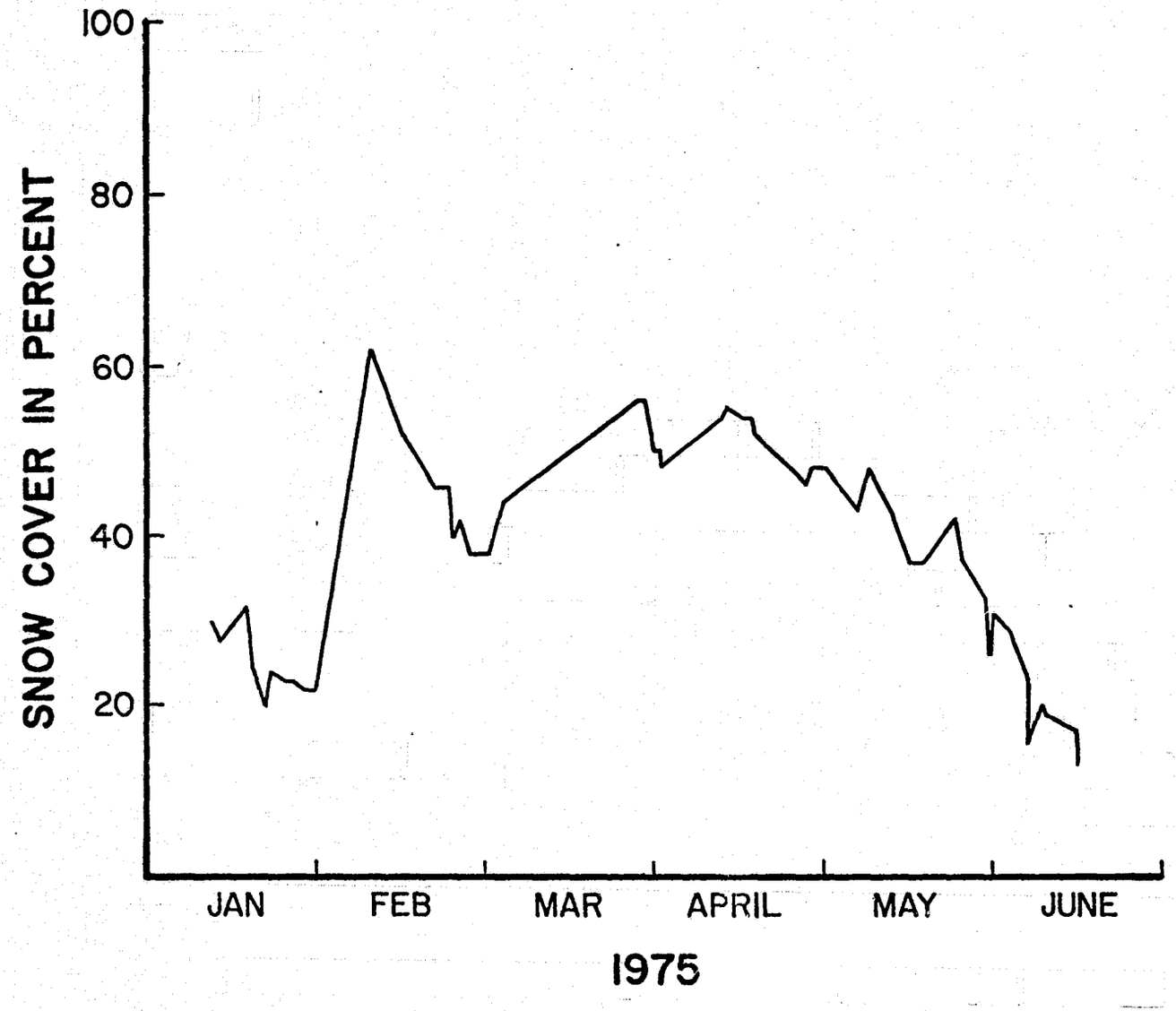



Figure 4. 1975 snow buildup and melt in the American River Basin from NOAA-4 VHRR data.

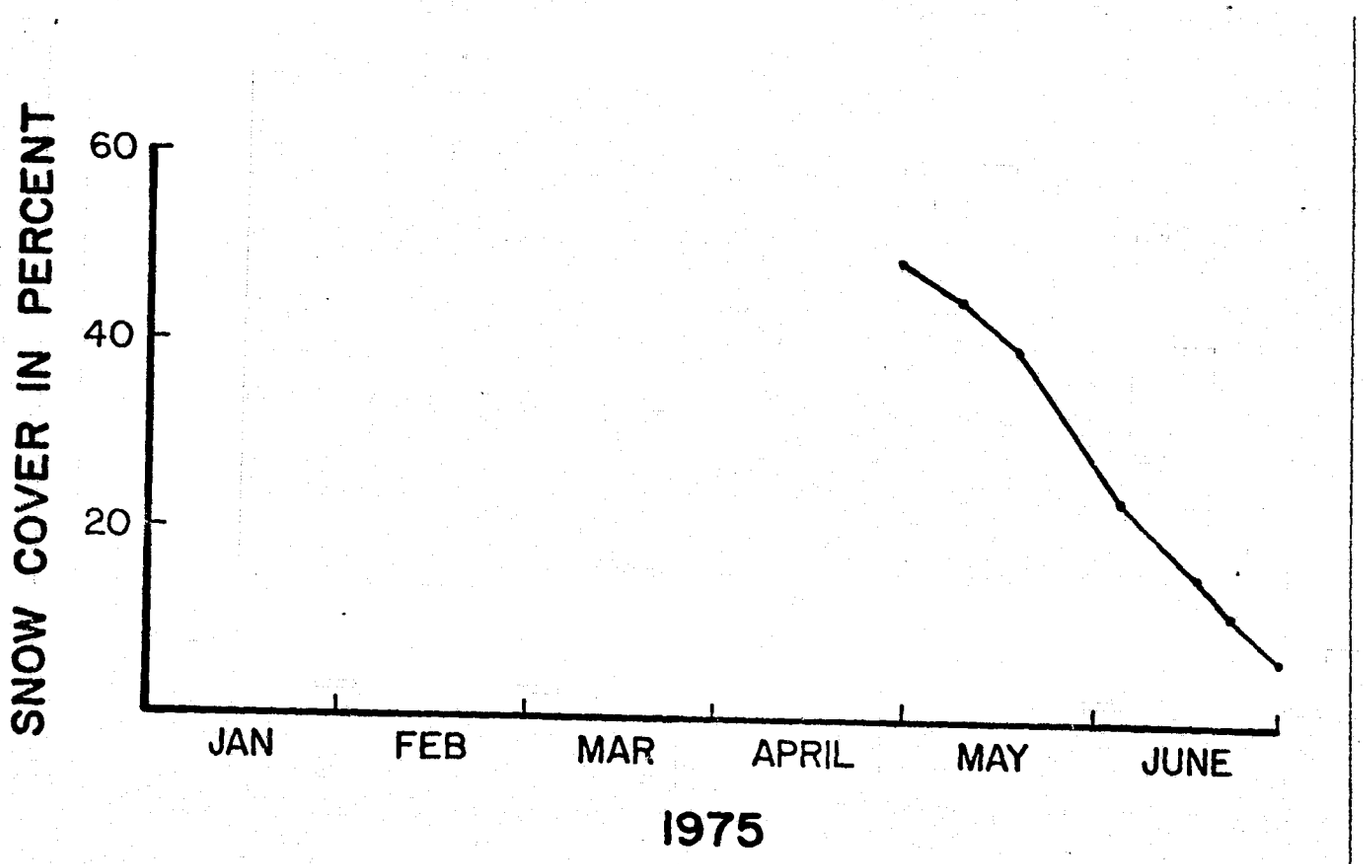



Figure 5. Areal snow extent in the American River Basin as determined by Environmental Products Branch/NESS from Landsat-1 and Landsat-2 MSS band-5 imagery.

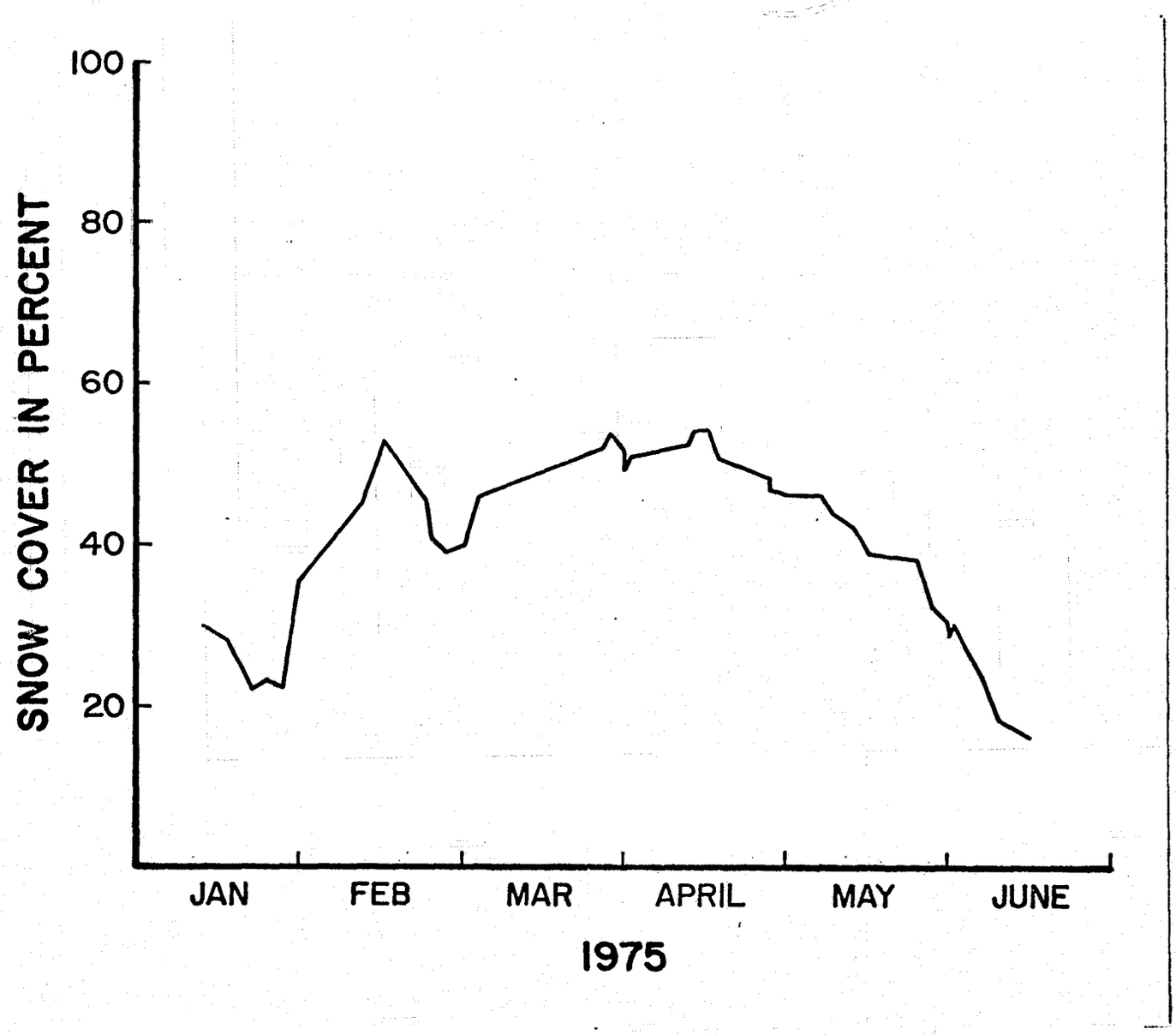



Figure 6. Three-day running mean of snow buildup and melt in the American River Basin from NOAA-4 VHRR data.

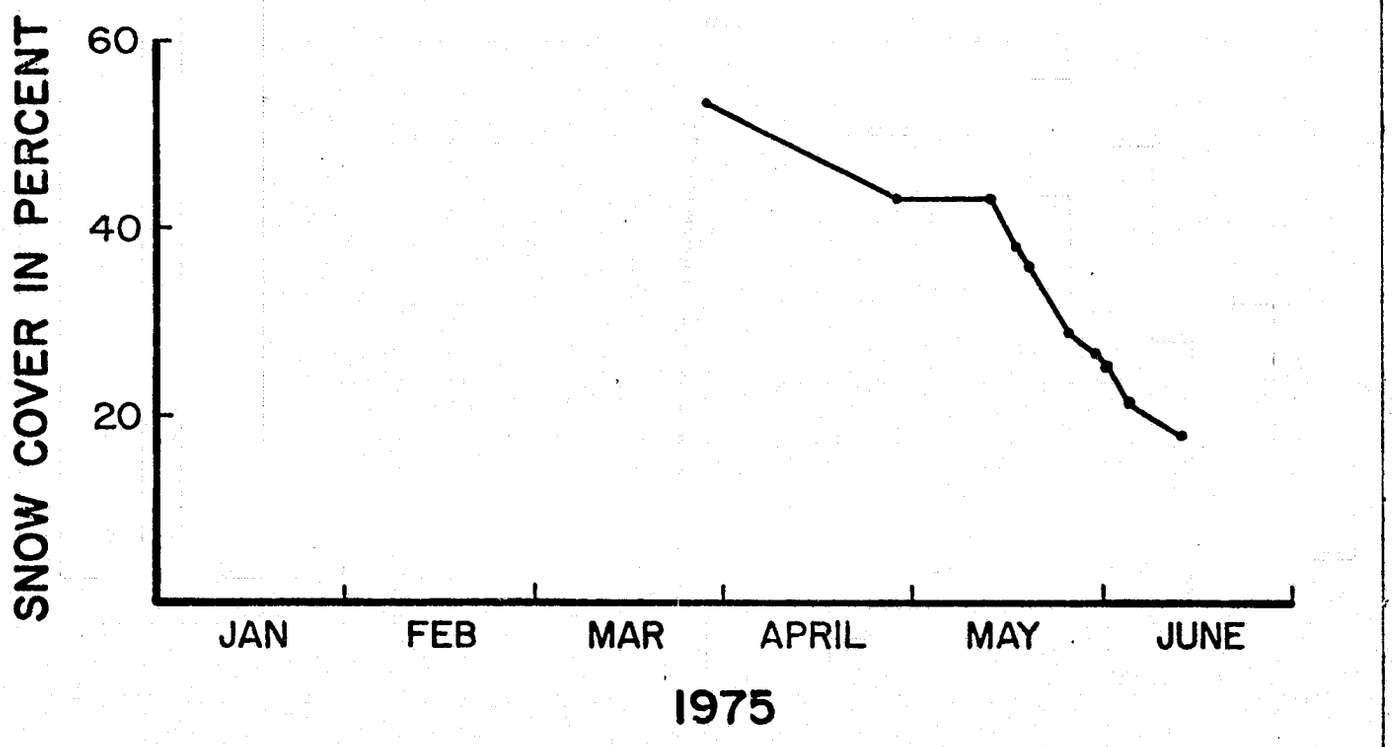



Figure 7. Areal snow extent in the American River Basin as determined from GOES-2 imagery.

blocked the movement of cyclonic storms into California. This figure is only 50% of the mean. Although the Blue Canyon weather station received 80% of normal precipitation in February, by 1 April the water equivalent of the snowpack in the American River was down to 32% of the mean. For the entire water year, the unimpaired runoff of the American River amounted to a scant 31% of the mean runoff. Table 1 shows the comparison of the water supply forecast with the observed flow. The difficulty of forecasting during extreme events such as prolonged drought is clearly evident here from the figures in the table.

Figure 8 shows the water equivalent of the snow at a high-altitude station. Note the steep dropoff to zero in mid-May, and the average dropoff, which reaches zero on 20 June.

4. The 1977 water year. The second drought year in a row plagued California. Runoff from the North Fork of the American River at North Fork Dam--an index station--was only 8% of median. The December monthly mean dischargeof 33.1 cfs and the daily mean of 29 cfs on 28 December were the lowest in 67 years of record. The drought was reportedly the worst in almost 100 years. In January the North Fork Dam station's monthly mean rose to 63.2 cfs which was still the lowest of record for the month in 36 years. Folsom Reservoir at month end was only 30% of normal maximum. The snowpack was far below the mean.

In February the snowpack increased slightly but streamflow remained below normal for the fourth consecutive month. The North Fork Dam gaging station recorded a monthly mean discharge of 77.2 cfs (6% of median), the lowest for the month in 36 years of record (see figure 9). Folsom Reservoir dropped to 27% of normal maximum.

In March the North Fork Dam gage recorded new low-flow records again.

Table 1. Observed and Forecast For the American River inflow to the Folsom Reservoir (in acre-feet x 1000) (based on data from California Department of Water Resources)

| Date | Forecast Period | Flow (cfs) | Observed Flow | Forecast Error |
|---|---|---|---|---|
| Feb. 1 | Apr-Jul | 420 | 312 | +35% |
| | Water yr. | 1,120 | 785 | +43% |
| Mar 1 | Apr-Jul | 485 | 312 | +55% |
| | Water yr. | 990 | 785 | +26% |
| Apr 1 | Apr-Jul | 300 | 312 | - 4% |
| | Water yr. | 755 | 785 | -10% |
| May 1 | Apr-Jul | 245 | 312 | -21% |
| | Water yr. | 700 | 785 | -11% |

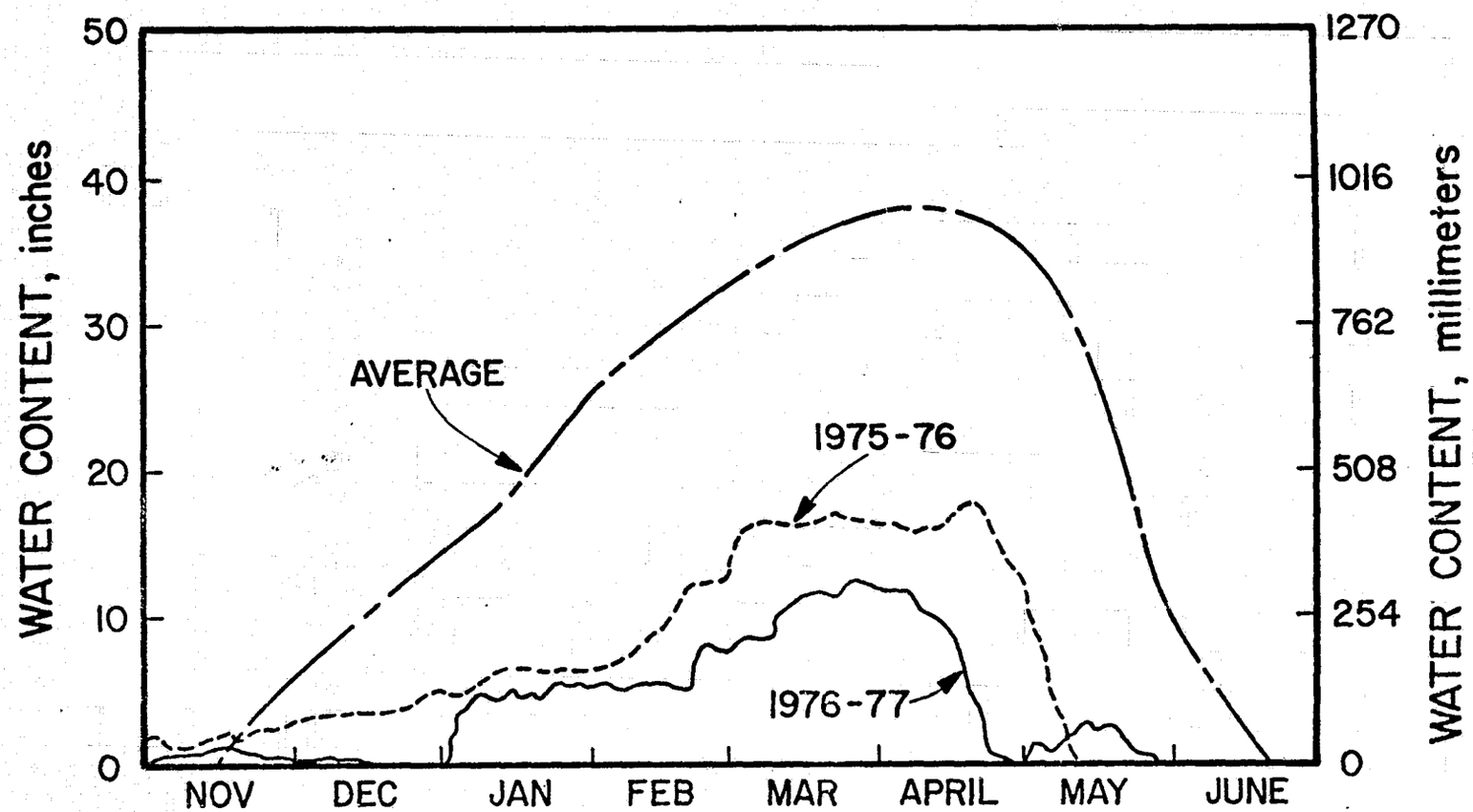



Figure 8. Water content of snow at Alpha (near Wrights Lake), elev. 7,600 ft. (2316 m), comparing 1975-76 and 1976-77 with average.

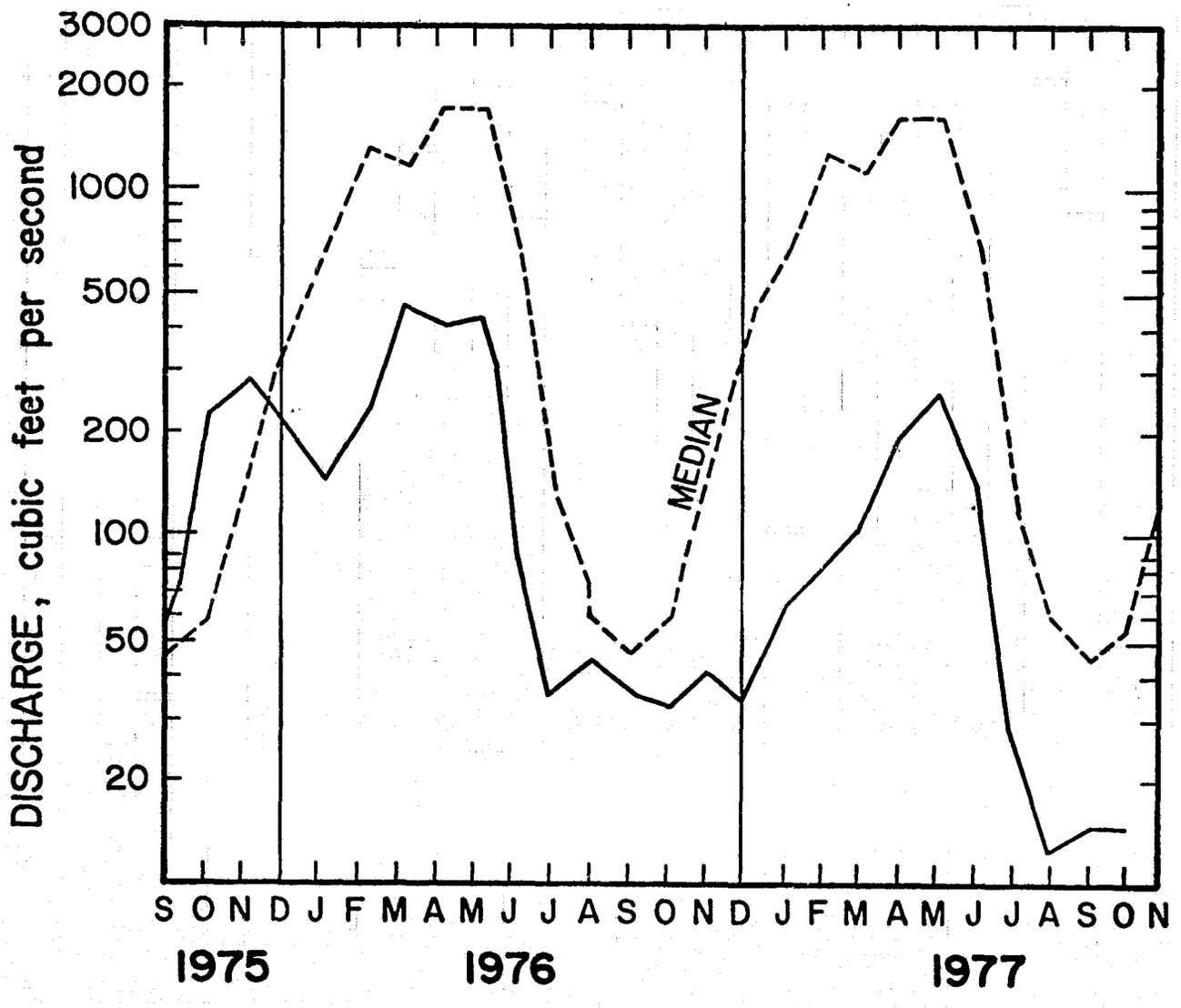



Figure 9. Monthly mean discharge of North Fork American River at North Fork Dam, Calif., for 1976 and 1977 water years.

The monthly mean of 109 cfs (9% of median) and the daily mean of 73 cfs on the 6th were the lowest for the month in 36 years of record. Folsom rose slightly to 29% of normal maximum.

In April new monthly lows were recorded. The month-end snowpack was far below normal (figure 8). Folsom reservoir was 30% of normal maximum. In May, the sixth consecutive monthly low flow record was set at North Fork Dam. Folsom Reservoir held at 30%. June was the ninth consecutive month of below-normal streamflow at North Fork Dam. Folsom dropped to 26% of normal maximum. As of 31 July, cumulative runoff for the first 10 months of the water year was only 12% of median! Folsom Reservoir continued to drop to 24% of normal maximum.

In August, the flow at North Fork Dam was 6 cfs less than the previous record low August mean (1931). The cumulative runoff for the first months of the water year was 12% of median. Folsom Reservoir was only 17% of normal maximum.

The monthly discharge of 14.7 cfs was the lowest of record for September, and the annual mean discharge was 88.4 cfs for the 1977 water year--the lowest of record.

5. Landsat MSS coverage and NOAA VHRR coverage. In 1975, during the snowmelt season, seven MSS measurements of basin snow extent were made (see Table 2). Only one pass was obscured by clouds. During the same period, 11 measurements were made using VHRR images, and 10 measurements were taken drom VISSR (GOES) images.

Figure 5 shows the snow-covered area depletion curve prepared from the Landsat MSS band 5 images. A simple regression of snowcover plotted as a function of Julian day yielded a parabolic correlation

TABLE 2

Landsat-derived snow extent measurements for the American River Basin, 1975.

| Satellite | Date | Percent Snowcover |
|---|---|---|
| Landsat-1 | 4/29/75 | 49 |
| Landsat-2 | 5/8/75 | 45 |
| Landsat-1 | 5/17/75 | 40 |
| Landsat-1 | 6/4/75 | 24 |
| Landsat-2 | 6/13/75 | 16 |
| Landsat-1 | 6/22/75 | 12 |
| Landsat-2 | 7/1/75 | 7 |

coefficient (r) of 0.99+ for the seven MSS measurements. Using 11 points measured from the VHRR, the same plot yielded an r of 0.97. Thus the use of Landsat snowcover data to forecast the date of snow-free conditions in the river basin is a distinct possibility. The major deterrant is the slow delivery of Landsat data to the user. The more timely delivery of NOAA VHRR-based SCA maps makes them a preferred source, at present.

6. GOES VISSR coverage. The NOAA satellite, GOES (Geostationary Operational Environmental Satellite), is useful for mapping snow by means of its Visible Infrared Spin Scan Radiometer (VISSR). The satellite system consists of two satellites over the equator, one at 75°W and the other at 135°W. The VISSR has a visible band (0.55-0.75μm) and a thermal IR band (10.5-12.5μm). Ground resolution of the visible band is roughly equivalent to the VHRR (1 km). The resolution decreases as the "look" angle increases; thus the far north (above 55°N) is not a suitable target for snow mapping. The oblique viewing angle also creates some panoramic distortion in the GOES images. Nevertheless the VISSR is capable of producing an image of the same area every 30 minutes, a feat no other satellite sensor performs. The advantages of VISSR data then are that it greatly increases the probability of securing a cloud-free image of a given river basin, and it permits multiple looks on a specific day, thereby revealing the effect of sun angle on snowcover detection and reflection.

A plot of 10 VISSR-derived measurements of snowcover are shown on figure 7. Snow-surface reflectance using the broadband VISSR is consistently less bright and less extensive owing to the near-IR shift of the VISSR spectral response curve (Schneider and McGinnis, 1977). The

reflectance of snow is greatly diminished in the near-IR as demonstrated by Strong et al. (1971), Wiesnet et al. (1974), and O'Brien and Munis (1975). Figure 10 demonstrates that the GOES VISSR consistently records less snow than Landsat MSS Band 5 and NOAA VHRR visible band.

In 10 measurements of the American River basin the VISSR read an average of 3.5% lower than corresponding VHRR values for the same day. The differences ranged from -1.5% to -6.5%.

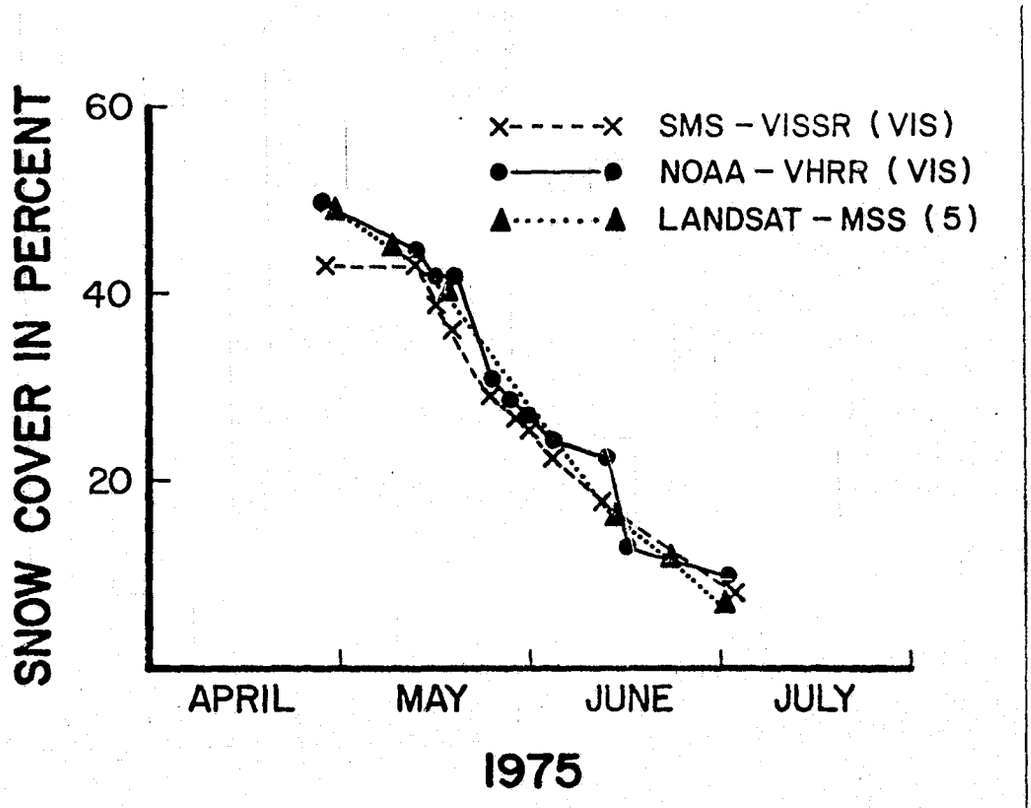



Figure 21. Comparison of SMS VISSR, NOAA VHRR, and Landsat MSS 5 sensors in mapping areal snow extent in the American River Basin for 1975.

Barnes, J.C., and Bowley, C.J., 1968, Operational Guide for Mapping Snow Cover from Satellite Photography, Allied Research Assoc., Inc., Concord, Mass., 116 pp.

Brown, A.J., 1975, Interpretation of Snowcover from Satellite Imagery for use in Water Supply Forecasts in the Sierra Nevada, in Rango, A., Ed., Operational Applications of Satellite Snowcover Observations, NASA SP-391, Washington, D.C., 430 pp.

Meier, M.J., 1975, Comparison of Different Methods for Estimating Snowcover in Forested, Mountainous Basins using Landsat (ERTS) Images, in Rango, A., Ed., 1975, Operational Applications of Satellite Snowcover Observations, NASA SP-391, pp. 215-234.

O'Brien, H.W. and Munis, R.H., 1975, Red and Near Infrared Reflectance of Snow, U.S. Army Cold Regions and Research Lab., USACRREL Research Rept. 332.

Rango, A., 1975, An overview of the Applications Systems Verification Test of Snowcover Mapping, in Rango, A., Ed., Operational Applications of Satellite Snowcover Observations, NASA SP-391, Washington, D.C., 430 pp.

Schneider, S.R., Wiesnet, D.R., and McMillan, M.C., 1976, River Basin Snow Mapping at the National Environmental Satellite Service, NOAA Tech. Memo. NESS 83, 19 pp.

Schneider, R., and McGinnis, D.F., Jr., 1977, Spectral Differences between VHRR and VISSR Data and their Impact on Environmental Studies, Proc. Amer. Soc. Photogramm., 43rd Ann. Mtg., Feb-Mar 1977, Washington, D.C., pp. 470-480.

Strong, A.E., McClain, E.P., McGinnis, D.F., Jr., 1971, Detection of Thawing Snow and Ice Packs through Combined use of Visible and Near-Infrared Measurements from Earth Satellites, Monthly Weather Review, Vol. 99, No. 11, pp. 828-830.

Wiesnet, D.R., 1974, The Role of Satellites in Snow and Ice Measurements, in Santeford, H.S., and Smith, J.L., Advanced Concepts and Techniques in the Study of Snow and Ice Resources, Nat. Acad. of Sciences, Washington, D.C., pp. 447-456.

Wiesnet, D.R., McGinnis, D.R., Jr., and McMillan, M.C., 1974, Evaluation of ERTS Data for Certain Hydrological Uses, Final Rept. to NASA/GSFC, Contract No. 432-641-14-04-03.

## Snowmelt in the American River Basin, California

### Introduction

Several studies (Wiesnet, et al., 1975, Thomas, et al., 1978) have attempted to derive various snowpack parameters using the multispectral approach available with Landsat MSS data. Early techniques using raw, uncorrected MSS reflectance counts (Wiesnet, et al., 1975) have been superseded by more sophisticated analyses that use computer programs (Thomas, et al., 1978). Results thus far are mostly preliminary, although measurement of snow extent has become routine and operational. Information concerning the density, moisture content, and the surface condition of the snowpack derived from MSS data is still speculative. In our attempt to extract information on snowpack variables from Landsat MSS computer compatible tapes (CCT's) of snow-covered scenes, the GE (General Electric) Image 100 Interactive Multispectral Image Analysis System was utilized.

### Description of the G.E. Image 100 System

The G.E. Image 100 Interactive Multispectral Image Analysis System (henceforth called the G.E. Image 100 in this report) is a user-oriented system designed for deriving useful information from remotely-acquired data, whether from satellites or aircraft. The G.E. Image 100 operates on the principle that all objects possess unique spectral characteristics or signatures. This signature uniqueness is used to "identify" similar features in an image by simultaneous analysis of signatures in multiple frequencies, such as the Landsat MSS. The G.E. Image 100 then assigns psuedo-colors or themes to those features having identical spectral characteristics. These themes may then be displayed on a color CRT, or super-imposed on the input image, or recorded.

Analysis of Landsat MSS Data

Landsat MSS CCT's for snowmelt periods during 1975 and 1976 were obtained for the portion of the Sierra Nevada that includes the American River basin. Snowpack extent during those two years differs widely. In 1975, the snowpack was normal to slightly above normal. 1976 was the third-driest winter since 1900. MSS CCT's were available for the dates given in Table 3. Only information from MSS bands 5 and 7 (0.6-0.7μm and 0.8-1.1μm, respectively) were utilized in the G.E. Image 100 analyses because of the atmospheric haze problem in MSS band 4 (0.5-0.6μm) and the preference of the longer near-IR wavelength/MSS band 7 in place of the narrow, often saturated, band 6 (0.7-0.8μm).

The analyses entailed reading the data from MSS band 5 and 7 into the G.E. Image 100 with a resultant color display of the American River basin in the composited bands on a cathode ray tube monitor contained on the Image Analyzer Console. Through interaction with the Graphics Display Terminal, a histogram was generated summing MSS band 5 and 7 response, pixel by pixel, in a bivariate graph, MSS band 5 as the ordinate and MSS band 7 as the abscissa. The pixels containing snow were grouped into three classifications as shown in Table 4. The ranges for each classification were selected by viewing the CRT display for various groupings of the bivariate MSS 5 and 7 pixel distribution and then "alarming" the Image Analyzer Console television monitor to note which pixels had been designated a given category. In general, the reflectance limits for both MSS bands varied only slightly from scene to scene for a particular classification. In retrospect, a constant set of limits could have been specified for the classification of all scenes. If this had been done,

TABLE 3. Dates of available Landsat CCT's covering American River basin, 1975 and 1976.

| 1975 | 1976 |
|---|---|
| 8 May | 14 April |
| 17 May | 23 April |
| 13 June | 20 May |
| 22 June | 29 May |
| 1 July | |

TABLE 4

RANGE OF REFLECTANCE IN ARBITRARY UNITS

FOR VARIOUS CLASSES OF SNOW

| Date of Scene | Fresh Snow | | Wet Snow | | Partial Snow | |
|---|---|---|---|---|---|---|
| | MSS-5 | MSS-7 | MSS-5 | MSS-7 | MSS-5 | MSS-7 |
| 5/8/75 | 96-127 | 44-63 | 127 | 16-43 | 72-127 | 16-43 |
| 5/17/75 | 89-127 | 44-63 | 127 | 15-43 | 70-126 | 15-43 |
| 6/13/75 | 96-127 | 45-63 | 127 | 16-44 | 84-126 | 16-44 |
| 6/22/75 | 96-127 | 44-63 | 127 | 13-43 | 86-127 | 13-43 |
| 7/1/75 | 96-127 | 45-63 | 127 | 16-44 | 86-127 | 16-44 |
| 4/14/76 | 91-127 | 44-63 | 127 | 16-46 | 66-125 | 16-46 |
| 4/23/76 | 92-127 | 45-63 | 127 | 19-44 | 72-127 | 19-44 |
| 5/20/76 | 88-127 | 44-63 | 127 | 17-43 | 88-126 | 17-43 |
| 5/29/76 | 115-127 | 45-63 | 127 | 22-44 | 85-126 | 22-44 |

certainly the number of pixels in a given classification would change, but not sufficiently to alter the proportion of snow type to total snowcover. Furthermore, fixed limits would not be affected by changes in class limits that may result from changes in sun elevation.

Images for the nine dates, with the three snow classifications are presented as Figs. 11a through 11i. These images were produced by a Dicomed processor and show high elevation snow as yellow, middle elevation snow as purple, and the low elevation snow as cyan. These three classifications are thought to represent fresh or nonmelting snow, melting snow, and partial snow cover, respectively. The remaining area contained within the American River basin, where vegetated, is reddish-brown; where bare rocks occur, the theme is gray. Gray pixels also seem to include some of the low elevation snow A comparison of the 8 May 1975 and 1 July 1975 images (Figs. 11a and 11e) reveals that large areas changed from gray to red-brown, i.e., from snow to vegetation. By July 1 the largest areas of gray are limited to the high elevations in the vicinity of the Sierra crest.

The percent of each snow type relative to the entire snow-covered area is provided in Table 5. Table 5 also compares computer-generated SCA to SCA obtained using conventional snowmapping procedures practiced in the NESS (Schneider, et al., 1975).

Comparison of the percentages of the three snow types reveals the lack of any consistent trend as snowmelt progresses. The percent of dry (yellow) snow decreases seasonally but erratically, with several reversals to larger percentages. Patterns for the categories of melting (purple) and partial (blue) snowcover are similarly erratic. These trends become more consistent, however, when the data are plotted separately

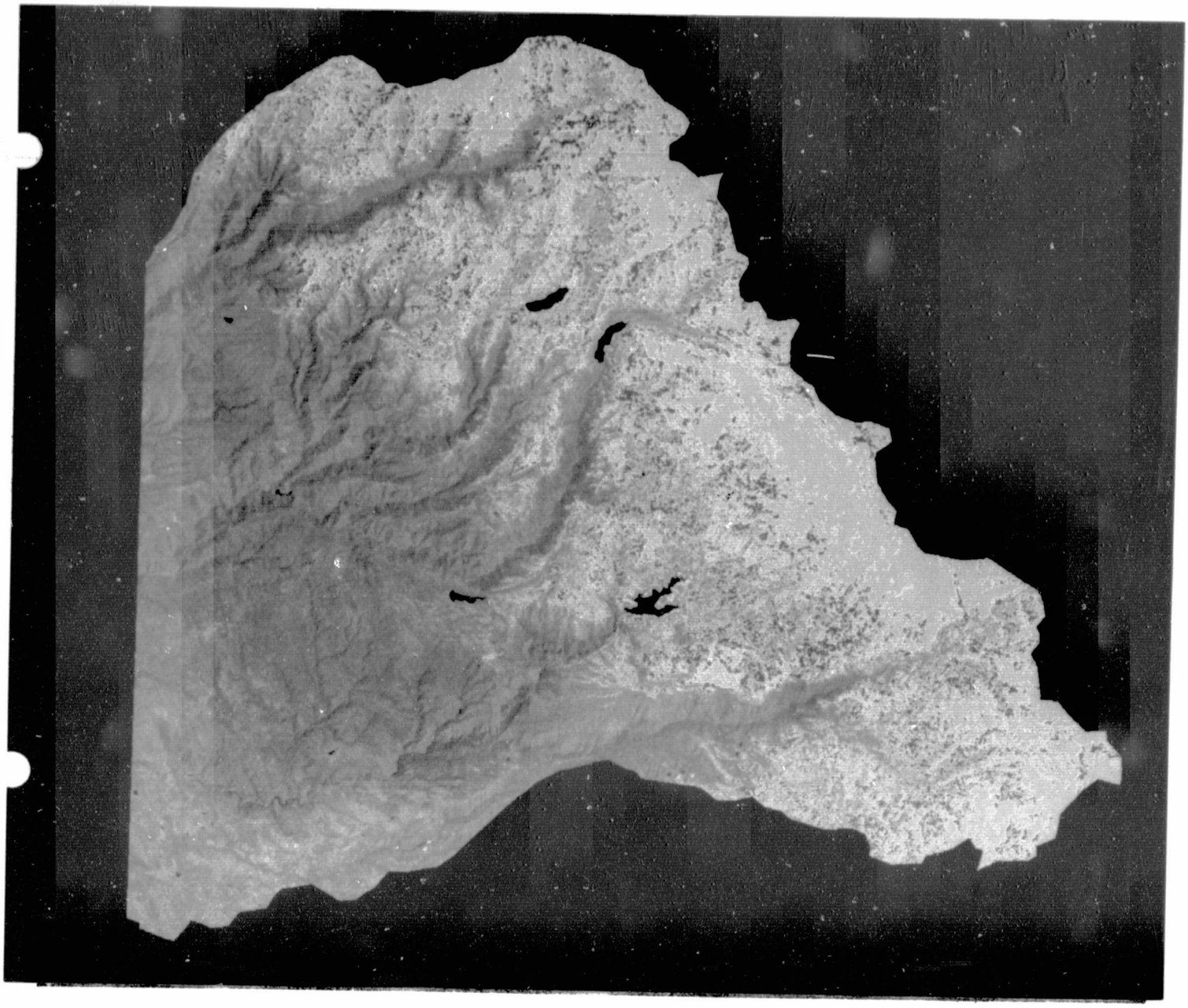


Fig. 11a. Computer-generated snow classification for 8 May 1975.

ORIGINAL PAGE IS
OF POOR QUALITY

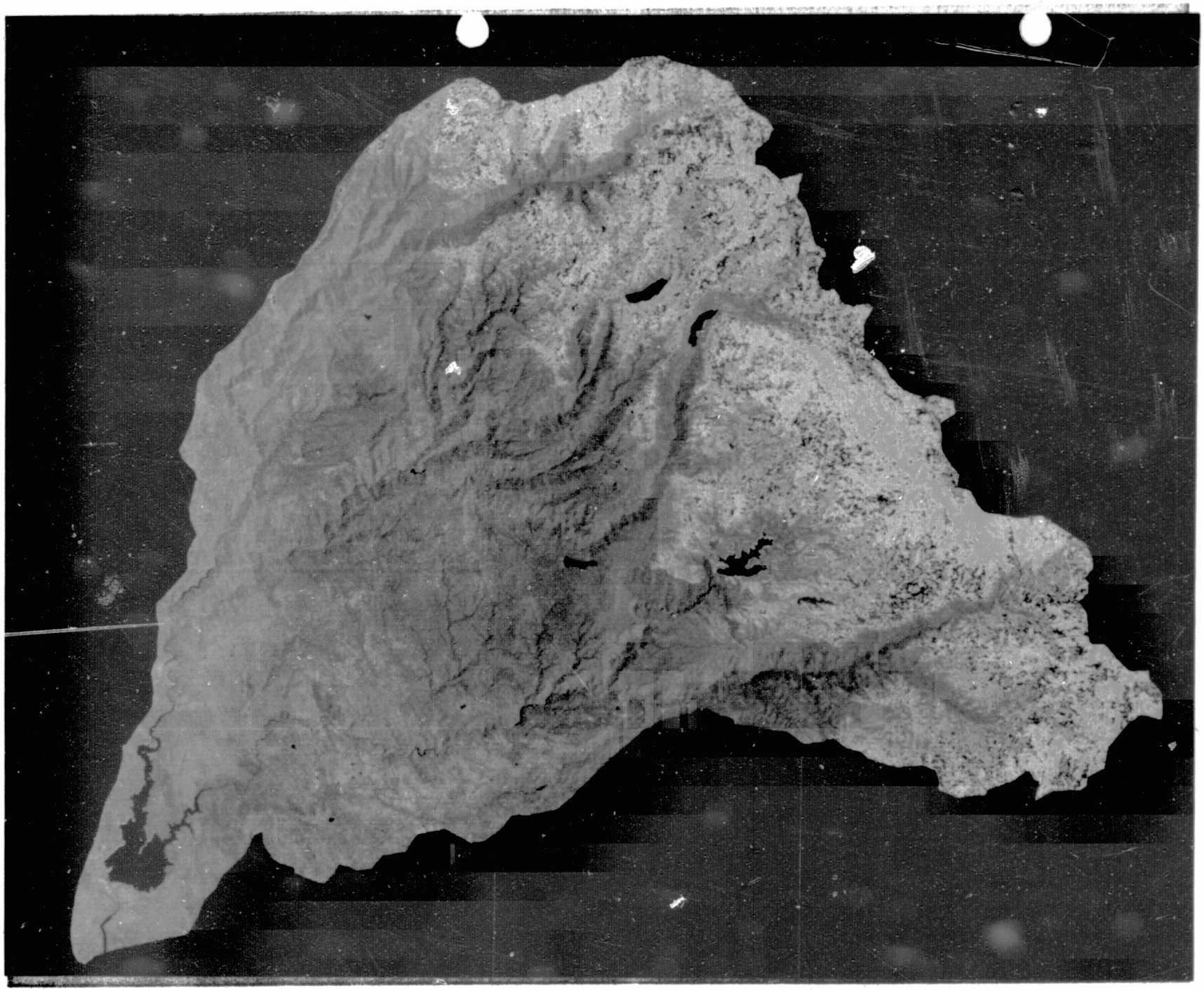


Fig. 11b. Computer-generated snow classification for 17 May 1975.



ORIGINAL PAGE IS
OF POOR QUALITY

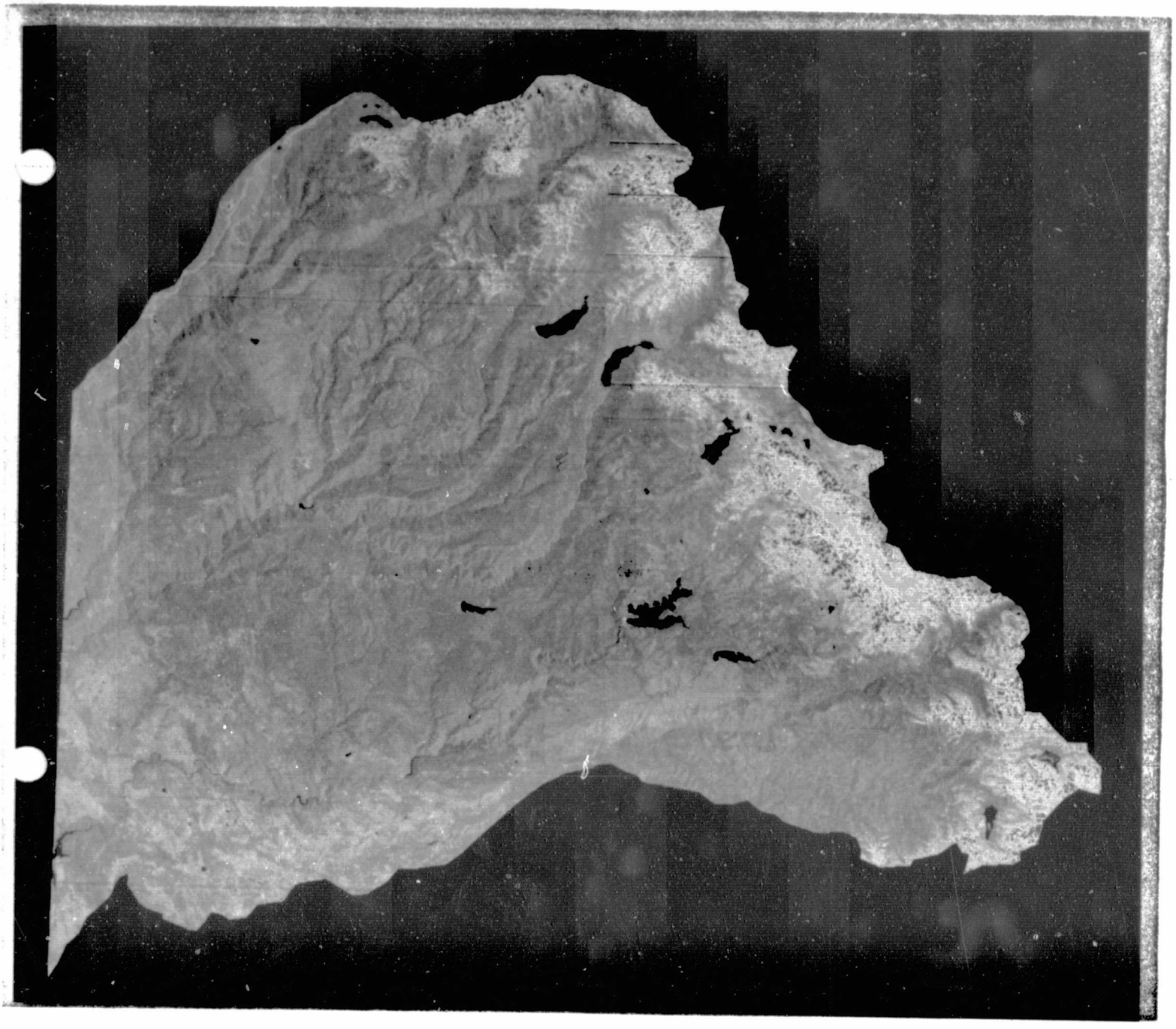


Fig. 11c. Computer-generated snow classification for 13 June 1975.

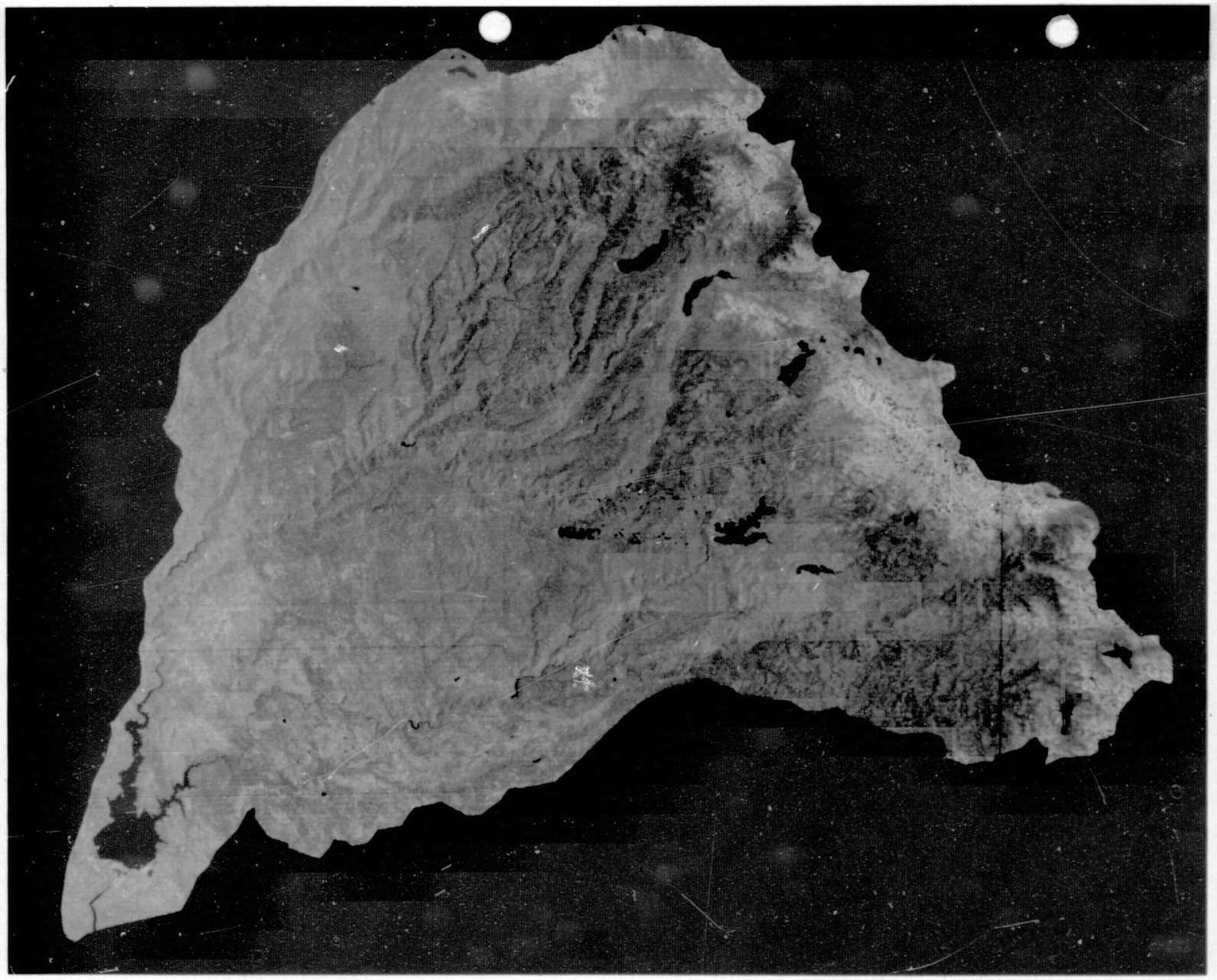


Fig. 11d. Computer-generated snow classification for 22 June 1975.

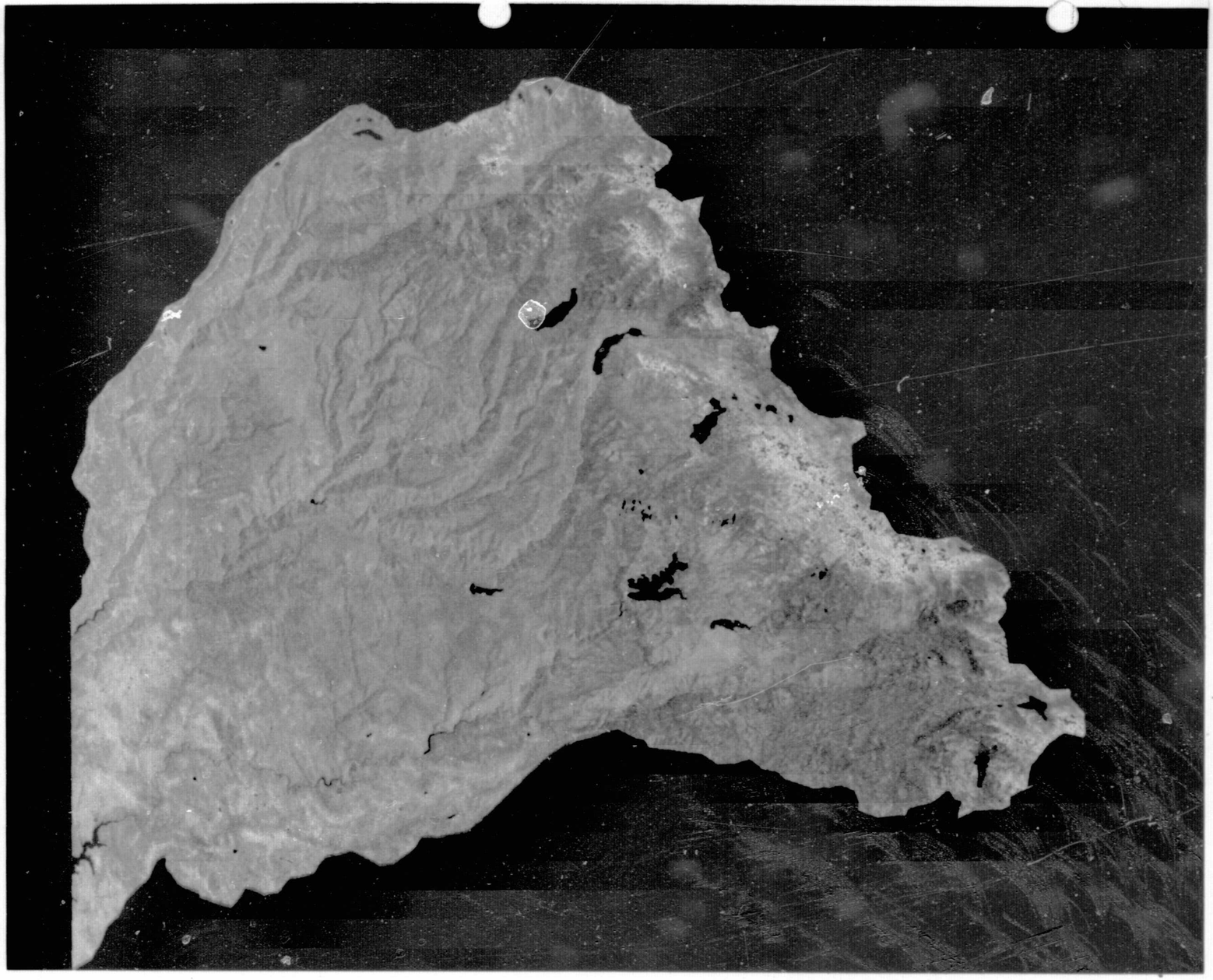


Fig. 11c. Computer-generated snow classification for 1 July 1975.

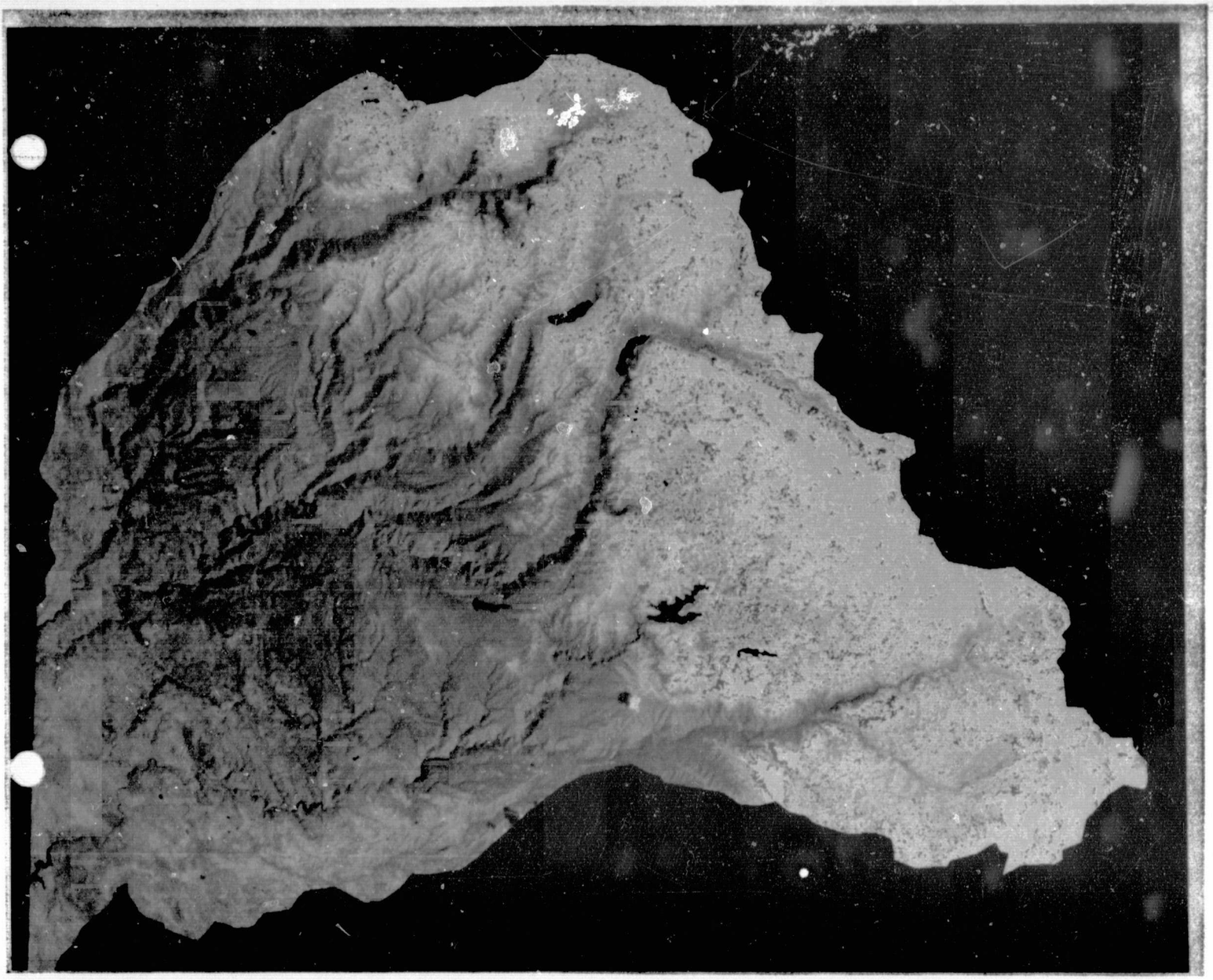


Fig. 11f. Computer-generated snow classification for 14 April 1976.

REPRODUCIBILITY OF THE
ORIGINAL PAGE IS POOR

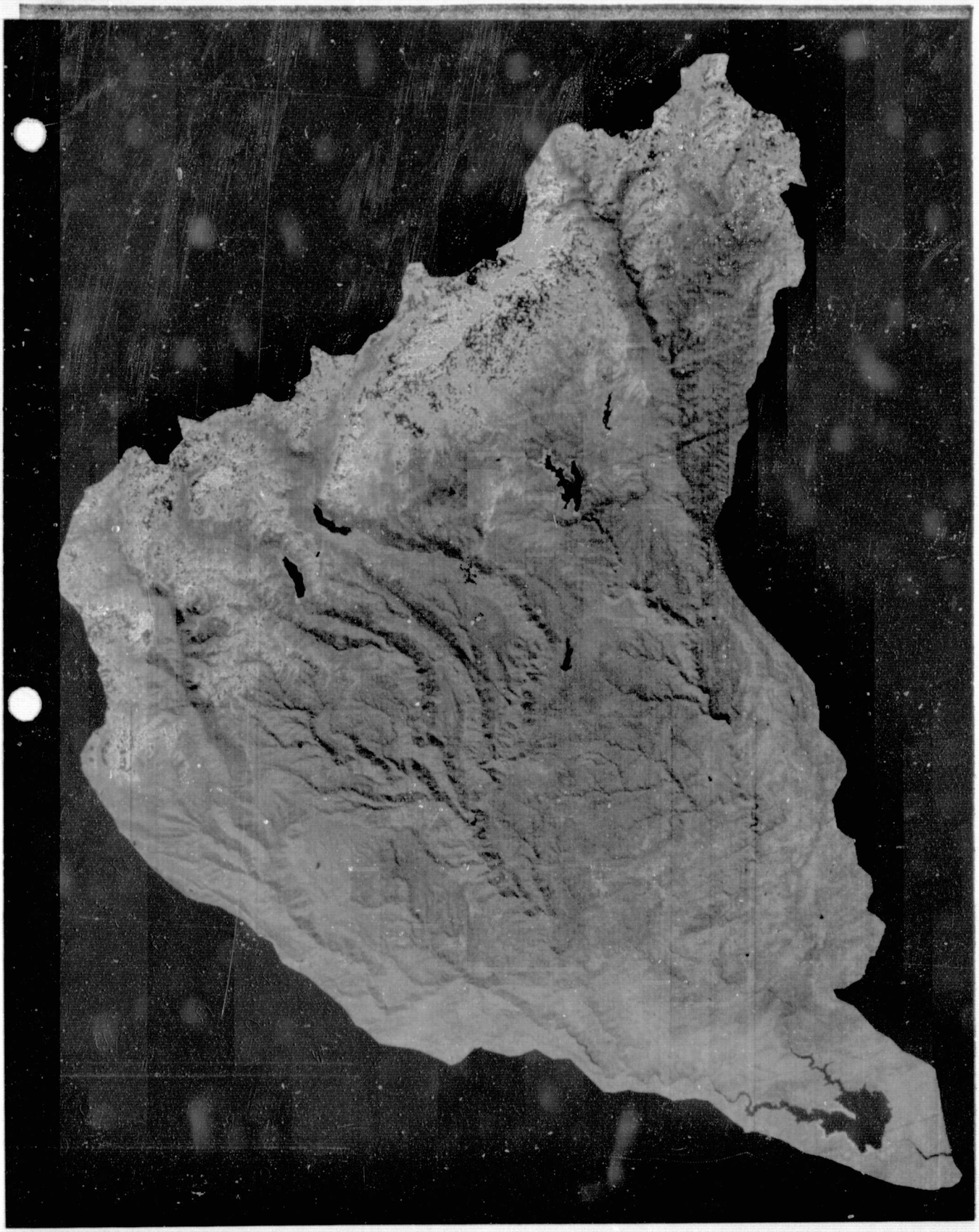


Fig. 11g Computer-generated snow classification for 23 April 1976.

REPRODUCIBILITY OF THE
ORIGINAL PAGE IS POOR

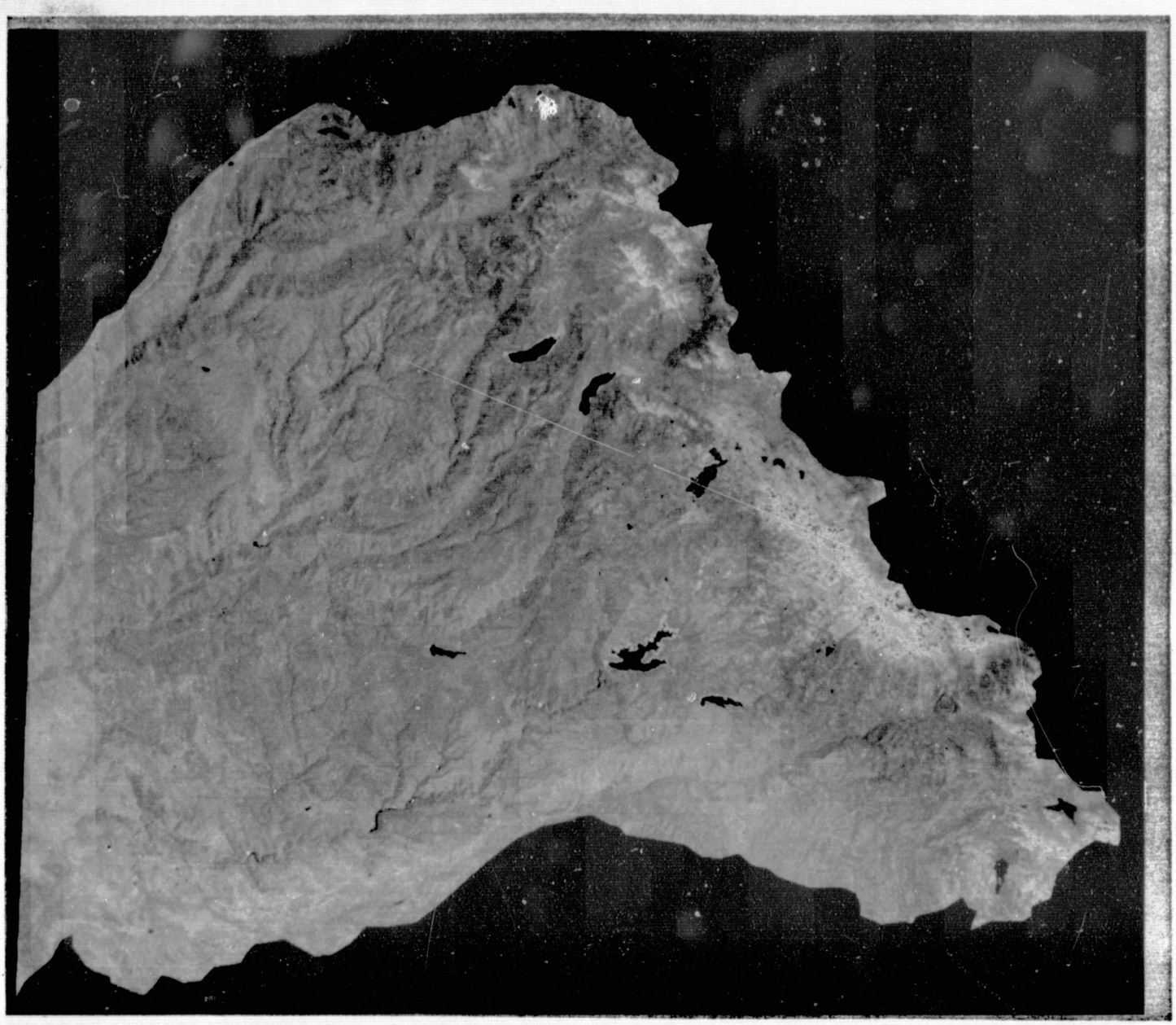


Fig. 11h. Computer-generated snow classification for 20 May 1976.

REPRODUCIBILITY OF THE
ORIGINAL PAGE IS POOR

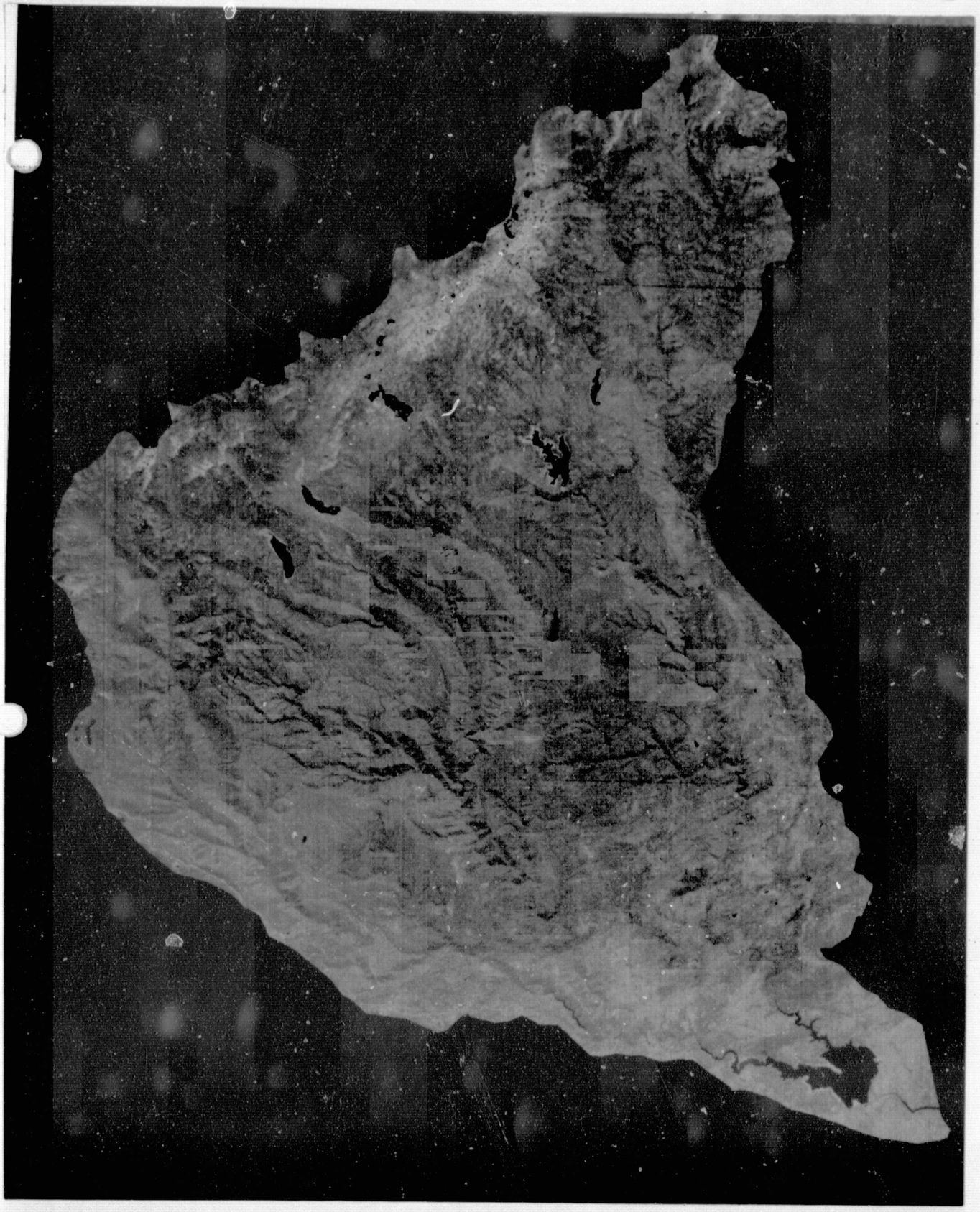


Fig. 11i. Computer-generated snow classification for 29 May 1976.

REPRODUCIBILITY OF THE
ORIGINAL PAGE IS POOR

Table 5. Comparison of Conventional Analysis vs. Computer-Generated Analysis and Breakdown of Snowcover by Class as Pe

| Date | Percent Snowcover Conventional Analysis (MSS-5) | Percent Snowcover Computed by G.E. Image 100 | Ratio GE 100/Conventional | Snowcover Breakdown by Type in Yellow | Purple |
|---|---|---|---|---|---|
| 8 May 1975 | 45 | 27 | 0.60 | 15 | 1 |
| 17 May 1975 | 40 | 20 | 0.50 | 7 | 3 |
| 13 Jun 1975 | 16 | 5 | 0.31 | 2 | <1 |
| 22 Jun 1975 | 12 | 2 | 0.17 | <1 | <1 |
| 1 Jul 1975 | 7 | 1 | 0.14 | <1 | <1 |
| 14 Apr 1976 | 41 | 21 | 0.51 | 13 | <1 |
| 23 Apr 1976 | 26 | 8 | 0.31 | 1 | 1 |
| 20 May 1976 | 7 | 1 | 0.14 | <1 | <1 |
| 29 May 1976 | 6 | <1 | 0.08 | <1 | <1 |



ORIGINAL PAGE IS OF POOR QUALITY

FOLDOUT FRAME

lysis vs. Computer-Generated Analysis and Breakdown of Snowcover by Class as Percent of Total Basin Area

| Percent Snowcover ted by G.E. Image 100 | Ratio GE 100/Conventional | Snowcover Breakdown by Type in Percent of Basin Yellow | Purple | Cyan |
|---|---|---|---|---|
| 27 | 0.60 | 15 | 1 | 11 |
| 20 | 0.50 | 7 | 3 | 10 |
| 5 | 0.31 | 2 | <1 | 3 |
| 2 | 0.17 | <1 | <1 | 1 |
| 1 | 0.14 | <1 | <1 | <1 |
| 21 | 0.51 | 13 | <1 | 8 |
| 8 | 0.31 | 1 | 1 | 5 |
| 1 | 0.14 | <1 | <1 | <1 |
| <1 | 0.08 | <1 | <1 | <1 |

2 [illegible]

by satellite, suggesting that sensor differences may exist between the MSS on Landsat-1 and the MSS on Landsat-2. Such differences would affect reflectance limits for a given snow classification and, possibly, to significant changes in the number of pixels placed in a given snow classification.

Another problem is the omission of the contribution that gray pixels make to the total snowcover Early in the snowmelt season when snow-free bare rock is at a minimum, most gray pixels appear to represent low elevation snow and should be included in the total pixel count for snow. However, inclusion of gray pixels as representative of snow in the late melt season would erroneously inflate the SCA, since most of these pixels would be representing bare rock rather than snow. It appears that the combination of MSS bands 5 and 7 is insufficient to differentiate between low-elevation snow and bare rock--at least for the American River basin. Inclusion of the percent of gray pixels in the American River basin would not solve the dilemma of fluctuation noted in Table 5.

Surface Data

A. Precipitation

During the 1975 snowmelt period of May and June only light amounts of snow fell. The heaviest snowfall, 13 cm, occurred on 20 May at Twin Lakes (2386 m) in the southeast corner of the American River basin. All snowfalls occurred between Landsat overpasses and were melted before the subsequent satellite view of the basin. Non-snow precipitation (rain) was limited to the first week of May and to 24 June with generally less than 0.5 cm of rain occurring sporadically. Thus the

timing of precipitation events neither affected the retreat of the snowline nor increased the surface reflectivity of the snow when examined by the MSS.

Snowfall occurred on 14 April 1976 the same day as one of the Landsat overpasses. There is some cloud contamination in the southeast portion of the image (Figure 11f), but a check of the NOAA-4 VHRR IR image (taken at approximately the same time as Landsat) failed to provide any information as to location or extent of the clouds. Evidently the clouds were low-level cumulus producing scattered, but at times, intense snow showers. One isolated cloud is readily apparent in the south-central portion of Figure 11f, having a similar theme as the snow. Another cloud can be found within the snowpack, located near the east-central edge of the basin boundary. Though the cloud itself is not separable from the surrounding snow, the shadow stands out as an island of gray and blue in a sea of yellow. Other clouds if present over the snowpack must be small, not casting discernable shadows. The overall cloud effect on the data displayed in Table 5 is thought to be small.

Except for the 14 April 1976 case, no occasional snowfalls are known. No precipitation effects in snow surface reflectance are noted for the remaining dates.

B. Temperature

Only eight stations in or adjacent to the American River basin report maximum and minimum temperatures to the National Climatic Center of EDS. One of these stations, Blue Canyon WSO airport, acquires temperatures every hour. Unfortunately Blue Canyon is not representative of stations in the high Sierra, having minimum temperatures 5-15$^{o}$C

higher than other American River basin locations. Maximum temperatures are quite similar for all stations, including Blue Canyon. Elevations of the stations ranged from 1572 m (5156 ft) to 2386 m (7829 ft).

For Blue Canyon, 1800 GMT temperatures (within 15 minutes of the Landsat overpass) average only 2.5°C less than the daily maximum, ranging from 0.5 to 4.0°C below the maximum ambient temperature. It is not known whether these 1800 GMT temperatures at Blue Canyon are representative of the temperatures at other areas in the American River basin for the same time. Copies of monthly thermographs for Twin Lakes, California, obtained from the Pacific Gas and Electric Company showed the 1800 GMT temperatures for the nine dates of Landsat coverage had climbed to 88 percent of the total diurnal rise in temperature. Temperatures at Blue Canyon averaged 78 percent of the diurnal rise by 1800 GMT (1000 local)--perhaps a lower figure than all other stations in the American River basin. Thus an assumption of 80 percent of the diurnal rise by 1800 GMT for Sierra stations appears conservative and acceptable for this study. These estimated 1800 GMT temperatures (i.e., minimum + 0.80 (maximum-minimum)) are presented in Table 6. No temperatures for any of the nine dates are known to be subfreezing during acquisition of the Landsat data. In fact, only on 14 April 1976 are temperatures consistently estimated to be less than 5°C at 1800 GMT.

Ancillary temperature data were obtained from Dr. James Smith of the USDA Forest Service and Mr. Barney Clorety of the Sacramento Municipal Utility District (Table 6). Similarly these data indicate subfreezing temperatures at 1800 GMT only on 14 April 1976 and then only above 2316 m. Upper air temperatures for 850 mb (1463 m) and 700 mb

TABLE 6. Estimated Surface and Upper Air Temperatures at or near Time of Landsat Overpass, in Degrees C.

| STATION | ELEVATION Meters | ELEVATION Feet | 1975 8 May | 1975 17 May | 1975 13 June | 1975 22 June | 1975 1 July | 1976 14 April | 1976 23 April | 1976 20 May | 1976 29 May |
|---|---|---|---|---|---|---|---|---|---|---|---|
| Blue Canyon WSO | 1609 | 5280 | 11.7* | 21.7* | 27.8* | 19.4* | 15.6* | 7.8* | 7.8* | 17.8* | 15.6* |
| Donner Mem. St. Pk. | 1810 | 5937 | 11.8 | 15.6 | 23.1 | 17.5 | 15.6 | 4.4 | 9.5 | 14.0 | 13.7 |
| Lake Spaulding | 1572 | 5156 | 12.7 | 19.9 | 26.8 | 20.1 | 16.8 | - | 14.9 | 17.2 | 12.8 |
| Squaw Valley | 1900 | 6235 | 10.7 | 14.4 | 23.4 | 18.1 | 16.7 | - | - | - | - |
| Tahoe City | 1899 | 6230 | 9.3 | 12.8 | 20.9 | 16.0 | - | 2.4 | 7.1 | 13.6 | 15.3 |
| Tahoe Valley FAA AP | 1906 | 6254 | 9.6 | 16.0 | 21.1 | 18.5 | 15.5 | 6.2 | 12.5 | 13.3 | 14.5 |
| Truckee R.S. | 1827 | 5995 | - | - | - | - | - | 4.5 | 9.2 | 13.6 | 17.1 |
| Twin Lakes | 2386 | 7829 | 8.6 | 19.1 | 19.6 | 13.4 | 11.9 | 4.8 | 8.6 | 10.9 | 9.8 |
| SMUD 1** | 1554 | 5100 | 18.6 | 25.2 | 31.2 | 24.7 | - | 12.7 | 14.3 | 22.0 | 19.3 |
| SMUD 2 | 1798 | 5900 | 16.2 | 21.9 | 30.2 | 21.3 | 18.5 | 8.3 | 16.3 | 18.3 | 17.0 |
| SMUD 3 | 2042 | 6700 | 13.0 | 19.8 | 25.7 | 17.6 | 13.6 | 7.3 | 15.3 | 16.8 | 15.3 |
| SMUD 4 | 2316 | 7600 | 10.6 | 14.9 | 20.6 | 16.0 | 11.1 | 0.6 | 9.3 | 10.9 | 11.0 |
| SMUD 5 | 2408 | 7900 | 14.9 | - | 26.5 | 19.8 | 19.8 | 2.0 | 12.9 | 14.2 | 13.5 |
| SMUD 6 | 2682 | 8800 | - | 18.8 | 22.6 | 16.4 | 16.4 | 0.5 | 14.5 | 12.6 | 12.5 |
| USDA CSSL | 2103 | 6900 | 12.7* | 16.6* | 21.7* | 16.8* | 13.4* | 4.9* | 11.7* | 12.2* | 12.2* |
| 850 mb | 1463 | 4800 | 13.3 | 16.0 | 26.3 | 19.3 | 14.3 | 5.0 | 11.3 | 12.8 | 13.8 |
| 700 mb | 3002 | 9850 | 1.0 | 6.0 | 10.8 | 7.0 | 5.0 | -6.5 | 0.3 | 3.0 | 2.8 |

* Actual 1800 GMT Temperature, Not Estimated.

**SMUD: Sacramento Municipal Unility District.

(3002 m) yield a similar finding (Table 6). Thus it is likely that even at the Sierra crest (above 3050 m) the snow was melting during each Landsat overpass with the single possible exception of 14 April 1976.

Comparison of Areal Snow Extent: Conventional vs. G.E. Image 100 Zoom

Areal snow extent as measured by Zoom Transfer Scope (ZTS) or by computer via the G.E. Image 100, decreases seasonally as expected. However, the decrease in snow extent is more precipitous in the computer-derived values. The ratio of SCA via the G.E. Image 100 to the SCA via the conventional NESS methods varies from 0.6 for 8 May 1975 to 0.08 for 29 May 1976. A close inspection of the Dicomed photographs provides at least one reason for part of the apparent rapid decrease in snowcover. Early during the spring melt (17 May 1975) the snowcover is more continuous, particularly at the high elevations (yellow) but becomes noticeably less continuous in the lowest elevation (cyan). As the area of "nonmelting" snow decreases, the area of "discontinuous" snow grows. Thus near the end of the snowmelt season, only few patches of "continuous" snow remain. The G.E. Image 100 system tallies snowcover pixel by pixel, and is not concerned with the continuous snowline. The experienced snowmapper draws an enveloping, smooth continuous line, containing the SCA, but does not analyzing for the the individual discontinuities. Two conventional snow-cover analyses are shown in Figures 12a and 12b, and were completed using the Dicomed photographs for (solid lines) 17 May and 22 June 1975. Conventional snow-cover maps using standard 1:1,000,000 MSS band-5 images are shown in Figures 13a (17 May 1975) and 13b (22 June 1975) and have been added to Figures 12a and 12b (dashed lines) to facilitate comparison. SCA for 17 May 1975 was 40 percent and 33 percent, respectively, for conventional vs. Dicomed (Fig. 13 vs. 12a) and for 22 June 1975 were 12 percent

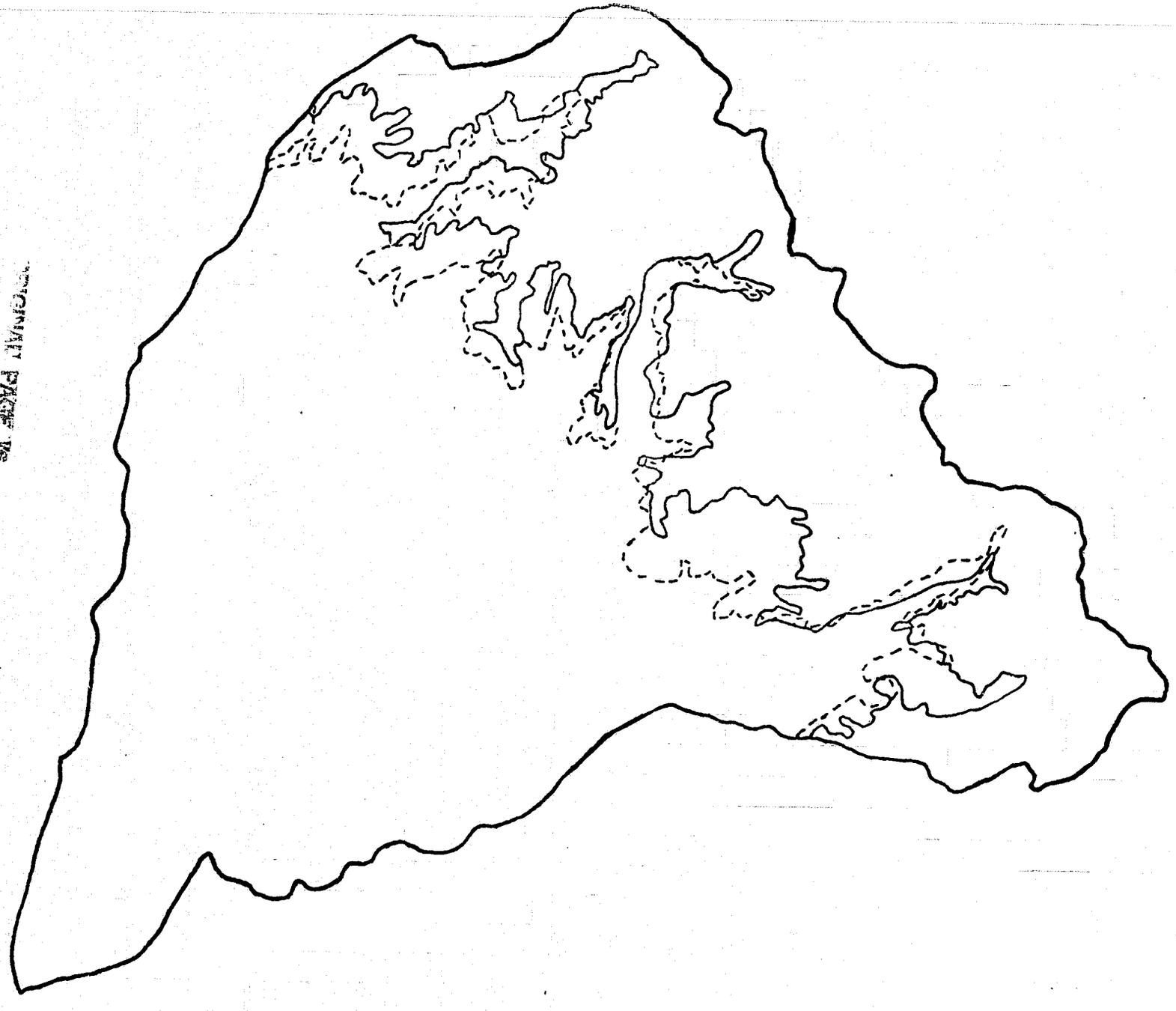


Figure 12a. Comparison of SCA as derived from Fig. 11b (solid line) with conventionally-derived SCA shown in Fig. 13a (dashed line) for 17 May 1975.



Figure 12b. Comparison of SCA as determined from Fig. 11d (solid line) with conventionally-derived SCA shown in Fig. 13b for 22 June 1975.



Figure 13a. Conventional SCA map for 17 May 1975.

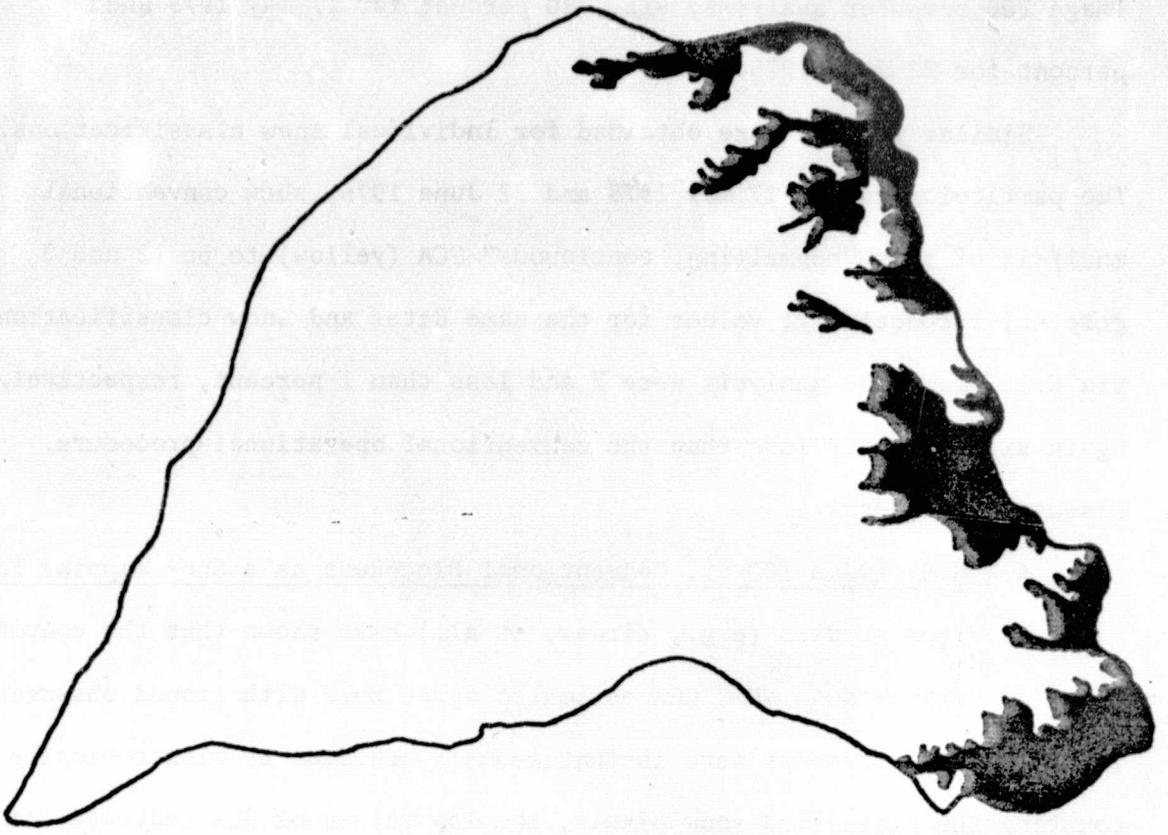


Figure 13b. Conventional SCA map for 22 June 1975.

and 9 percent, respectively, for conventional vs. Dicomed (Fig. 13b) vs. 12b). All SCA values are well above the amounts achieved by G.E. Image 100 computer analyses, viz., 20 percent for 17 May 1975 and 2 percent for 22 June 1975.

Similar results were obtained for individual snow classifications. Two particular cases, 17 May 1975 and 22 June 1976, show conventional analysis of this "nonmelting, continuous" SCA (yellow) to be 12 and 2 percent, respectively; values for the same dates and snow classification via G.E. Image 100 analysis were 7 and less than 1 percent, respectively--again significantly less than the conventional operational procedure.

Discussion of Results

A. G.E. Image 100 vs. Conventional Procedure as a Snow Mapping Tool

Previous studies (e.g., Kirdar, et al.) have shown that the conventionally derived NOAA NESS SCA estimates agree well with ground observations. Though SCA measurements were instantaneously achieved by electronically counting the classified snow pixels, the low values of SCA indicate the apparent difficulty of the G.E. Image 100 to properly define the various themes representing snow-covered area as reviewed by the MSS of Landsat. Most likely the discontinuous snow (blue) is located in a mixture of coniferous forests and open areas, common throughout the Sierra Nevadas. The snow quickly melts from the trees, but often remains as deep as 2 meters on the ground Unfortunately the forest partially obscures the Landsat MSS view of the snow-covered ground beneath.

Another possibility for the observed differences in the two procedures used to calculate SCA could occur from the greater detail in area measurement obtained through the multispectral analysis. There are snow-free areas within the snowpack which are too numerous and too minute to measure accurately with a compensating planimeter, but these small

melt areas or wind blown areas can be detected and tallied with the automatic planimeter function of the G.E. Image 100.

Whatever the cause of the observed differences in the two techniques to map and measure snow, snow mapping is apparently best viewed synoptically using 1:1,000,000 MSS 5 images rather than the pixel by pixel (80-meter resolution) procedure followed by the G.E. Image 100. The NESS operational snow mapping program described by Schneider, et al. (1975) has proved its usefulness as attested in communication received by real-time users of NESS-derived SCA values. For the present, manually prepared snow maps and resultant SCA values are timely and cost effective. Digital snow mapping using GOES data in near-real time is being done for six basins located in or near the Sierra Nevada, including the American River basin (Tarpley, et al., in press). Plans to expand the procedure to the remaining NESS basins are under consideration. Even if the G.E. Image 100 system produced equivalent snow maps matching those done by the conventional procedure, the technique would be more time-consuming (one must wait for CCT's) and costlier.

would be more time-consuming and costlier.

B. Snow Classification using the G.E. Image 100

Surface air temperature, interpolated to the time of Landsat overpass, and upper air analyses indicate that the entire snowpack was melting at 1800 GMT for all dates, with the possible exception of 14 April 1976. On this date the freezing level may have been slightly lower than the 3050 m crest of the Sierras. The snowpack differences shown in the Dicomed (colored) images cannot then be attributed to melting or non-melting snow. Rather the colors are more likely representative of the number of hours of above-freezing temperatures the snow has encountered or the frequency of freeze-thaw cycles. Both of these parameters directly effect the grain size of the snow and thus the reflectivity of the snowpack (O'Brien and Munis, 1975).

A second factor affecting measured MSS reflectances involves land cover classification. The predominent land cover at elevations where snow exists ranges from Ponderosa pine at the lower elevations, and fir and spruce in middle elevations, to Lodge-pole pine at the highest elevations. In the middle and upper elevations near and along the Sierra crest, large areas of sparse vegetation and bare rock predominate. In this region the Image 100 performs adequately, distinguishing snow from rocks when the snowline lies above 1800 m (5905 ft). At lower elevations early in the snowmelt season (see Figures 11a-c; 11f-g), the classification scheme used omits the lowest elevation snowcover by categorizing the snow as bare rock. The effect of snow on Ponderosa pine, fir, and spruce evidently results, at Landsat resolution, in a land use pattern that appears so similar to bare rock that the combined information in MSS bands 5 and 7 is insufficient to differentiate between

snow and bare rock. Information contained in MSS bands 4 and 6 would not aid in the separation of snow from bare rock and thus the problem must remain unresolved using the present MSS system.

Clouds appear similar to snow (see Fig. 11f) probably because of the low saturation level in band 5. Cloud shadows over the snowpack are classified as bare rock (see Fig. 11f, 14 April 1976). Snow classification images from the drought year of 1976 wrongly identify the bare, dried peripheries of the reservoirs exposed by low water levels as bare rock.

An interesting observation is the limited amount of snow classified as "melting snow" (i.e., purple) in figures 11a-i. Most of the snow classified as "partial cover" (i.e., cyan) should probably be placed in the "melting" snow category as well, especially as most of the partial-cover snow lies at lower elevations than the "melting" snow (purple). The 8 May 1975 image (Figure 11a) is a good example. Ice House Reservoir at elevation 1657 m (5437 ft), located southeast of the largest ice-free reservoir (Union Valley Reservoir) in the American River basin, appears purple or classified as "melting" snow in its east and west ends. For a pixel to be so classified the snow must saturate MSS band 5 and yet be a much lower reflector in MSS band 7 (reflectance not to exceed 44 on an arbitrary scale of 0 to 63). Areas that are cyan maintain an identical range in MSS band 7 but are permitted to have MSS band 5 values as low as 70 on a scale of 1 to 127. Based on the range of MSS band 5 and 7 values for each classification and knowing that temperatures were above freezing everywhere in the basin at the time of the satellite overpass, it appears to be more appropriate to classify purple snow as middle metamorphosed snow and cyan snow as late

metamorphosed snow (or initially melting and actively melting snow, respectively). Yellow snow would be better labeled early metamorphosed snow rather than fresh snow since the date of last snowfall may have occurred several weeks prior to the satellite overpass. These classifications are purely arbitrary and without sufficient ground truth cannot be substantiated. However, these classifications appear to be more realistic than the ones proposed earlier in this section.

The apparent reason for the small number of pixels colored purple is the result of only one value being acceptable for MSS band 5, viz., 127 or saturation. This restriction permits only 31 possible combinations of MSS band 5 and 7 reflectances for the purple snow category. Possible combinations for yellow and cyan snow are 780 and 1,922, respectively, or 25 and 62 times as many opportunities to have a yellow or blue pixel than one that is purple. Table 7 presents the ratios of snow classified as "Yellow" and "cyan" to the snow placed in the "purple" category. Only once, 14 April 1976, when the lowest surface temperature of all nine cases occurred, did the measured ratios exceed those expected by chance. In other words, there were generally more purple-alarmed pixels than would be expected to occur in a purely random process.

Similarly, when comparing yellow and cyan classifications, the occurrence of yellow pixels in proportion to cyan pixels exceeds that expected by chance, except for the 23 April 1976 case. Thus the cyan snow classification is less common in comparison to chance and to both the purple and yellow snow classification. Statistics are easily generated; however, to grasp the real significance of the thematic approach to snow separation by type is much more difficult. Without sufficient ground truth and because of the saturation of the MSS by snow, the thematic approach using Landsat MSS data generally cannot provide meaningful results.

TABLE 7. Number of Pixels by Snow Type and Comparison of Yellow and Cyan-Snow-to Purple Snow in Percent

| | 8 MAY 1975 | | 17 MAY 1975 | | 13 JUNE 1975 | | 22 JUNE 1975 | | 1 JULY 1975 | |
|---|---|---|---|---|---|---|---|---|---|---|
| Snow Type | No. of Pixels | Ratio Snow type: purple snow | No. of Pixels | Ratio Snow type: purple snow | No. of Pixels | Ratio Snow type: purple snow | No. of Pixels | Ratio Snow type: purple snow | No. of Pixels | Ratio Snow type: purple snow |
| Purple | 10,389 | 1 | 29,411 | 1 | 4138 | 1 | 3587 | 1 | 1116 | 1 |
| Yellow | 156,852 | 15.10 | 80,022 | 2.72 | 18,544 | 4.48 | 6614 | 1.84 | 4996 | 4.48 |
| Cyan | 116,197 | 11.18 | 108,036 | 3.67 | 29,441 | 7.11 | 13,537 | 3.77 | 8213 | 7.36 |

| | 14 APRIL 1976 | | 23 APRIL 1976 | | 20 MAY 1976 | | 29 MAY 1976 | |
|---|---|---|---|---|---|---|---|---|
| Snow Type | No. of Pixels | Ratio Snow type: purple snow | No. of Pixels | Ratio Snow type: purple snow | No. of Pixels | Ratio Snow type: purple snow | No. of Pixels | Ratio Snow type: purple snow |
| Purple | 292 | 1 | 12,208 | 1 | 647 | 1 | 877 | 1 |
| Yellow | 135,079 | 462.60 | 15,833 | 1.30 | 5058 | 7.82 | 1071 | 1.22 |
| Cyan | 91,148 | 312.5 | 60,624 | 4.97 | 6005 | 9.28 | 3299 | 3.76 |



ORIGINAL PAGE IS OF POOR QUALITY

Summary

From G.E. Image 100 computer tapes, Dicomed color images of Landsat scenes were generated. Various colors, each assigned to a bivariate range of MSS band 5 and 7 arbitrary reflectances, were used thematically in an attempt to classify the changing condition of the American River basin snowpack. From the histogram of MSS 5 and 7 values three classifications or themes were readily apparent and were thought to represent partial snowcover (cyan), melting snow (purple), and fresh or nonmelting snow (yellow). Inspection of available surface and upper air temperatures revealed that melting conditions existed on all Landsat overpasses with the possible exception of 4 April 1976. On this date, it is likely that the highest elevation snow surface (above 2500 m) was at or slightly below freezing at the 1800 GMT satellite acquisition.

Rather than separate melting from non-melting snow, the thematic approach has apparently divided the snow into various degrees of metamorphism. Possible classifications of these three categories could be actively melting or late metamosphosed snow as cyan, early melting or middle metamorphosed snow as purple, and initially melting snow or early metamorphosed snow as yellow. Unfortunately snowpack ground truth information in this basin was sparse to nonexistent and precluded any precise evaluation of the snowpack condition.

Another shortcoming noted in the G.E. Image 100 thematic separation was the inability to note a spectral difference between lowest elevation snow and bare rock. This inability is most critical late in the snow-melt season when the snowline has receded sufficiently to expose large areas of bare rock. At this time of year, classifying bare rock as low-elevation snow would lead to inflated values for total snowcover.

The G.E. Image 100 computer system is quite capable of handling the sophisticated multispectral techniques necessary to develop themes for snowpack classification. Unfortunately the Landsat MSS sensor limits the G.E. Image 100's usefulness because of low energy-level saturation and inadequate multispectral information. Not until the MSS system is improved by eliminating these problems will substantial progress result in a worthwhile assessment of snowpack parameters.

Saturation limits of future MSS's must be raised to avoid the currently-occurring saturation of the MSS when imaging snowfields. The AVHRR on TIROS N, NOAA's new operational polar-orbiting satellite, has saturation limits that exceed the reflectance observed from snowpacks and demonstrates thas sensor saturation need not be a problem. Preliminary research has been completed regarding the spectral response of various natural snow samples in the visible and near-IR (O'Brien and Munis, 1975). Research at CRREL is currently being conducted, in situ, on the effects of various substracts on snow reflectance. These new data combined with CRREL's previous study should provide insight into which visible and near-IR spectral regions provide useful information concerning snowpack properties.

## References


Thomas, I.L., Lewis, A.J., and Ching, N.P., 1978: Snowfield Assessment from Landsat, Photogrammetric Engineering and Remote Sensing, Vol. 64, No. 4, pp. 493-502.

Wiesnet, D.R., McGinnis, D.F., McMillan, M.C., 1975: Evaluation of ERTS Data for Certain Hydrological Uses, Final Report to NASA/GSFC, Contract No. 432-641-14-04-03, 92 pp.

Schneider, S.R., McMillan, M.C., and Wiesnet, D.R., 1975: River Basin Snow Mapping at the National Environmental Satellite Service, NOAA Tech. Memo. NESS 86, 19 pp.

Kirder, E., Schumann, H.H., and Warskow, W.L., 1977: The Application of Aerial and Satellite Snow-Mapping Techniques for Multi-purpose Reservoir System Operations in Arizona, Proc. of the 45th Annual Meeting of the Western Snow Conf., pp. 95-99.

O'Brien, H.W. and Munis, R.H., 1975: Red and Near-IR Spectral Reflectance of Snow, Proc. of the Operational Applications of Satellite Snowcover Observations Workshop, NASA SP-391, pp. 345-360.

Tarpley, J.D., Schneider, S.R., Danaher, E.J., and Myers, G.I., in press, An All-Digital Approach to Snow Mapping using Geostationary Satellite Data, presented at Workshop on Operational Applications of Satellite Snowcover Observati-ns, Reno, Nevada, April 16-17, 1979.

## Snow in Forest Areas

### Introduction

Snow mapping in dense forested areas, whether deciduous or coniferous, was recognized as difficult from the inception of our research into snow mapping at NESS. A summary of the findings of a report prepared for NESS by Eschner et al. (1977) investigating the problem of snow monitoring in forested areas via remote sensing follows.

### Objectives

The study (Eschner, et al., 1977) comprised three principal efforts: (1) a quantitative consideration of masking effects resulting from vegetative and topographic characteristics, (2) a detailed analysis of snow reflectance under vegetative cover using Landsat MSS and NOAA VHRR data, and (3) experimental mapping of snow extent via manual, digital, and electronic methods. Data used included NOAA digital VHRR visible and thermal tapes, Landsat digital MSS tapes, ground observations of reflectance, and low-altitude photography.

### Data

The handling of the NOAA digital VHRR data required the development of various software programs; a description of the five required programs is provided in the report (Eschner, et al., 1977, pp. 18-21). Based on techniques described by Algazi, et al. (1976) and Legeckis and Pritchard (1976), the VHRR data were corrected for geometric and panoramic distortions as well as the problem of skew. Programs for processing digital Landsat data were developed concurrently with the NOAA software.

### Data Analysis

A correlation analysis between NOAA VHRR visible brightness and site characteristics such as percent conifer, slope and roughness, slope and shading, and snow depth, as tabulated in Table 8, showed

**Table 8.** Correlation Analysis over Snow Survey Sites (After Eschner, et al., 1977)

| Correlation Coefficients, r's | NOAA Visible Brightness, expressed as: | | | |
|---|---|---|---|---|
| | Raw | Corrected | % tile | Normal'd |
| Snow Depth | .15 | .06 | .03 | .10 |
| Percent Conifer | .20 | -.29 | .27 | .17 |
| Slope/Roughness | .22 | -.14 | .23 | .21 |
| Slope/Shading | .08 | .01 | .07 | .07 |

only weak correlations. Such weak correlations did not warrant the use of a regression equation to estimate snow depth based on site characteristics and visible brightness. The lack of correlation is apparently caused by the poor signal-to-noise nature of the VHRR data.

Table 9 statistics demonstrate that the smaller range of the Landsat MSS response suggests greater sensitivity and better signal-to-noise ratio than the NOAA VHRR visible band.

Contrary to earlier findings of Wiesnet et al. (1975), who reported a decrease in reflectance of snow in the Cascade Mountains as a function of increasing wavelength, Eschner, et al. (1977) in the Adirondack Mountains measured a maximum response (i.e., reflectance) in the near-IR. Table 10 presents a summary of the grouped MSS data (for deciduous, conifer, and open areas), first as raw data (digital counts) then in terms of radiance ($\mu W/cm^2sr$). The findings are graphed in Figure A.4.1 and show in general an increase in radiance for all types of ground cover with increasing wavelength. The only exception is the result for deciduous forests on 25 February 1976 where the band 6 radiance of $2.18\mu W/cm^2sr$ fell below the band 5 value of $2.32\mu W/cm^2sr$. Eschner et al. (1977) attribute the increased reflectance of forested areas "to the high density of vegetation present in the study area" (adjacent to Cranberry Lake) and in the northeast in general. This explanation may have credence over coniferous sites, but would not apply to deciduous forests where no apparent explanation exists for the noted increased radiance.

Hard-copy visible-band NOAA VHRR imagery, analyzed following the procedure described by Schneider et al. (1976), yielded snow extent maps in close agreement with ground surveys. Some difficulty was noted

Table 9. Satellite Imagery Data Ranges, 1976 Dimensionless Values, Absolute Scale of 0 to 255. (After Eschner, et al., 1977).

| | | 96 Percentile Limits | Range | Mode | Mean | St. Dev. | Look Angle α |
|---|---|---|---|---|---|---|---|
| NOAA (visible) | 15 Jan | 183-224 | 41 | 205 | 204 | 11 | .328 |
| | 17 Jan | 191-233 | 42 | 223 | 220 | 11 | .280 |
| | 19 Jan | 192-231 | 39 | 223 | 224 | 12 | .210 |
| | 23 Jan | 201-230 | 29 | 215 | 225 | 11 | .096 |
| | 23 Feb | 196-231 | 35 | 223 | 228 | 14 | .144 |
| | 25 Feb | 186-228 | 42 | 215 | 227 | 18 | .203 |
| | 24 Mar | 188-226 | 38 | 215 | 229 | 19 | .371 |
| | 7 Apr | 209-230 | 21 | 223 | 220 | 6 | .057 |
| | 9 Apr | 209-232 | 23 | 223 | 220 | 6 | .112 |
| Landsat (band 5) | 25 Feb | 23-177 | 154 | 43 | 66 | 39 | |
| | 24 Mar | 20-153 | 133 | 45 | 60 | 31 | |

All units are digital counts on a scale of 0-255.

Table 10. Landsat Image Brightness and Radiance Estimates. (After Eschner, et al., 1977)

| | | Digital Count (0-255) Band | | | | Radiance Estimate ($\mu w/cm^2 sr$) Band | | | | # pixels sampled |
|---|---|---|---|---|---|---|---|---|---|---|
| | | 4 | 5 | 6 | 7 | 4 | 5 | 6 | 7 | |
| 25 Feb 76 | deciduous | 66 | 73 | 78 | 61 | 2.60 | 2.32 | 2.18 | 3.87 | 329 |
| | conifer | 40 | 38 | 49 | 40 | 1.57 | 1.21 | 1.37 | 2.54 | 95 |
| | open | 147 | 169 | 144 | 82 | 1.43 | 1.33 | 0.99 | 1.29 | 315 |
| 24 Mar 76 | deciduous | 58 | 56 | 72 | 54 | 2.28 | 1.78 | 2.01 | 3.43 | 298 |
| | conifer | 31 | 24 | 46 | 41 | 1.22 | 0.76 | 1.29 | 2.60 | 168 |
| | open | 118 | 111 | 102 | 40 | 1.15 | 0.87 | 0.70 | 0.63 | 240 |

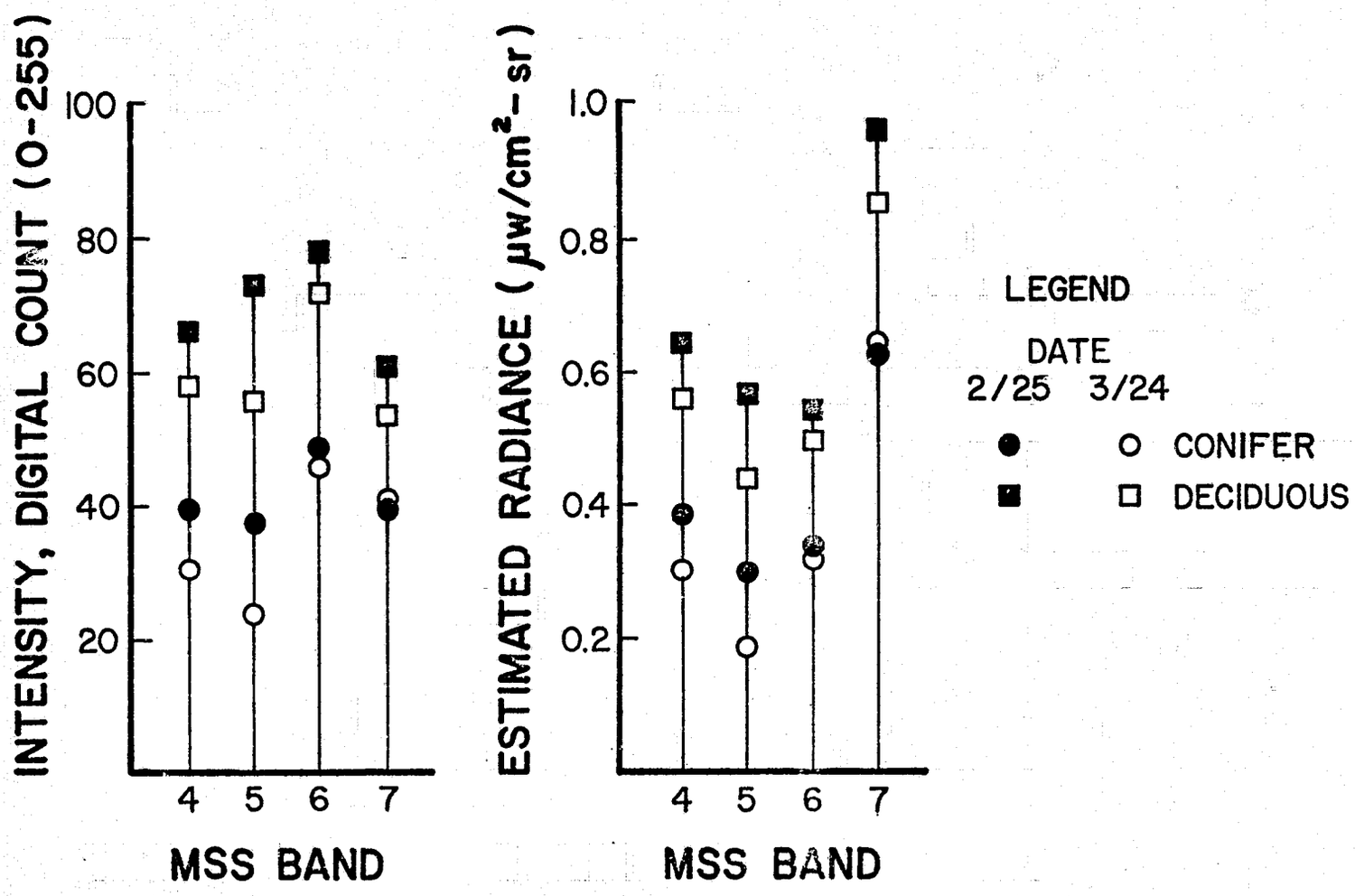



Figure 14. Graph showing Landsat brightness levels and radiation estimates of snowcover in deciduous and conifer areas of the Adirondack Mountains. (after Eschner, et al., 1977).

in the analysis of 1976 images prior to late March when the snow-covered Adirondack region consistently appeared as dark as the non-snow areas to the south.

Digital analysis of the VHRR data from 7 April 1976 required an averaging technique to remove noise in the data. Once the noise-induced "salt and pepper" tone was removed, the resulting product resembled snow maps produced using standard VHRR imagery and the Zoom Transfer Scope. The digital analysis technique for snow mapping is more advantageous than conventional hard-copy photograpic interpretation in at least two aspects. The imagery may be geometrically corrected for precisely relating image data to watershed boundaries, and ground observations may be more accurately located on an image to assist in determining the threshold level separating snow from non-snow areas.

Summary

NOAA visible VHRR digital data present little information on snow conditions in the Adirondacks during winter and early spring. This lack of information appears to be caused by a poor signal-to-noise ratio in the data. After mid-March, discrete areas of high reflectance correspond well to areas of snowcover indicated by ground surveys, providing timely information to the hydrologist during the spring run-off period. Digital generation of snow maps from VHRR visible data is hampered by noise in the data, but the application of a simple averaging technique was found to greatly increase the utility of the data. This procedure is more precise, but more costly than either the manual or computer-assisted interpretation of snow from hard-copy NOAA imagery.

The increased near-infrared response observed in Landsat MSS 6

and 7 from dense coniferous and deciduous forests warrants further examination. Future spectral studies involving the discrimination of fresh and metamorphosed snow should consider the effects of varying vegetation type and density as a function of resolution element size.

References: (Section on Snow in Forest Areas)

Algazi, R., 1976: An Integrated Study of the State of California using Remote Sensing Techniques, Annual progress report, University of California, Davis, pp. 58-70.

Eschner, A.R., Lillesand, J.M., and Meisner, D.E., 1977: Satellite Remote Sensing of Snowcover in the Adirondack Mountains, Final Report, 88 pp., NOAA/NESS Grant No. 04-5-158-43.

Legeckis, R. and Pritchard, J., 1976: Algorithm for Correcting the VHRR Imagery for Geometric Distortions due to the Earth's Curvature and Rotation, NOAA Tech. Memo. NESS 77, 15 pp.

Schneider, S.R., McMillan, M.C., and Wiesnet, D.R., 1976: River Basin Snow Mapping at the National Environmental Satellite Service, NESS Tech. Memo. NESS 83, 27 pp.

Wiesnet, D.R., McGinnis, D.F., and McMillan, M.C., 1975: Evaluation of ERTS Data for Certain Hydrological Uses, Final Report to NASA/GSFC, Contract No. 432-641-14-04-03, 92 pp.

Snowcover Runoff Relation in American River Subbasins

## I. Introduction

The monitoring of changes in the extent of snowcover began with the advent of operational satellites. The feasibility of using snowcover changes to extract useful information regarding resultant snowmelt runoff was reported by Rango and Salomonson (1977), Salomonson and MacLeod (1972), and the U.S. Department of Interios (1974). of Rango and Salomonson involved correlating the snow-covered area (SCA) at its greatest extent, viz., April 1-20, (just before the beginning of the melt season) with seasonal runoff volume for April-July. Two watersheds in the Himalayan region were studied, yielding correlations of 0.91 and 0.94 (r) for straight line best fits. These high correlations must be tempered by the fact that only six and eight years of data were available for the two regressions.

## II. Description of Subbasins

A natural extension of the snowmelt-runoff studies is to shorten the period of runoff forecasts, for example, reducing 3-month volumes to monthly or perhaps weekly or daily runoff estimates based in part on changes in satellite-deserved SCA. Because we have gathered a considerable amount of Landsat data on the American River basin, it was decided to concentrate on subbasins of the American River. Only three subbasins of the American River have gaging stations on streams whose flows are unregulated upstream of the gage. These stations are Pilot Creek above Stumpy Meadows Lake (11431800), drainage area 30.3 $km^2$ (11.7 $mi^2$); Duncan Creek near French Meadows (11427700), drainage area 25.74 $km^2$ (9.92 $mi^2$); and North Fork of Middle Fork American

River near Foresthill (11433260), 230.3 $km^2$ (88.9 $mi^2$). The higher elevations of each of these subbasins receive snow during the winter and spring seasons--though the snow depth and cover within each subbasin vary greatly from year to year. The range in elevation is 1606 to 2195m for Duncan Creek, 1304 to 1725m for Pilot Creek, and 396 to 3189m for North Fork of Middle Fork American River. None of the gages predate 1960 and range from 13 to 18 years in length of record. Figure 15 shows the location of the three subbasins within the American River. Figures 16a, 16b, 16c, show details of Duncan Creek, Pilot Creek, and North Fork of Middle Fork American River basins, respectively.

III. Data and Data Analysis

Average daily runoff values, in cubic feet per second, are published yearly by the U.S. Geological Survey in cooperation with individual state agencies (USGS, 1973-76). The 12-month period of record begins on the first of October and is known as the water year. Thus the 1973 water year covers the period October, 1972 through September, 1973. Plots of the daily discharge for the three subbasins for the year 1973, 1975, and 1976 are presented in Figure 17a for Duncan and Pilot Creeks, and in Figure 17b for North Fork of Middle Fork American River, respectively. Satellite-derived SCA in terms of percent of basin are listed in Table 11. Note that Landsat data are available for only a few dates per year, only twice for the drought year 1976. To compensate for the paucity of Landsat-derived SCA, NOAA VHRR SCA data were combined with the Landsat estimates thus providing a more complete record. SCA regressions were performed

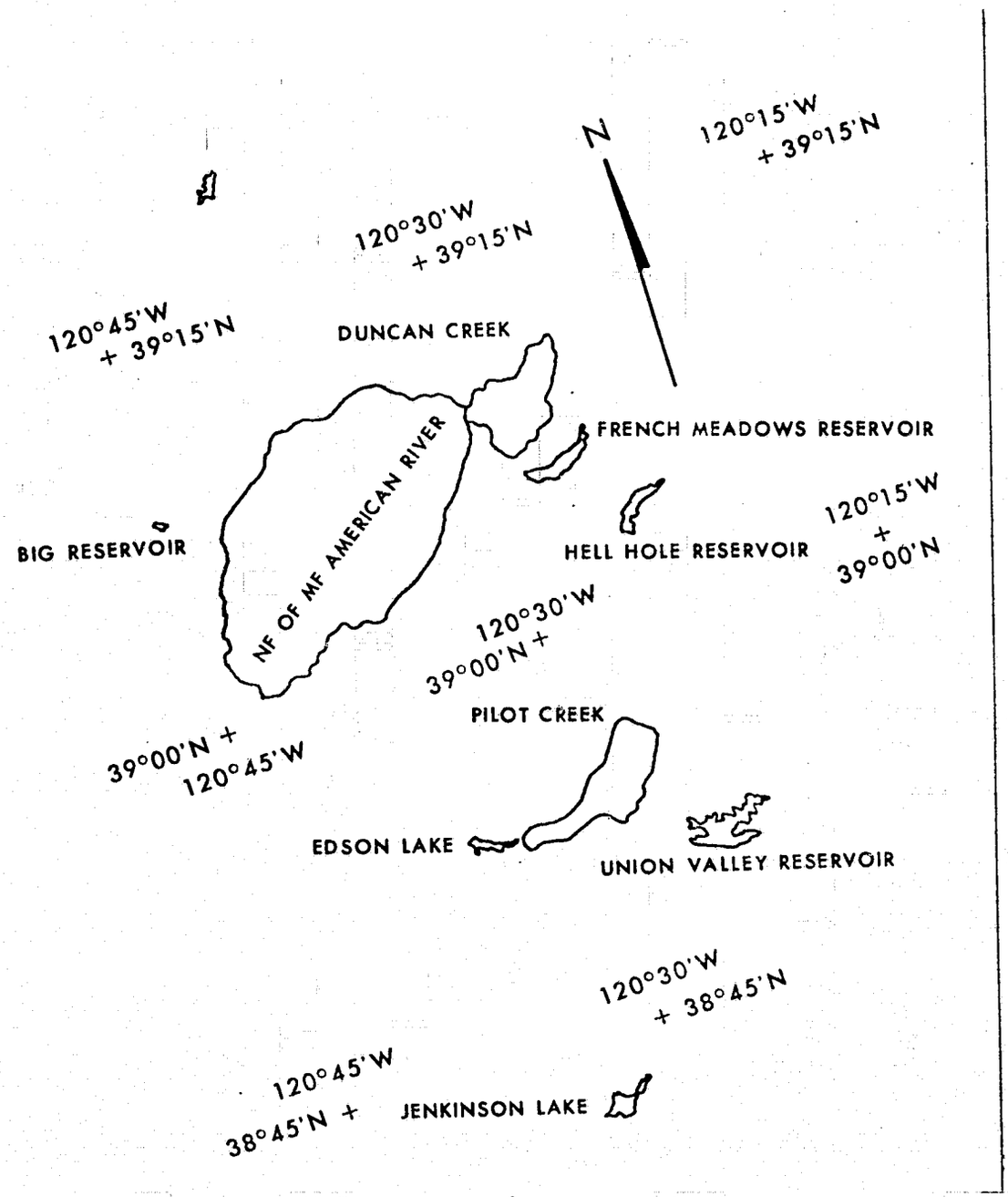



Figure 15. Sketch map showing the location of the Duncan Creek, Pilot Creek, and North Fork of Middle Fork American River subbasins.

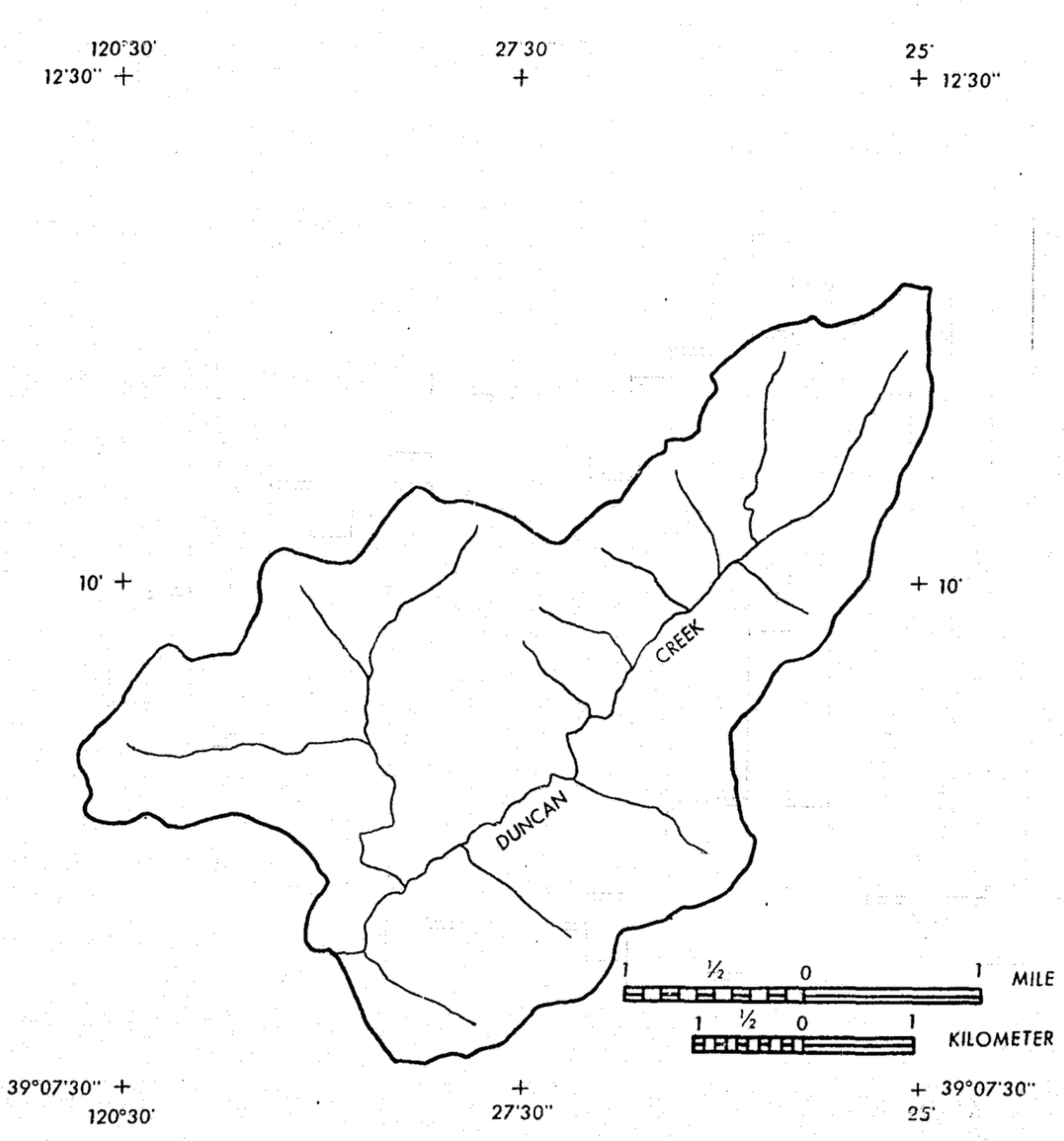



Figure 16a. Map of the Duncan Creek subbasin.

REPRODUCIBILITY OF TH
ORIGINAL PAGE IS POOR

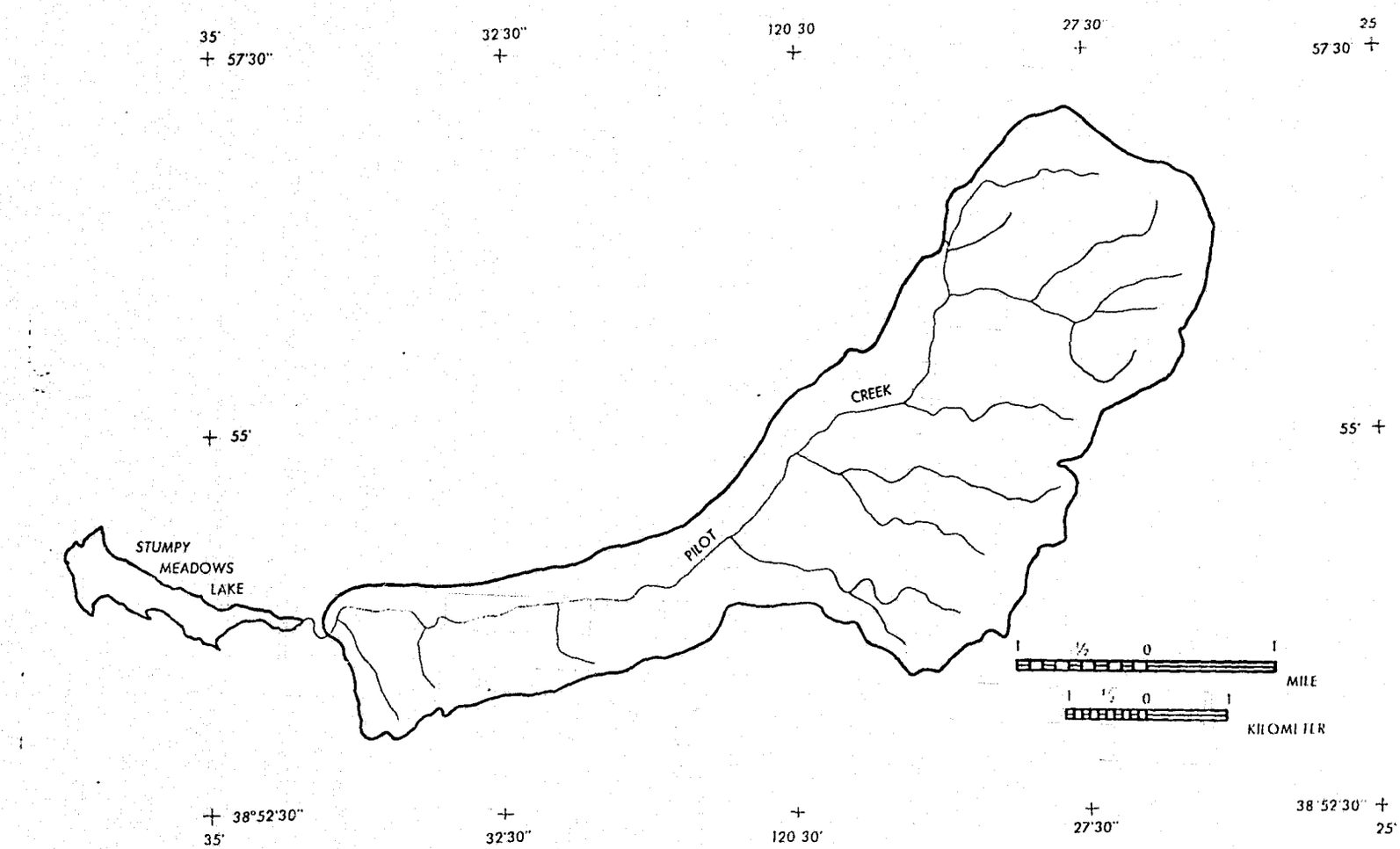



Figure 16b. Map of the Pilot Creek subbasin.

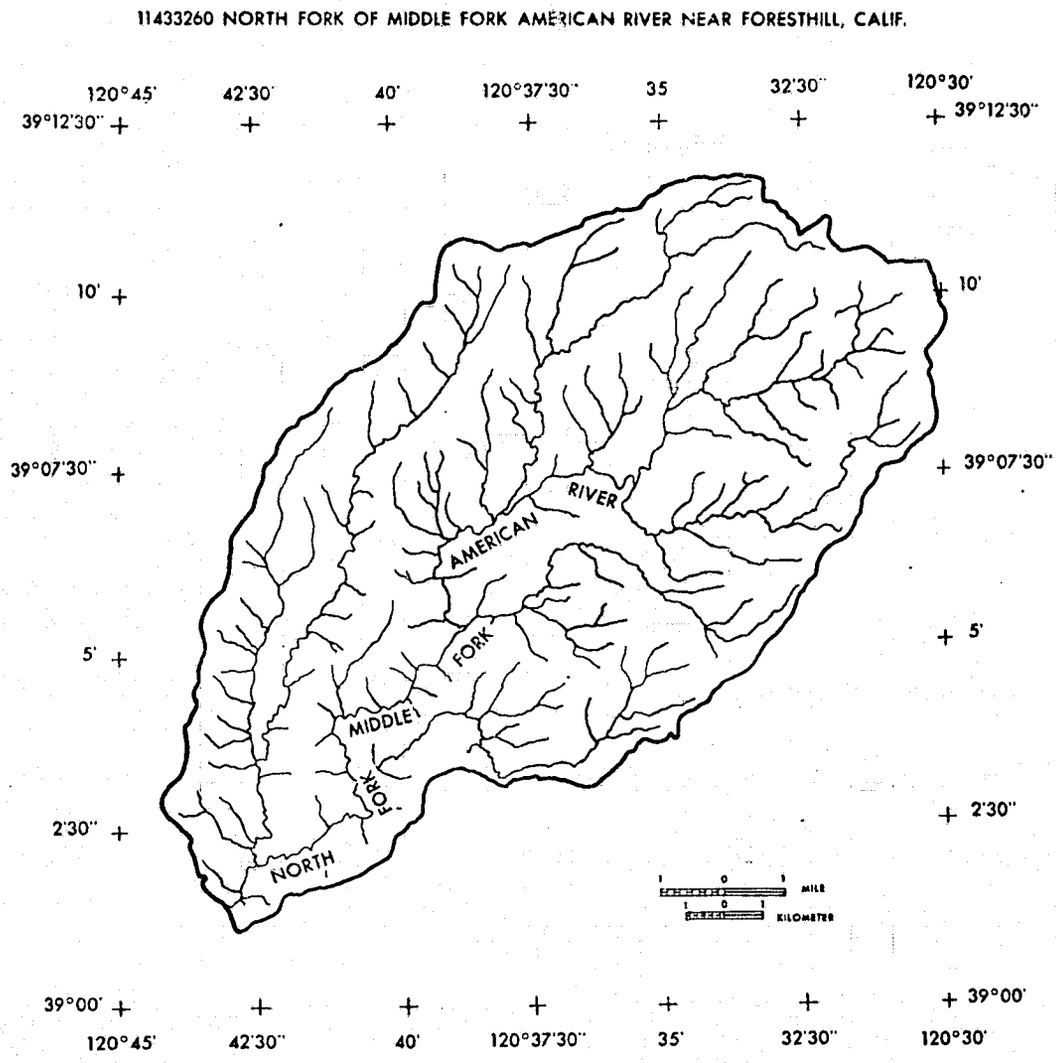



Figure 16c. Map of the North Fork of Middle Fork American River subbasin.

REPRODUCIBILITY OF TH
ORIGINAL PAGE IS POOR

ORIGINAL PAGE IS OF POOR QUALITY

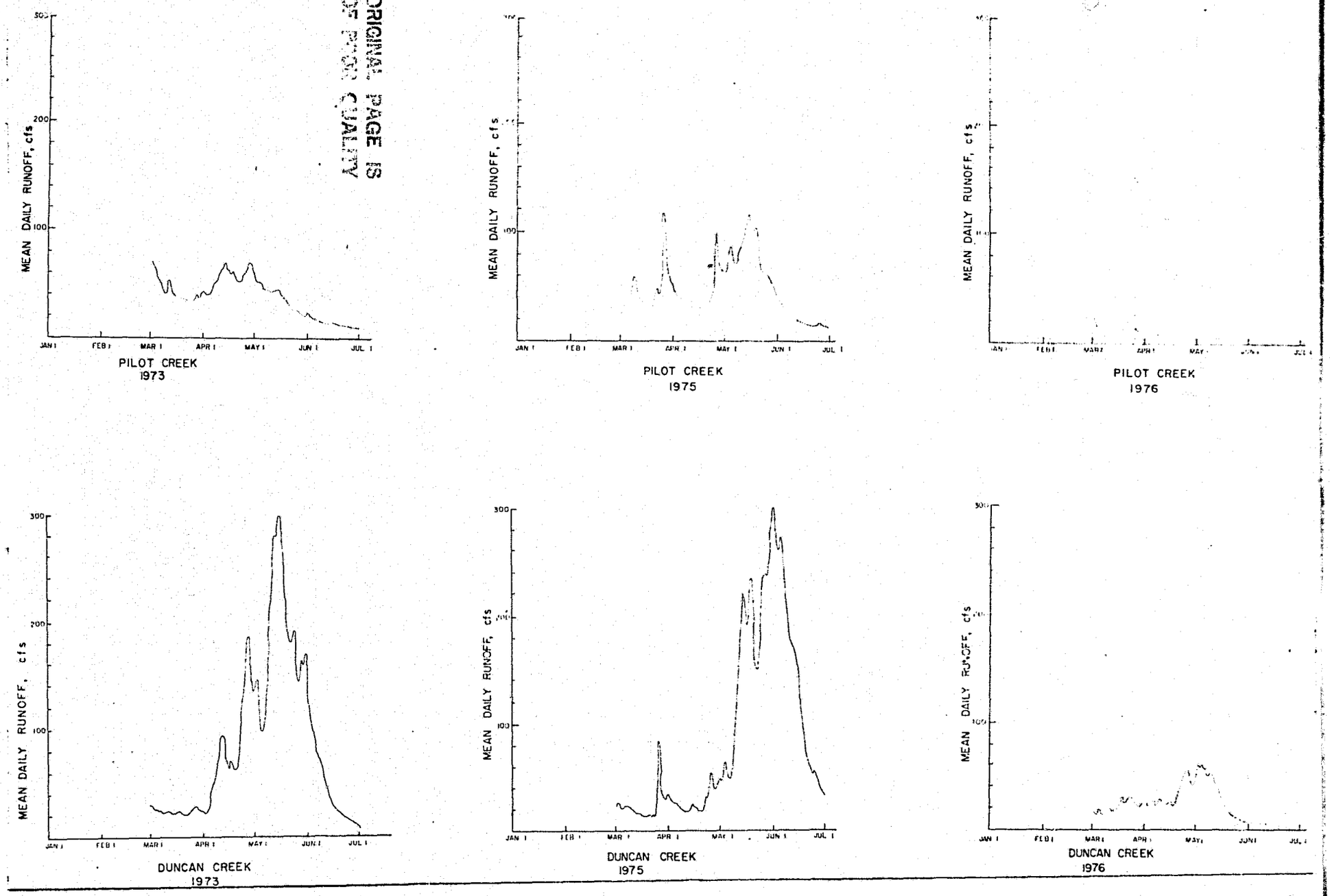



Figure 17a. Daily discharge hydrographs of Pilot Creek and Duncan Creek for March-June 1973, 1975, and 1976.

REPRODUCIBILITY OF THE
ORIGINAL PAGE IS POOR

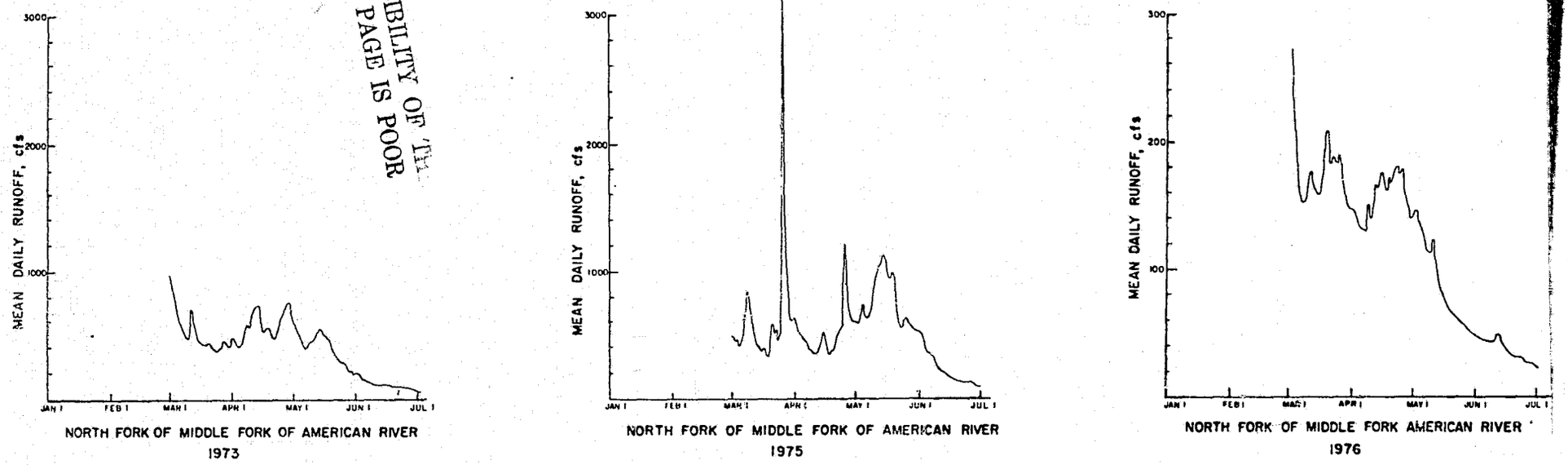



Figure 17b. Daily discharge hydrographs of North Fork of Middle Fork American River for March-June 1973, 1975, and 1976.

Table 11. Snow Cover Area of American River Subbasins in Percent for 1973, 1975, 1976 using Landsat MSS Band 5 Imagery

| Date | AMERICAN RIVER SUBBASINS | | |
|---|---|---|---|
| | N.F. of M.F. American River | Duncan Creek | Pilot Creek |
| 4/3/73 | 48 | 85 | 64 |
| 4/21/73 | 40 | 93 | 48 |
| 5/9/73 | 19 | 92 | 24 |
| 5/27/73 | 4 | 62 | 0 |
| 4/11/75 | 74 | 91 | 84 |
| 5/8/75 | 40 | 93 | 73 |
| 5/17/75 | 25 | 86 | 22 |
| 6/4/75 | 4 | 67 | 0 |
| 4/14/76 | 29 | 75 | 69 |
| 4/23/76 | 8 | 47 | 0 |

relating NOAA-derived and Landsat-derived American River SCA as well as regressing individual subbasin SCA's against the American River SCA's (Landsat data only). Even though the data were sparse, meaningful relationships were found for Pilot Creek and the North Fork (NF) of the Middle Fork (MF) of the American River and are given below:

NOAA vs. Landsat, American River Basin

1973: $y = 1.18 + 1.01x$, $r = 0.99$ y = Landsat-derived SCA

1975: $y = 6.99 + 1.22x$, $r = 0.99$ x = NOAA-derived SCA

1976: $y = 0.81 + 0.98x$, $r = 0.99$

N.F. of M.F. American River

1973: $y = -29.00 + 1.56\ (1.18 + 1.01x) = -27.16 + 1.58x$

1975: $y = -29.00 + 1.56\ (-6.99 + 1.22x) = 39.90 + 1.90x$

1976 $y = -29.00 + 1.56\ (0.81 + 0.98x) = -27.74 + 1.53x$

x = NOAA-derived American River basin SCA, in percent

y = N.F. of M.F. American River basin SCA, in percent

REPRODUCIBILITY OF T
ORIGINAL PAGE IS POOR

Pilot Creek

1973: $y = 21.90 + 1.71\ (1.18 + 1.01x) = -19.88 + 1.73x$

1975: $y = 21.90 + 1.71\ (-6.99 + 1.22x) = -33.85 + 2.09x$

1976: $y = 21.90 + 1.71\ (0.81 + 0.98x) = -20.51 + 1.68x$

x = NOAA-derived American River basin SCA, in percent

y = Pilot Creek SCA, in percent

Data for Duncan Creek were too scattered and showed no apparent relationship to American River SCA.



C-2

A thorough but somewhat outdated study of the snowmelt process is presented in Snow Hydrology (1956). The study indicates that temperature is a good index to snowmelt, to be explicit, the number of degrees that the maximum temperature exceeds the freezing point. Leaf (1975) has incorporated SCA into a computerized short-term streamflow forecast model, that also includes the residual snowpack water equivalent as an independent variable. For our study of the American River basin, several independent parameters were regressed in an attempt to estimate daily runoff flows (in cfs). The independent variables include SCA (for the American River basin and for the individual subbasin), the number of degress the daily maximum temperature exceeded freezing in degrees F, the snow on the ground (inches), snowfall (inches), the water equivalent of the snowpack (inches), and the amount of precipitation (in inches of water). A final independent parameter was Julian day. All data were available on a daily basis, except SCA. Missing values of SCA were estimated by linear interpolation when rather uniform maximum temperatures occurred and precipitation was absent. Adjustments in the estimated SCA were made to account for snowfalls, widely varying temperatures or large rainfalls. Most adjustments involved less than several percent change in SCA. Estimates of SCA were made taking into account as many meteorological variables as possible; nevertheless some subjectivity was introduced in the decision process. The daily parameters, including the dependent variable, runoff, were punched onto computer cards and run through a packaged stepwise, multivariate regression on the NESS IBM 360/195. Because of the high correlation between SCA for the American River basin and the two subbasins (0.94 to 0.99), a second run was made

exchanging SCA values. Data were available for 1973, 1975, and 1976; but no regression analysis were performed for Pilot Creek for 1976 because of the rapid melt of the snowpack and the very low, almost constant, runoff.

## IV. Discussion of Results

Multiple regression correlation coefficients (r's) ranged from 0.74 to 0.96. The regression analyses usually included only three of the seven independent variables; the others contributed little to reduce the variance (sums of squares). Of the 10 analyses performed, only two required more than three variables to reach the maximum reduction in the variance. For these cases, five variables were used. Two other analyses required only two variables to reach maximum r.

Snow-covered area, by providing the largest reduction in the sums of squares, was the most important variable in six of 10 runs, occurring as the second and third most important parameter twice, respectively. Precipitation and day of the year were each most efficient in reducing the sums of squares twice. Snow on the ground appeared as only the second-most useful variable in the analyses, but did so in eight of the ten runs. In third place, in addition to SCA, were day of year (four times) and precipitation, twice. For the two cases when five variables were used, snowfall occurred once in both the fourth and fifth positions, water equivalent of the snowpack once in fourth position, and day of year once in fifth place.

The occurrence of SCA as an important variable in all the regression analysis is noteworthy. Further, the SCA for the American River basin in four of the five cases reduced the variance slightly

more than did the SCA for the individual subbasins. The reason for this slightly greater reduction is not known, but is of little significance because of the high correlation between the two variables. It suggests that one need not rely on the higher resolution, less frequent Landsat imagery to provide SCA. Rather, the lower resolution NOAA data should suffice in estimating runoff of small watersheds (as small as 30.3 $km^2$) as long as the SCA of the subbasin correlates well with the larger, NOAA VHRR-size river basin.

The other useful variables are standard meteorological or hydrologic parameters, and though some are not acquired at many observation stations (such as snow on the ground and snowfall), these variables are usually available near, if not within, the basin perimeter. In this study, Blue Canyon Weather Service Office (WSO) supplied the snow parameters ndd is located approximately 75 km from the subbasins.

There is an indication that the parameters used are not always well-correlated with runoff. For both basins, 1975 regressions have very low r's of 0.74 and 0.75. For this year the Pilot Creek SCA was only the third most important parameter for reducing the sum of squares. SCA was still the most effective parameter for the NF of the MF American River, but accounting for an r of only 0.54. Obviously other factors affected the runoff during 1975--factors not included in the chosen parameters. A check of the hydrographs for the NF of MF American River show 1975 to be rather irregular with three distinct peaks during the snowmelt season beginning in late March. 1976 shows a much different hydrograph response having only one double-peaked maximum with a long, almost smooth, recession

curve. It was 1976 that the correlation coefficient was the highest and was accomplished using only the day of year and SCA variables.

## V. Summary

In summary, a simple regression model of readily available meteorological parameters, satellite-derived SCA, and day of year provides estimates of daily average runoff with r's in excess of 0.89. Such estimates are obtained during snowmelt seasons where the hydrograph is very regular, i.e., having one well-defined peak followed by a rather smooth, recession curve. During snowmelt seasons punctuated with many precipitation events, the regression model performs poorly. Thus SCA appears to contain information for those who are interested in better quantifying daily runoff in the American River basin and possibly for quantifying runoff in other Sierra Nevada basins similar to the American River. The potential to predict runoff, indirectly, in much smaller subbasins, the size of 30 $km^2$, in the American River using SCA was demonstrated.

## References


Corps of Engineers, U.S. Army, North Pacific Division, 1956: Snow Hydrology, 437 pp.

Leaf, C.F., 1975: Applications of Satellite Snow Cover in Computerized Short-Term Streamflow Forecasting, in Operational Applications of Satellite Snowcover Observations, A. Rango (Ed.), pp. 175-186.

Rango, A., Salomonson, V.V., 1977: Seasonal Streamflow Estimation in the Himalayan Region Employing Meteorological Satellite Snow Cover Observations, Water Resources Research, Vol. 13, No. 1,

Salomonson, V.V., and N.H. MacLeod, 1972: Nimbus Hydrological Observations over the Watersheds of the Niger and Indus Rivers, 4th Annual Proceedings, Earth Resources Review, NASA Doc. MSC 05937, pp. 5-1 to 5-11.

U.S. Department of Interior, 1974: Snow Mapping and Runoff Forecasting Examination of ERTS-1 Capabilities and Potential Benefits from an operational ERS System, Interim report, Contract 14-08-001-13519, Office of Econ. Anal., Washington, D.C.

U.S. Geological Survey, 1973-1976: Water Resources Data for California Water Year 1973-76, Vol. 4, USGS Water-Data Report CA-73-076-4.

# SOIL MOISTURE STUDIES

## Introduction

The need for improved soil moisture estimates is demonstrated by the crude approximation currently used for hydrologic design (USDA, SCS, 1957) and streamflow estimates (Burnash, et al, 1973). Most soil moisture values are actually based on precipitation values from rain gages that are weighted by a decay function of time or on accumulated 5-day antecedent rainfall. Soil moisture measurements are rarely taken in situ, and when taken individually are point values, undoubtedly unrepresentative of the entire river basin. There is a real need for areally averaged soil moisture values that reflect the condition of the watershed and its response to rainfall more accurately.

Basin-wide soil moisture estimates are best obtained from remote platforms such as aircraft or satellites. Sensors scanning in such portions of the electromagnetic spectrum as the near-IR (Merritt and Hall, 1973), thermal (Idso, et al., 1975, Jackson, et al., 1976), gamma ray (Feimster, et al, 1975), and microwave (Schmugge, 1976; Schmugge, et al., 1976a; Schmugge, et al, 1976b) have been used in an attempt to obtain basin-wide soil moisture. An extensive study of active microwave work with soil moisture has been done by Batlivals and Ulaby (1977), while work by Schmugge, et al. (1976a) covers the passive microwave area. Unfortunately the resolution of satellite-borne passive microwave data is currently limited to approximately 25 km.

Field studies were conducted near Phoenix, Arizona, and near Luverne, Minnesota, as part of this Landsat-2 investigation. The objective of the investigation is to monitor soil moisture at NOAA test

sites and to compare ERTS (Landsat) spectral reflectance measurements with not only ground truth (soil samples) but with concurrent gamma-ray aircraft data collected and furnished by ongoing in-house NOAA research, and with concurrent NASA PMIS overflights.

Phoenix Test Site

Description of Site and Overview of Experiment

The test site in the Phoenix area was selected for several reasons: 1) it is irrigated land, thus affording a variety of soil moisture; 2) the fields are regular and set along straight lines oriented north-south; 3) it had been studied previously in 1974 (Schmugge, et al, 1976b); and 4) cloud-free conditions are relatively frequent. The experiment was timed to coincide with that time when a large number of bare fields were either planted in cotton or were being prepared for planting; therefore soil moisture conditions would vary widely. Figure 1 shows the general location of the test sites, and figures 2a-c present detailed maps of each field and the location of soil samples in each field.

The experiment involved participants from NASA/JSC and GSFC, USDA/SCS, NOAA/NESS, EG&G and Bittinger and Associates, as well as students from Arizona State University. Various remote sensors collected data in the gamma ray, microwave, visible, thermal and near-IR portions of the spectrum for correlation with the soil moisture values determined from soil samples taken in the fields. Table 1 summarizes the remotely sensed data sources.

The goal of the combined experiment was to evaluate the usefulness of remote sensors for monitoring soil moisture. The major thrust centered on

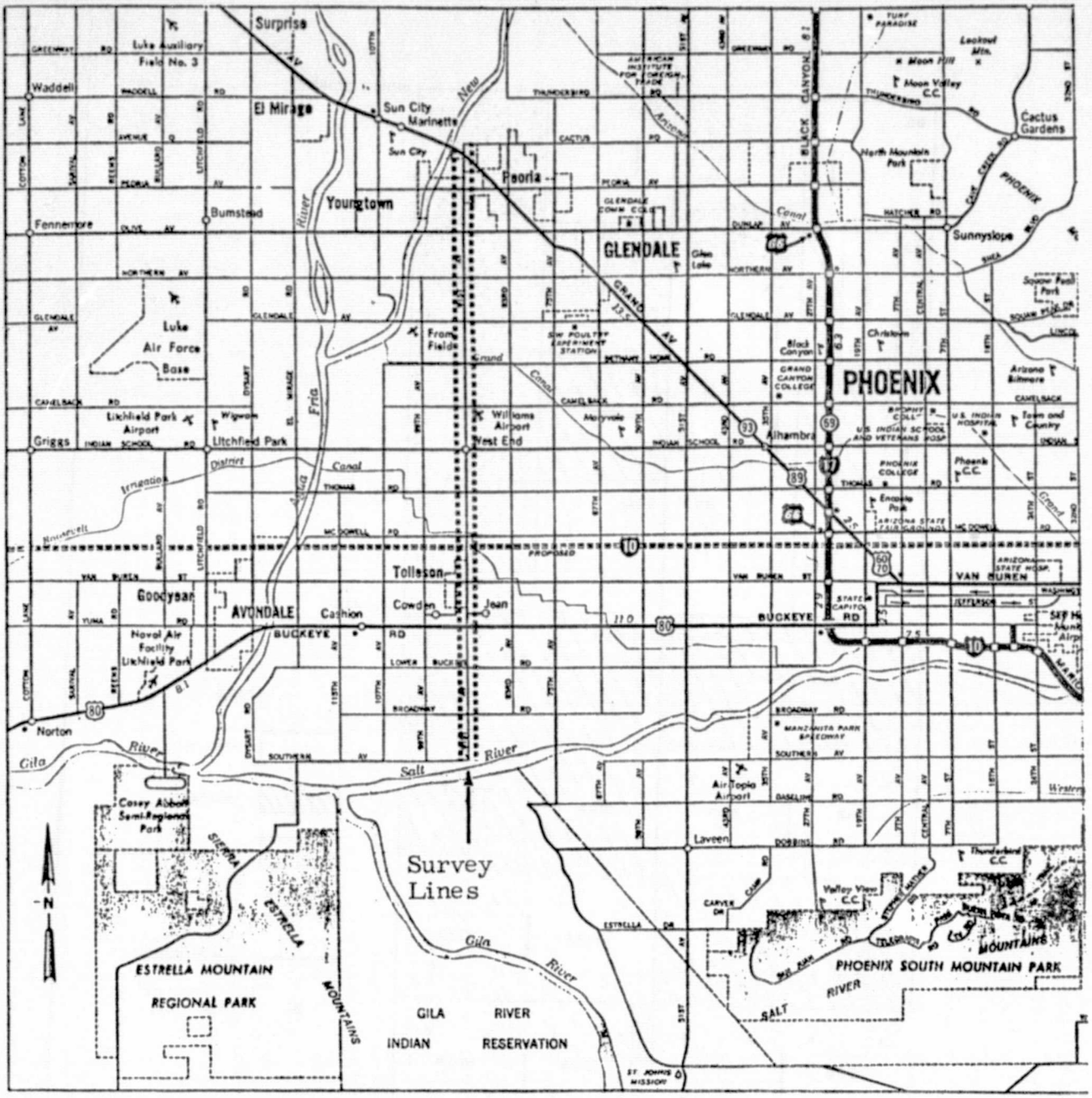



Fig. 1. Index map showing the two survey lines near Phoenix, Ariz.



ORIGINAL PAGE IS
OF POOR QUALITY

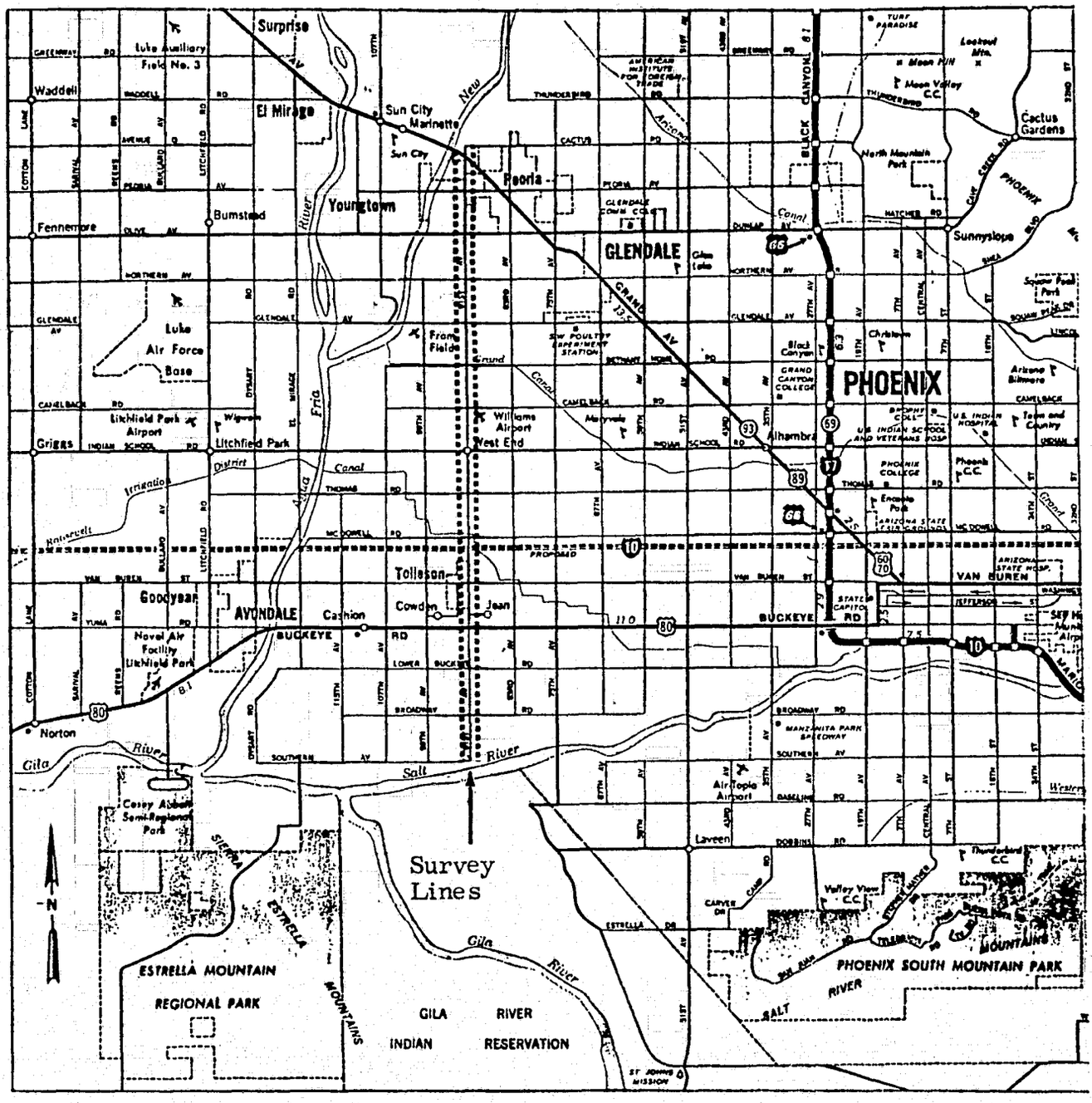



Fig. 1. Index map showing the two survey lines near Phoenix, Ariz.



ORIGINAL PAGE IS
OF POOR QUALITY

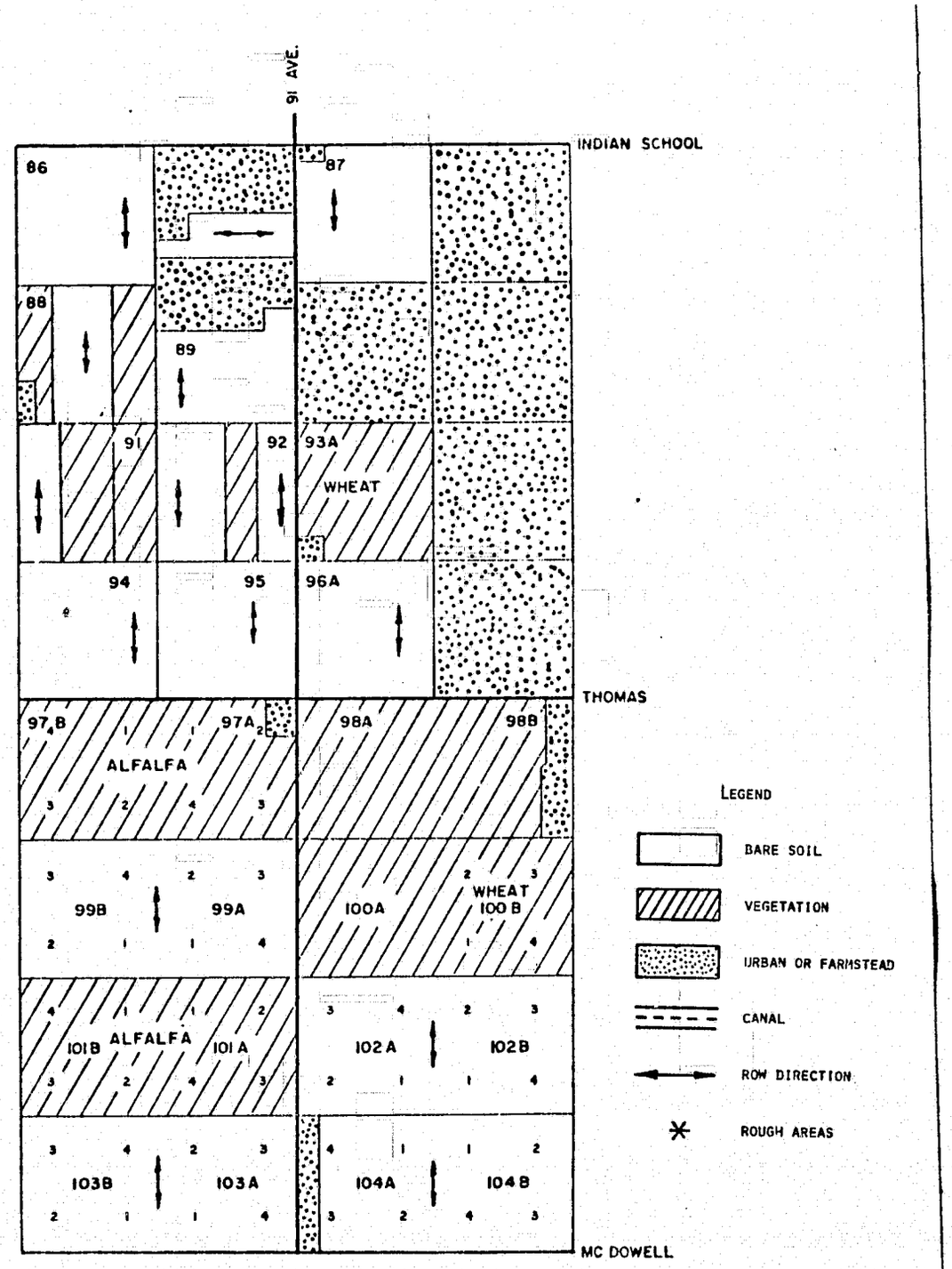
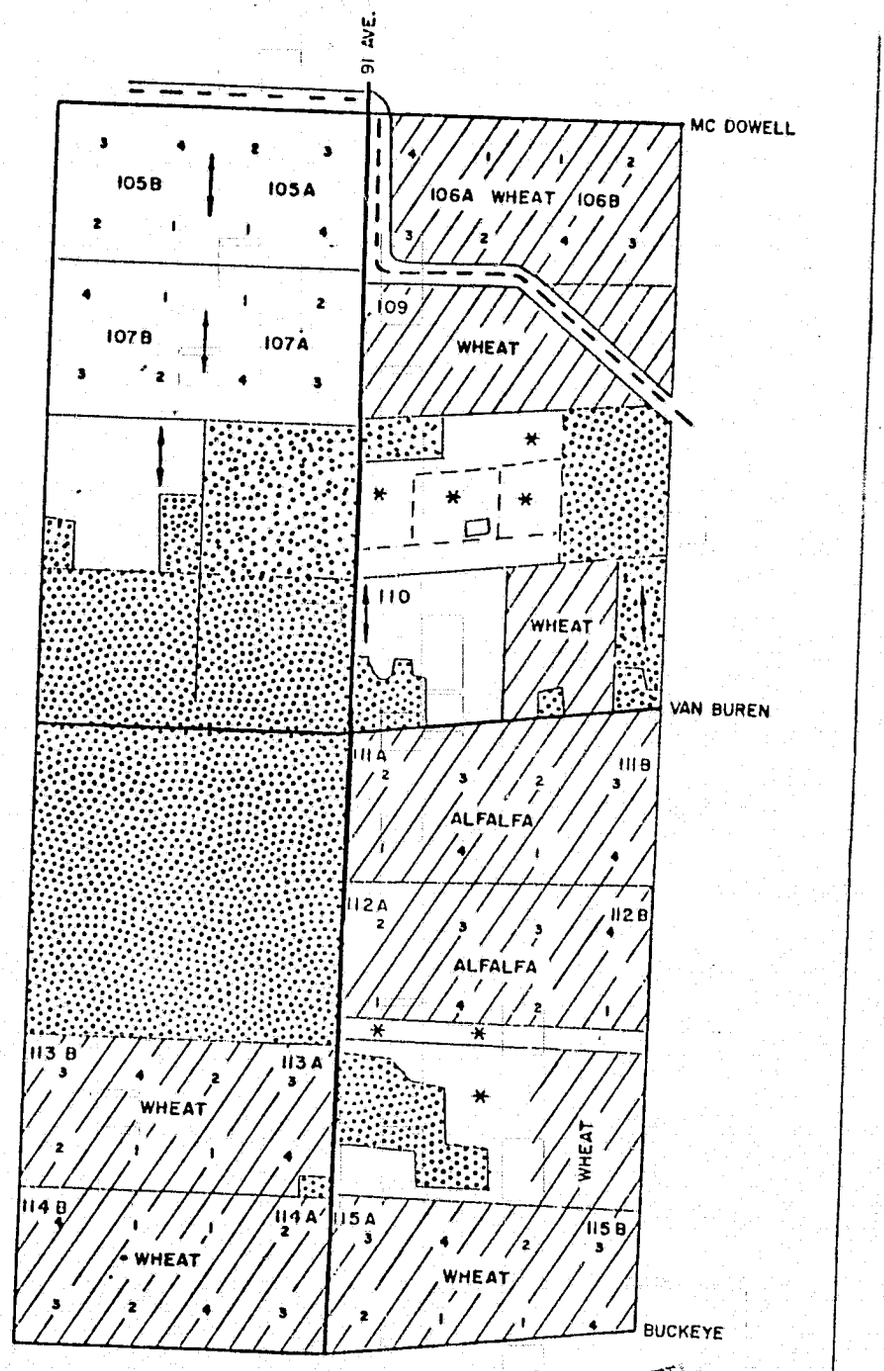



Fig. 2a. Map showing northern third of test site near Phoenix, Arizona, with details as to land use, row direction, and field sampling locations (from Blanchard, 1975, Appendix B).




REPRODUCIBILITY OF TH...
ORIGINAL PAGE IS POOR

Fig. 2b. Map showing middle third of test site near Phoenix, Arizona, with details to land use, row direction, and field sampling locations. Legend found on Figure 2. (from Blanchard, 1975, Appendix B)

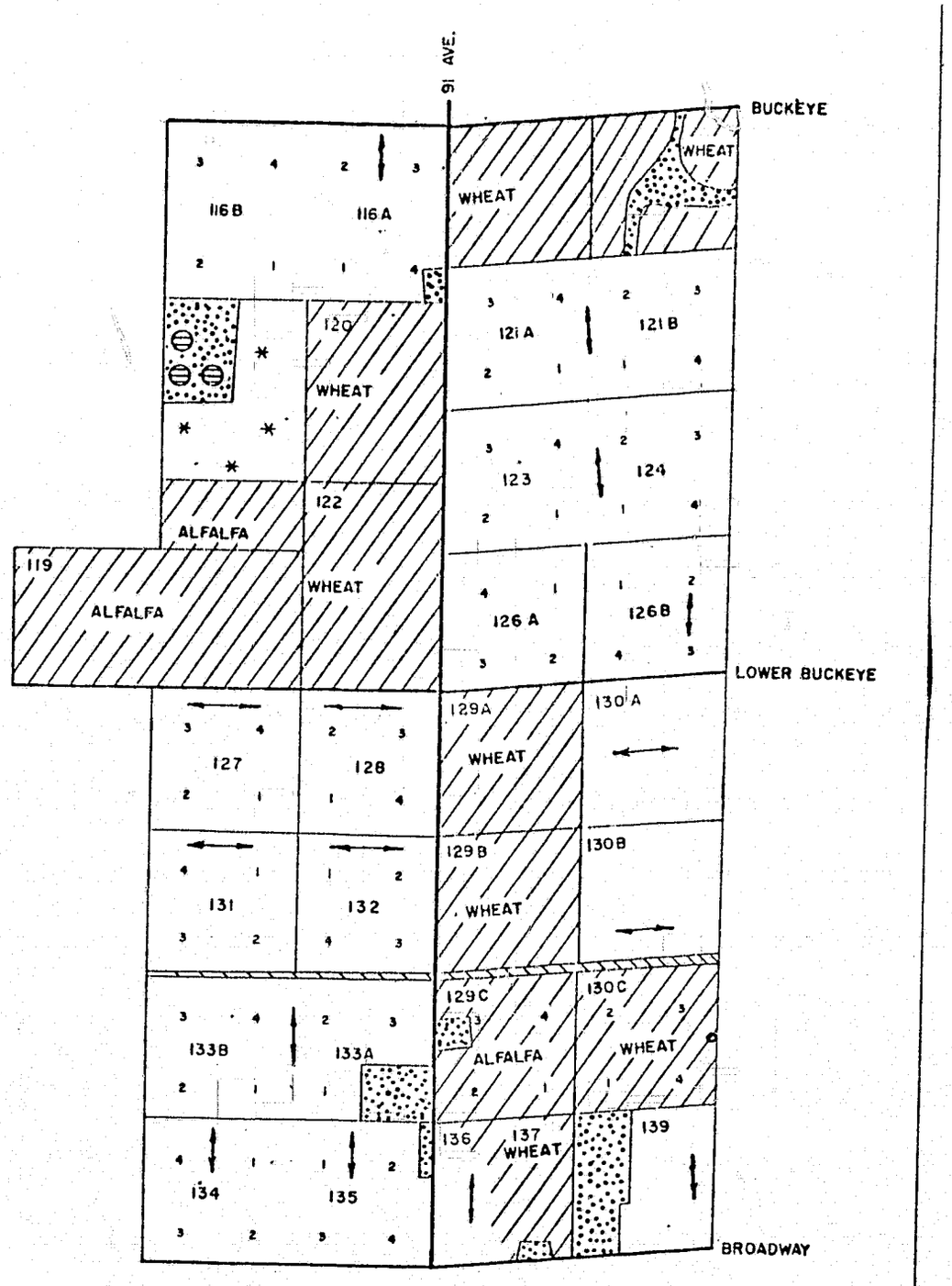



Fig. 2c. Map showing southern third of test site near Phoenix, Arizona, with details as to land use, row direction, and field sampling locations. Legend found on Figure 2. (from Blanchard, 1975, Appendix B)

TABLE 1. Summary of remote sensors used to collect data of Phoenix test site.

| Wavelength | Sensor | Platform | Supplier | Date Collected | Altitude |
|---|---|---|---|---|---|
| 0.5-1.1μm | MSS | Landsat | NASA | 3/17/75 | 900 km |
| 10.5-12.5μm | VISSR | SMS-2 | NOAA | 3/18/75 | 37,500 km |
| 2.8 cm | PMIS | P-3 | NASA | 3/18/75 | 0.5 & 0.8 km |
| 21 cm | MFMR | P-3 | NASA | 3/18/75 | 0.5 & 0.8 km |
| 1A ($10^{-11}$cm) | NaI(Tl) (gamma ray) | Beechcraft | EG&G | 3/18/75 | 0.15 km |

TABLE 2. Net $^{40}K$ and $^{208}Tl$ gamma photopeak count rate from the March 18, 1975 survey. (From Feimster, et al., 1976)

| Survey Line* | Spectrum No. | Time of Day | Net Gamma Count Rate in Photopeak (cpm) $^{40}K$ | $^{208}Tl$ |
|---|---|---|---|---|
| 1A | 203 | AM | 2397 | 534 |
| 1B | 207 | AM | 2777 | 592 |
| 1C | 211 | AM | 2785 | 598 |
| (Average values for survey line segment) | | | (2673) | (577) |
| 1A | 225 | PM | 2734 | 573 |
| 1B | 226 | PM | 2621 | 583 |
| (Average values for survey line segment) | | | (2628) | (585) |
| (Average values for whole line) | | | (2651) | (581) |

*The symbols A, B, and C refer to the successive passes over line 1.

microwaves (NASA) with secondary efforts involving gamma ray, near-IR and thermal (NOAA) data.

Soil Sampling and Soil Moisture Data

Sampling was done at four points in each 16.9-hectare field selected. Points were located approximately one-fourth the width of the field from the adjacent boundaries (see sampling locations, figures 2a-c) and are thus at or near the centers of each quadrant of the field.

Primary tillage practice was listing, i.e., the furrowing of the soil in which row crops are sown in the furrows. Most fields, bare particularly, had listed furrows where irrigation water is distributed along the furrow, and moisture reaches the listed ridges by infiltration and capillary movement. At each data point five samples were collected on the tops of ridges and five were collected at the bottom of furrows.

The ten samples collected at each location were as nearly representative as physically possible of the 0-1 cm, 1-2 cm, 2-5 cm, 5-9 cm, and 9-16 cm depth zones. These sampling depths were chosen by the NASA/ Texas A&M team to test theoretical models of microwave emission. Weighted composite averages were calculated to represent composite soil moisture from the surface to the bottom of each zone to be used in the development of empirical models for determination of soil moisture with microwave equipment.

A report by Blanchard (1975) provides details of the sampling techniques and sampling processing. Appendix A to his report gives all soil moisture values including various soil moisture averages for different depths and for entire fields. Location of the fields and soil temperature data are also provided.

Microwave Study

The relation of passive microwave to changes in soil moisture has been studied at the Phoenix test site each year from 1972 to 1975 (Schmugge, et al, 1976a; 1976b; and Schmugge, 1976). The results of the various experiments, culminating in 1975, showed that radiometers operating at 21 cm have good sensitivity to soil moisture variations, about a 50°K change as soil dries from field capacity. The sensitivity is maintained even for a moderate vegetation canopy. For wavelengths less than 3 cm, vegetation effectively screens the soil surface thereby limiting the usefulness of microwave radiometers for soil moisture sensing. Further study is needed to determine whether the additional polarization obtained at off-nadir orientations is worth the sacrifice of poorer spatial resolution. For a complete review of the microwave investigations one should consult the above referenced reports.

Gamma Ray Study

The purpose of the survey was to determine soil moisture by detecting differences in the terrestrial gamma flux attenuation as a function of soil moisture content. Most of the gamma radiation from the naturally occurring radioelements in the soil, measured above ground, originated within a few centimeters of the surface. The presence of moisture in the soil causes an effective increase in soil density resulting in an increased attenuation of the gamma flux for wet soil and a corresponding lower flux above the ground surface. Selected samples of the surface soil, analyzed gravimetrically, provide the necessary calibration data to allow a quantitative determination of aerial measurements. The EG&G aerial measurements of terrestrial passive gamma radiation were performed simultaneously with the NASA microwave measurements and the ground

sampling, and offers an independent set of data from which to establish correlations and evaluate the NASA microwave data.

The survey lines along which soil moisture measurements were made consisted of two 16-mile (25 km) long lines situated 1,200 feet (375μ) on either side of 91st Avenue in the western section of Phoenix as shown in figure 1. These lines were oriented in a north-south direction and covered flat farmland, most of which was unvegetated. The character of the region surveyed is illustrated in more detail in figures 2a-c, with indications of the location of ground-based soil sampling points.

Equipment

The EG&G aircraft survey consisted of measuring the natural terrestrial gamma-ray emission using an unshielded fourteen crystal array of 4-in by 4-in NaI(Tl) detectors. The gamma radiation comes primarily from the naturally occurring $^{40}K$ in the surface soil, together with $^{214}Bi$ and $^{208}Tl$ from the uranium and thorium decay chains. The aerial radiation measurements included the collection of gross gamma counts and gamma energy spectra. The gross gamma-count system consisted of an amplifier discriminator computer unit that counted and recorded the total number of gamma rays of energy greater than 50keV that were detected during a one-second interval. The gross gamma-count rate (number of gamma rays detected per second) was digitally recorded along with aircraft position and altitude every second. As a backup and complement to the digital recording of the gross-count data, a record was made on a continuous strip chart of the gross gamma-count rate and the radar altitude as a function of time. The data collecting system

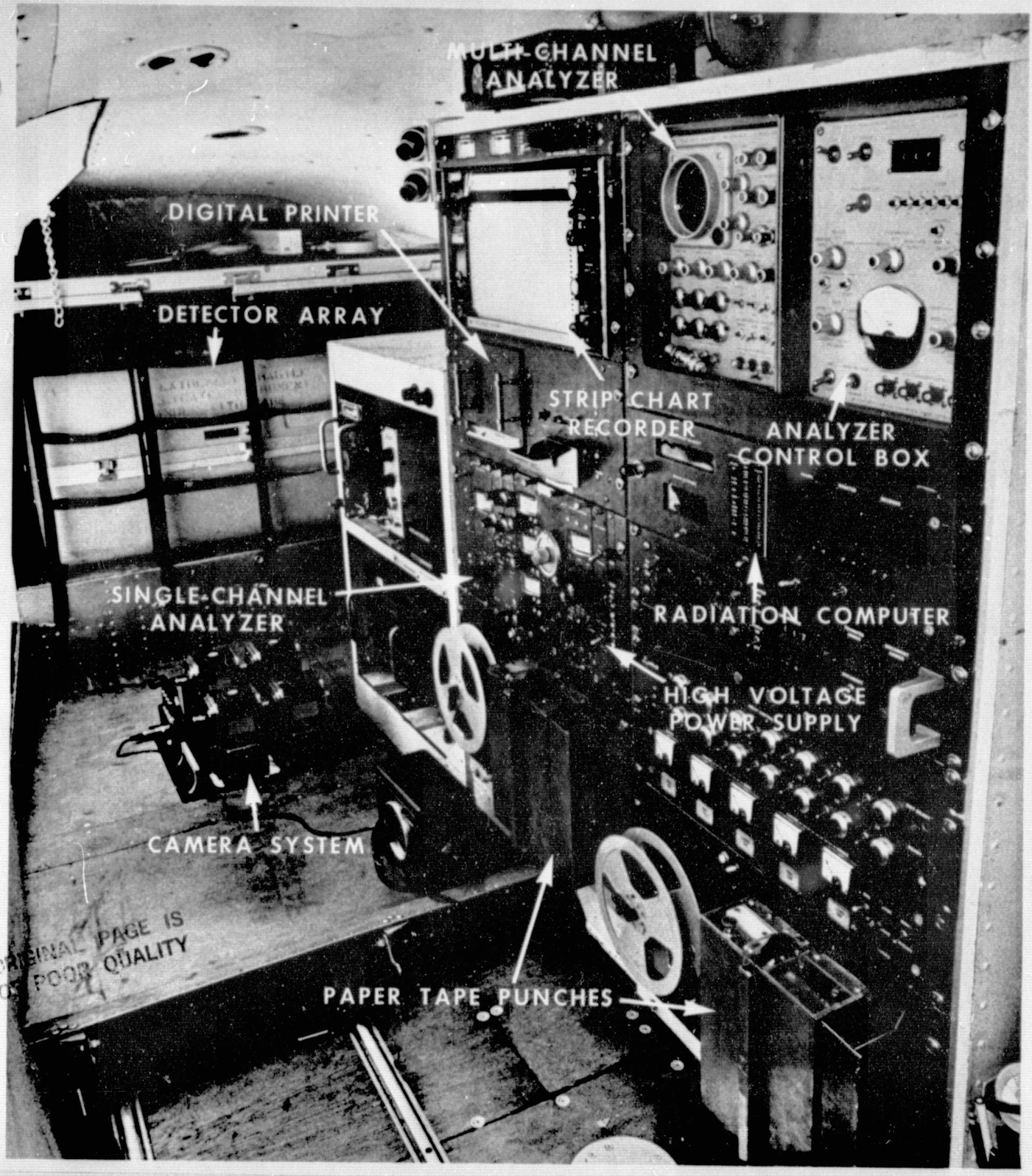
is shown in figure 3. An air filter sampler was also available on the aircraft to measure the concentration of radioactive airborne radon daughters which are the principal background contributors to the measured terrestrial radiation signals.

Technique

The detection system together with associated electronics was flown on a Beechcraft Twin Bonanza aircraft at an altitude of 150 m (500 ft) above the terrain and at a speed of about 140 knots. The two flight lines were surveyed three times in succession just after sunrise on March 18 and three times again in the early afternoon of the same day. The position of the aircraft and its altitude above terrain were measured and recorded every other second by a radar navigation computer system. The position and altitude measurements are accurate to ±106 m (±350 ft) and ±6 m (±20 ft), respectively. At an altitude of 150 m (500 ft) the field of view of the detectors covered an area of approximately 350 hectares

for the mean energy of gamma radiation from naturally occurring radioelements.

All flights were timed to coincide with the NASA P-3 aircraft survey and the ground sampling work. The gross gamma counts were measured by the array of fourteen 4-in by 4-in NaI crystals nn board the survey aircraft. The data were recorded once every two seconds, providing a data point for every 150 m (500 feet) of survey line traveled. These data were averaged on a mile-by-mile basis. In addition, the gamma energy spectrum was recorded at eight-mile intervals during the survey, or twice per survey line. The spectral data were used to sum gamma




ORIGINAL PAGE IS OF POOR QUALITY

Fig. 3. View of the interior of the gamma ray survey aircraft showing the detector package and the electronic data collection system. (from Feimster, et al, 1975)

REPRODUCIBILITY OF TH
ORIGINAL PAGE IS POOR

counts in the $^{208}Tl$ photopeak region and in the $^{40}K$ photopeak region. Soil moisture determinations were made using the three independent analyses of gamma flux attenuation from gross counts between 50 keV and 3.0 MeV, as well as using the $^{208}Tl$ and the $^{40}K$ photopeak gammas. All three sets of data, including previous measurements, were later employed in determining soil moisture values.

In order to establish the magnitude of the airborne radon daughter gamma background during this survey, air filter samples were taken twice during the morning survey and twice during the afternoon survey. The filters trapped radioactive radon daughters which commonly attach themselves to aerosol particles in the size range between a fraction of a micron to a few tens of microns. Additionally, the gamma ray count rate was measured while flying the aircraft at 150 m (500 ft) over nearby Lake George where one would expect no terrestiial gamma radiation to be present--as another evaluation of the airborne radon daughter contribution to the measurements.

Results

The gamma count rates in the photopeaks for $^{40}K$ and $^{208}Tl$ were determined by first subtracting the non-terrestrial background counts (due to the aircraft, cosmic rays and airborne radon daughters) from the respective pulse height-spectrum windows (see figure 4), i.e., channels 91 through 104 for $^{40}K$ and channels 168 through 184 for $^{208}Tl$. These net photopeak count rates were then adjusted to correspond to that for transport of these terrestrial gammas through an air mass of 17 g/cm$^2$ (equivalent to an altitude of 150 m (500 ft) at average pressure and temperature). Table 2 gives a listing of net photopeak count rates for

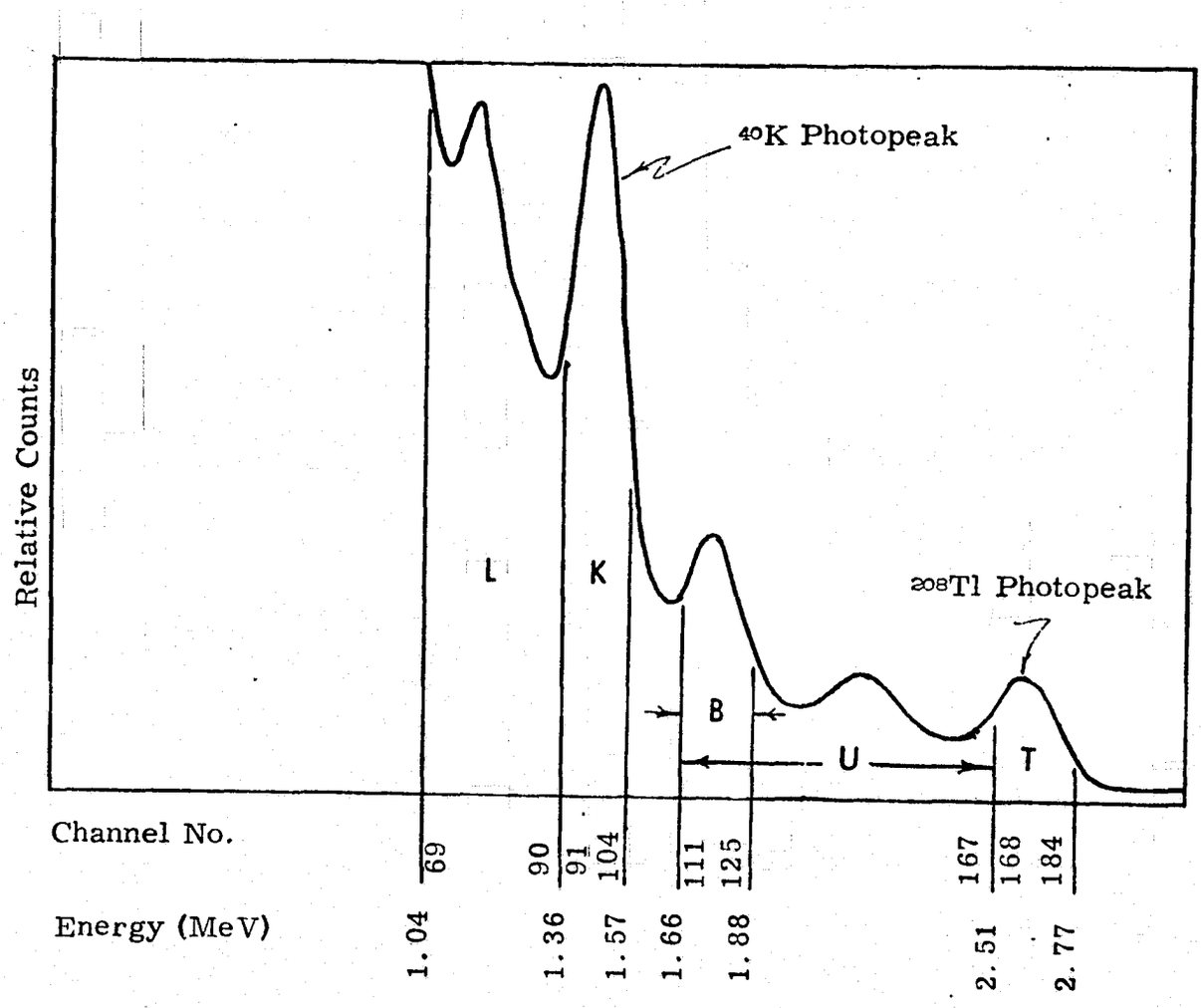



Fig. 4. Definition of the gamma energy spectral pulse height windows used in the photopeak area equations. The letter labels refer to the following: T (counts in the $^{208}Tl$ window); U (counts in the window occupied by the higher energy $^{214}Bi$ gammas from the uranium decay chain); B (counts in the 1.6 MeV $^{214}Bi$ photopeak window); K (counts in the $^{40}K$ photopeak window); and L (lower energy background gamma counts around the 1.12 MeV $^{214}Bi$ photopeak. (from Feimster et al, 1975)

$^{40}K$ and $^{208}Tl$ for each survey line flown on March 18, 1975, and values averaged over repeated flights.

The ratio of gamma flux $\Gamma_1/\Gamma_2$ measured for two different soil moisture conditions $M_1$ and $M_2$ has the form

$$\frac{\Gamma_1}{\Gamma_2} = \frac{1 + M_2}{1 + M_1} \qquad \text{Eq. (1)}$$

Eq. (1) is used with the tabulated $^{40}K$ and $^{208}Tl$ photopeak count rates given in Table 2, the $^{40}K$ and $^{208}Tl$ photopeak count rate for November 21, 1972, (2740 cpm and 583 cpm, respectively) and the soil moisture for November 21, 1972, (19%) to determine the soil moisture values for the March 18, 1975, survey. It should be noted that this can only be done for survey line 1 (west of 91st Avenue) since only that line was surveyed previously, a necessary prerequisite for determining the value of $M_1$ of Eq. (1).

The calculated soil moisture values, employing the $^{40}K$ and the $^{208}Tl$ photopeak area methods are:

M ($^{40}K$) = 22%

M ($^{208}Tl$) = 20%

The third method of determining soil moisture from aerial measurements of terrestrial gamma radiation employs analysis of the gross gamma count rates between 50 keV and 3.0 MeV. If there is negligible airborne radon daughter contribution to the signal, the net terrestrial gross count rate is determined by subtracting the gamma background count rate due to the aircraft and cosmic rays. The net count rate is then adjusted to correspond to that for transport of 17 g/cm$^2$ as was done for the $^{40}K$

and $^{208}Tl$ count rates. Occasionally, however, substantial airborne radon daughters are present during the surveys. Two approaches were used to establish the magnitude of the radon daughter background. The first was to determine this background contribution by utilizing (1) the change in the rario U/K of the gamma count rates in the two pulse height windows U and K (see figure 5), on November 21, 1972, and March 18, 1975, (2) the (counts/sec)/(counts/min) due to airborne radon daughters in the U pulse height window as determined by experimental lake overflights, (3) a knowledge of the $^{40}K$ photopeak and radon daughter counts on November 21, 1972, and (4) a knowledge of the $^{40}K$ photopeak count on March 18, 1975. These values are, respectively

1) U/K (November 21, 1972) = .44 U/K (March 18, 1975) = 0.46
2) Airborne radon count over water in U pulse height = 0.82 (counts/sec)/(counts/min)
3) $^{40}K$ photopeak count (November 21, 1972) = 2740 cpm

   radon daughter count (November 21, 1972) = 600 cps
4) $^{40}K$ photopeak count (March 18, 1975) = 2665 cpm

With this data it is possible to determine the total <u>average nonterrestrial</u> gross count rate by proceeding through the following computations:

Uranium terrestrial gross count rate (November 21, 1972)

$$= 0.82\ (U/K)(^{40}K) - \text{airborne radon daughter count count}$$

$$= 0.82\ (0.44)\ (2740) - 600 \qquad \text{(Eq. 2)}$$

$$= 389 \text{ cps}$$

REPRODUCIBILITY OF THE
ORIGINAL PAGE IS POOR

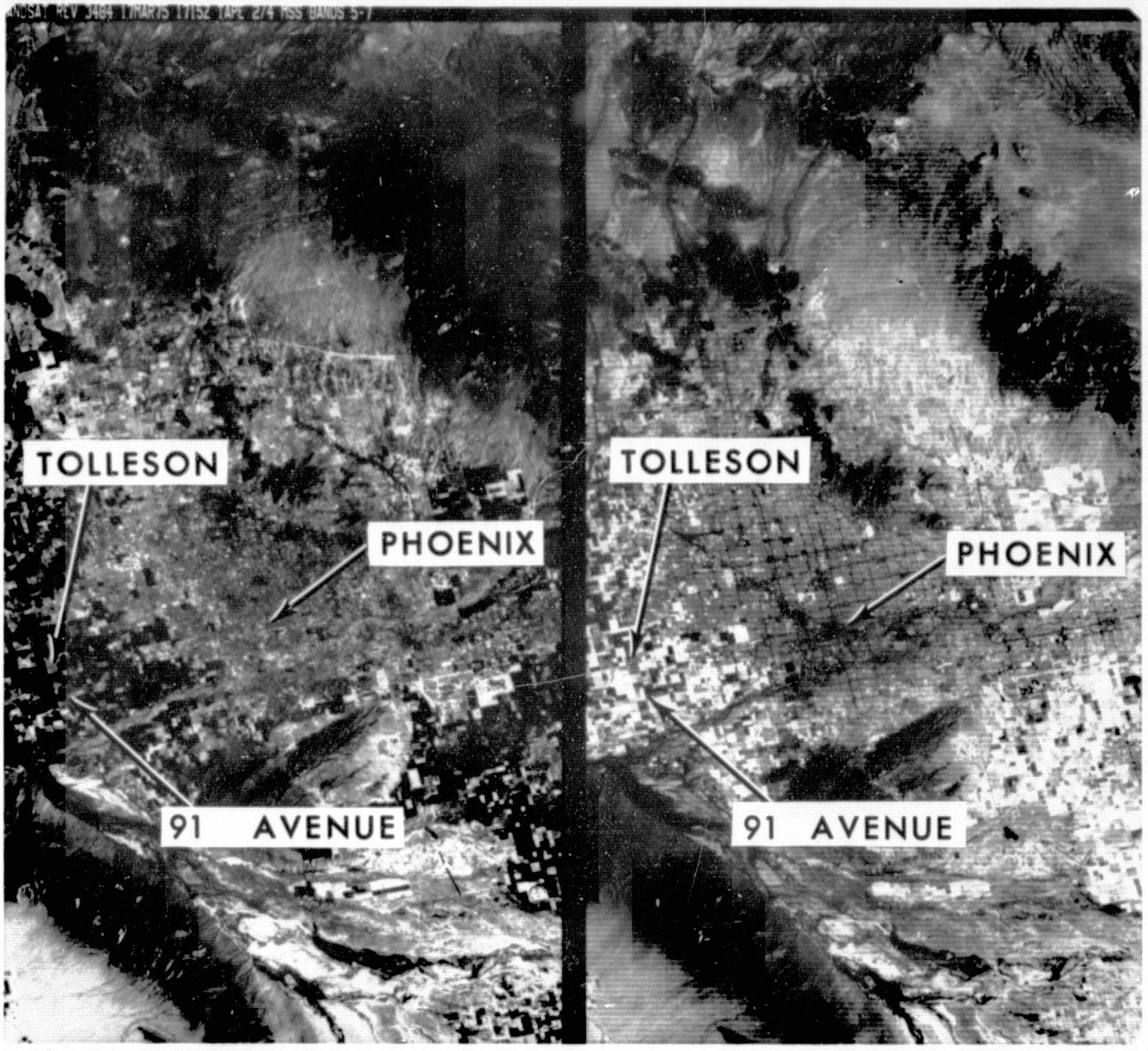



Fig. 5. Portion of Landsat-1 image (3/17/75, 1967-17154, orbit 13,484) covering Phoenix and the area to the west of the city including the test site at Tolleson, Arizona. MSS band 5 (0.6-0.7μm) on left, MSS band 7 (0.8-1.1μm) on right. Computer-generated and enhanced.

ORIGINAL PAGE IS
OF POOR QUALITY

Total uranium daughter (radon + terrestrial) count rate (March 18, 1975)

$$= 0.82\ (U/K)\ (^{40}K)$$

$$= 0.82\ (0.46)\ (2665) \qquad \text{(Eq. 3)}$$

$$= 1005 \text{ cps}$$

$U_{NET}$ gamma count rate (March 18, 1975)

= (Eq. 2)

- (Percent change in $^{40}K$ photopeak count between dates)

x (Eq. 2)

$$= 389\ (0.03 \times 389) \qquad \text{(Eq. 4)}$$

$$= 377 \text{ cps}$$

REPRODUCIBILITY OF THE
ORIGINAL PAGE IS POOR

Radon gamma count rate (March 18, 1975)

= (Eq. 3) - (Eq. 4)

$$= 1005\text{-}377 \qquad \text{(Eq. 5)}$$

$$= 628 \text{ cps}$$

Therefore, total average nonterrestrial gross count component for flight line is (radon + aircraft background + cosmic)

$$= ((\text{Eq. 5}) + 290 + (137e^{(15\text{-pressure})}))/2.55 \qquad \text{(Eq. 6)}$$

$$= 1129 \text{ cps (at } 13.90 \text{ lbs/in}^2 \text{barometric pressure)}$$

By determining the total $^{214}Bi$ photopeak areas in the U pulse height window for each flight line segment, approximate values for the radon and the total nonterrestrial background component for each line were computed as shown above. The results are tabulated in Table 3. The second method used to establish the contribution of the gamma count rate from the airborne radon was to compute an adjusted gross count (corrected for the nonterrestrial component) that corresponds to the new soil moisture computed for March 18, 1975, as described earlier. The adjusted gross

TABLE 3. Nonterrestrial background determined from the estimated radon activity using the U/K method. (Nonterrestrial bkg = radon + aircraft + cosmic**). (From Feimster, et al., 1976)

| Gamma Counts* in the U pulse height windows (cpm) | Pressure** ($lb/in^2$) | Radon Activity in the gross count channel (cps) | Nonterrestrial bkg in the gross count channel (cps) |
|---|---|---|---|
| 938 | 13.16 | 556 | 1131 |
| 1027 | 14.12 | 645 | 1222 |
| 1223 | 14.12 | 841 | 1329 |
| 1031 | 14.12 | 649 | 1138 |
| 1334 | 14.16 | 952 | 1437 |
| 1203 | 14.16 | 821 | 1306 |
| 1033 | 14.09 | 651 | 1139 |
| 1560 | 14.13 | 1178 | 1666 |
| 1376 | 14.16 | 994 | 1522 |
| 986 | 13.64 | 604 | 1102 |

* These data represent Lake Roosevelt; Lines 1AN, 2AS, 1BN, 1BS, 2BS, 1CN, 1CS, 2CS; and finally Lake Roosevelt. The line indication such as 1AN means line 1, first pass, north half, etc.

**Cosmic radiation flux C is dependent upon the pressure according to $C = 137\ e^{(15-P)/2.55}$.

TABLE 4. Nonterrestrial background computed from the adjusted gross count rate, fitted to photopeak area data. (From Feimster, et al., 1976)

| Line | Gross Count Rate (cps) | Fitted Adjusted Gross Count Rate (CPS) | Resultant Nonterrestrial bkg (cps) |
|---|---|---|---|
| 1A (AM) | 3682 | 2500 | 1307 |
| 1B (AM) | 3780 | 2500 | 1399 |
| 1C (AM) | 3776 | 2500 | 1389 |
| 1A (PM) | 3837 | 2500 | 1381 |
| 1B (PM) | 3526 | 2500 | 1070 |
| 1C (PM) | 3065 | 2500 | 1009 |

count rate for March 18, 1975, can be solved for by the equation:

$$\Gamma_2 = \frac{\Gamma_1(1 + M_1)}{1 + M_2} \qquad \text{(Eq. 7)}$$

where

$\Gamma_1$ and $M_1$ = adjusted gross count rate and soil moisture, respectively, on November 21, 1972

$\Gamma_2$ and $M_2$ = Unknown adjusted gross count rate and known soil moisture from photopeak area data on March 18, 1975.

The average adjusted gross count rate and soil moisture during November 21, 1972 was 2553 cps and 19%, respectively. The average soil moisture value determined from the photopeak area analysis of the March 18, 1975, survey data was computed to be 21.5% (average of the moisture values computed from the $^{40}K$ and $^{208}Tl$ photopeak areas). Substituting the appropriate values into (Eq. 7), the adjusted gross count rate is:

$$\Gamma_2 = \frac{2533 \text{ cps } (1.190)}{(1.215)} = 2500 \text{ cps} \qquad \text{(Eq. 8)}$$

To solve for the nonterrestrial component (radon + aircraft background + cosmic), the adjusted gross count is subtracted from the total gross count. The subtraction is accomplished by making use of the following two equations:

$$GC_{NET} = GC_{TOT} - (\text{aircraft background} + \text{radon} + \text{cosmic}) \qquad \text{(Eq. 9)}$$

$$GC_{ADS} = GC_{NET}\, e^{0.054\,(AM-17)} \qquad \text{(Eq. 10)}$$

where

$GC_{NET}$ = total gross count less the nonterrestrial component

$GC_{TOT}$ = total gross count

$GC_{AJD}$ = net gross count adjusted for air mass attenuation

AM = air mass

The total gross count ($GC_{TOT}$) is measured, and the expected adjusted gross count ($GC_{ADJ}$) was established from the peak area soil moisture data (Eq. 8). Combining equations gives:

$$GC_{ADJ} = (GC_{TOT} - \text{aircraft background} + \text{radon} + \text{cosmic}/2.55) \times e^{0.054(AM-17)} \quad \text{(Eq. 11)}$$

Solving for the nonterrestrial component leads to:

$$(\text{aircraft background} + \text{radon} + \text{cosmic}) = GC_{TOT} - GC_{ADJ}\, e^{-0.054\,(AM-17)} \quad \text{(Eq. 12)}$$

Substituting the values for the aircraft and cosmic, the equation becomes:

$$(290 + \text{Radon} + 137e^{(15-p)/2.55}) = GC_{TOT} - GC_{ADJ}\, e^{-0.54(AM-17)} \quad \text{(Eq. 13)}$$

This allows computation of the total nonterrestrial component as well as the radon singly. Table 4 lists the values that are computed from this equation. Example 1 considers the first case in Table 4.

Ex. (1)

$GC_{TOT} = 3682$

$AM = 17.91$

$GC_{ADJ} = 2500$

$$(\text{aircraft background} + \text{radon} + \text{cosmic}) = GC_{TOT} - GC_{ADJ}e^{-0.054(AM-17)}$$

$$= 3682 - 2500e^{-0.054(1791-17)}$$

$$= 1302 \text{ (nonterrestrial component)}$$

Substituting: aircraft background = 290

$$\text{cosmic} = 137\, e^{(15-p)/2.55}$$

$$\text{Radon} = 1302\text{-}290\text{-}137\ e^{(15-14.12)/2.55}$$

$$= 819 \text{ cps}$$

This adjusted gross count rate was used for the two-segment average of each pass made over the survey line listed in Table 4.

Soil Moisture Ground Measurements

Four points were sampled to a depth of 15 cm in each of 46 fields (16 vegetated, 30 bare) on each side of two flight lines in the following intervals: 0-1 cm, 1-2 cm, 2-5 cm, 5-9 cm and 9-15 cm. At each point, five samples were taken from the top and five samples from the bottom of the furrows. Average moisture contents for each of the four points were computed from each respective five interval samples. Soil moisture computed from soil samples and weighted to a depth of 9 cm were chosen to compare with the aerial data. The weighing equation for the 9-cm depth is written as:

$$\%\ \text{moisture (0-9 cm)} = 1/9\ (\%\ \text{mois. (0-1 cm)} + \%\ \text{mois. (1-2 cm)} + 3 \times \%\ \text{mois. (2-5 cm)} + 4 \times \%\ \text{mois. (5-9 cm)}$$

Table 5 lists all the areas that samples were taken from and their corresponding moisture values weighted for a 9-cm depth using the above relationship.

The results in Table 6 show that moisture values computed from the gross count rate of the aerial data of March 18, 1975, are slightly higher than the ground-based measurements during the same period as measurements taken on November 21, 1972, and March 18, 1975. The average of the ground sampling moisture values was very nearly the same as the moisture value computed from the photopeak area data.

As explained earlier, the gross count data are affected by the

TABLE 5. Soil moisture values from soil samples weighted for the sampled 9-cm soil depth. (From Feimster et al., 1976)

| Field | Average soil moisture values (% by weight of soil) North Point | South Point |
|---|---|---|
| 97 (A&B) | 23.19 | 22.53 |
| 99 " | 19.78 | 19.43 |
| 101 " | 19.78 | 17.88 |
| 102 " | 29.98 | 31.75 |
| 103 " | 23.59 | 23.97 |
| 104 " | 27.25 | 28.98 |
| 105 " | 25.89 | 26.81 |
| 106 " | 30.30 | 27.90 |
| 107 " | 31.30 | 33.78 |
| 111 " | 22.89 | 28.27 |
| 112 " | 27.71 | 29.74 |
| 113 " | 27.27 | 28.98 |
| 114 " | 20.53 | 18.69 |
| 115 " | 24.77 | 27.75 |
| 116 " | 22.95 | 21.22 |
| 121 " | 15.56 | 20.99 |
| 123 & 124 | 24.10 | 23.09 |
| 126 (A&B) | 19.17 | 18.77 |
| 127 & 128 | 19.03 | 19.40 |
| 129 & 130 | 16.90 | 13.49 |
| 131 & 132 | 21.09 | 19.94 |
| 133 (A&B) | 9.38 | 8.20 |
| 134 & 135 | 18.11 | 14.47 |

TABLE 6. Comparison of soil moisture values determined from ground sampling and from aerial measurements. (From Feimster, et al., 1976)

| Location on line 1 (mile no.) | Soil Moisture (% by weight) Results from soil samples Nov 21, 1972 | Results from soil samples Mar 18, 1975 | Results from aerial measurements Mar 18, 1975 |
|---|---|---|---|
| 9 | 21.3 | 21.3 | 16.6 |
| 11 | 28.8 | 26.7 | 32.2 |
| 12 | 22.3 | 22.1 | 25.6 |
| 13 | 18.2 | 16.2 | 19.1 |
| Avg. value for entire survey line | 19.0 | 21.56±4.3 | 24.3±6.1* 21.5** |

* These results are from the mile-by-mile gross gamma count rate analysis.

**These results are from the analysis of gamma photopeak data, averaged over the entire survey line.

airborne radon activity which is the major cause of the differences shown in Table 6 of the ground-based moisture determination and those from the aerial gross count data.

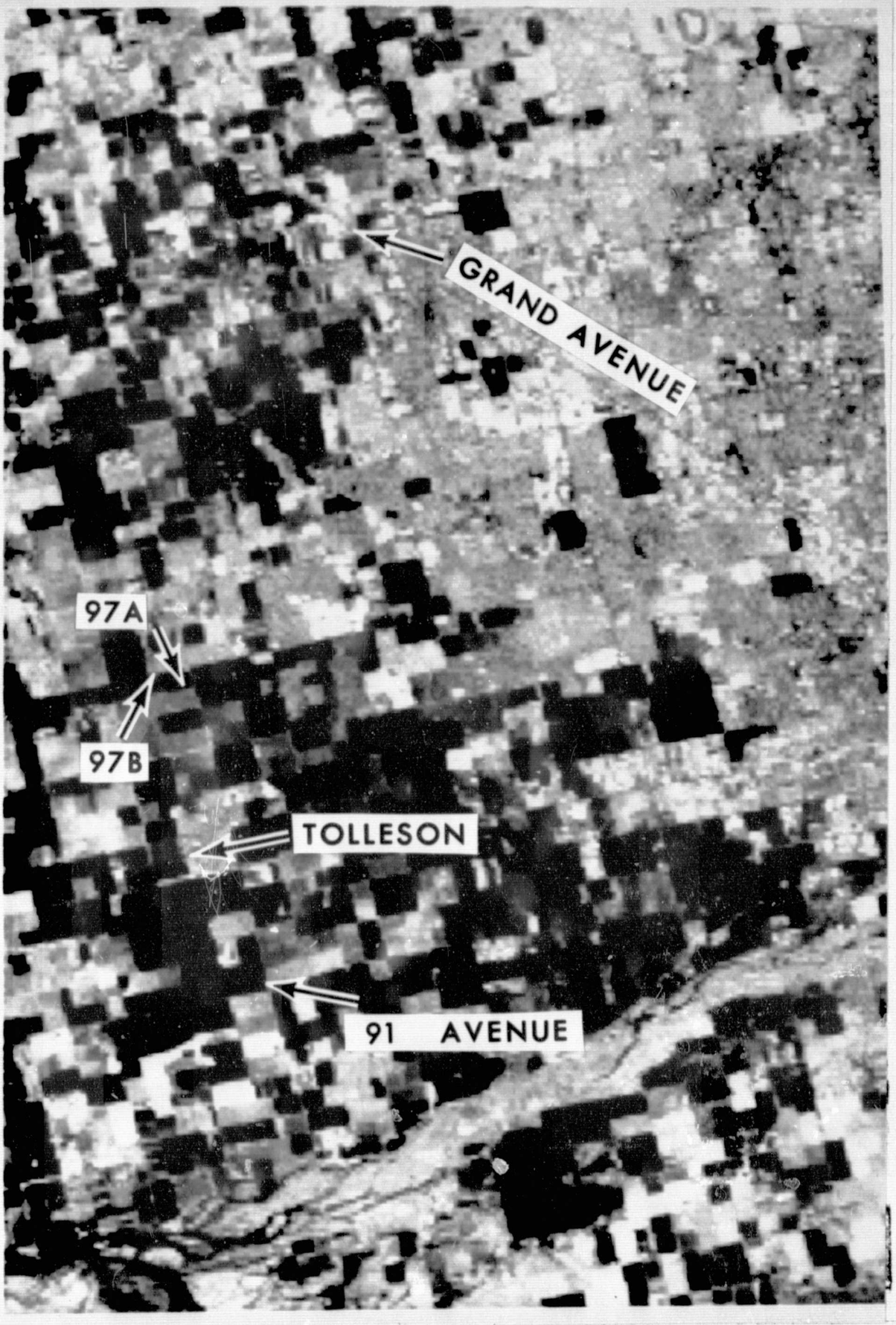
Landsat Investigation - Visible and Near-IR

Introduction

Findings of previous investigators (Sabatini, et al, 1971; Steiner and Guterman, 1966; Merritt and Hall, 1973; Planet, 1970; and Angstrom, 1925) indicate that the reflectance of soils decreases in the visible and near-IR as soil moisture increases above the wilting point. The change in reflectance is also dependent to a significant degree on the soil type, with dark soils showing a greater change than light soils. The availability of Landsat-1 data (Orbit 13,484 ID 1967-17154) on the day preceding the ground observations at Phoenix permitted a test of the above-mentioned investigators' findings.

Procedure

The March 17, 1975, Landsat data were displayed pictorially in Digital Muirhead Display images (DMD's) from 7-track CCT's with bands 5 and 7 side-by-side (see figure 5). The test site along and on either side of 91st Avenue was located in the imagery and enlarged, figure 6a and 6b, to better view the area. A microfilm composite of the area in rectified 32 by 32 pixel arrays provided the quantitative data used in the regression analyses. One such array is presented in figure 7 showing 94, 95, 96a, 97A, 97B, 98A, 99A, 99B, and 100A. fields / Even though the images appear "blocky" due to the enlargement, the 80-meter resolution of the MSS still allowed 25-35 satellite data points per field. Variation in the number of points was a function of a given field's boundaries with respect to the scan lines of the MSS.




ORIGINAL PAGE IS
OF POOR QUALITY

Fig. 6a. Enlarged segment of MSS band 5 shown in Figure 5, covering test site and the immediate vicinity around Tolleson, Arizona.

REPRODUCIBILITY OF THE
ORIGINAL PAGE IS POOR

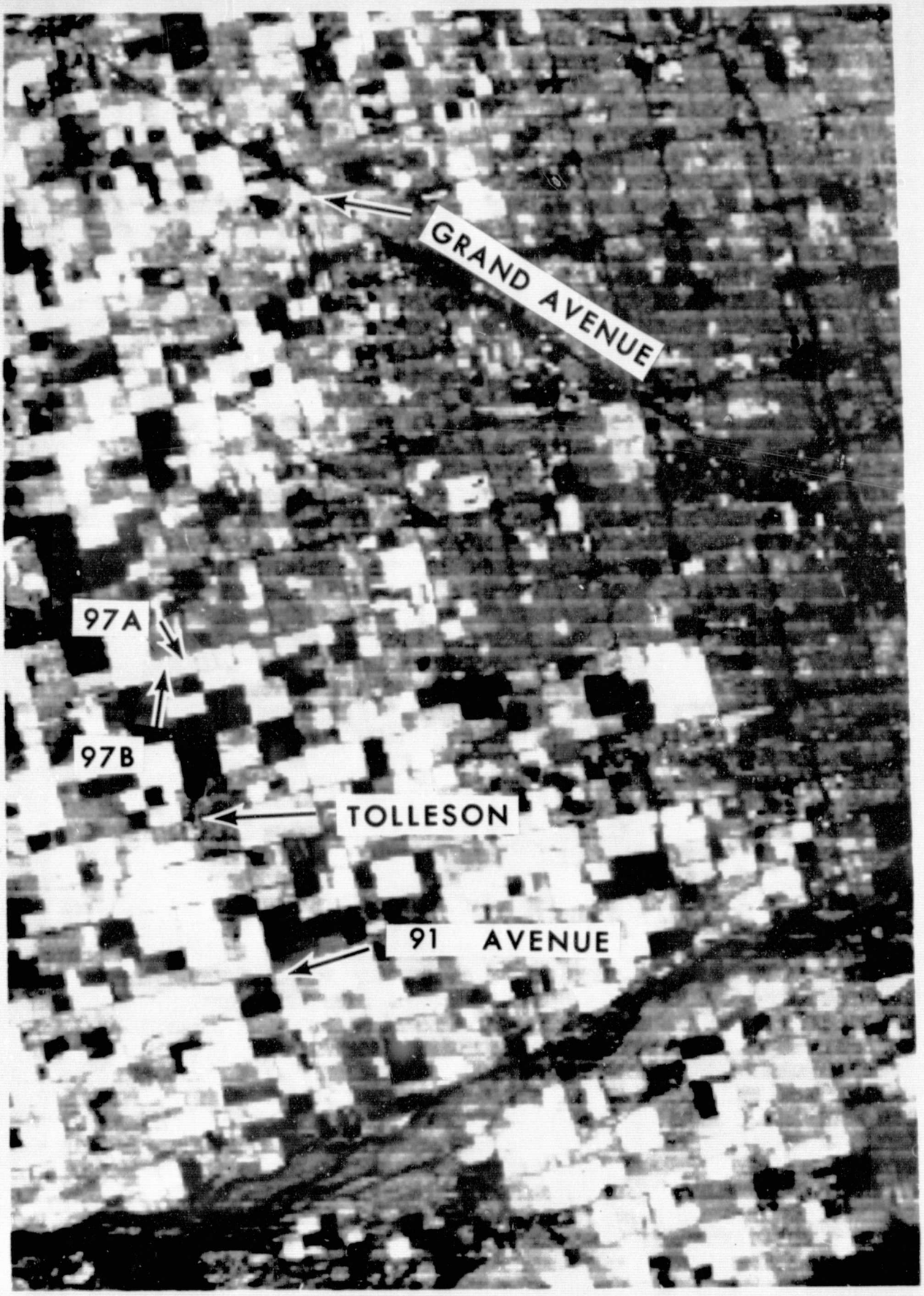



Fig. 6b. Enlarged segment of MSS band 7 shown in Figure 5, covering test site and the immediate vicinity around Tolleson, Arizona.

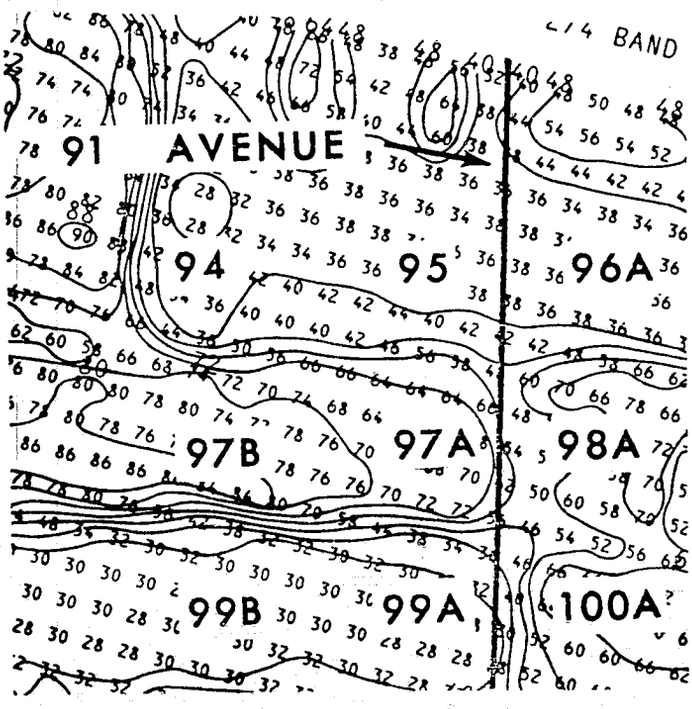



Fig. 7 Example of full-resolution contoured microfilm printout of MSS band 7 raw data counts, covering fields 94, 95, 97A, 97B, and portions of fields 91, 92, 93A, 98A, 99A, 99B, and 100A.

ORIGINAL PAGE IS
OF POOR QUALITY

The satellite values were averaged for each field for direct comparison with the averaged soil moisture values taken from Blanchard's (1975) report. As the reflectance measured by the MSS is essentially from the surface of the vegetation or soil, field soil moisture values of the top one centimeter (for both top and bottom of the furrow) from the following morning's data survey (March 18, 1975) were used to correlate with Landsat MSS readings. The difference in time between the two data sets--about 24 hours--is not as critical as comparing early morning and late afternoon values on the same day. Jackson et al. (1975) showed that there is a recovery of soil moisture, an upward flux of moisture, beginning several hours before sunset, to partially replace those losses (up to 75% when the soil surface is relatively dry) due to evapotranspiration during the day. The recovery may be seen in figure 8. Satellite MSS reflectance values and soil moisture values for vegetated and bare fields were compared.

Results and Discussion

Plots of the various MSS band reflectances versus soil moisture in percent are presented in figures 9a-d and 10. There appears to be little change in reflectance for vegetated fields in either of the visible bands, MSS 4 and 5. However, in the near-IR (MSS 6 and 7), there is an increasing reflectance in both bands with increasing soil moisture for alfalfa, but not for wheat. Apparently the additional moisture is manifest in a more vigorously growing alfalfa plant, giving a brighter response in bands 6 and 7. The same does not seem to be true for wheat.

All bare fields showed a decrease in reflectance as soil moisture

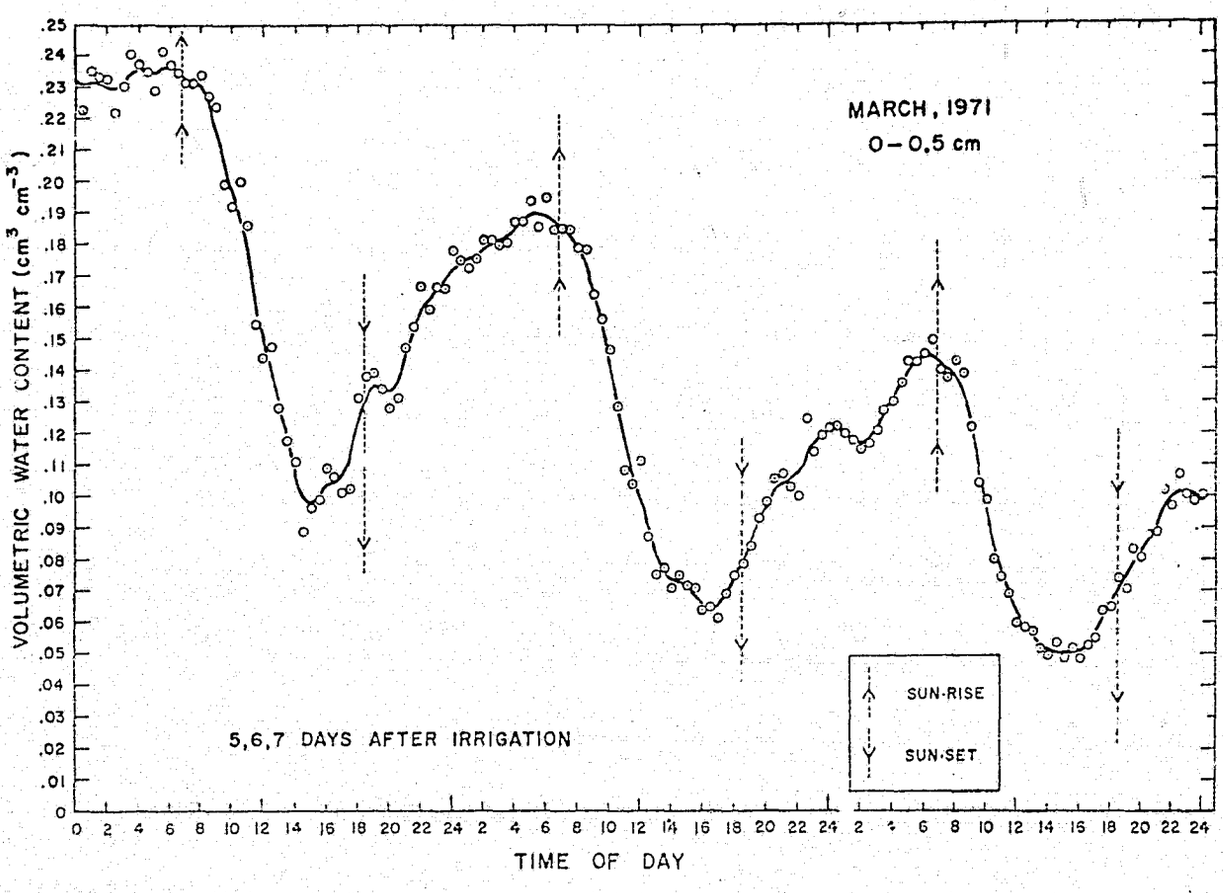



Fig. 8. Volumetric water content in the 0.0 to 0.5-cm increment versus time for 3 days during March 1971. The solid line represents smoothed data and the symbols represent the measured values. (from Jackson, 1973)

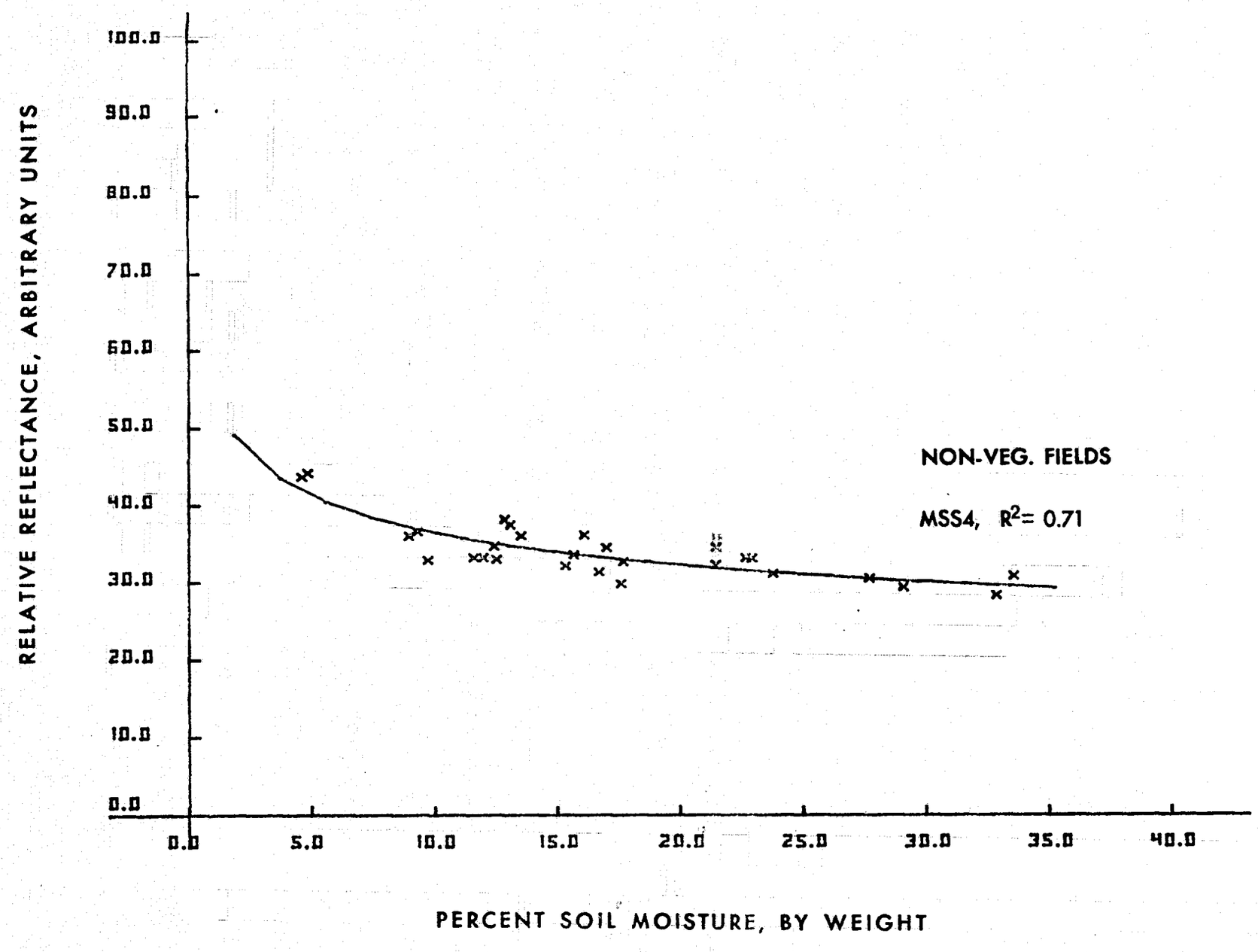



Fig. 9a. Regression analysis of percent soil moisture vs. MSS reflectance raw counts, MSS band 4, bare fields only (power fit).

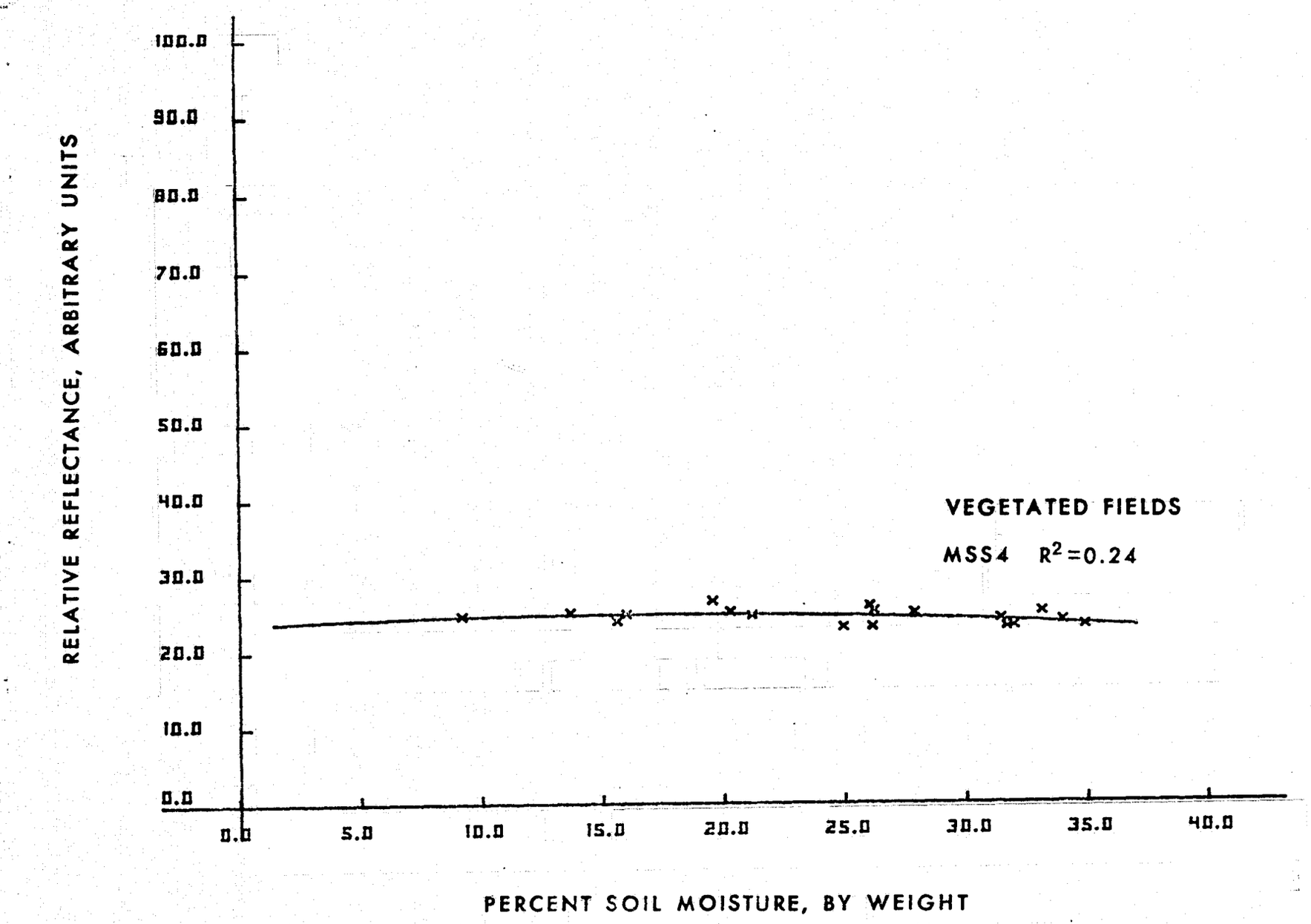



Fig. 9b. Regression analysis of percent soil moisture vs. MSS reflectance raw counts, MSS band 4, vegetated fields only (parabolic fit).

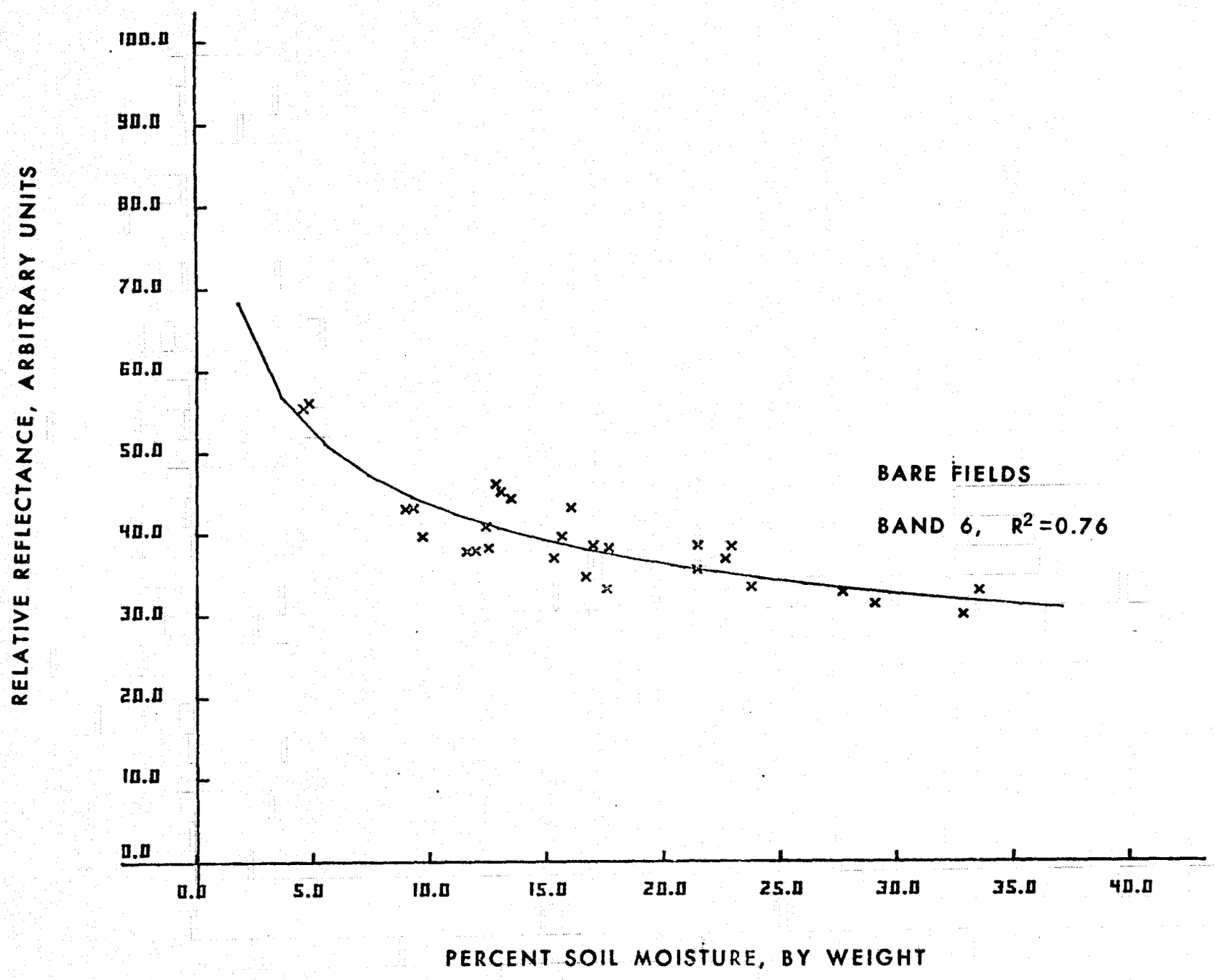



Fig. 9c. Regression analysis of percent soil moisture vs. MSS reflectance raw counts, M band 6, bare field only (power fit).

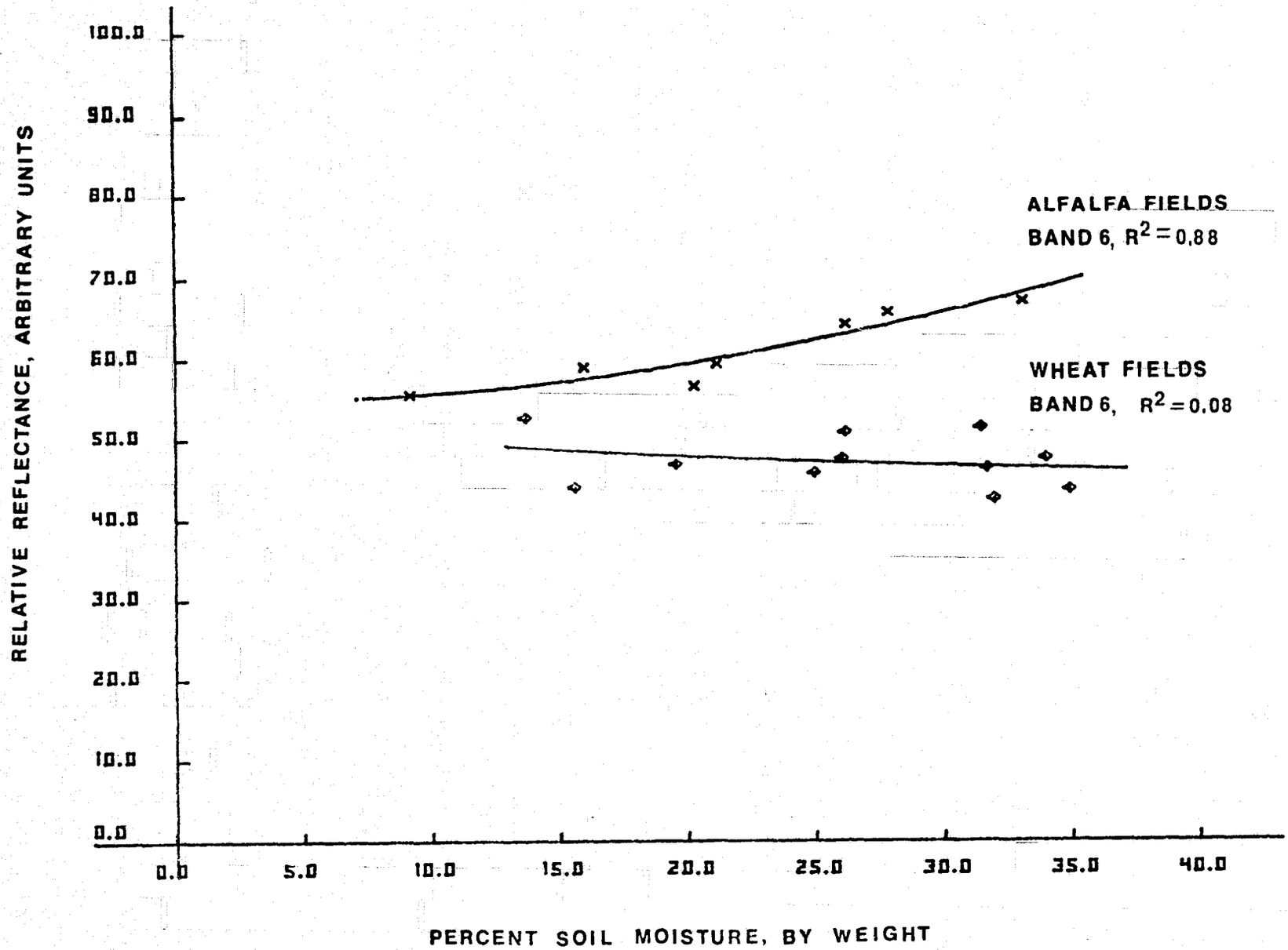



Fig. 9d. Regression analysis of percent soil moisture vs. MSS reflectance raw counts, MSS band 6, vegetated fields only, alfalfa (parabolic fit) and wheat (power fit) separated.

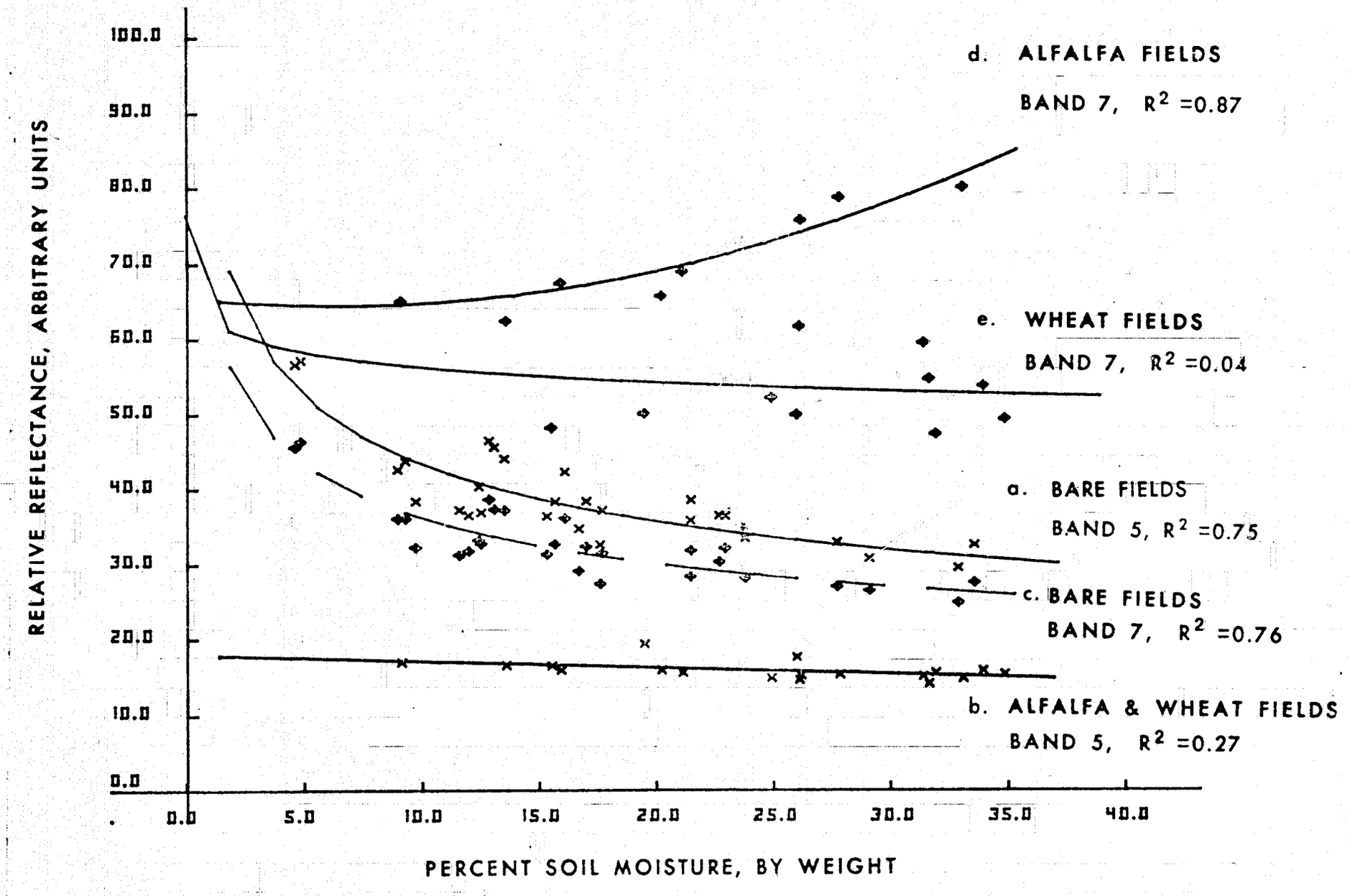



Fig. 10. Combined plots of MSS bands 5 and 7 raw counts vs. soil moisture: a) MSS band 5, bare fields only (power fit); b) MSS band 5, vegetated fields only (straight-line fit); c) MSS band 7, bare fields only (power fit); d) MSS band 7, alfalfa only (parabolic fit); and e) MSS band 7, wheat only (logarthmic fit).

increased, with a power fit to the data consistently supplying the best correlation of the five available curves for data fitting. The amount of variance, $r^2$, ranged from 0.71 for MSS 4 to 0.76 for MSS 6 and 7; $r^2$ for MSS 5 was 0.75. Even though the fits were good, most of the reflectance decrease occurred between 5 and 20 percent soil moisture with very little further decrease from 20 to 35 percent.

Only 18 data points were available for vegetated fields, 8 from fields growing alfalfa and 10 from fields in wheat. The two visible bands in the MSS, 4 and 5, showed no change in reflectance as soil moisture varied from 5 to 35 percent. The brightness of wheat fields in the near-IR (MSS 6 and 7) also indicated almost no dependency on soil moisture changes. The alfalfa fields in the near-IR increased in reflectance as the soil moisture increased. Unlike the curve for bare fields, near-IR reflectance values did not level off at high soil moisture. Rather the reflectance increased at a slightly increasing rate. One possible explanation for the differences noted between wheat and alfalfa is that the alfalfa provides a solid canopy; but the wheat, being only 22-30 cm (9-12 inches) high, did not provide a complete vegetative cover, and thus the satellite was integrating the response of both bare soil and vegetation. The alfalfa apparently responded to the increased soil moisture by growing more vigorously and appearing more reflective.

Though visible and near-IR remote sensors provide some indication of soil moisture at the surface of bare fields, the correlations are best between 5 and 20 percent soil moisture.

Figure 11 shows Landsat MSS band 7 raw data (full resolution) superimposed on a false color near-IR aerial photograph. The aircraft

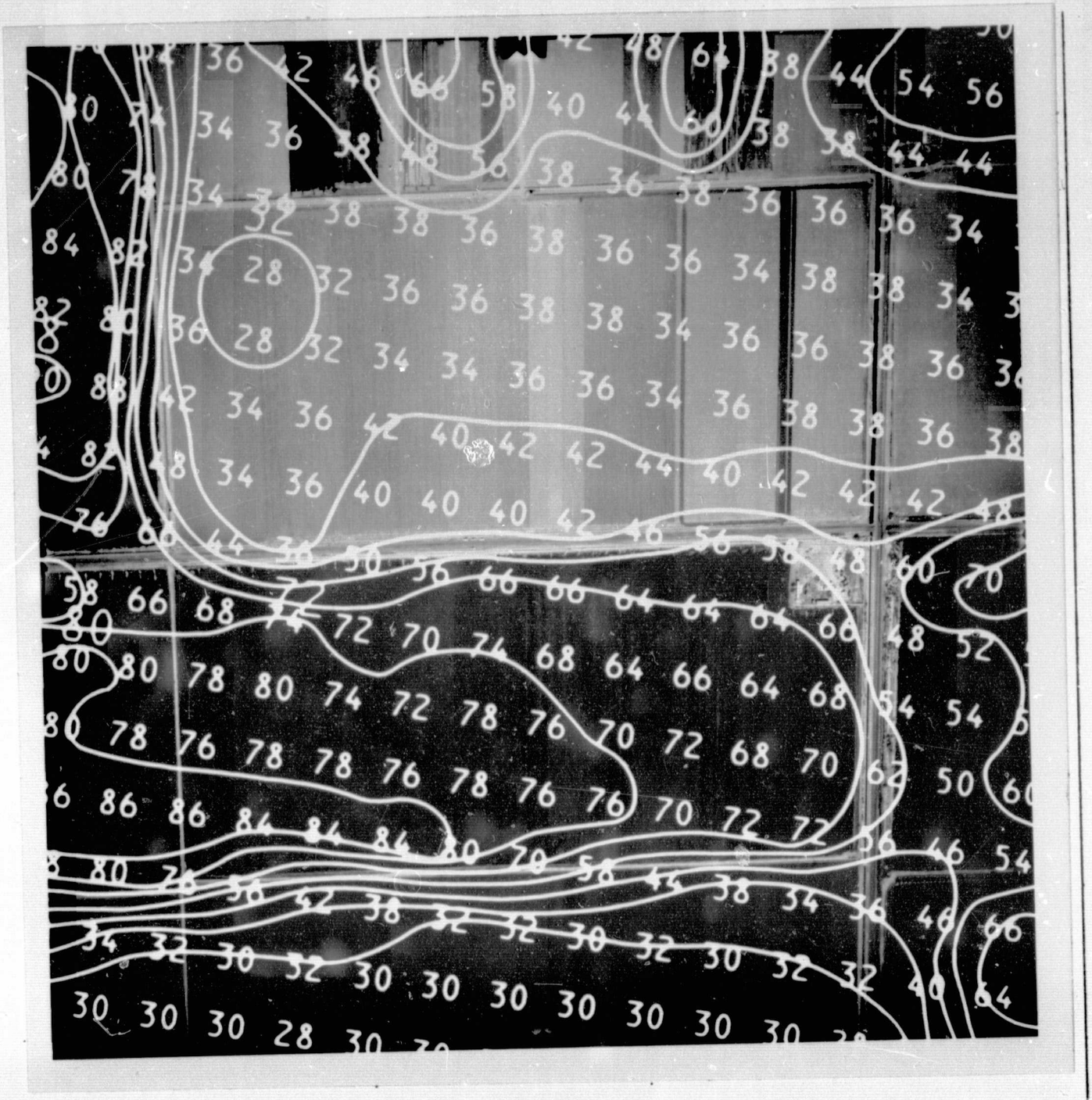


Fig. 11. False-color aerial photogaaph of fields 94, 95, 97A, 97B as well as portions of fields 91, 92, 93A, 98A, 99A, 99B, and 100A, overprinted with MSS band 7 raw data from Landsat-1 image (3/17/75, 1967-17154). See Fig. 7.

REPRODUCIBILITY OF THE
ORIGINAL PAGE IS POOR

data were collected on the afternoon of March 18 near 1 P.M. local time; the Landsat values were obtained at 10:00 A.M. local time on March 17. The area is west of Phoenix and covers a portion of the test site located north of Tolleson. 91st Avenue runs vertically (N-S) through the right (east) portion of the image. Red areas indicate actively growing vegetation. The large rectangular area just below the center of the image is test fields 97A and B, planted in alfalfa. Acquisition of soil moisture values, obtained close to the time of aircraft overpass, differed from the Landsat-acquired near-IR information by approximately 27 hours. However, as shown by Jackson et al. (1975), the effects of differences in observation times are somewhat compensated by the nocturnal replenishment of surface soil moisture from reserves deeper in the ground. Surface (0-2 cm) moisture values (in percent of dry weight) for fields 97A and B ranged from 13.70 to 27.65. The driest areas occurred in field 97A adjacent to 91st Avenue; the wettest along the western (left) edge of field 97B. As shown in figure 10 a general increase in Landsat MSS band 7 values for alfalfa fields occurs as soil moisture increases. MSS band 7 values range from 64 in the drier portion of field 97A to 84 at the wettest locations in field 97B. This proportional relationship of soil moisture to MSS band 7 values was found to exist for all alfalfa fields sampled in the study (see figure 10).

The amount of useful information from visible and near-IR is miniscule when compared to that provided by passive microwaves and potentially from the thermal IR. Further efforts to predict soil from remote platforms should place the emphasis on the microwave portion of the spectrum and thermal IR where the most favorable results have

been achieved. For vegetated fields, though the MSS data were limited, crops growing complete canopies such as does alfalfa, may manifest increases in soil moisture by growing more vigorously.

NOAA Investigation - Thermal IR

Another area of the spectrum that might provide some information on soil moisture and its change with time is the thermal IR at 10.5-12.5μm. Work done by Idso, et al. (1975) indicate that if the soil type is known, the amplitude of the diurnal surface soil temperature wave is a function of the water content in the surface layer. Maximum values of surface soil temperatures were observed about 1.5 hours after local noon; minimum surface soil temperatures just before sunrise.

The 30-minute interval between observations by NOAA's SMS/GOES satellites allows measurements of temperatures near the daily extremes and thus could closely measure the daily amplitude of surface soil temperatures. A computer program has been developed by J. Pritchard (personal communication) that subtracts any two SMS/GOES tapes. An example is shown in figure 12. The difference between the two indicated observations is in the center, the subtrahend on the left, and the minuend on the right.

Unfortunately, two problems exist with the data that preclude its usefulness as a potential soil-moisture monitor. Figure 13 vividly displays the problem of low resolution. In this image the blockiness of the individual 8-km resolution pixels is evident. Moreover the entire Phoenix test site area does not even fill one 8 by 8 km pixel (being only 3 km by 8 km). The test site's approximate location is indicated, as are other more easily identified landmarks. The second problem involves the difficulty in obtaining taped SMS/GOES data. This

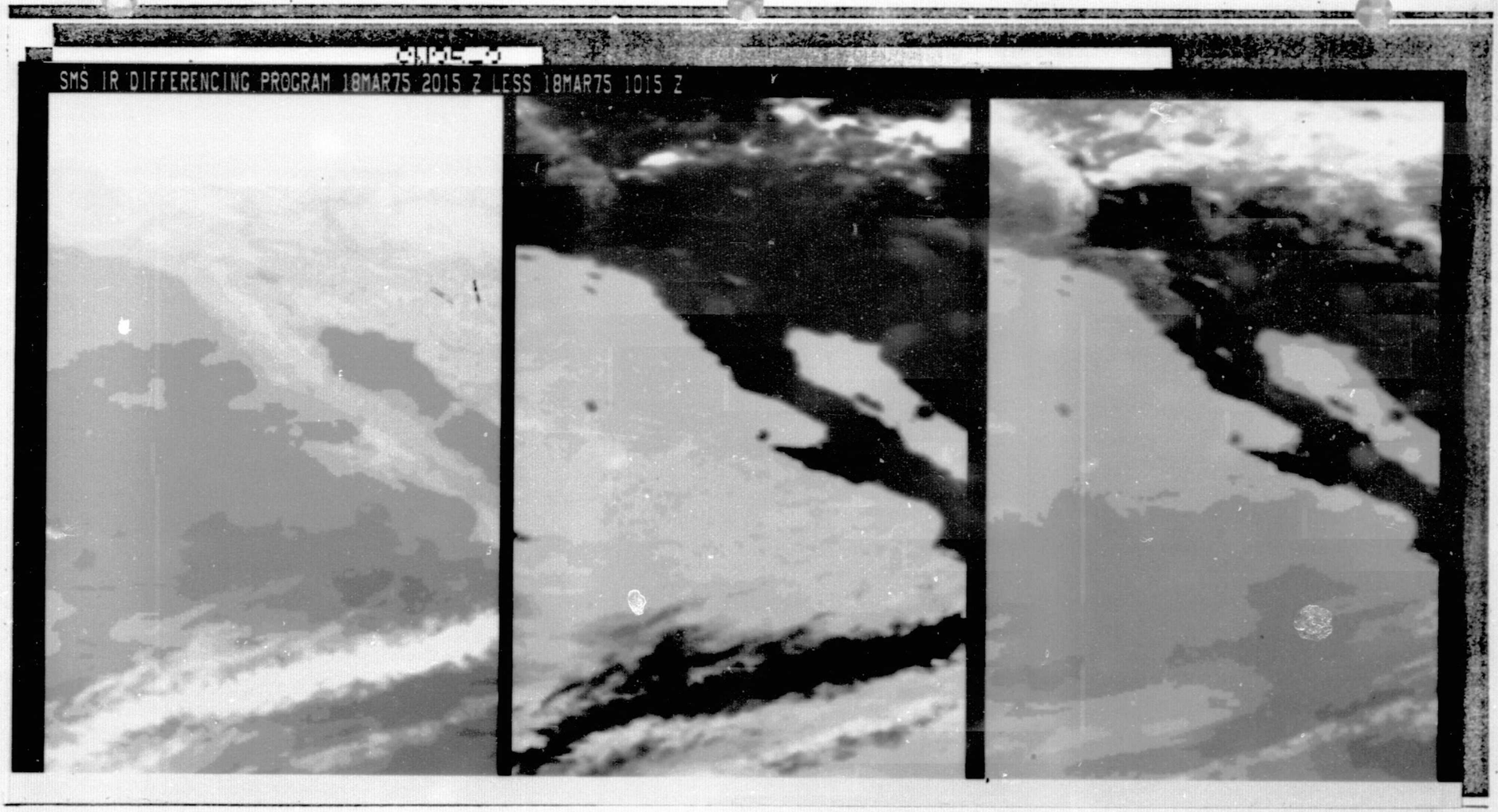



Fig. 12. SMS-2 8-km resolution thermal-IR (10.5-12.5 m) imagery of southwestern North America and eastern Pacific Ocean. Image on left was observed at 2015 GMT on 3/17/75. Image on right was observed at 1015 GMT on 3/18/75. Image in center was obtained by subtracting temperatures measured on 3/18/75 from those measured on 3/17/75.

ORIGINAL PAGE IS OF POOR QUALITY

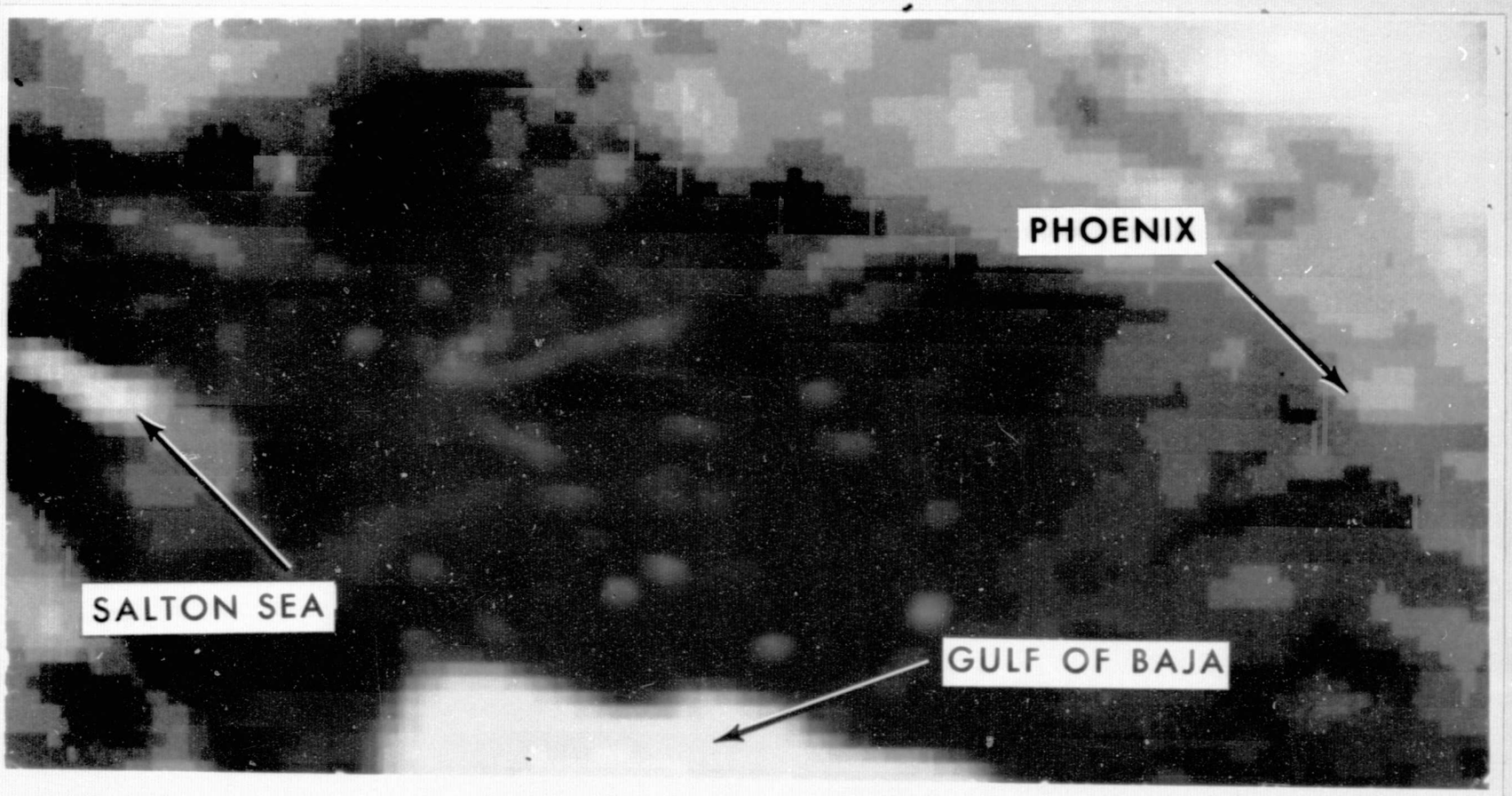



Fig. 13. Enlarged portion of 8-km thermal-IR (10.5-12.5 m) image acquired by SMS-2 at 1015 GMT on 3/18/75. Area viewed covers southwestern U.S. (including Phoenix test site) and portions of Baja, California, and the Gulf of Baja.

example was obtained only by special request, as GOES tapes are not archived. The reason for not saving tapes is lack of storage facilities. Thus until tapes at an improved resolution from thermal sensors on geosynchronous satellites become a reality, the potential for a remote thermal soil moisture monitor will not be realized.

Conclusions

Estimates of soil moisture were obtained from visible, near-IR gamma ray and microwave data. Attempts using GOES thermal-IR were unsuccessful due to poor resolution (8 km), even though laboratory studies support the thermal inertia concept as a valid means to measure soil moisture fluctuations. Microwaves were the most effective at soil moisture estimates, with and without vegetative cover. Gamma rays provided only one value for the entire test site, produced by many data points obtained from overlapping 150-meter diameter circles. Even though the resulting averaged value was near the averaged field moisture value, this method suffers from atmospheric contaminants (randon daughters), the need to fly at low altitudes (150 m) and the necessity of prior calibration of a given site. Visible and near-IR relationships are present for bare fields but appear to be limited to soil moisture levels between 5 and 20 percent. The densely vegetated alfalfa fields correlated only with near-IR reflectance. Soil moisture values from wheat fields showed no relation to either visible or near-IR MSS data.

Summary of soil moisture

The study, involving aircraft and remote sensors, evaluated the effectiveness of portions of the electromagnetic spectrum to estimate soil moisture. Tests were made at two sites, viz., Phoenix Arizona, and Luverne, Minnesota, using data collected by visible, near-IR, thermal IR, microwaves and gamma-ray sensors. The results of these studies indicate the greatest potential for remote soil moisture monitors to be thermal IR and microwave sensors. Operationally both suffer from a lack of resolution. Microwaves can also penetrate vegetation and the soil surface to provide average soil moisture estimates to almost 8 centimeters deep. Thermal inertia estimates are of necessity obtained from bare fields and can only indirectly determine moisture conditions of the subsurface layer.

Findings of the gamma-ray surveys are within range of field data. However, the method has no future in any satellite program, being limited to very low altitude (150 m) aircraft flights. The technique necessitates at least one previous flight over a given region to calibrate the system. Noise from radon daughters must be taken into account. The gamma-ray soil moisture technique does provide a check for systems such as remote passive microwaves where coarser resolution prevails.

Visible MSS data from Landsat correlated with soil moisture only when the soil was bare, and would thus be a very limited tool to maintain year-round monitoring of soil-moisture variations. The near-IR appears somewhat more promising showing correlation with bare ground and some correlation with changes in soil moisture when a vegetative cover is present (alfalfa). But results for wheat, for the sparse data

available, indicated no relationship between satellite near-IR reflectance and soil moisture. The overall results of the Landsat MSS data are marginal at best and are far inferior to those soil-moisture estimates obtained by the microwave technique.

Future

The continued development of sensors for future satellites provides the hope that a better understanding of soil moisture variations will be possible via remote sensing. In particular there were five satellites launched in 1978, each containing one or more sensors collecting data pertinent for soil moisture evaluation. Landsat-3, launched on March 5, unlike its predecessors, has a thermal channel in the 10.5-12.5μm portion of the spectrum. Unfortunately outgassing problems have continually plagued the thermal channel resulting in an increased NEΔT (noise equivalent temperature increment) now exceeding 2.5°C. This degradation will, at some point, make the data totally useless, likely by June 1979.

Though still 1-km in resolution, the daily coverage provided by the thermal-IR of the AVHRR (Advanced VHRR) on TIROS-N, placed in orbit on 13 October 1978 has a lower noise level, only 0.1°C NEΔT (noise equivalent difference in temperature), than the IR scanners on board earlier NOAA satellites. The HCMR (Heat Capacity Mapping Radiometer) on board the HCMM satellite, oribiting the Earth since 26 April 1978, has a 500 m resolution with a 1½ to 3½-day cycle (8-day cycle for thermal inertia measurements). The thermal information collected by these three satellites will permit the furtherance of studies such as the one presently being done in Phoenix (Jackson, et al., 1975). The HCMM satellite scattered

a significant loss of power on 28 February 1979 resulting in restricted data collection beginning 10 March 1979.

The other two satellites launched in 1978 are Seasat-A and Nimbus-G. Both satellites collected information of Earth in the microwave region of the spectrum. Seasat-A was launched on 26 June 1979; Nimbus-G on 24 October 1978.

Both Nimbus-G and Seasat-A have onboard the Scanning Multi-frequency Microwave Radiometer (SMMR). Unfortunately the resolution (25 to 125 km) and wavelengths (6.6, 10.69, 18, 22.235, 36 GHz) are not optimum for soil moistrre evaluation. The active microwave system on Seasat-A, known as SAR (Synethic Aperture Radar), imaged ocean and limited land areas at 1.35 GHz with a resolution of 25 m. This very high resolution imagery, though not in the optimum soil moisture wavelength range of 4.25 to 5.25 GHz, should provide useful information regarding soil moisture evaluation, particularly at areas the size of agricultural units (65 hectares). A massive power failure occurred 10 October 1978 terminating all functions of the spacecraft.

## References


Angstrom, A., 1925, The Albedo of Various Surface of Ground Geograf, Ann. 7, 323-343.

Batlivala, P.P. and Ulaby, F.T., 1977, Feasibility of Monitoring Soil Moisture using Active Microwave Remote Sensing, The Univ. of Kansas Center for Research, Inc., RSL Technical Report 264-12, NASA/JSC Contract NAS 9-14052.

Blanchard, B.J., 1975, Ground Truth Report 1975 Phoenix Microwave Experiment, Texas A&M Univ., Remote Sensing Center, College Station, Texas.

Bowers, S.S. and Hanks, R.J., 1965, Reflection of Radiant Energy from Soils, Soil Science, 100, pp. 130-138.

Burnash, R.J.C., Ferral, R.L., and McGuire, R., 1973, Generalized Streamflow Simulation, Cooperative development by Joint Federal and State River Forecast Center, Sacramento, Calif., 203 pp.

Condit, H.R., 1970, The Spectral Reflectance of American Soils, Photogrammetric Engineering, Sept. 1970, pp. 955-966.

Feimster, E.L., Fritzsche, A.E., 1975, Soil Moisture Survey at Luverne, Minnesota , EG&G Report EGG-1183-1975, Las Vegas, Nev., 29 pp.

Feimster, E.L., Fritzsche, A.E., and Jupiter, C., 1975, Soil Moisture Survey Experiment at Phoenix, Arizona, EG&G Report No. EGG-1183-1974, Las Vegas, Nev., 30 pp.

Idso, S.B., Schmugge, T.J., Jackson, R.D. and Reginato, R.J., 1975, The Utility of Surface Temperature Measurements for the Remote Sensing of Surface Soil Water Status, Journal of Geophysical Research, Vol. 80, No. 21, pp. 3044-3049.

Idso, S.B. and Ehrler, R.L., 1976, Estimating Soil Moisture in the Root Zone of Crops: A Technique Adaptable to Remote Sensing, Geophysical Research Letters, Vol. 3, No. 1, pp. 23-25.

Jackson, R.D., Reginato, R.J. and Idso, S.B., 1975, Timing of Ground Truth Acquisition during Remote Assessment of Soil-Water Content, Remote Sensing of Environment, Vol. 6, No. 4, pp. 249-255.

Merritt, E.S. and Hall, C., 1973, Soil Moisture Estimation Applications of Nimbus-3 HRIR-D (0.7-1.3μm) Observations, Final Report, Earth Satellite Corp., Contract No. 2-37098, 45 pp.

Orlov, D.L., 1966, Quantitative Patterns of Light Reflectance on Soils: I. Influence of Particles (aggregate) Size on Reflectivity; Diklady Soil Sci., No. 13. Supplement.

Planet, W., 1970, Some Comment of Reflectance Measurement of Wet Soil, Remote Sensing of Environment, Vol. 1, pp. 127-129.

Sabatini, R., Raochevsky, G. and Sissala, J., 1971, Nimbus Earth Resources Technical Report N.Z. Contract No. NAS-21617, NASA, Goddard Space Flight Center.

Schmugge, T., 1976a, Preliminary Results from the March, 1975 Soil Moisture Flight, NASA/Technical Memorandum, TMX 71197, 16 pp.

Schmugge, T., 1976b, Remote Sensing of Soil Moisture, NASA X-913-76-118.

Schmugge, T., Wilheit, T., Webster, Gloersen, P., 1976a, Remote Sensing of Soil Moisture with Microwave Radiometers-II, NASA TN D-8321, Wash., D.C., 34 pp.

Schmugge, T., Blanchard, B., Burke, W., Paris, J., Wang, Jr., 1976b, Results of 1974 Soil Moisture Flight, NASA TN C-8199, Wash., D.C., 58 pp.

Shockley, W.G., Knight, S.J., and Limpscomb, 1962, Identifying Soil Parameters with an Infrared Spectrometer. Proc. of the Second Symp. on Rem. Sens. of the Environ., Univ. of Michigan press, Ann Arbor.

Steiner, D. and Guterman, T., 1966, Russian Data on Spectral Reflectance of Vegetation, Soil and Rock Types, European Research Office, U.S. Army Contract DA-91-591-EUC-3863/OI-652-0106.

Stoner, E.R. and Horvath, E.H., 1971, The Effect of Cultural Practices on Multispectral Response from Surface Soil, Proc. 7th Int. Symp. of Remote Sens. Environ., Vol. III, pp. 2109-2113.

Blanchard, M.B., Greeley, R., and Goettleman, R., 1974, Use of Visible, Near-Infrared and Thermal Infrared Remote Sensing to Study Soil Moisture. NASA Technical Memo TM X-62, 543, 4 pp.

NOAA, 1975. Climatological Data--South Dakota, Vol. 79, No. 10, Environmental Data Service, National Climatic Center, Asheville, N.C.

Reginato, R.J., Idso, S.B., Vedder, J.F., Jackson, R.D., Blanchard, M.B., and Goettleman, R., 1976. Soil Water Content and Evaporation Determined by Thermal Parameters obtained from Ground-based and Remote Measurements. J. Geophys. Res., 81, 1617-1620

USDA, 1949. Soil Survey of Rock County, Minnesota Series 1938, No. 21.

REPRODUCIBILITY OF THE
ORIGINAL PAGE IS POOR

## LUVERNE, MINNESOTA SOIL MOISTURE SURVEY

### Description of Test Site

The Luverne soil moisture survey area lies in the extreme southwest corner of Minnesota, approximately 30 miles northeast of Sioux Falls, South Dakota (see figure 14). The test site is 8 miles long and is south of Luverne, Minnesota, and parallel to U.S. Highway 75 (see figure 15). The elevation of the test area is between 1,400 and 1,500 feet above mean sea level with slopes varying from 0 to 8%. Soil types consist mainly of silty clay loams and alluvial soils located near flood plains (see figure 16) and most of the acreage grown in corn, alfalfa, hay, and wheat (USDA, 1949).

### Soil Moisture Experiments

During the period of this study two soil moisture experiments were attempted in the Luverne test site area. The first was performed May 11-12, 1975, and the second on October 17, 1975. During both of these test periods, ground truth, meteorological conditions and aircraft and satellite remote sensing platforms were to be used to evaluate soil moisture conditions. Unfortunately during the May 11-12 test period cloud contamination prevented the use of satellite data and during the October 17 study no Landsat overpass was scheduled and no ground truth was collected.

### The May 11-12, 1975 Experiment

On May 11, light rain showers persisted until approximately 9:30 a.m. After these early morning showers, slow clearing commenced and by noon mostly clear skies prevailed. By 2:00 p.m., however, scattered showers and thunderstorms developed and continued throughout the afternoon. National Weather Service records for Luverne indicate 0.47 inches of rain

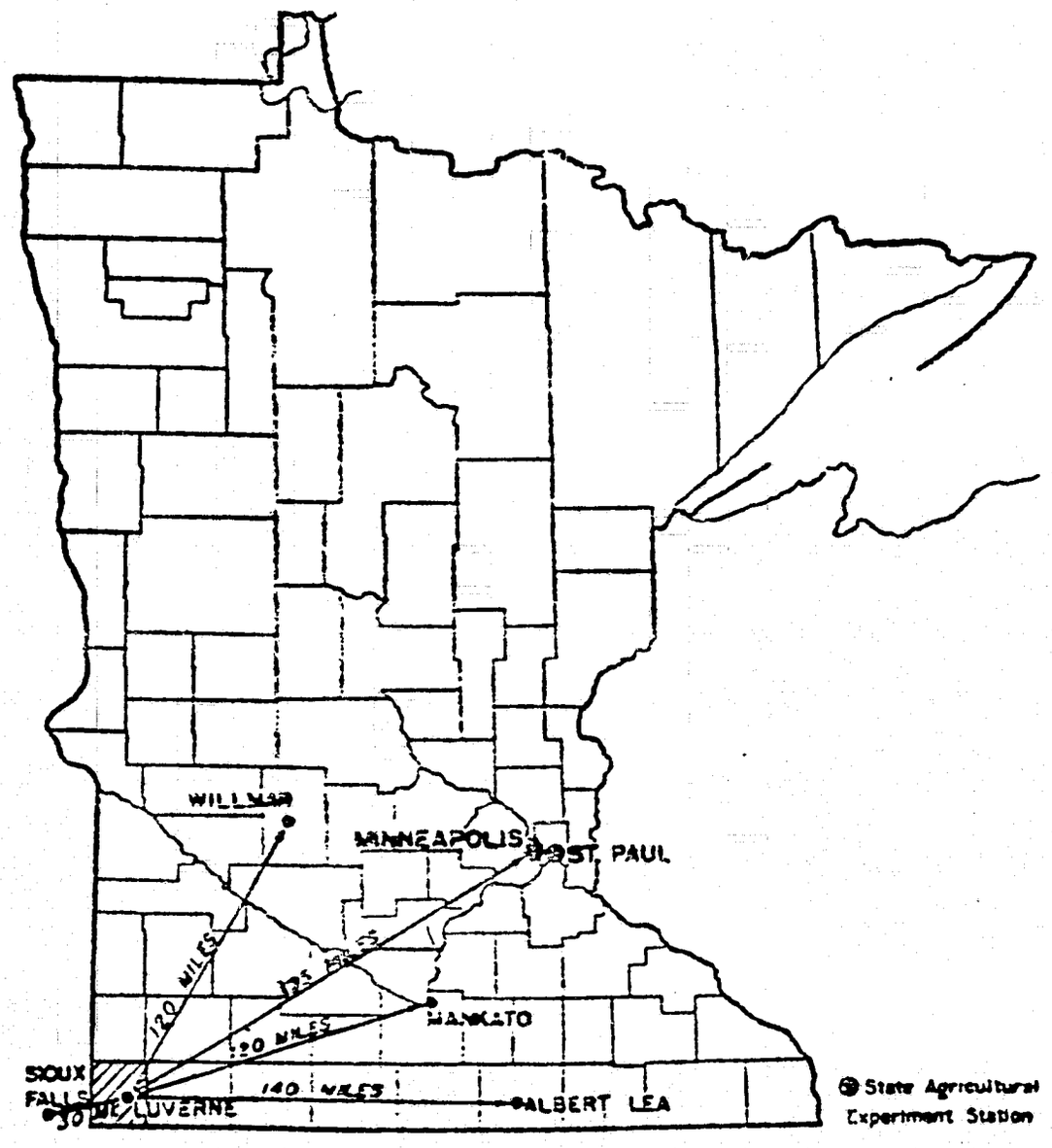



Fig. 14. Index map of Minnesota showing the location of Luverne.

REPRODUCIBILITY OF THE
ORIGINAL PAGE IS POOR

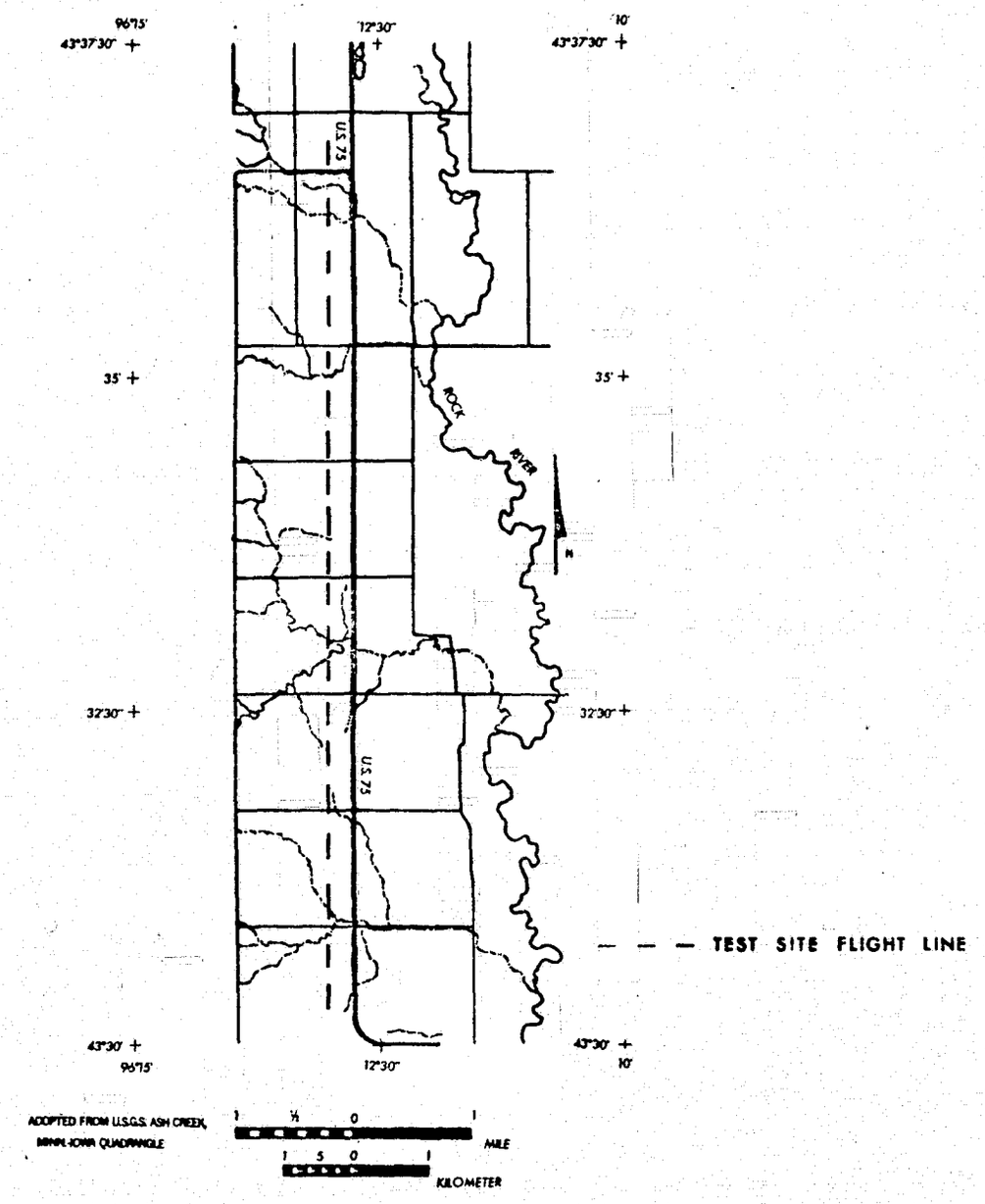
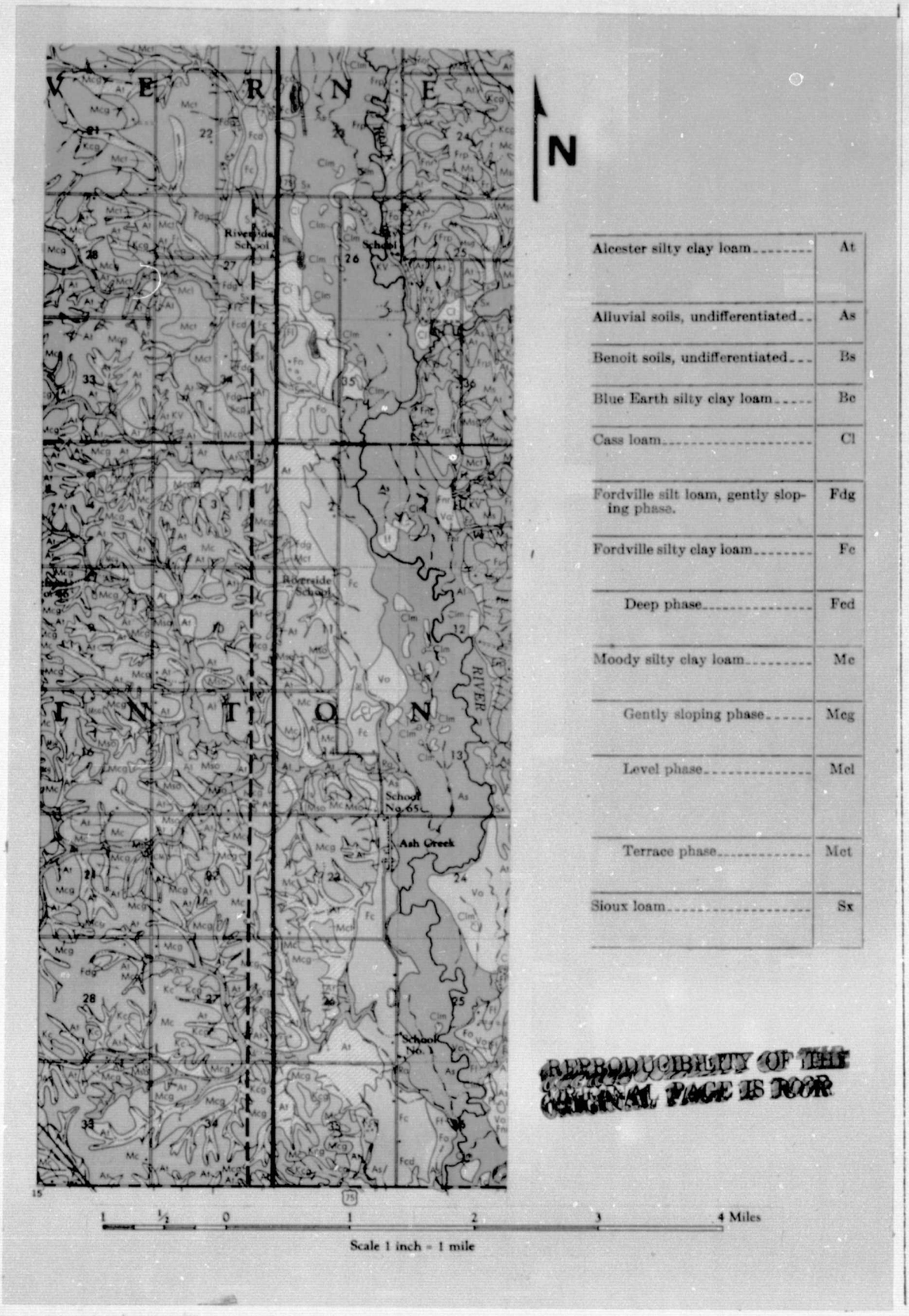



Fig. 15 Map of Luverne, Minnesota, test site showing flight line.




| | |
|---|---|
| Alcester silty clay loam | At |
| Alluvial soils, undifferentiated | As |
| Benoit soils, undifferentiated | Bs |
| Blue Earth silty clay loam | Be |
| Cass loam | Cl |
| Fordville silt loam, gently sloping phase. | Fdg |
| Fordville silty clay loam | Fc |
| Deep phase | Fcd |
| Moody silty clay loam | Mc |
| Gently sloping phase | Mcg |
| Level phase | Mcl |
| Terrace phase | Mct |
| Sioux loam | Sx |

REPRODUCIBILITY OF THE ORIGINAL PAGE IS POOR

Fig. 16. Soil map of Luverne, Minnesota, test site. U.S. Highway #75 is shown by dark bold line. Test site line is shown by dashes. Map taken from USDA soil map of Rock County, Minnesota.

for the day. Because of the inclement weather the planned EG&G gamma-ray aircraft underflight was cancelled, the Landsat overpass imagery proved unusable due to cloud cover over the test site, and no ground truth was collected.

Fortunately May 12 was without inclement weather and the EG&G aerial survey for the measurement of natural terrestrial gamma radiation was carried out. The purpose of the survey was similar to the passive gamma ray survey performed over the Phoenix test site, i.e., to determine soil moisture by detecting differences in the terrestrial gamma flux attenuation as a function of soil moisture content. Initially it was hoped to establish correlations between 1) the NASA Landsat-2 satellite measurements of the terrestrial near-infrared and optical signals and 2) the soil moisture determined from ground-based sampling. The EG&G aerial measurements of terrestrial gamma radiation were planned to be simultaneous with the NASA satellite measurements and the ground sampling thus providing an independent set of data from which to establish correlations and evaluate the NASA near-infrared data. The planned comparisons were not possible, however, because, as mentioned previously, of heavy cloud cover during the time that the satellite was due to pass over the area.

A. Equipment

The equipment used for the Luverne gamma ray survey was the same as that used for the Phoenix gamma ray survey. (see p. B-10 of this report for details).

B. Technique

This section on technique is taken largely from Feimster and Fritzsche, 1975. The Luverne, Minnesota, survey included five lines

approximately 8 miles long, three flown in the north-south direction and two in the east-west direction, oriented parallel and perpendicular to U.S. Highway #75, respectively. Radiological data used to compute soil moistures were collected over Line A, shown in figures 17 and 18. This line is located 1000 ft west and parallel to Highway #75.

A Twin Beech Bonanza aircraft carrying radiation detection instrumentation as shown in figure 5, and flying at an altitude of 500 ft (152 m) above the terrain, made four passes over each of the five survey lines. The flights were timed to coincide with the ground sampling work.

Details of the technique are given in the Phoenix test site section and are not repeated here.

C. Results

The predominant gamma rays from natural radioelements in the soil include the 2.6MeV $^{208}$Tl gammas from the thorium decay chain, a family of $^{214}$Bi gammas from the uranium decay chain ranging over values of 0.61, 0.76, 0.93, 1.12, 1.76 and 2.2 MeV, and the 1.46 MeV gammas from $^{40}$K. A typical terrestrial gamma-ray pulse height spectrum as measured by a large NaI(Tl) crystal is illustrated in figure 4. The gamma counts under the $^{208}$Tl photopeak, between pulse height channels number 168 and 184, contain no background contribution from the airborne $^{214}$Bi radon daughters, since the $^{214}$Bi gammas are at lower energy values; the $^{40}$K photopeak data provide an abundance of counts, and can be separated from higher energy $^{214}$Bi Compton tails through a spectral stripping analysis. The gross count data, integrated over the range between 50 keV and 3.0 MeV offers the advantage of excellent counting statistics and

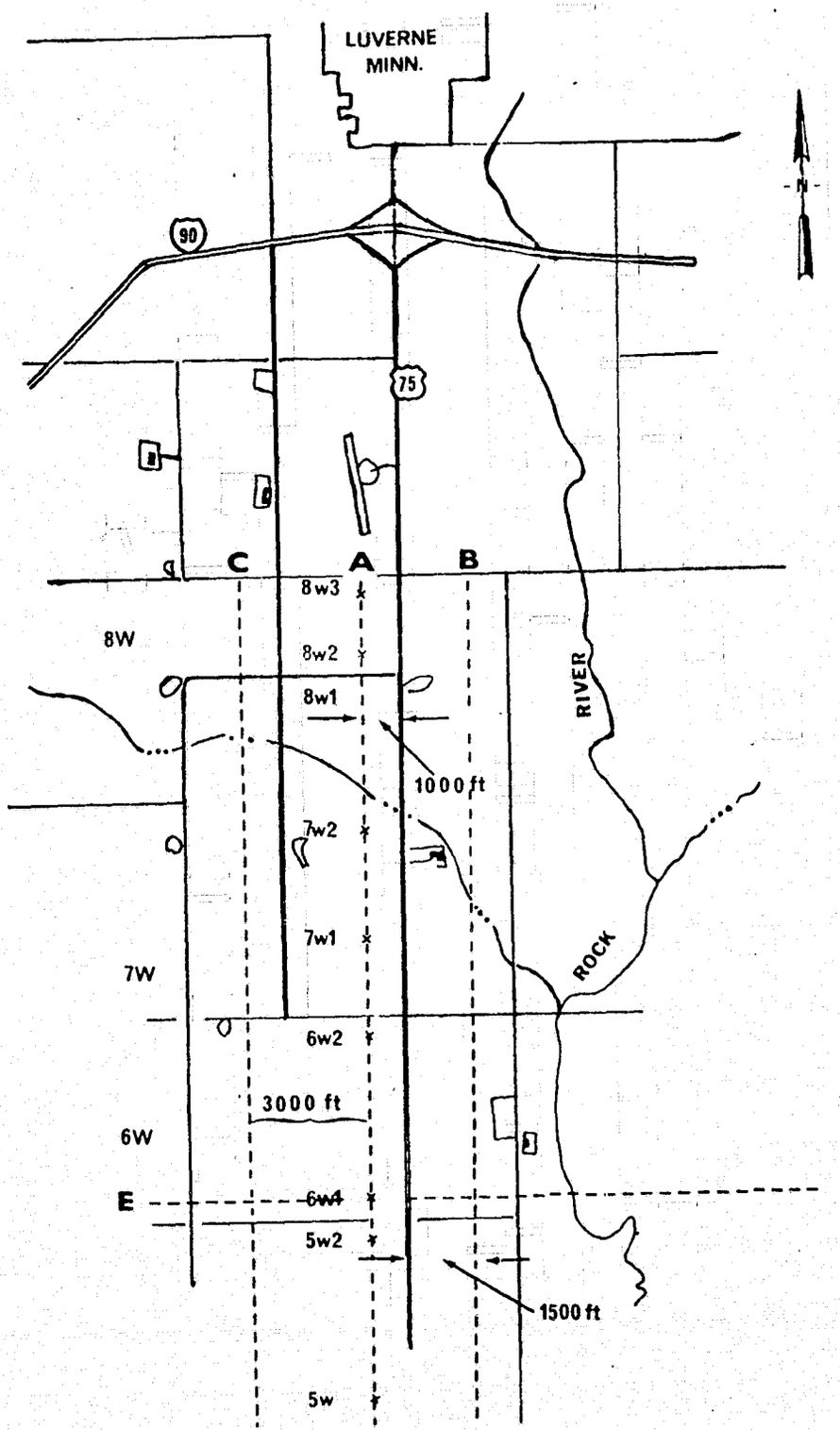



Fig. 17. Luverne, Minnesota, survey flight pattern-north half. The dashed lines labeled A through C and E indicate the positions of survey lines (from Feimster and Fritzsche, 1975).

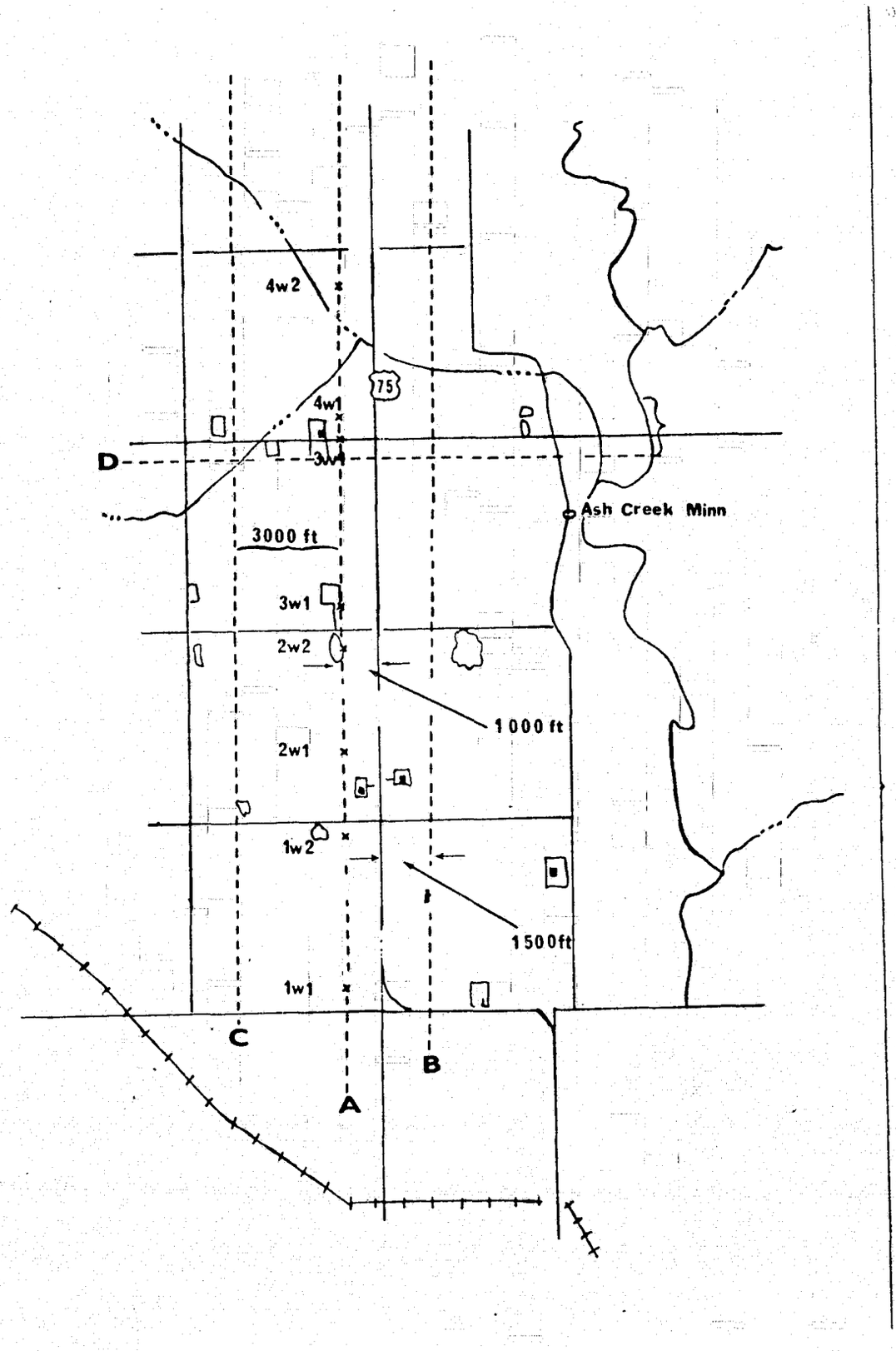



Fig. 18. Luverne, Minnesota, survey flight pattern-south half. The dashed lines labeled A through D indicate the positions of survey lines (from Feimster and Fritzsche, 1975)

good spatial resolution (on a mile-by-mile basis). However, a correction for airborne radon daughters has to be applied to the gross count.

The gamma-count rates in the photopeaks for $^{40}K$ and $^{208}Tl$ were determined by first subtracting the non-terrestrial background counts (due to the aircraft, cosmic rays and airborne radon daughters) from the respective pulse height spectrum windows (see Figure 6, channels 91 through 104 for $^{40}K$ and channels 168 through 184 for $^{208}Tl$). These net photopeak count rates were then adjusted to correspond to that for transport of these terrestrial gammas through an air mass of 17 $g/cm^2$ (equivalent to an altitude of 500 feet at average pressure and temperature). Table 7 gives a listing of net photopeak count rates for $^{40}K$ and $^{208}Tl$ for survey line A flown on May 12, 1975, and values averaged over repeated flights.

The ratio of gamma flux $\Gamma_1/\Gamma_2$ measured for two different soil moisture conditions $M_1$ and $M_2$ has the form

$$\frac{\Gamma_1}{\Gamma_2} = \frac{1+M_2}{1+M} \qquad \text{(Eq. 14)}$$

Eq. (14) is used with the tabulated $^{40}K$ and $^{208}Tl$ photopeak count rates given in Table 1, the $^{40}K$ and $^{208}Tl$ photopeak count rate for March 6, 1973 (1730 cpm and 482 cpm, respectively) and the soil moisture for March 6, 1973, to determine the soil moisture for the May 2, 1975 survey. It should be noted that this can only be done for survey line A (west of U.S. #75) since only that line was surveyed previously; a necessary prerequisite for determining the value of Eq. (14).

The calculated soil moisture values, employing the $^{40}K$ and the $^{208}Tl$



REPRODUCIBILITY OF THE ORIGINAL PAGE IS POOR

TABLE 7. Net $^{40}K$ and $^{208}Tl$ gamma photopeak count rates from the May 12, 1975 survey of Line A at Luverne, Minnesota (from Feimster and Fritzsche, 1975)

| Spectrum No. | Pass No. | Net Gamma Count Rate in Photopeak (cpm) $^{40}K$ | $^{208}Tl$ |
|---|---|---|---|
| 55 | 1 | 1859 | 556 |
| 60 | 2 | 1907 | 540 |
| 65 | 3 | 1841 | 537 |
| 71 | 4 | 1905 | 542 |
| | Avg. | 1878 | Avg. 544 |

photopeak area methods are:

M ($^{40}$K) = 32%

M ($^{208}$Tl) = 28%

The third method of determining soil moisture from aerial measurements of terrestrial gamaa radiation employs and analysis of the gross gamma-count rates between 50 KeV and 3.0 MeV as explained in the Phoenix test site section. Correcting the gross gamma count for the airborne radon contribution is most often achieved by air filter data analysis (see Feimster and Fritzsche, 1975 Appendix A). Table 8 lists data collected by filter and radon values computed from these filter data of May 12, 1975 and March 6, 1973.

To validate the air filter data, a method called U/K ratio was employed. The significant elements of this method are:

1. The uranium photopeak to potassium photopeak count rate ratio is computed for any two surveys under consideration. These are labeled U and K as parts of the gamma energy spectrum defined in figure 6.

2. If the U/K ratio increased from one soil moisture survey to the next, then the radon daughter contribution to the gamma count rate has increased in both the energy spectra and in the gross count rate. The U/K ratio is unaffected by soil moisture changes.

Table 9 lists the U/K ratio computations for the March 6, 1973 and May 12, 1975 data. Since the U/K ratio decreased from the first to the second survey, then the airborne radon must have decreased. This result supports the air filter results (in Table 8) which show the radon contribution decreasing from 600 cps to 165 cps.

The air filter method is used for the soil moisture analysis in this

TABLE 8. Air Filter Data (from Feimster and Fritzsche, 1975)

| Date | Air Filter Count Rate (per 3 min.) | Background Count Rate (per 3 min.) | Net Filter Count Rate (per 3 min.) | Gross Gamma[1] Count Rate ($sec^{-1}$) | Filter[2] Factor | Location | Excess[3] Gross Gamma Count Rate ($sec^{-1}$) |
|---|---|---|---|---|---|---|---|
| 5/12/75 | 4260 | 962 | 3298 | 1100 | .18 | Lake | 165 |
| | 1794 | 877 | 916 | | | Land | |
| 3/6/73 | 3778 | 1617 | 2161 | 1200 | .32 | Lake | |
| | 3524 | 1604 | 1920 | | | Land | 600 |

[1]The gross gamma count rate is the gamma count rate per second in the primary detector array.

[2]The filter factor is the gross gamma count rate less the aircraft and cosmic ray contributions divided by the net filter count rate.

[3]The excess gross gamma count rate is due to airborne radon daughters. It is computed from the filter factor times the net filter count rate.

TABLE 9. Gamma spectral data used in U/K ratio computations (from Feimster and Fritzsche, 1975).

| Survey Date | Gamma count rate in selected pulse height window* K (cpm) | U (cpm) | Ratio U/K |
|---|---|---|---|
| 3/6/73 | 1719 | 1285 | 0.75 |
| 5/12/75 | 1877 | 616 | 0.33 |

*Refer to pulse height window definition in Figure 4.

report, because it yields an absolute magnitude for airborne radon. The U/K ratio yields the change in concentration for airborne radon only. The contributions of airborne radon to the primary detector signal as given in Table 2 are: 165 cps for May 12, 1975 and 600 cps for March 6, 1973. The cosmic + aircraft contribution was 500* cps. Therefore, the non-terrestrial background was 1100 cps on March 6, 1973 and 665 cps on May 12, 1975. These non-terrestrial background count rates were subtracted from the gross count rates along each mile of survey line, giving the net terrestrial gross count rate averaged over a survey distance of one mile. Table 10 shows the adjusted gross count rate per mile for four passes made over Line A. The adjusted gross count rates averaged mile-by-mile basis as shown in Table 11.

To support the soil moisture values computed from aerial data, 81 soil samples were taken and their moisture content measured. Moisture values from these samples were supplied by Twin Cities Testing and Engineering, Sioux Falls, South Dakota. Their method was to weigh the samples before and after drying and compute the soil moisture values determined from the ratio of the wet minus dry weights divided by dry weights. Table 12 compares the moisture values on a mile-by-mile basis (Table 12a) and a 2-mile basis, determined from the aerial data and the moisture values from the ground sampling data for the two survey dates. Some discrepancy is generally expected between the ground and aerial data. As explained earlier, moisture values acquired by the aerial system are computed form data averaged over approximately a ¼ sq. mi. area opposed to point samples taken to compute ground based soil moistures.

As a check for data acquisition consistency of the aerial system, several passes were made over each survey line. A plot, figure 19, of

*Cosmic count rate = 290 + 137e(15 - pressure)/2.55) cps.

TABLE 10. Adjusted and averaged adjusted gross count rates per mile for line A (from Feimster and Fritzsche, 1975).

| | May 12, 1975 | | | | | March 6, 1973 |
|---|---|---|---|---|---|---|
| Pass No. | 1 | 2 | 3 | 4 | | |
| Mile | | | | | Average | Average |
| 1 | 2293 | 2315 | 2359 | 2262 | 2307 | 1930 |
| 2 | 2400 | 2484 | 2377 | 2343 | 2391 | 1969 |
| 3 | 2553 | 2499 | 2531 | 2501 | 2508 | 2195 |
| 4 | 2570 | 2552 | 2552 | 2531 | 2552 | 2304 |
| 5 | 2492 | 2530 | 2486 | 2485 | 2498 | 2248 |
| 6 | 2549 | 2578 | 2519 | 2491 | 2534 | 2266 |
| 7 | 2443 | 2496 | 2447 | 2413 | 2450 | 2308 |
| 8 | 2462 | 2441 | 2397 | 2447 | 2436 | 2239 |

Note: Units of gross count are counts $sec^{-1}$.

Table 11. Soil moisture for May 12, 1975 computed from averaged adjusted gross count rates in Table 10 and March 6, 1973 soil moisture data (from Feimster and Fritzsche, 1975).

| | March 6, 1973 | | May 12, 1975 | |
|---|---|---|---|---|
| Mile | Gross Count Rate ($sec^{-1}$) | % Soil* Moisture | Gross Count Rate ($sec^{-1}$) | % Soil+ Moisture |
| 1 | 1930 | 47 | 2307 | 23 |
| 2 | 1969 | 47 | 2391 | 21 |
| 3 | 2195 | 46 | 2508 | 28 |
| 4 | 2304 | 51 | 2552 | 36 |
| 5 | 2248 | 41 | 2498 | 27 |
| 6 | 2266 | 41 | 2534 | 26 |
| 7 | 2308 | 43 | 2450 | 35 |
| 8 | 2239 | 35 | 2436 | 24 |
| Averages | 2182 | 44 | 2460 | 28 |

*The soil moisture on March 6, 1973, was obtained from ground-based measurements.

+The soil moisture on May 12, 1975, was obtained from the airborne gross count rate data from both March 6 and May 12 and the soil moisture data of March 6, 1973 (see Equation 14).

REPRODUCIBILITY OF THE
ORIGINAL PAGE IS POOR

TABLE 12. Comparison of the airborne gross count rate method and the ground-based soil moisture measurements per mile (from Feimster and Fritzsche, 1975).

| Mile | Soil Moisture (%) Airborne | Ground Based |
|---|---|---|
| 1 | 23 | 25 |
| 2 | 21 | 26 |
| 3 | 28 | 39 |
| 4 | 36 | 28 |
| 5 | 27 | 23 |
| 6 | 26 | 27 |
| 7 | 35 | 30 |
| 8 | 24 | 29 |
| Average | 28 | 28 |

TABLE 12a. Comparison of airborne gross count rate method and the ground-based soil moisture measurements per 2 miles (from Feimster and Fritzsche, 1975).

| Miles | Soil Moisture Airborne | Ground Based |
|---|---|---|
| 1-2 | 22 | 25.5 |
| 3-4 | 32 | 33 |
| 5-6 | 26.5 | 25 |
| 7-8 | 30.5 | 29.5 |
| Average | 28 | 28 |

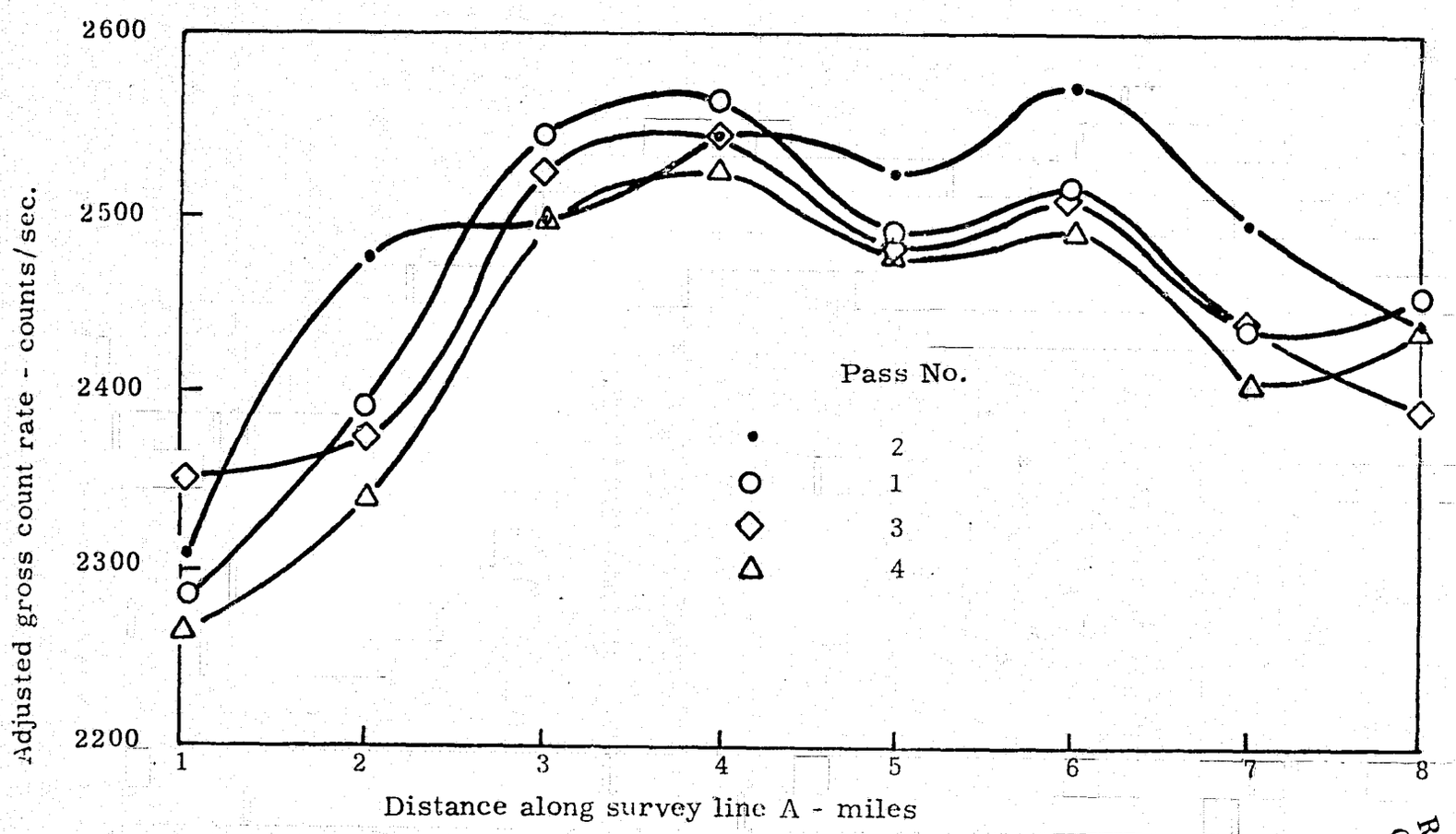



Fig. 19. Average adjusted gross count rate per mile for each of the four passes of line A (from Feimster and Fritzsche, 1975).



REPRODUCIBILITY OF THE ORIGINAL PAGE IS POOR

the variation of the adjusted gross gamma count rate during each pass over survey Line A, using gross count rate versus time, illustrates acquisition consistency during this survey. The difference between corresponding points of each curve is due primarily to counting error which is approximately (count rate)$^{\frac{1}{2}}$/(count rate) at a 68% confidence level; i.e., $\pm$ one standard deviation.

Figure 20 shows the relationship between the ground sampled soil moisture values values computed per mile and the soil moistures per mile from the adjusted gross count aerial data.

D. Conclusions

The airborne gamma-ray results indicate a range of values for soil moisture for the survey at Luverne, Minnesota, on May 12, 1975, from 28% to 39%. The spread in these values is due to:

1. The statistical counting uncertainty of the photopeak area methods.

2. The airborne radon concentration uncertainty in the gross count rate method.

3. The uncertainty in the ground measurements of the baseline soil moisture, i.e., that soil moisture obtained from soil samples on March 6, 1973.

The $^{40}K$ and $^{208}Tl$ photopeak methods gave average soil moisture values of 32% and 28%, respectively. The adjusted gross-count rate method gave an average soil moisture value of 28%, with mile-by-mile values ranging from 21% to 36%. Ground measured soil moisture values ranged from 23% to 39% with the average value being 28%. Thus, the three methods of surveying soil moisture by airborne $\gamma$-ray gives results consistent with

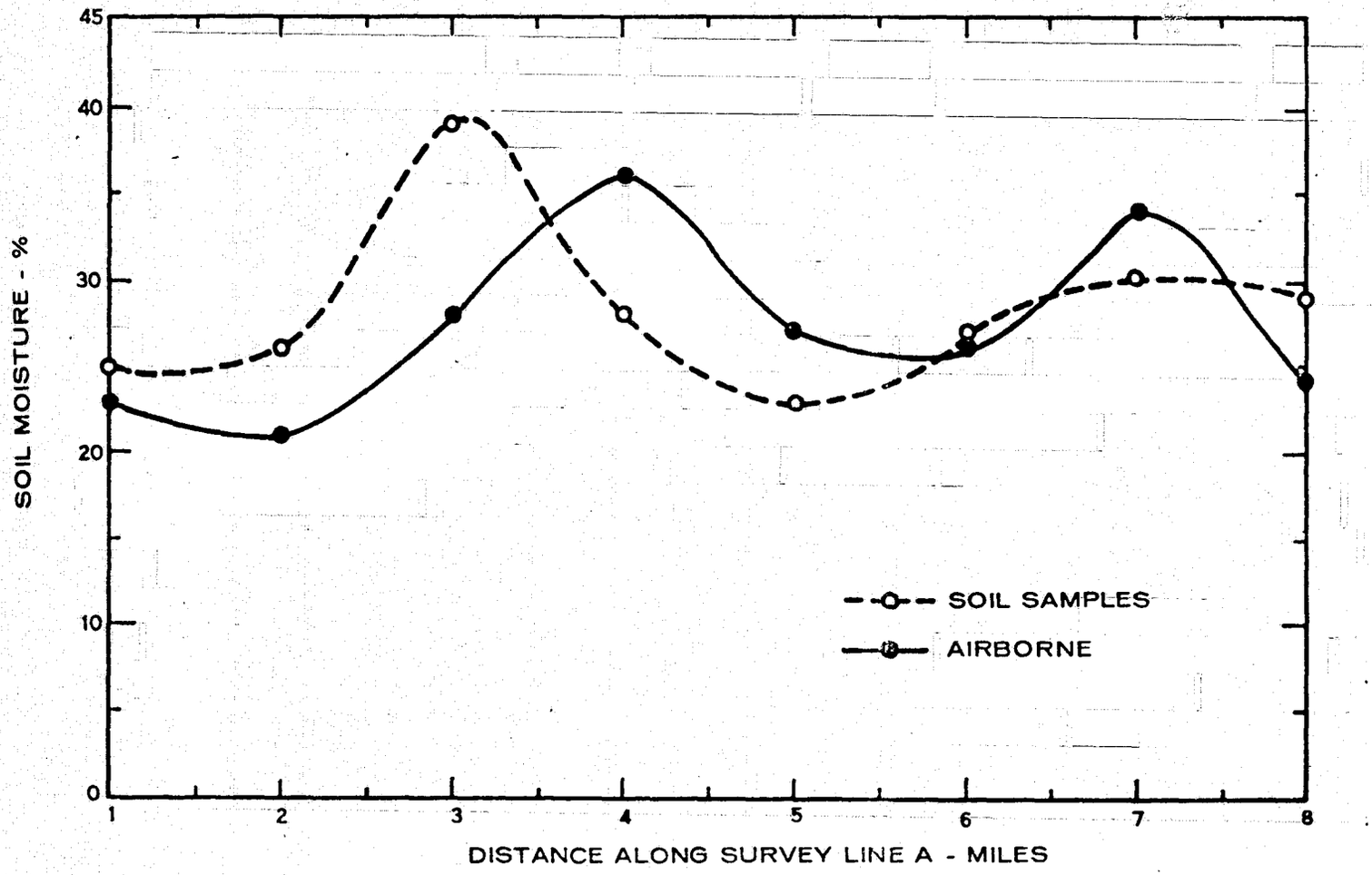



Fig. 20. Average soil moisture per mile from airborne adjusted gross count rate and from soil samples (from Feimster and Fritzsche, 1975).

those obtained by ground truth. The photopeak methods, however, appears more useful in measuring the long-line soil moisture average, whereas the adjusted gross-count rate method can be used to measure soil moisture in one mile increments.

To improve the accuracy of the airborne gamma-ray soil-moisture measurements, the following experiments and procedures are recommended:

a. Increase the amount of soil samples taken to reduce the true soil moisture uncertainty.

b. Improve the systematic method of recovering soil samples with respect to location and sampling density on the survey line. This could be accomplished by permanently marking the soil sample sites for future sampling. However, due to crop rotation and field tillage, this may be impractical except for selected site locations.

c. Reduce the error in the airborne system due to radon. To accomplish this, the variable spatial distribution of radon daughters in the air would need to be determined, as well as determining the varying relative humidity and temperature more accurately.

d. Establish a more accurate relationship of gamma-ray flux to soil moisture through more soil moisture surveys or ground-based experiments in a laboratory-controlled situation.

The October 17, 1975 Experiment

On October 17, 1975, the NASA P-3 aircraft was scheduled to overfly the Luverne, Minnesota, test site. The sensors aboard include an 11-channel multispectral scanner, six AMPS cameras and filters, one Zeiss camera, and one PRT-5 radiation thermometer. The characteristics of the scanner and camera systems are listed in Tables 13, 14, and 15, respectively. The PRT-5 radiation thermometer is used to measure gross apparent radiation in the 8 to 14μm range. The instrument has a 2° field of view

TABLE 13. $M^2S$ Characteristics

| Channel | Spectral Bandwidth | Remarks |
|---|---|---|
| 1 | .370-.413 | |
| 2 | .440-.490 | |
| 3 | .495-.535 | |
| 4 | .540-.580 | |
| 5 | .580-.620 | Inoperative |
| 6 | .620-.660 | |
| 7 | .660-.700 | |
| 8 | .700-.740 | Inoperative |
| 9 | .760-.860 | |
| 10 | .970-1.060 | |
| 11 | 8.000-13.000 | |

TABLE 14. AMPS Characteristics

| Station # | Focal Length | Filter Bandpass | Remarks |
|---|---|---|---|
| 1 | 6" | 875-925 nm | Black and white IR |
| 2 | 6" | 700-800 nm | Not ordered |
| 3 | 6" | 500-800 nm | Color IR |
| 4 | 6" | 400-700 nm | Aerial color |
| 5 | 6" | 625-675 nm | Not ordered |
| 6 | 6" | 525-575 nm | Not ordered |

TABLE 15. Zeiss Characteristics

| | Focal Length | Filter Bandpass | Remarks |
|---|---|---|---|
| | 6" | 520-850 nm | Color IR film |

TABLE 16. Soil Types found in Fields A, B, C, and D

| Field | Predominant Soil Types | Description |
|---|---|---|
| A | Fordville Silty Clay Loam<br>Sioux Loam | Well drained nearly level to gently sloping soils of the stream terraces. They are underlain, generally within 3 feet of the surface, by sand and gravel. |
| B | Cass Loam | Soil of the flood plains. Subject to temporary high water table and frequent floods. |
| | Fordville Silty Clay Loam | Same as Field A. |
| | Sioux Loam | Same as Field A. |
| C | Fordville Silty Clay Loam | Same as Field A. |
| D | Moody Silty Clay Loam | Well drained soil of the Loessal uplands. |

and a response time of 5 milliseconds. Incoming radiated energy, continuously compared to a 55°C internal reference, is converted into a voltage, which is directly related to the energy difference between the target and the reference. This voltage is displayed on the indicator as

equivalent blackbody temperature to an accuracy of 0.5°C.

Unfortunately, because of a very short notice that the P-3 aircraft was to overfly the test site area, there was no time to organize a ground data collection effort. Also no Landsat overpass was available for this day. Thus the resulting aircraft data cannot be verified by using ground data or satellite information as planned.

Weather over the test site was clear and temperature at the time of the overflight was near 16°C. Weather records at nearby Sioux Falls, South Dakota, indicate little or no precipitation from October 14-17. Three overflights (lines 7, 8, and 9) were made over the test site parallel to U.S. Highway #75. Of these three passes line 7 had the test site line too near the edge of the imagery, line 8 has the test site line somewhat off center of the imagery, and line 9 was centered on the imagery. Owing to delays in securing data tapes and problems with the computer reduction of line 9, line 8 was analyzed instead of line 9.

A. Zeiss and AMPS Data

Of the seven Zeiss and AMPS camera stations available as data sources on the October 17, 1975, flight, only four were ordered for analysis. The filter band passes selected were 400-700 nm (AMPS aerial color), 500-800 nm (AMPS color IR), 875-925 nm (AMPS B&W IR), and 520-850 nm (Zeiss color IR). After examining the imagery, four fields labeled A, B,, C, and D, were selected for further study (figure 21). The fields, shown in the Zeiss and AMPS images (figures 22 through 39) were selected because 1) the imagery showed them to be devoid of vegetation, and 2) comparison of the soil types also showed them to be similar, i.e., loam. Specific soils for each field are listed in Table 16.

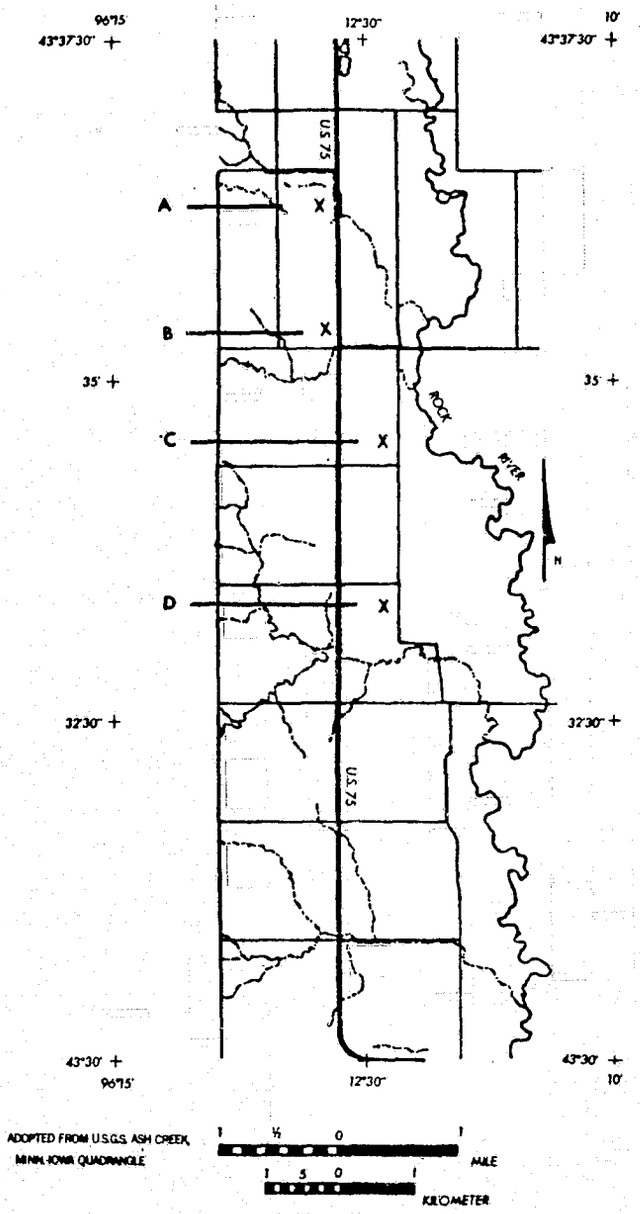



Fig. 21. Location of the four fields selected in the October 17, 1975 soil moisture experiment.

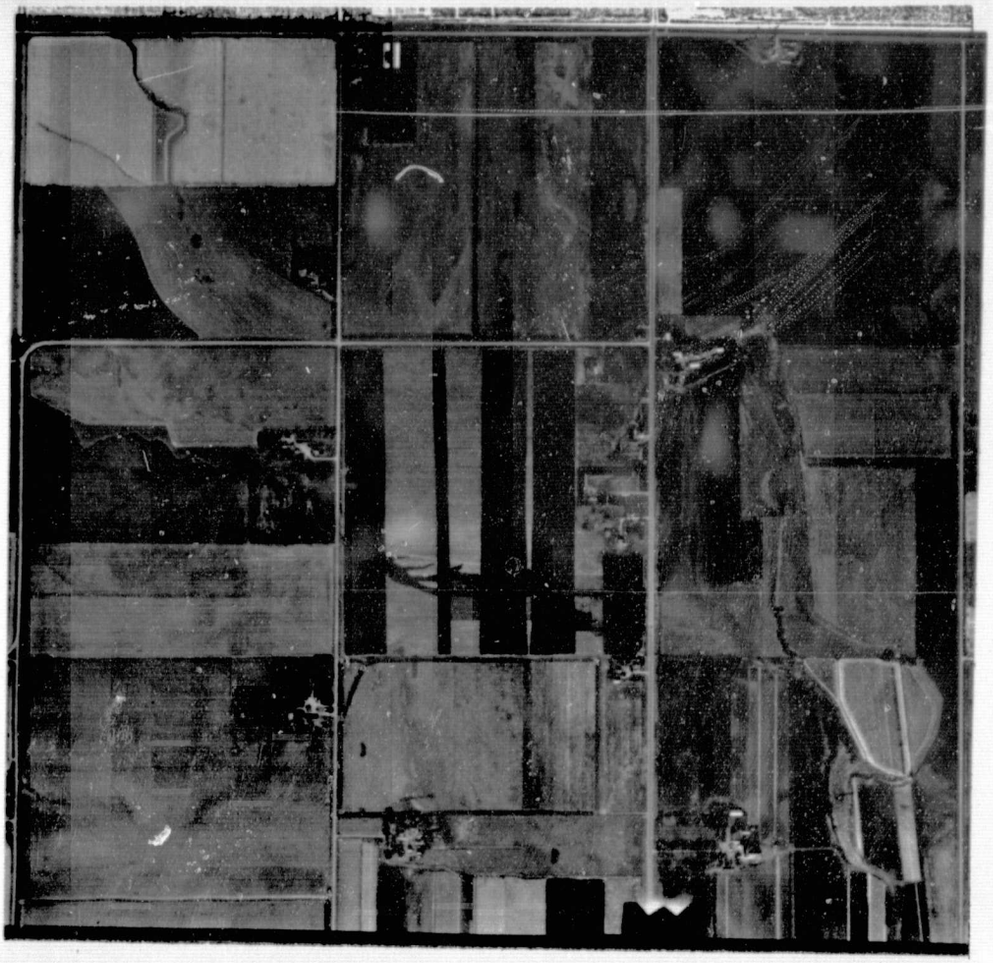


Fig. 22. Zeiss color IR photograph of field A.

ORIGINAL PAGE IS
OF POOR QUALITY

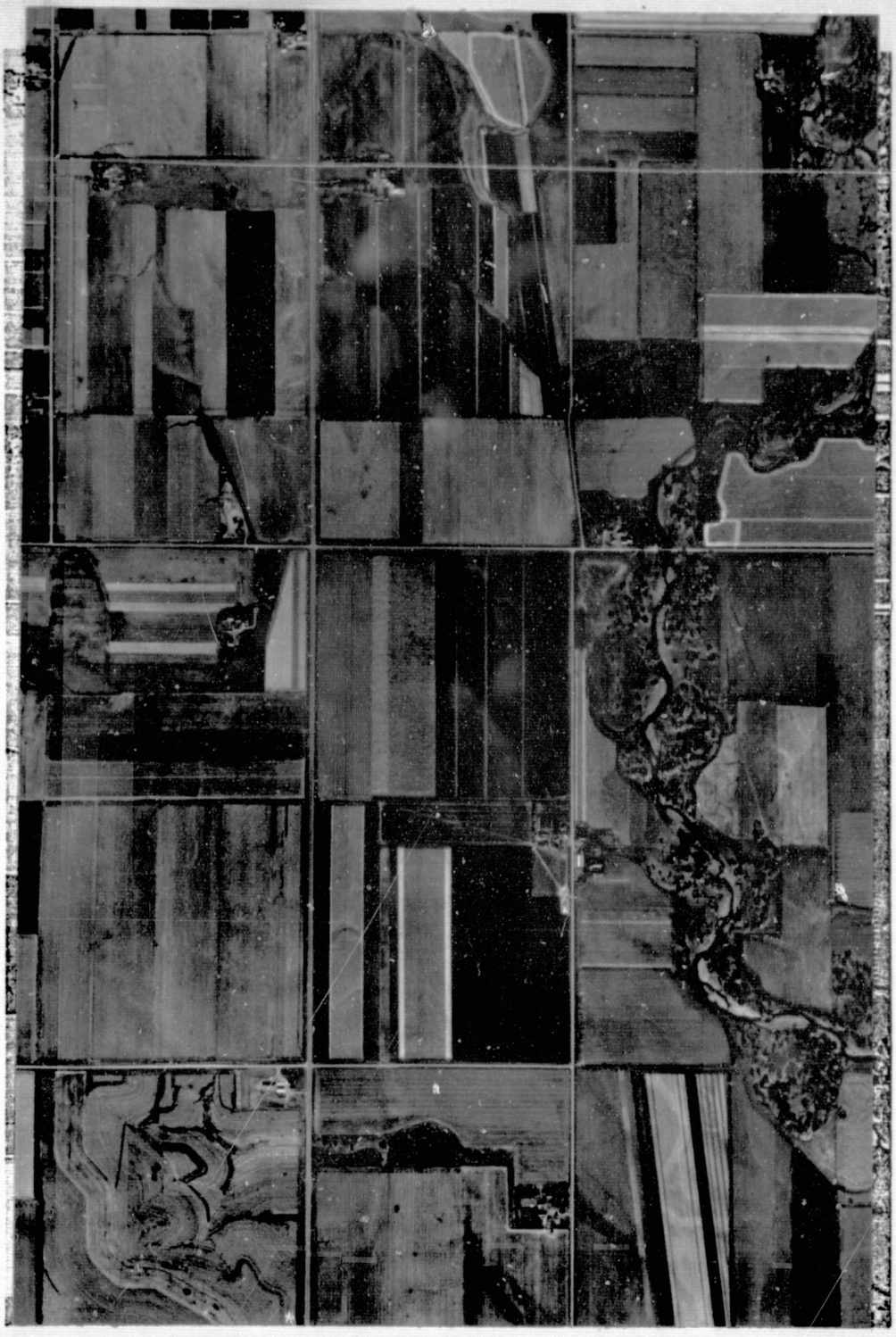


Fig. 23. Zeiss color IR photograph of fields B and C.

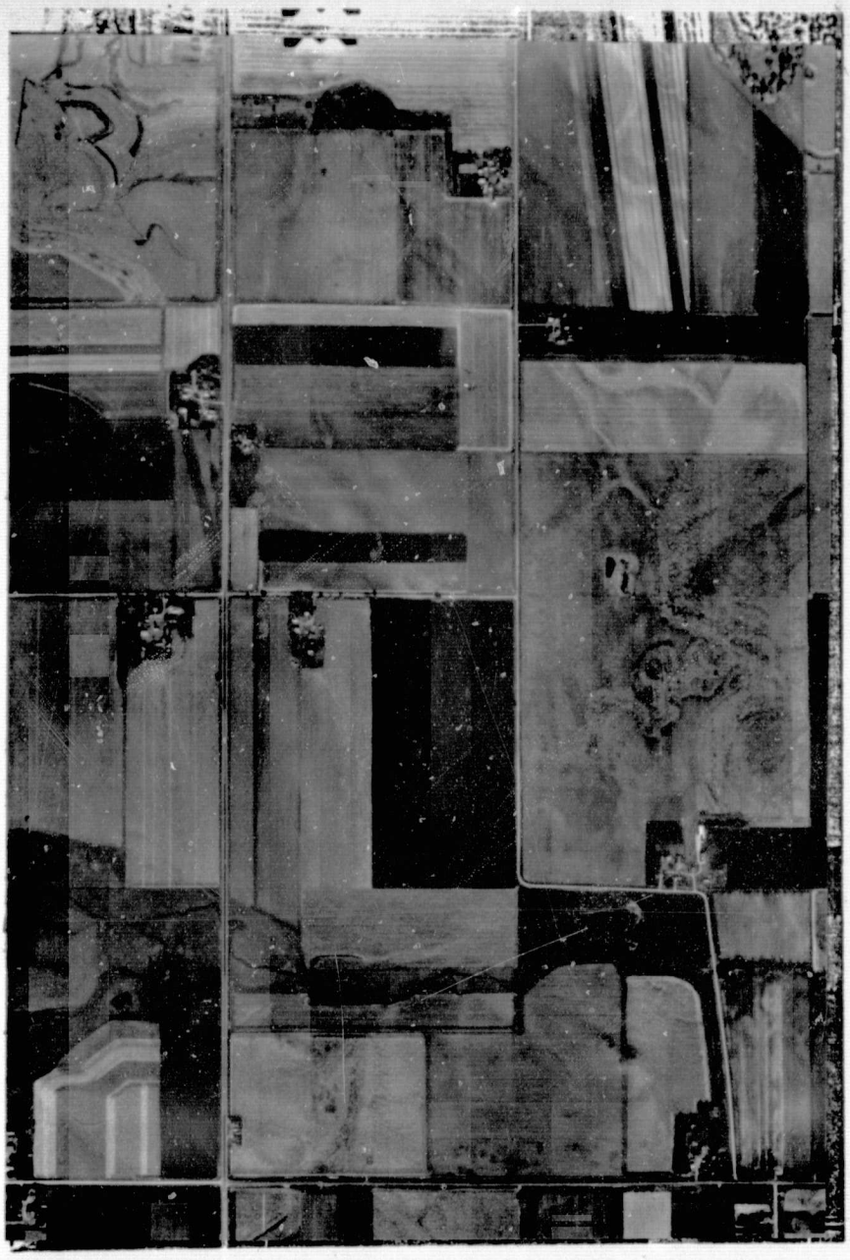


Fig. 24. Zeiss color IR photograph of field D.

ORIGINAL PAGE IS
OF POOR QUALITY

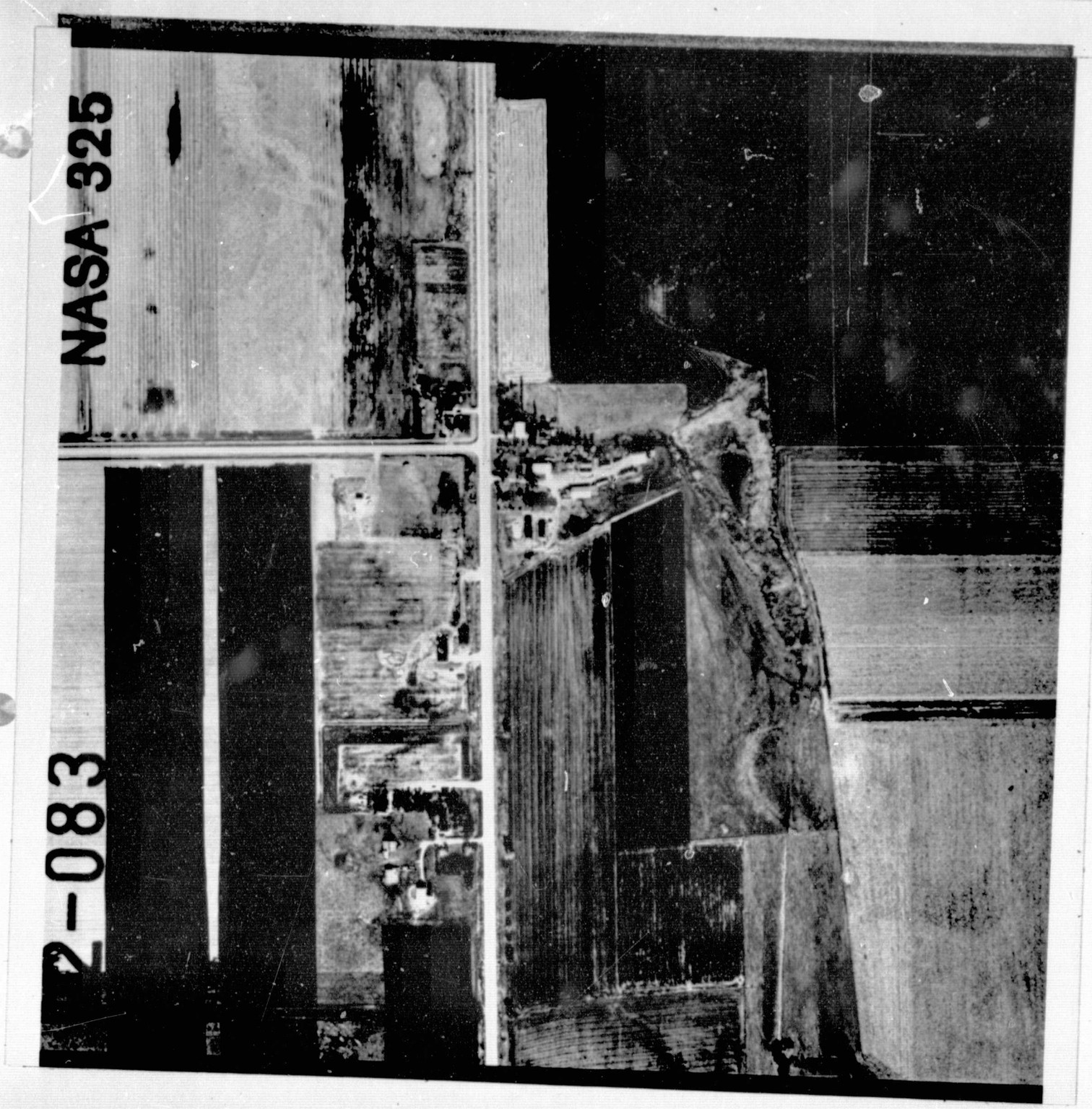



Fig. 25. AMPS aerial color photograph of field A.

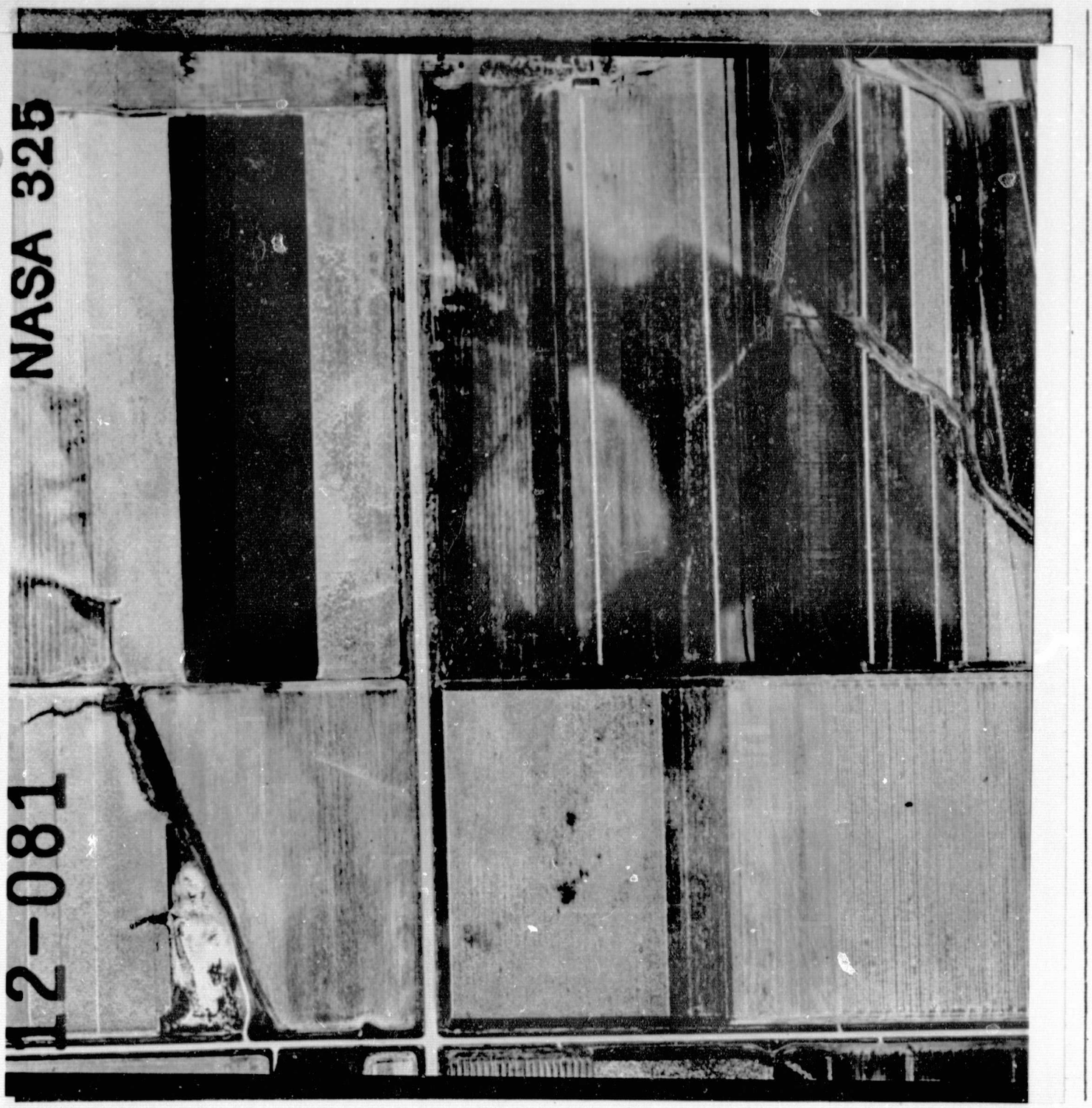



Fig. 26. AMPS aerial color photograph of field B.

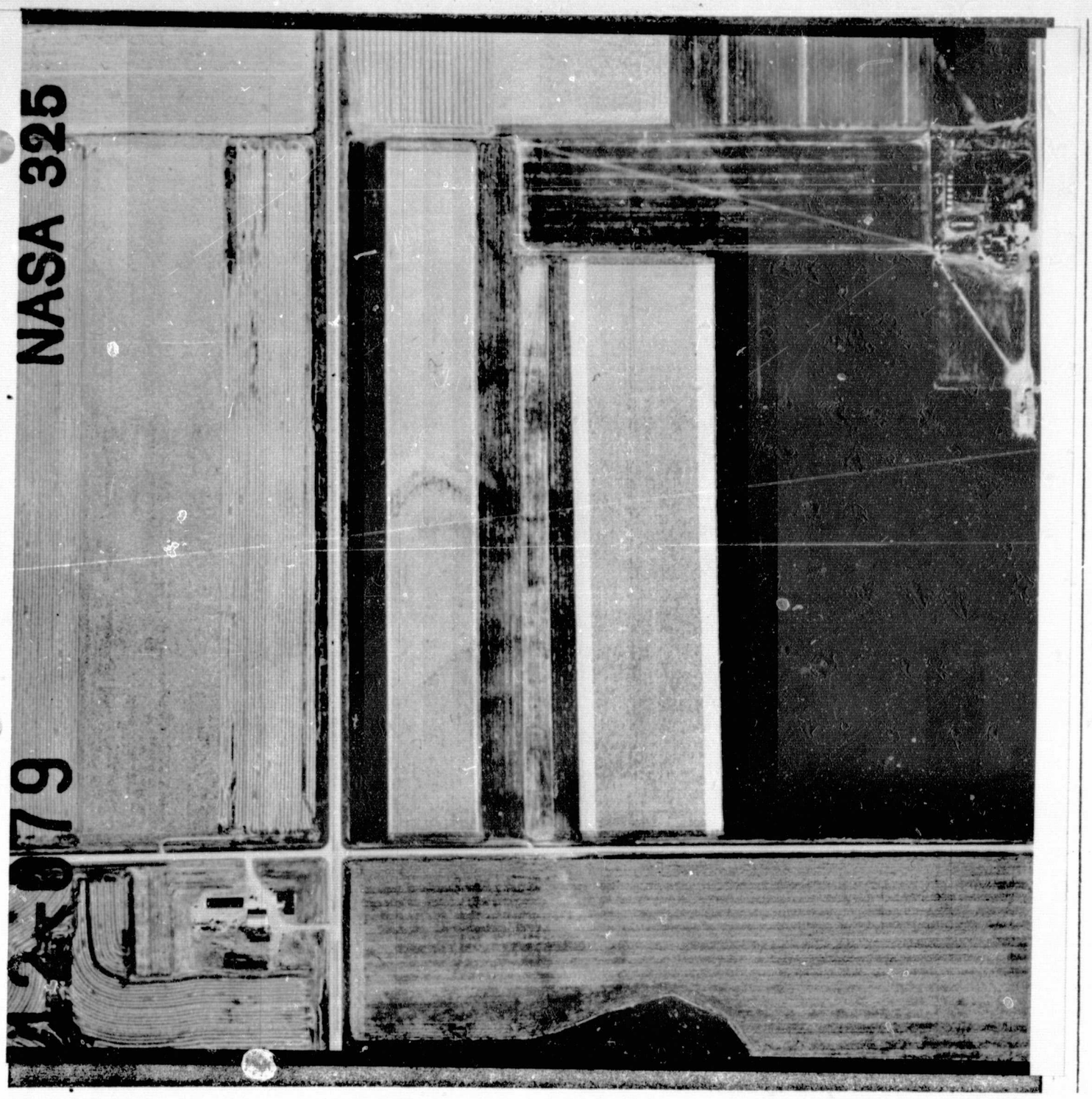



Fig. 27. AMPS aerial color photograph of field C.

ORIGINAL PAGE IS
OF POOR QUALITY




Fig. 28. AMPS aerial color photograph of northern section of field D.

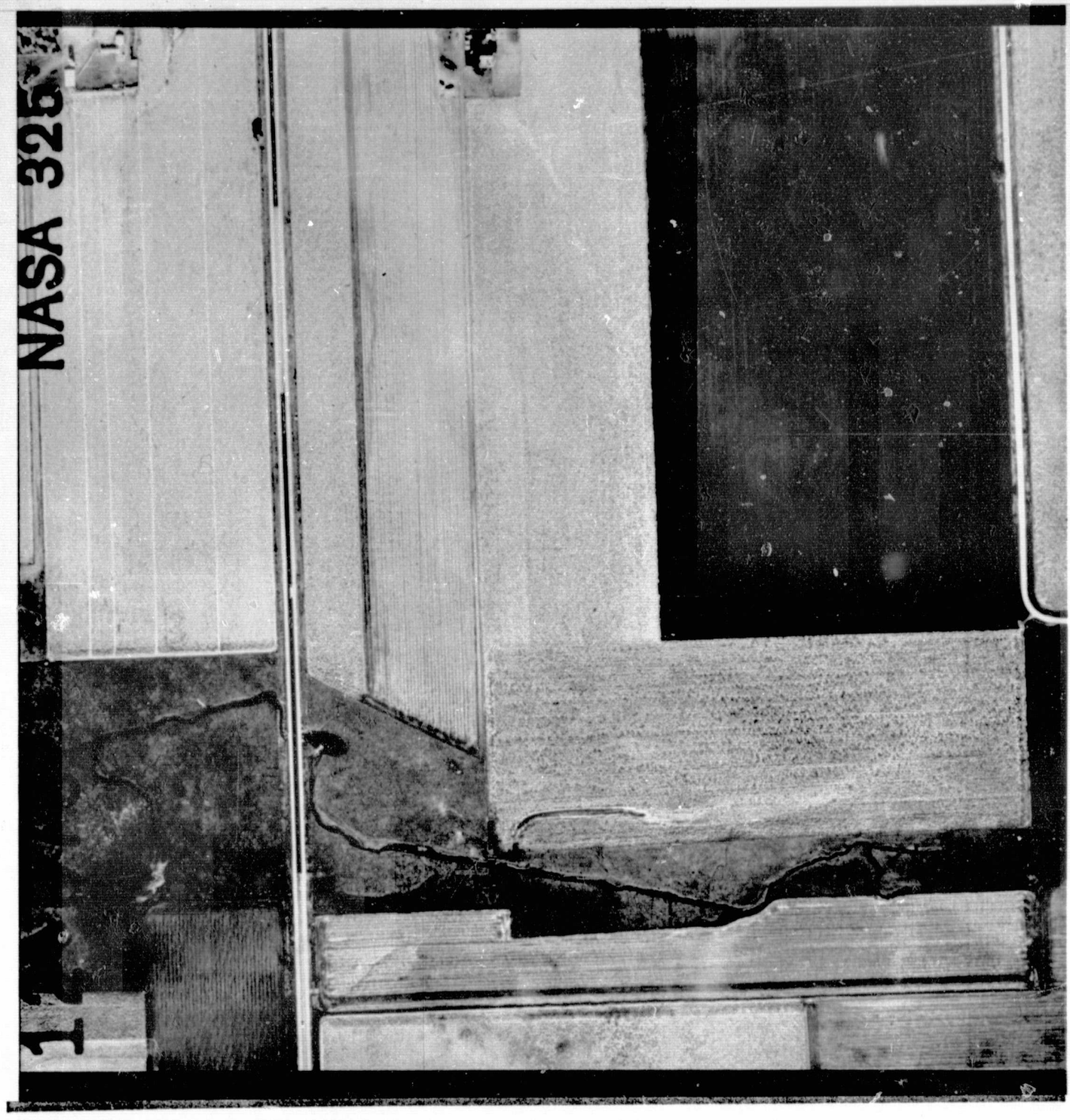



Fig. 29. AMPS aerial color photograph of southern section of field D.

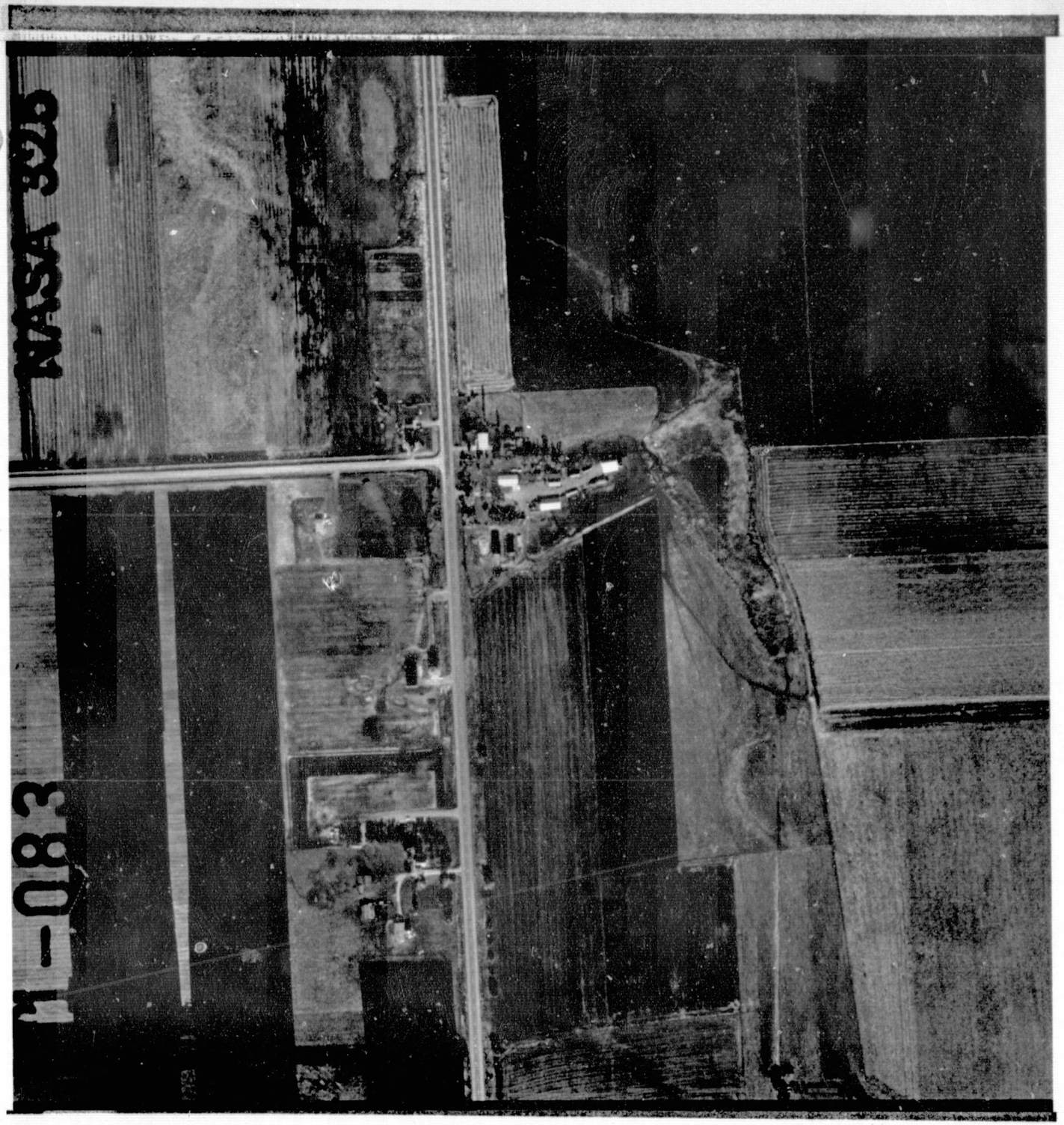



Fig. 30. AMPS color IR photograph of field A.




Fig. 31. AMPS color IR photograph of field B.

ORIGINAL PAGE IS
OF POOR QUALITY

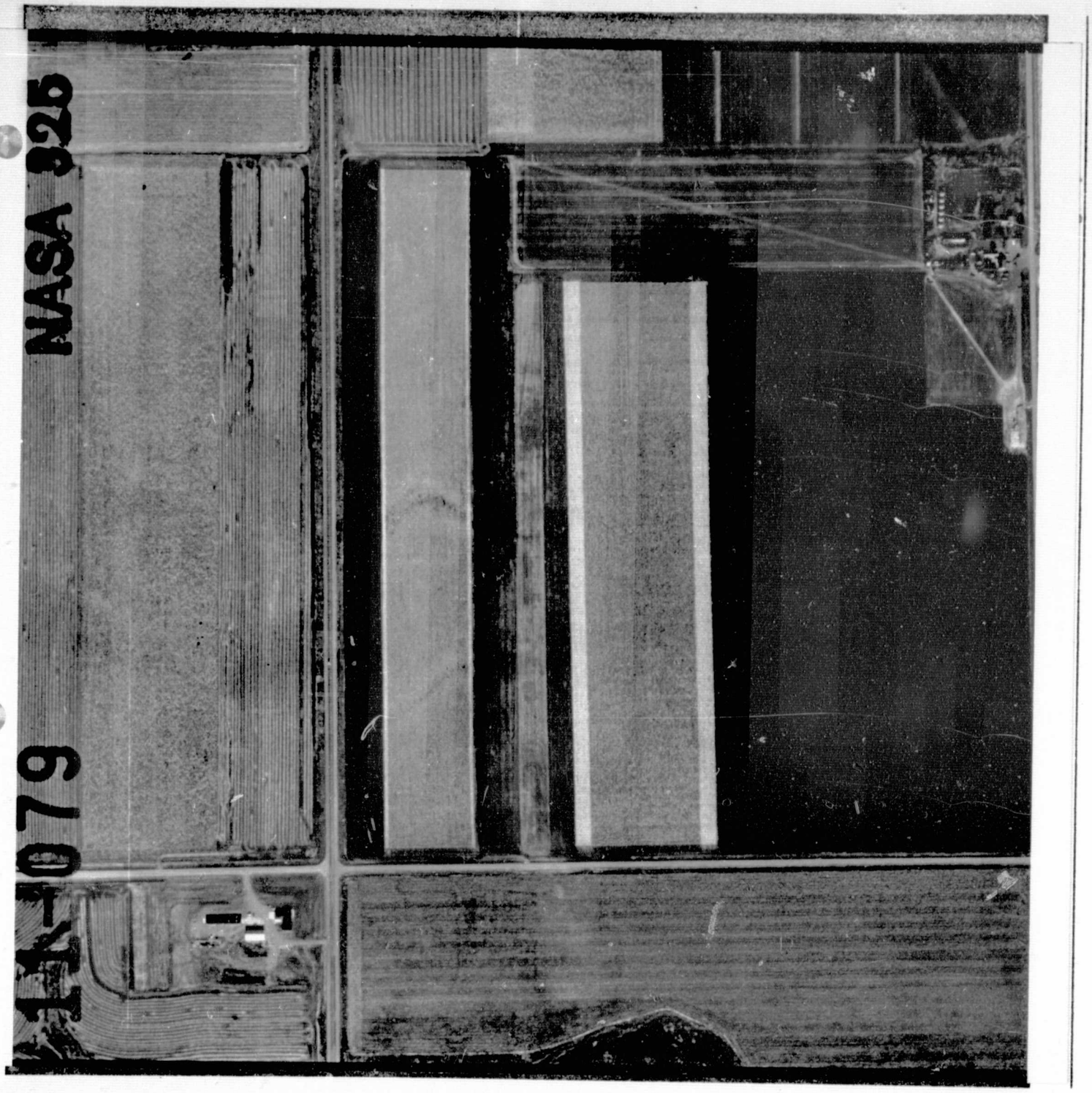



Fig. 32. AMPS color IR photograph of field C.




Fig. 33. AMPS color IR photograph of northern section of field D.

REPRODUCIBILITY OF THE
ORIGINAL PAGE IS POOR




Fig. 34. AMPS color IR photograph of southern section of field D.

ORIGINAL PAGE IS
OF POOR QUALITY

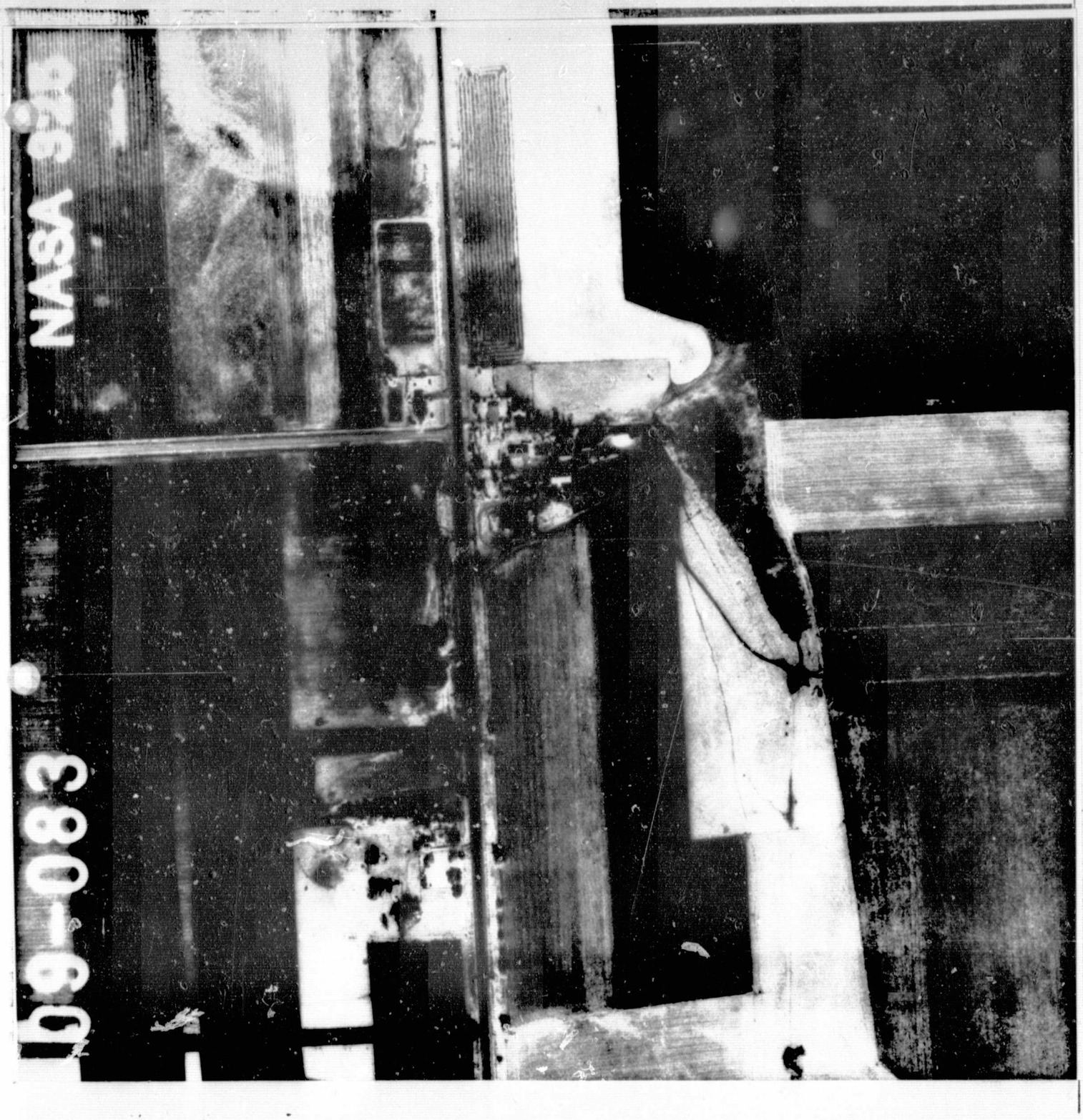



Fig. 35. AMPS black and white IR photograph of field A.

REPRODUCIBILITY OF THE
ORIGINAL PAGE IS POOR

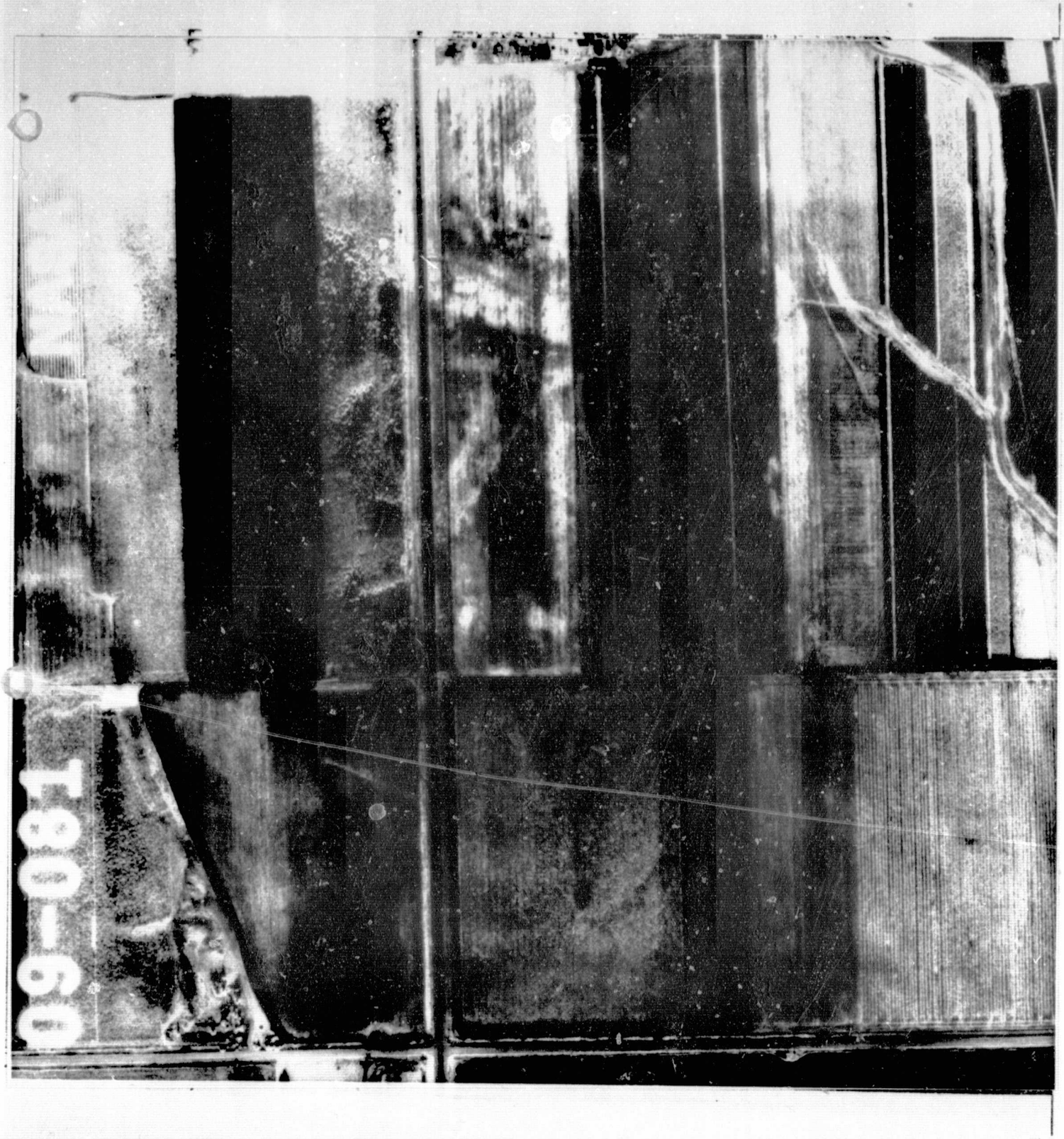



Fig. 36. AMPS black and white IR photograph of field B.

ORIGINAL PAGE IS
OF POOR QUALITY

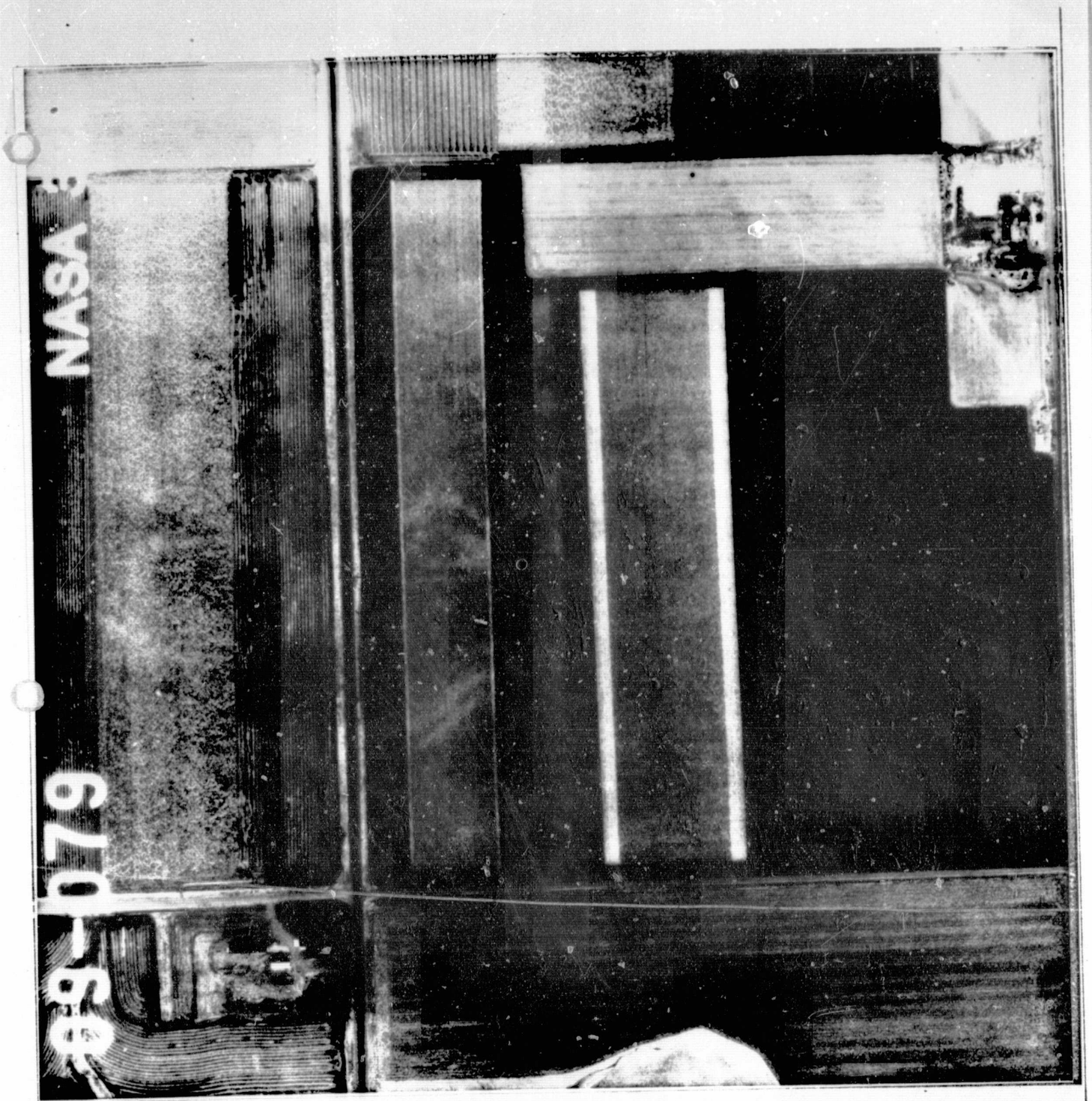



Fig. 37. AMPS black and white IR photograph of field C.

REPRODUCIBILITY OF THE
ORIGINAL PAGE IS POOR

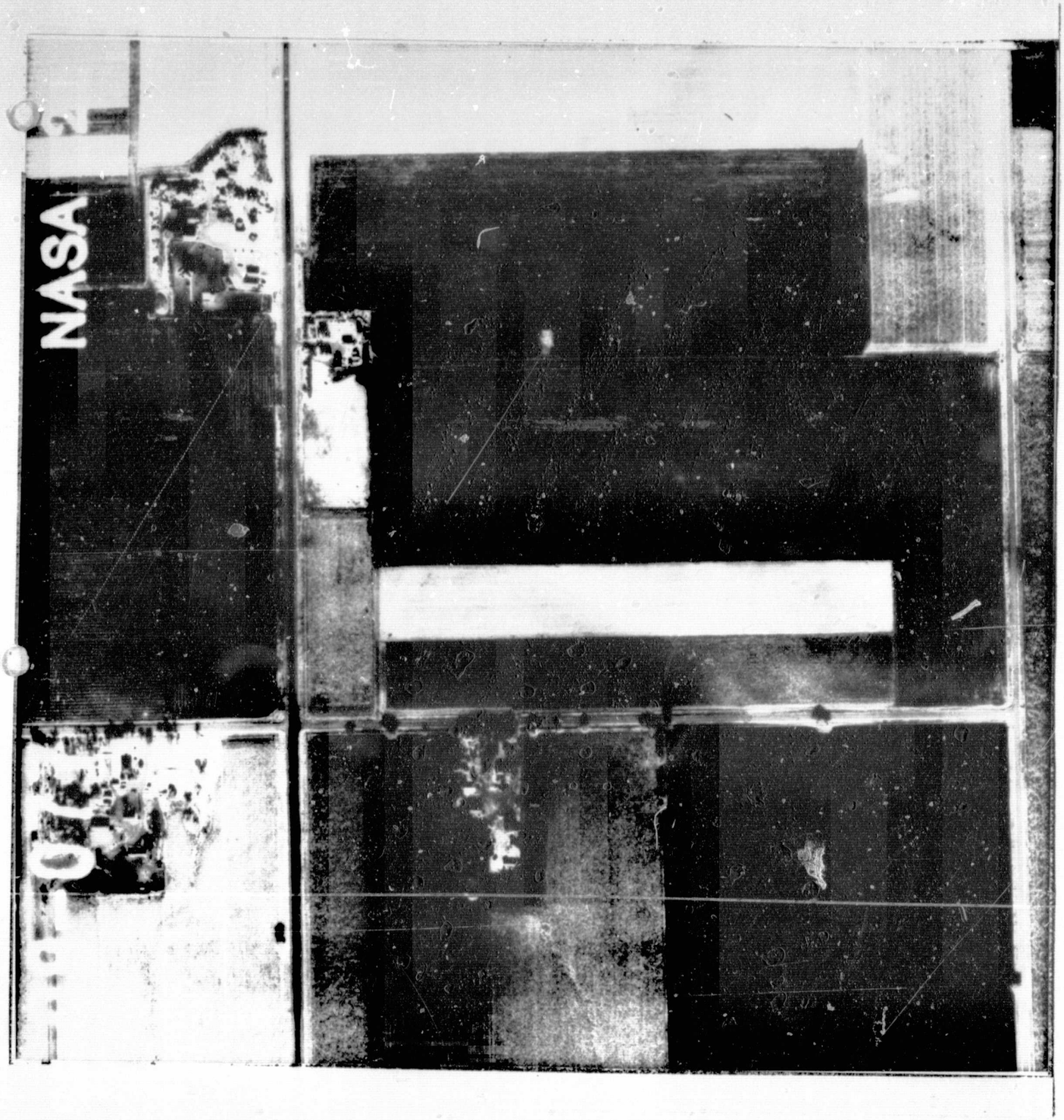



Fig. 38. AMPS black and white IR photograph of the northern section of field D.



Fig. 39. AMPS black and white IR photograph of the southern section of field D.

ORIGINAL PAGE IS
OF POOR QUALITY

Since the four fields are similar, any difference between them can only be attributed to texture or soil moisture differences. The Zeiss and AMPS imagery, however, does not permit quantitative analysis of the field texture or soil-moisture conditions. Therefore, a quantitative analysis to detect texture or soil moisture differences, if any, between three fields was undertaken using the 11-channel multispectral scanner digital data.

B. Multispectral Scanner Data

Condit (1970) has shown through laboratory studies that general soil types and wet and dry soil conditions can be differentiated using five characteristic wavelengths; 0.440μm, 0.540μm, 0.640μm, 0.740μm, and 0.860μm. From these five wavelengths a characteristic curve relating percent reflectance to wavelength can be constructed for three general soil types, i.e., chernozem, pedalfer, and laterite. Furthermore, these curves show certain changes when the soil type is changed from a dry to a wet state. Since the multispectral scanner onboard the NASA P-3 aircraft included the five wavelength channels used in Condit's experiments, a study was performed to determine if the results could be duplicated using the four bare fields of the October 17 experiment over Luverne. According to Condit's analysis the four bare fields should have a curve similar to that of figure 40, a chernozem type soil curve of which the soil types of the four fields are included.

To derive the curves from the scanner data, the digital values for all wavelengths were converted to radiance values using an algorithm supplied by NASA/JSC. Contoured microfilm of the radiance values of the four fields was then generated for seven wavelengths of which the five used by Condit were included. The mid-wavelength values used were

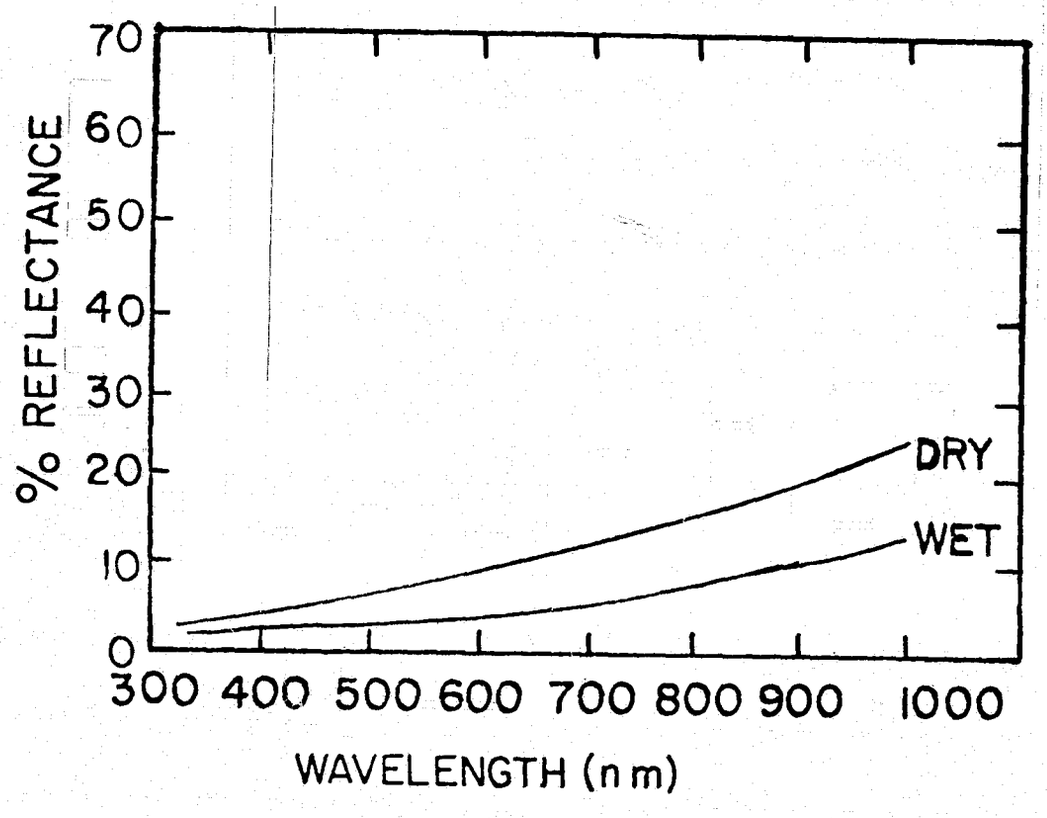



Fig. 40. Typical laboratory curve of chernozem-type soil (from Condit, 1970), percent reflectance vs. wavelength.

0.465μm, 0.515μm, 0.560μm, 0.640μm, 0.680μm, 0.810μm, and 1.015μm. Two other visible spectral channels (0.600 and 0.720 m) were available on the $M^2S$ but were not used due to malfunctions in both channels. A typical contoured radiance value microfilm product is shown in figure 41.

Plots of the average field radiance vs. wavelength for fields A, B, C, and D are shown in figures 42-45. Table 17 is a tabulation of the average field radiances for each field vs. wavelength as well as the mean and standard deviation of the radiances for a specified wavelength. Using Table 17, a comparison of the mean radiance values and standard deviations of each spectral bandwidth to the average radiance value of each field shows that only field D differs statistically from the other fields. Since the soil types of the four fields are the same, the possibilities accounting for this difference include vegetation, soil moisture, or soil particle size and soil structure. Examination of the Zeiss and AMPS imagery (see figures 22-39) reveals no vegetation in field D. Differences in soil moisture between field D and the other fields is possible but somewhat unlikely since (1) no measurable rain was recorded during the three days prior to the aircraft overflight, and (2) there is no field irrigation in this area during the late fall (e.g., October). During this time, however, many of the fields undergo tillage treatment. Stoner and Horvath (1971) have demonstrated that soil surfaces disturbed by tillage treatments exhibit a decrease in reflectance for the rougher soil surfaces. Other studies (Bowers and Hanks, 1965; Orlov, 1966; and Shockley et al., 1962) conclude that increasing particle diameter results in a decrease of reflectivity. Therefore the statistically higher radiance values in field D could be

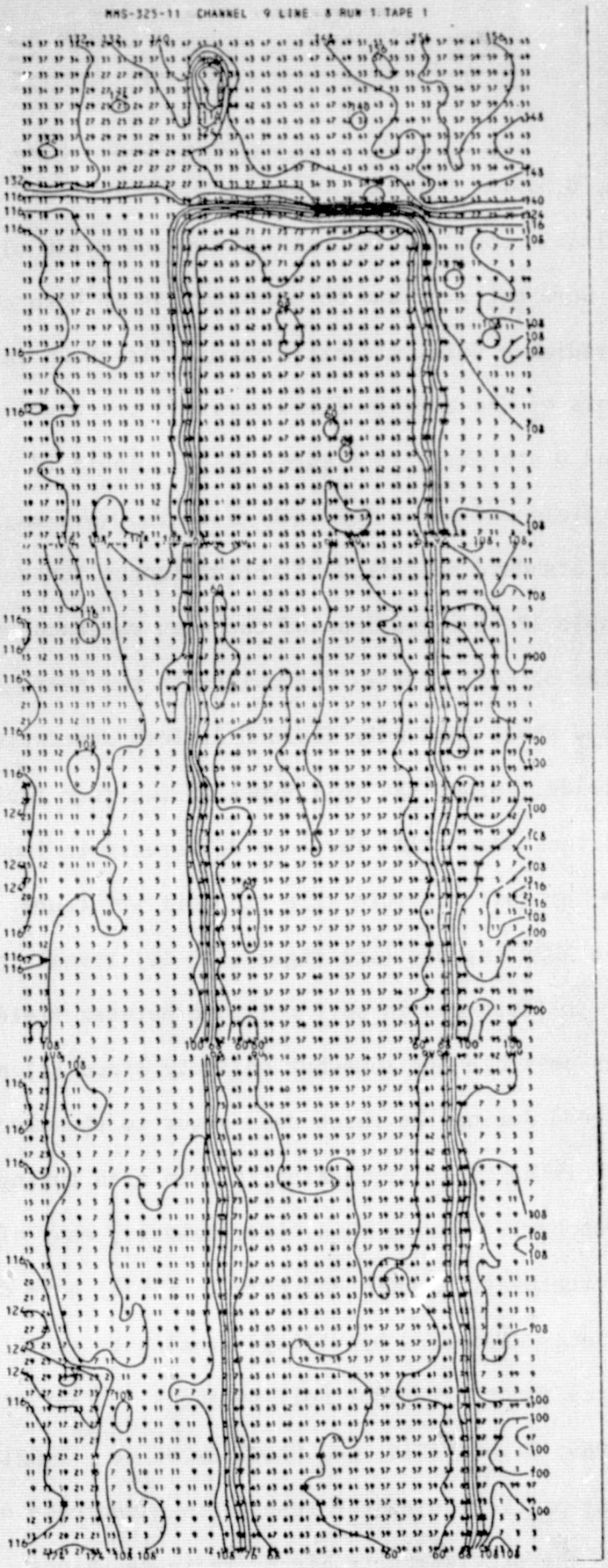



Fig. 41. Contoured radiance values for the channel 9 (0.760-0.860μm) of the multispectral scanner. Field B is shown.

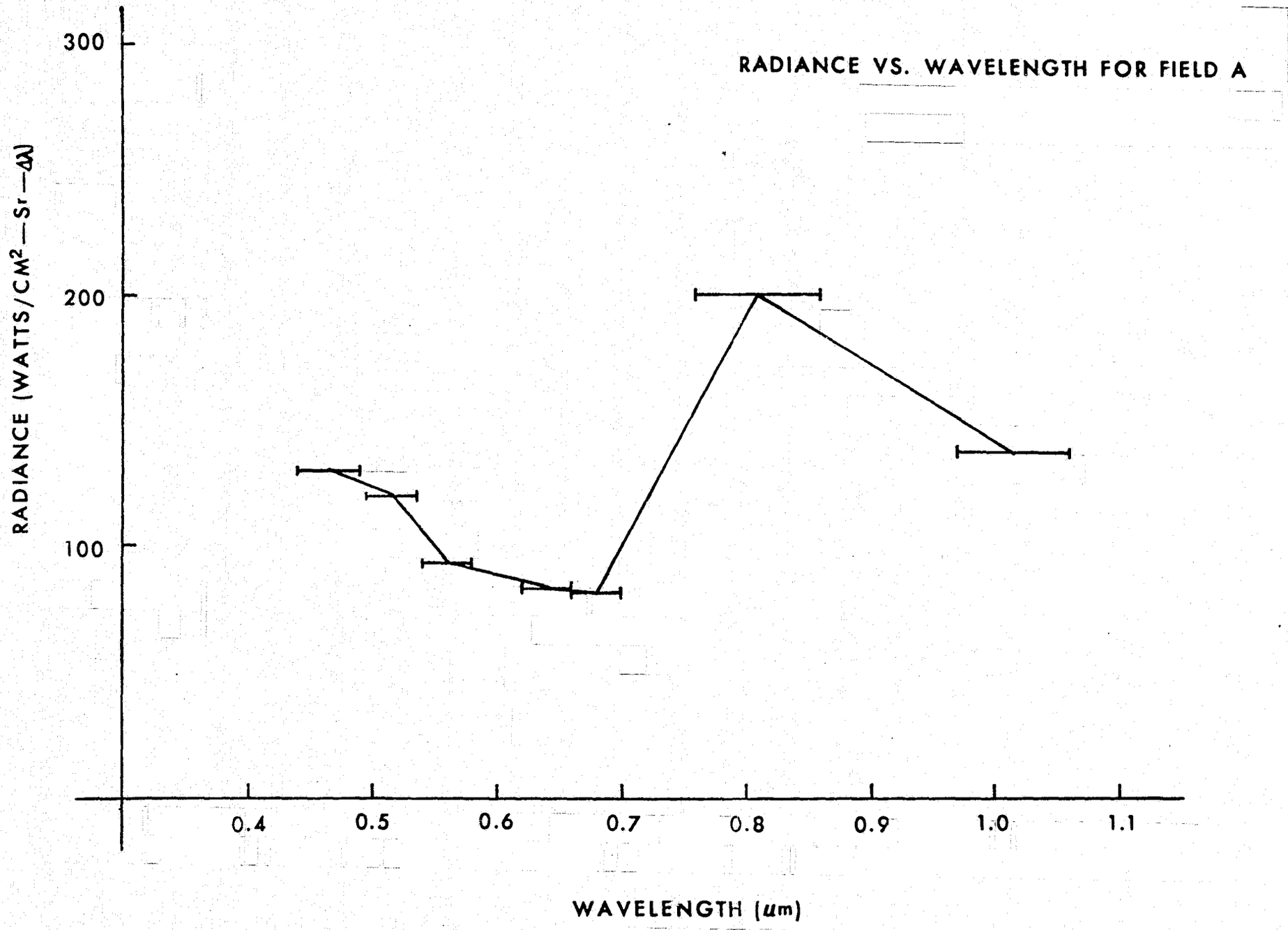



Fig. 42. Plot of average field radiance vs. wavelength for field A.

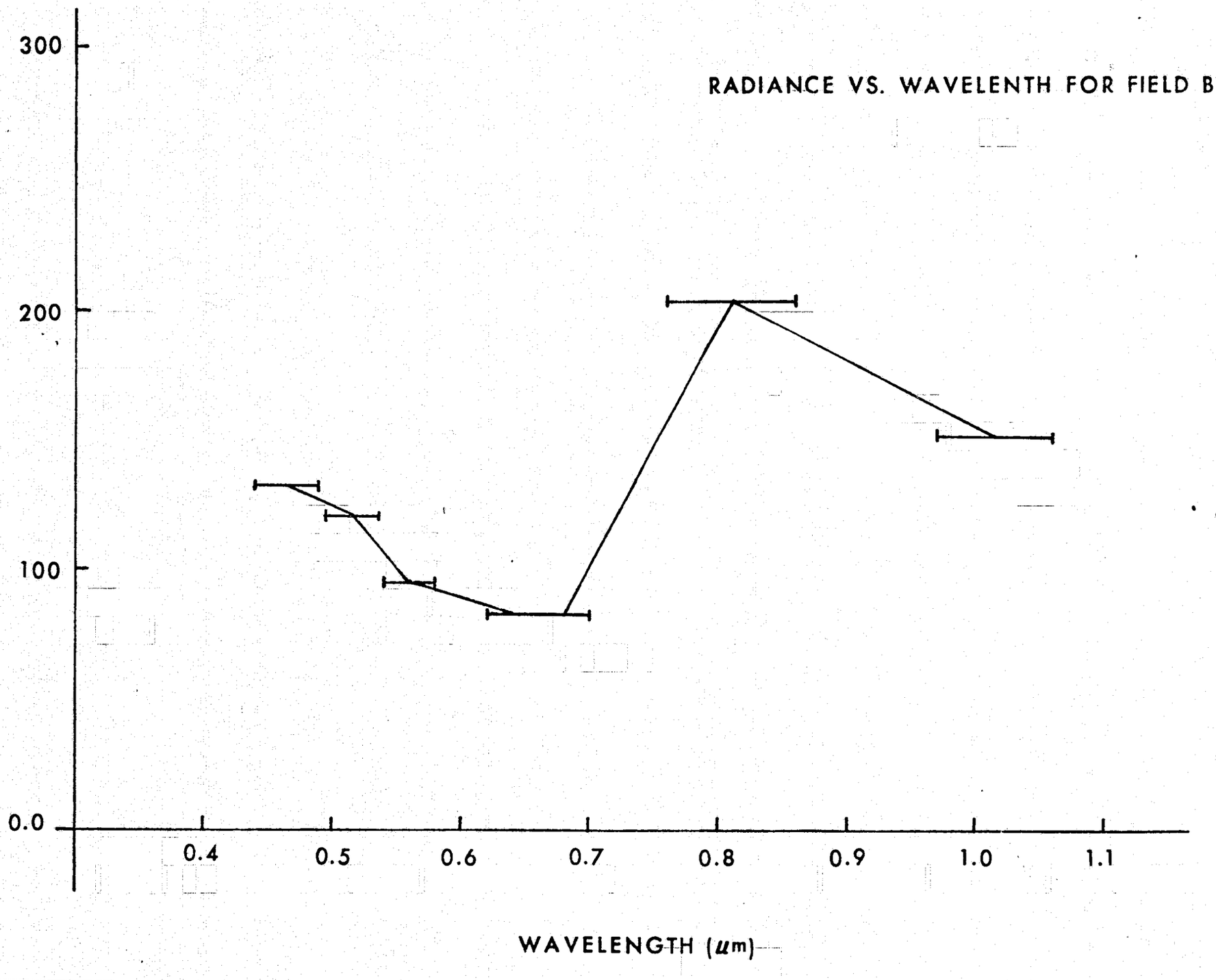



Fig. 43. Plot of average f. .d radiance vs. wavelength for field B.

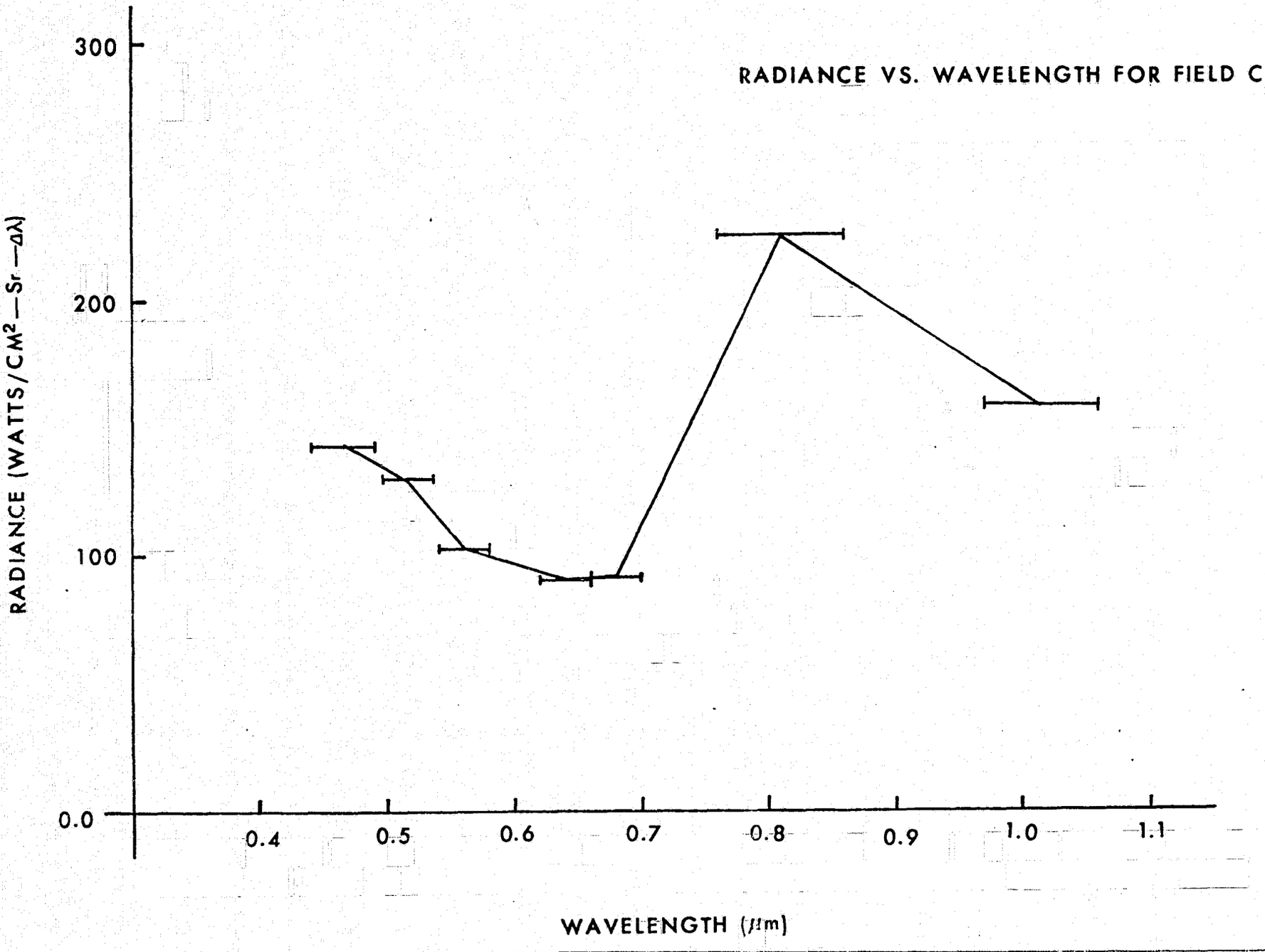



Fig. 44. Plot of average field radiance vs. wavelength for field C.

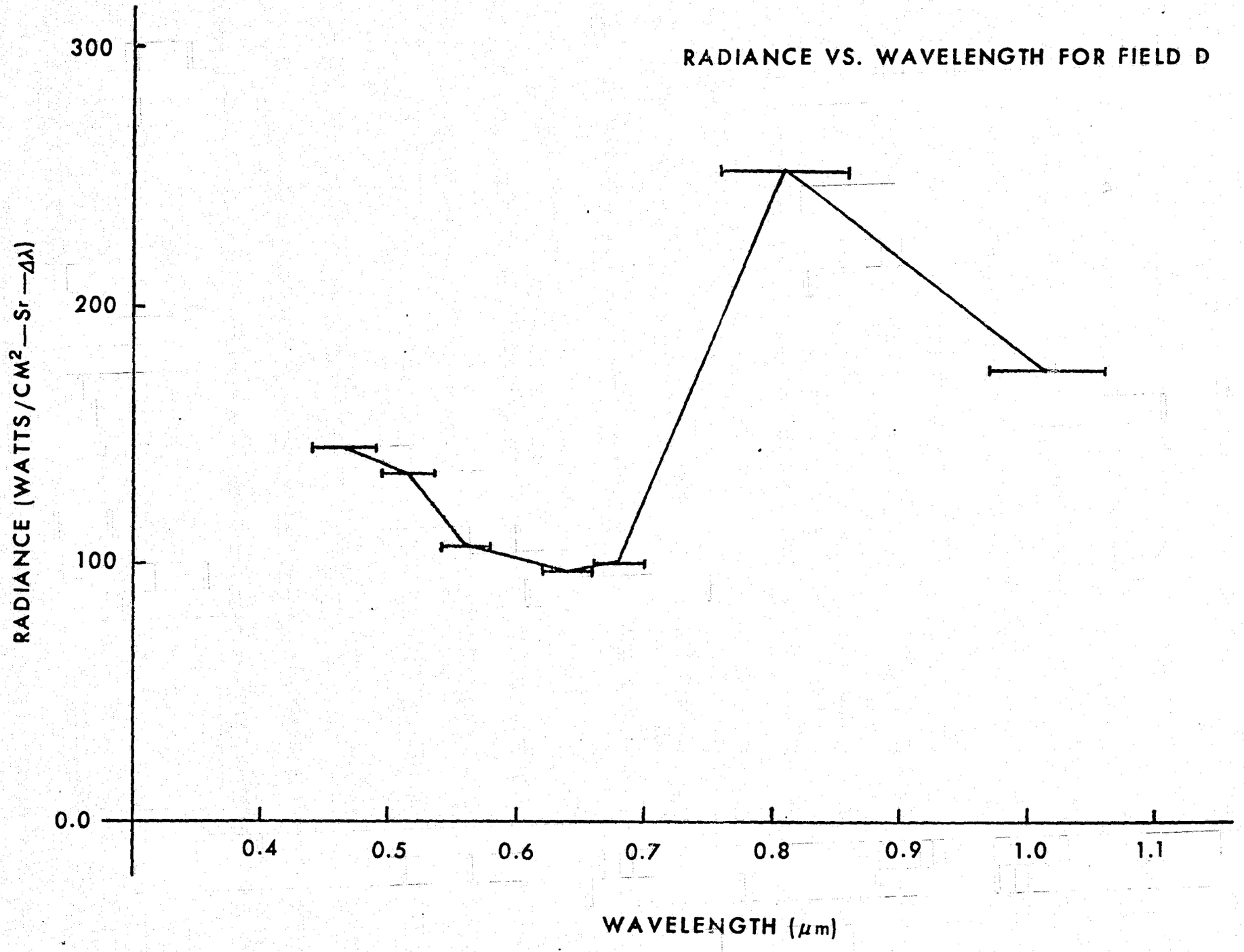



Fig. 45. Plot of average field radiance vs. wavelength for field D.

TABLE 17. $M^2S$ Spectral Band vs. Field Radiance

| Spectral Band (μm) | Average Field Radiance (Watts/$cm^2$-Sr-Δλ) | | | | | |
|---|---|---|---|---|---|---|
| | Field A | Field B | Field C | Field D | $\overline{X}$ | S |
| .440-.490 | 130 | 133 | 143 | 145 | 137.8 | 7.4 |
| .495-.535 | 120 | 121 | 130 | 135 | 126.5 | 7.2 |
| .540-.580 | 93 | 95 | 102 | 107 | 99.3 | 6.5 |
| .620-.660 | 83 | 83 | 90 | 96 | 88.0 | 6.3 |
| .660-.700 | 82 | 82 | 92 | 100 | 89.0 | 8.7 |
| .760-.860 | 200 | 205 | 225 | 252 | 220.5 | 23.6 |
| .970-1.060 | 137 | 152 | 160 | 175 | 156.0 | 15.9 |

accounted for by recent tillage in the other three fields. However, as mentioned previously, no ground data is available to verify this postulation.

A comparison of the $M^2S$-derived radiance vs. wavelength plots of fields A, B, C, and D (see figures 42-45) to Condit's laboratory curve of reflectance vs. wavelength for chernozem type soil (see figure 40) reveals several differences. The $M^2S$ data shows a decrease in radiance from 0.440μm-0.700μm, an increase from around 0.700μm to 0.860μm, and then another decrease from approximately 0.860μm to 1.060μm. This contrasts with Condit's curve which shows a general increase in reflectance vs. wavelength from 0.300μm to 1.000μm. The differences are not totally unexpected as field spectra often have differences with reflectance spectra from soils measured with spectrophotometer measurements in the laboratory. These differences arise because of (a) $O_2$, $CO_2$, and $H_2O$ absorption reducing incoming solar radiation in certain spectral bands, (b) variable solar illumination in different conditions, (c) soil texture and structure, and (d) solar intensity peaks at 0.5μm, falling off rapidly at shorter and longer wavelengths. Even though the laboratory and field curves do not correlate, it is encouraging to note that the $M^2S$ data provided an identical spectral "signature" for four fields of the same soil type.

C. $M^2S$ Thermal IR Data and PRT-5 Data

Several experiments (Blanchard, et al., 1974; Idso et al., 1975; and Reginato et al., 1976) have been performed demonstrating good relationships between soil-surface temperature and soil-moisture content. A summary of these relationships is found in Schmugge (1976b). Since no

ground truth was available for the October 17 experiment, no comparison was possible between it, the PRT-5 radiation thermometer, and the $M^2S$ channel 11 thermal IR data. Because the "footprint" of the PRT-5 sensor is approximately .11 km and line 8 of the aircraft data was not centered over the test line, the PRT-5 data does not include any of the fields A, B, C, or D. Therefore no comparison is possible between the PRT-5 temperature data and the temperatures derived from the $M^2S$ thermal IR data.

D. Landsat Data

The closest date for useable Landsat data for the October 17th experiment was October 1st. Since the test date and Landsat overpass date were not coincidental, the only comparison which can be made between the two is to determine whether the individual fields A, B, C, and D, which are visible on the $M^2S$ imagery can be distinguished on Landsat imagery. The purpose of the comparison is to determine if Landsat data can be used as an aid in studying individual fields in the Luverne, Minnesota test site.

Figure 46 is a side-by-side comparison of the channel 4 band (.54-.58μm) of the $M^2S$ data band 5 (.5-.6μm) of Landsat. The Landsat data has been photographically enlarged to approximate the scale of the $M^2S$ aircraft imagery. Field A through D have been labeled on the $M^2S$ image as well as other scene location features. The Landsat imagery has been similarly labeled. The result is poor field differentiation in band 5 for this area during October. None of the test fields can be located.

Figure 47 is a side-by-side comparison of the channel 10 band (0.97-1.06μm) of the $M^2S$ data and band 7 (0.80-1.1μm) of Landsat. Once again the test fields and scene location features have been labeled. Even

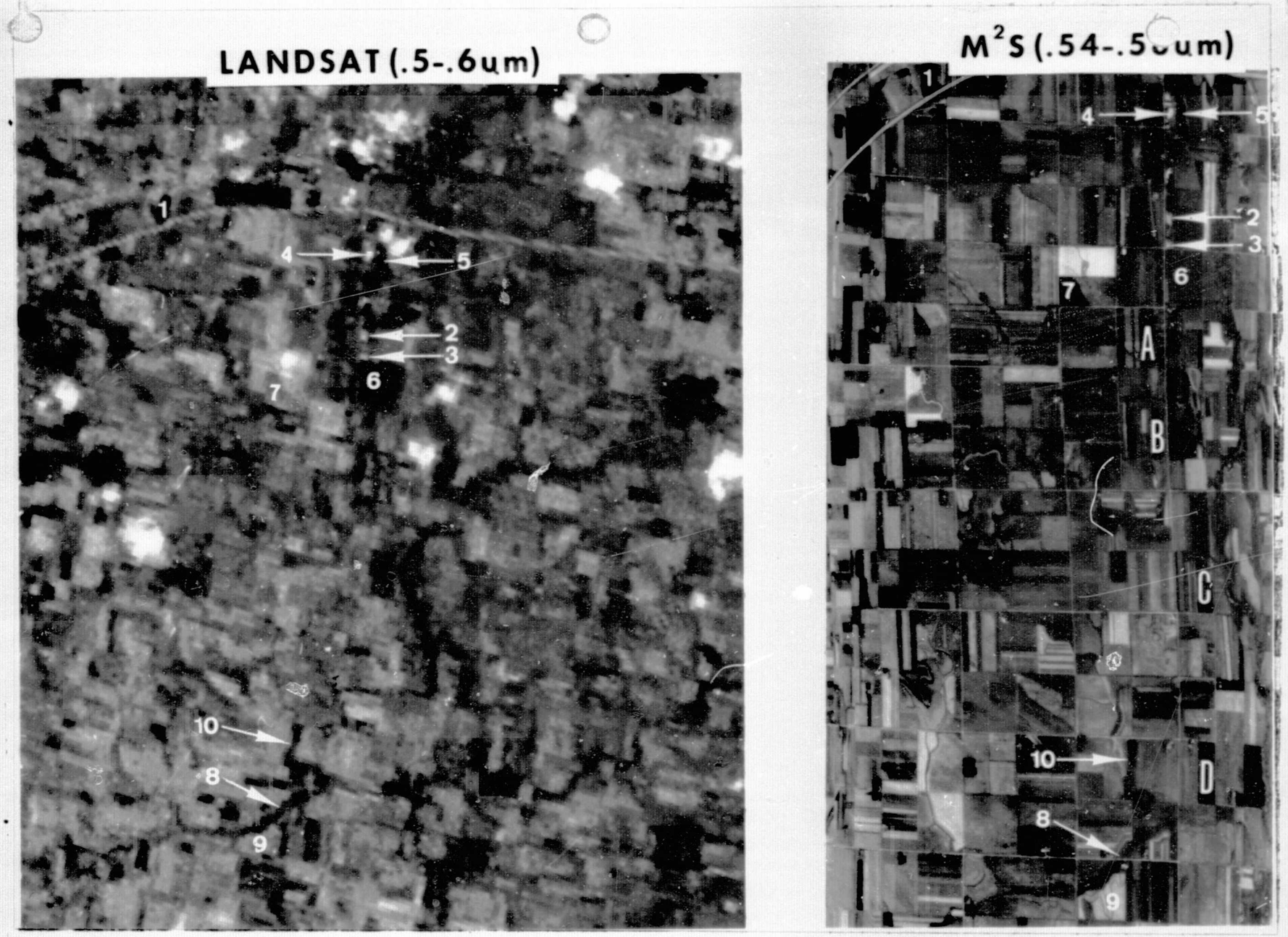



Fig. 46. A comparison of the channel 4 band (0.54-0.58μm) of the $M^2S$ and band 5 (0.5-0.6μm) of Landsat-2. Identical features on both bands are numbered.

ORIGINAL PAGE IS
OF POOR QUALITY

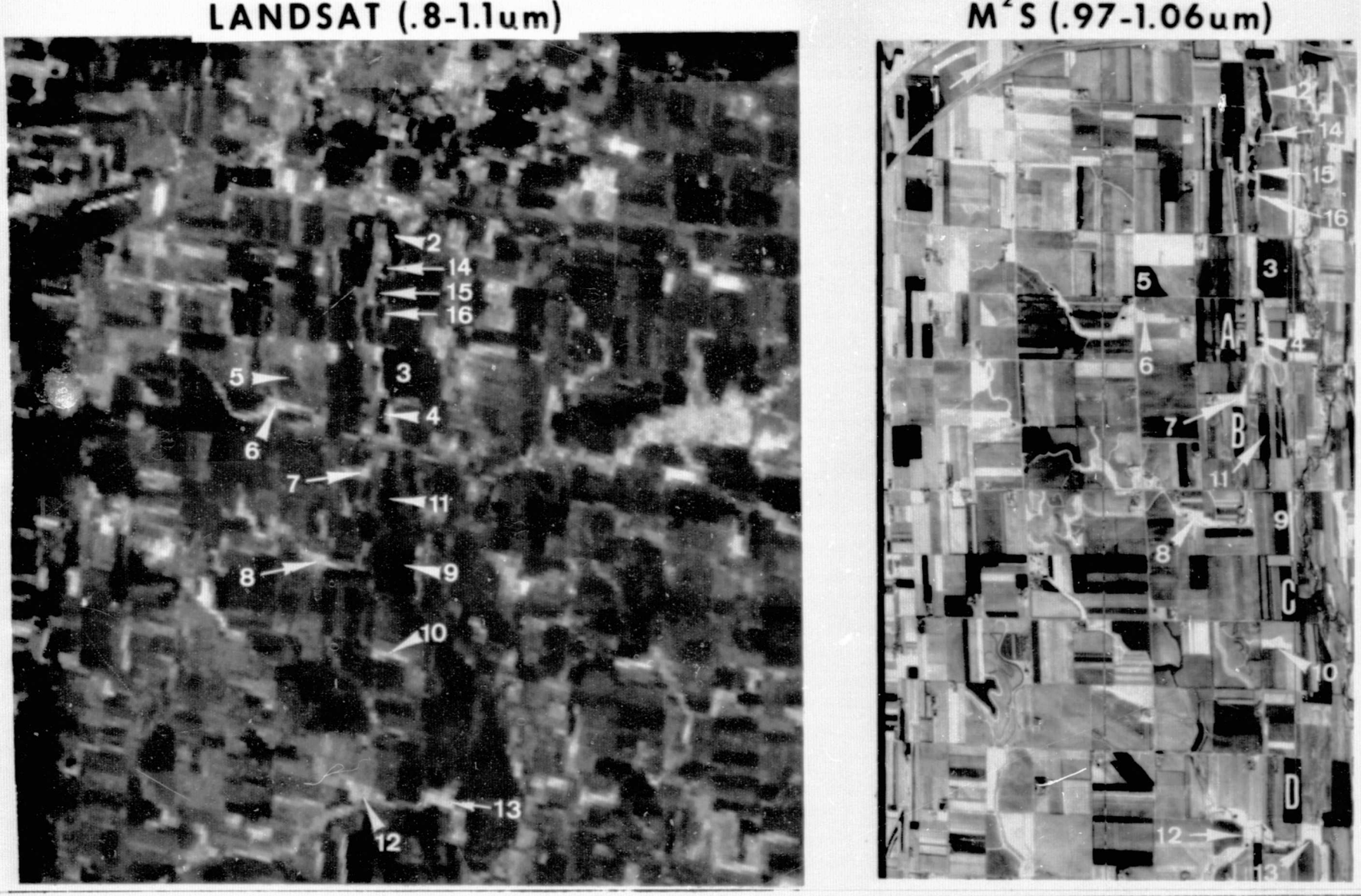



Fig. 47. A comparison of the channel 10 band (0.97-1.06μm) of the $M^2S$ and band 7 (0.8-1.1μm) of Landsat-2. Identical features on both bands are numbered.

through the test fields are not shown in band 7 of Landsat, it is much easier to distinguish individual fields during October in band 7 than in band 5. The question still arises as to why the test fields A through D do not appear on the October 1st satellite imagery. Other bare fields (e.g., 5 and 9) the size of the test fields do appear in band 7. According to the climatological data for October (NOAA, 1975) there was only one day of appreciable rainfall (.21 inches on October 9th) between the time of the satellite imagery and the subsequent aircraft imagery. Thus, different moisture conditions cannot account for the difference. The answer may be because the fields had not yet been tilled by October 1st after the fall harvest but were by October 18th, the time of the aircraft data.

Conclusions

Owing to the lack of ground data during the October 17, 1975 experiment, no conclusions can be drawn concerning soil moisture measurements using remote sensing techniques. Three conclusions, however, were derived from the remote sensing data. They are (1) multispectral data can be used to assign a spectral "signature" to specific soil types, (2) knowing prior meteorological conditions, statistical analysis of multispectral data can be used in nonirrigated areas to give a qualitative determination of field roughness, and (3) Landsat MSS band 7 data can be used as an aid in remote sensing studies of individual fields which are within the resolution limitations of the satellite data.

REPRODUCIBILITY OF THE
ORIGINAL PAGE IS POOR